Doctoral Thesis UAB No.

Biotechnological Applications of Artificial Microtissues

Presented by

Carlota Díaz Sánchez-Bustamante

Dipl. Biotechnology UAB

born 13.10.1980

citizen of Spain

Directed by

Prof. Dr. Martin Fussenegger

Department of Chemistry and Applied Biosciences

Institute of Chemical and Bio-engineering

ETH, Zurich

Barcelona, 2008

TABLE OF CONTENTS

Summary

Advances in tissue engineering and cell-based therapies will require the development of a range of specific technologies. These include systems for the cultivation of primary cells in three dimensions (3D) to form artificial tissues, efficient gene transduction technologies, and human-compatible gene regulation systems for adjustable molecular interventions all of which should enable the rational reprogramming of mammalian cells to achieve desired cell phenotypes, functionality, and to optimize cellular productivity.

The aim of this thesis is to (i) study and modulate the (electro) physiological properties of artificial myocardial microtissues by BMP-2 regulation to control and to regenerate cardiac functionality, (ii) study, induce and characterize differentiation and transdifferentiation processes of adipose- and bone-microtissues by overexpression of BMP-2 and ΔFosB genes in order to treat bone-related diseases such as osteoporosis, and (iii) evaluate artificial microtissue productivity to optimize mammalian production processes. Finally, the purpose is also to automate artificial microtissue production in order to satisfy requirements for industrial scale applications.

Scaffold-free artificial microtissues represent an alternative to existing tissue engineering strategies for cell-based therapies and tissue regeneration, as well as for cell-based biopharmaceutical applications. Within a research context, artificial microtissues could be used as a cell culture model to study/screen novel molecules/genes/proteins that are involved in different cellular processes (e.g. differentiation, proliferation, apoptosis, protein synthesis and secretion), while in a development context, artificial microtissues could be used as a tool to evaluate such target molecules/genes/proteins for their therapeutic action. Finally, once a therapeutic molecule/protein is identified, artificial microtissues may provide a more suitable or optimized environment for therapeutic protein production.

Sumario

Avances en ingeniería de tejidos y en terapias celulares requerirán el desarrollo de un nuevo abanico de tecnologías. Estas incluirán sistemas de cultivo de líneas primarias en tres dimensiones (3D) con el fin de construir tejidos artificiales, sistemas de transducción eficientes y sistemas de regulación genética compatibles en humanos para ajustar intervenciones moleculares. Todo ello permitirá reprogramar las células animales con el objetivo de obtener fenotipos deseados y de optimizar la productividad celular.

El objetivo de esta tesis es (i) estudiar y manipular las propiedades (electro) fisiológicas de los tejidos artificiales de miocardio mediante la regulación de BMP-2 para controlar y regenerar la funcionalidad cardiaca, (ii) estudiar, inducir y caracterizar los procesos de diferenciación y transdiferenciación de microtejidos adiposos y oseos mediante la sobre expresión de los genes BMP-2 y ΔFosB para tratar enfermedades relacionadas con el tejido oseo como la osteoporosis, y (iii) evaluar la productividad de los microtejidos artificiales para optimizar los procesos de producción con células animales. Por último, el objetivo es también automatizar la producción de microtejidos artificials para satisfacer las necesidades de la industria.

Microtejidos libres de scaffold no solo presentan una alternativa a la ingeniería de tejidos para terapias celulares y regeneración de tejidos, sino también tienen un gran potencial en estudios celulares para aplicaciones en la industria bio-farmacéutica. Mientras en el área de investigación, los microtejidos artificiales presentan un modelo para el estudio de nuevos genes y proteínas implicadas en diferentes procesos celulares (diferenciación, proliferación, apoptosis, síntesis de proteínas, etc.), en el area de desarrollo, los microtejidos artificiales representan una herramienta para el análisis de dichos genes y proteínas por su acción terapéutica. Finalmente, una vez la proteína terapéutica ha sido identificada, los microtejidos artificiales podrían proveer un ambiente más beneficioso para la producción de proteínas terapéuticas.

General Introduction

Engineering Artificial Microtissues

Tissue engineering is an interdisciplinary field that applies the principles of engineering and life sciences towards the development of biological substitutes that restore, maintain, or improve tissue function [1, 2].

2D vs. 3D Cell Culture

In vitro cultivation of mammalian cells is predominantly carried out by growing cells on adhesive monolayer cell culture surfaces (i.e. in two-dimensions, 2D). However, the *in situ* environment of a cell in a living organism has a three-dimensional (3D) architecture. The cells not only adhere to each other, but are also embedded in an extracellular matrix (ECM) containing proteins such as collagens, integrins, laminin and fibronectin [3], which affect cell shape [4], polarity [5], tension [6], proliferation [7], differentiation [8] and help communication between the cells [9] (Figure 1). Local disruption of the ECM by pharmacologic or genetic means results in selective programmed cell death (apoptosis) amongst adjacent cells [10, 11]. Cell functionality depends on such cell shape, cell-cell communication, cell-ECM interactions and on a signal gradient. Critically, this molecular gradient plays a key role in biological differentiation, determination of cell fate, organ development and signal transduction. Such gradients cannot be replicated in two dimensions. As a tissue consists of living cells organized within this complex structural and functional framework of 3D ECMs, it is no surprise that cells grown in flat monolayers miss many biological subtleties [12, 13].

Cell communication and the cellular environment determine gene expression and cellular biological behavior starting in the earliest stages of embryonic development [14]. For example, embryonic cells (non-malignant tissue) implanted into an unusual location transform to malignancy and to cancer, whereas implantation of the same cells into the correct location leads to normal embryogenesis.

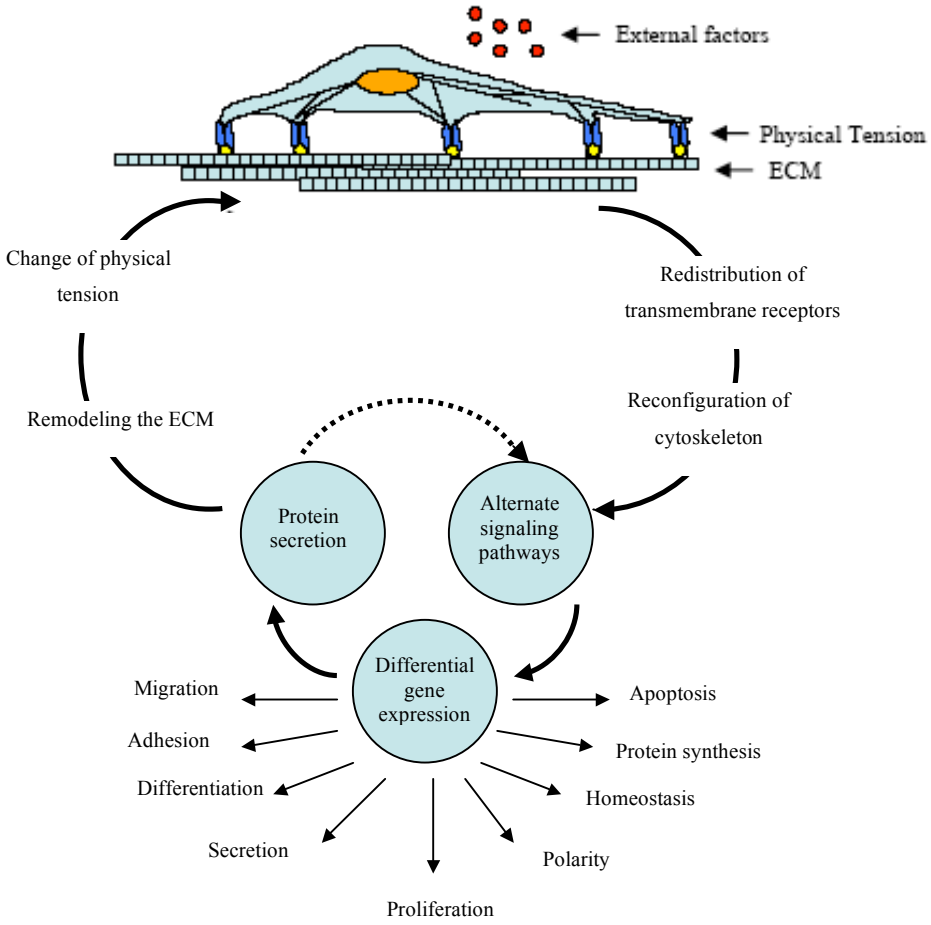

Figure 1: Role of three-dimensional shape, tension, external factors and extracellular matrix (ECM) on migration, adhesion, differentiation, secretion, proliferation, polarization, homeostasis, protein synthesis and apoptosis. Adapted from [13].

Due to the inability of 2D cell culture technologies to produce tissue-like phenotypes, biologists are progressively turning to 3D cell culture technologies [12, 15]. There are already many ongoing applications of 3D cell culture systems; in (i) tissue modeling or remodeling [16, 17], (ii) embryoid body characterization and studies of embryonic development [18], (iii) studies of cell-cell interactions, particularly with respect to drug resistance of multicellular tumors [11, 19, 20], (iv) gene/drug-function studies for cell-based therapies and studies of cell phenotype and differentiation stages, (v) therapeutic orientated studies, particularly for cancer research (necrosis, drug resistance, angiogenesis, metastasis, and proliferation) [21-24].

3D Cell Culture Systems

There are three principal tissue engineering strategies for treating diseased or injured tissues in patients. Implantation of: (i) biomaterials without additional cells which are used to convey biological signals to surrounding tissues to recruit cells and to promote inherent regeneration; (ii) cells together with a biomaterial scaffold that acts as a framework for developing tissues; and (iii) cells without any biomaterial which spontaneously form tissues.

Scaffold-based 3D cell culture systems are currently the standard technology for (micro)tissue generation. The scaffold serve as a substrate on which cell populations can attach, migrate, proliferate, differentiate, and be used as a drug carrier and delivery device to induce specific cellular functions [25, 26]. Critical variables in scaffold design and function includes the biomaterials themselves, including bulk materials, surface chemistry, mechanical properties, initial environment in the area of the scaffold, and late scaffold environment, which is often determined by degradation characteristics [27]. A host of different materials have been used in tissue engineering applications: (i) synthetic organic materials (polymers, hydrogels), (ii) synthetic inorganic materials (such as hydroxyapatite, ceramics, metals), (iii) organic material of natural origin (such as collagen, alginates, matrigel), and (iv) inorganic materials of natural origin (such as coralline, hydroxyapatite) [28]. However, such matrices contain biological information and elicit biological responses, which may differ from the response found in the natural microenvironment [29]. Despite considerable advances [30], current approaches to engineer cell-surface interactions do not entirely mimic the complexity of signals through which surrounding tissue regulates cell behavior such as induction of angiogenesis [13].

Scaffold-free 3D cell culture systems are an alternative to the use of biomaterials and are based upon cell self-assembly. Self-assembly can be characterized as the autonomous organization of cells into structures without human intervention. Such processes are common throughout nature occurring for example during histogenesis and organogenesis, and relying upon cell-cell and cell-ECM interactions to enable the organisms and its developing parts to gradually acquire their final shape [31]. As tissue engineers aim to not only create desirable organs but also to better understand of cell-cell and cell-matrix adhesion, cell self-aggregates represent ideal models for fulfilling these

requirements [32]. Therefore, strategies employing natural reaggregation processes to assemble monodispersed cells in a tissue-mimicking manner represent a valuable extension of current scaffold-based initiatives. Scaffold-free reaggregation may occur following (i) cultivation in shake flasks, gyratory shakers, roller bottles or non-adhesive surfaces [33, 34] (ii) centrifugation-based compression [35], (iii) maintenance in cell culture inserts [36], or (iv) gravity-enforced assembly in hanging drops [37].

Hanging-drop Technology

Originally pioneered for the production of embryoid bodies and blastocysts to study differentiation potential of stem cells [38], gravity-enforced assembly of microtissues in hanging drops has been found to be compatible with a variety of cell types [39]. Importantly, hanging drop technology enables self-tissue organization resulting in 3D biological structures of a prescribed size without compromising intracellular crosstalk or creating biocompatibility-associated issues [37, 39]. Hanging drop technology has been extensively used in areas such as cancer therapies due to the ability of multicellular tumor spheroids (MCTS) to reproduce tumor microenvironment more accurately than 2D cultures [11, 21, 22, 24, 40-42]. The microenvironment of the tumor is deeply involved in cancer initiation, progression, and especially in chemotherapeutic sensitivity (multicellular resistance) [43]. Microtissues formed in hanging drops have been also used for gene-function analysis of differentiation phenomena and development [44] and for the designing of functional microlivers, microcartilage and microhearts [45, 46] (Figure 2).

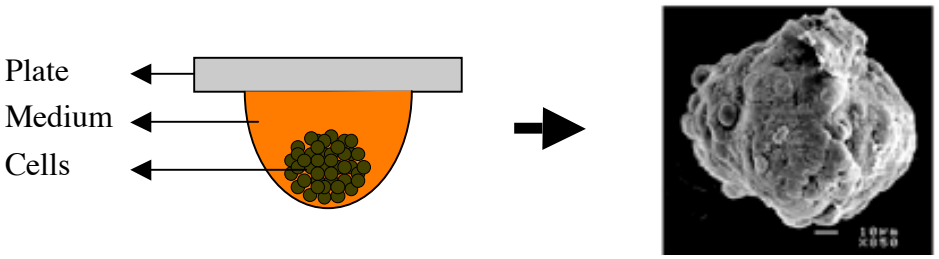

Figure 2. Gravity enforced self-assembly of microtissues in hanging drops. Droplets of a single cell suspension are placed onto a surface and cultivated upside down. After 1-4 days, depending on the cell type, cells form a cellular reaggregate.

Overall, gravity-enforced microtissue production has demonstrated its potential to (i) control tissue size in order to avoid oxygen and nutrients limitations of the *in vitro* culture [37], (ii) develop an ECM [47], (iii) maintain tissue-specific functionality [37], (iv) provide complex feeder structures for sensory neurons to differentiate [48] and for endothelial cells to vascularize [45, 49], (v) supports seamless integration of implants into host tissues [50] and (vi) offer tissue-like environments to improve drug/gene function correlations in current discovery programs [51, 52].

Gene Transfer and Gene Regulation of Artificial Microtissues

The major goal of gene therapy is to introduce a functional gene into a target cell to restore protein production, which either does not occur or is deficient due to a genetic disorder or metabolic disease [53, 54]. Over the past years a number of gene transfer vehicles have been developed, which include both nonvirus- and virus-based gene delivery systems [55-57]. Viral delivery systems are based on recombinant viruses delivering genetic information to the host cells by utilizing the viral infection process.

Lentiviruses

Lentiviruses are complex members of the *Retroviridae* family. The name is derived from *lentus* (slow) because of the prototypic slow progression of neurological diseases in sheep caused by the *maedi visna virus*. The most known lentivirus is the human immunodeficiency virus (HIV). Retroviruses are enveloped particles, 80 to 100 nm in diameter, which contain linear single-stranded RNA with positive polarity [58]. They infect target cells by fusion with cell membrane and convert viral RNA into a DNA intermediate through the viral-encoded reverse transcriptase enzyme and, through the integrase enzyme, they integrate this DNA molecule into the host genome where it resides as a provirus [59]. Compared to other retroviruses, lentiviruses contain several accessory genes (*tat, rev, nef, vpr, vif, and vpu*), some of which are known to play a regulatory role (*tat* and *rev*) and some others to have important functions during the viral life cycle and viral pathogenesis (Figure 4) [60]. However, the outstanding characteristic of lentiviruses are their ability to infect not only mitotic cells, but also non-dividing,

terminally differentiated cells [61, 62] because the preintegration complex can traverse the intact membrane of the nucleus in the target cell [63].

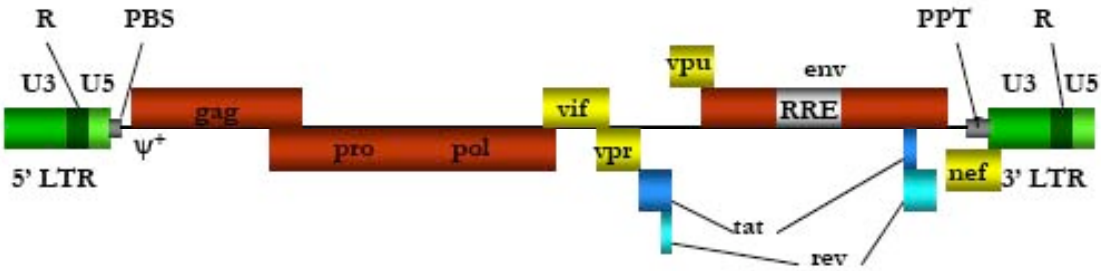

Figure 4: Schematic representation of the wild-type HIV provirus. The virus genome contain the 5' long terminal repeat [5'LTR, formed by the unique 3 prime (U3), a repeat (R) and the unique 5 prime (U5)], the primer-binding site (PBS), the extended packaging signal (ψ+) contained in the *gag* coding region (coding for the main structural proteins), the *pro* and *pol* coding regions (encoding the enzymes required for the viral lifecycle), the accessory genes *vif*, *vpr*, *vpu* and *nef* (which play important roles in the infectivity and pathogenesis of the virus), the *env* gene (coding for the envelope proteins), the regulatory genes tat and rev, the REV response element (RRE), the central polypurine track (PPT), and the 3' long terminal repeat (3'LTR; like 5'LTR formed by U3, R and U5).

In general, the genome of viruses encodes genes and *cis*-acting elements. While the coding sequences contain the genetic information of the structural and regulatory proteins required for the life cycle of the virus (infection, virus entry, replication and propagation) the *cis*-acting elements are essential for the packaging of the viral genome and integration in the host genome. To generate replication-deficient viral vectors, all protein-encoding sequences are removed from the virus and replaced by a therapeutic gene (or gene of interest), leaving the *cis*-acting sequences intact [53, 64-66]. The non-replicative viral particles, containing the genetic information of the therapeutic gene, are produced by transfecting the producer cells with the viral vector together with other vectors that provide the viral proteins in *trans*. Many different viral vectors are currently available for gene therapy [53, 67].

Lentiviral Vectors

Lentiviral vector systems typically include the transfer vector, which contains the transgene cassette, flanked by *cis*-acting elements required for encapsidation, reverse transcription and integration. These include (i) 5'LTR and 3'LTR, (ii) a relevant part of the *gag* gene containing the packaging signal (ψ^+), which is necessary for virus packaging, (iii) the *env*-derived sequences encompassing the Rev response element (RRE), allowing the transport of full length or singly spliced mRNA from the nucleus to the cytoplasm, and (iv) the polypurine tracts (cPPT and PPT) which support nuclear import of the proviral DNA in the transduced cell. The 3'LTR contains a large deletion in the U3 region (ΔU3) which results in transcriptional inactivation of LTR and reduces the risk of recombination with the wild-type virus [53, 68]. These engineered vectors have been referred to as self-inactivating vectors (SIN) and have markedly increased the safety of lentivirus-derived vectors. In addition to the transfer plasmid the helper and the envelope plasmids supply all the *trans*-acting elements necessary for the information about structural proteins, enzymes, and the envelope protein (VSV-G) which are all required for the production of non-replicating lentiviral particles [66] (Figure 5).

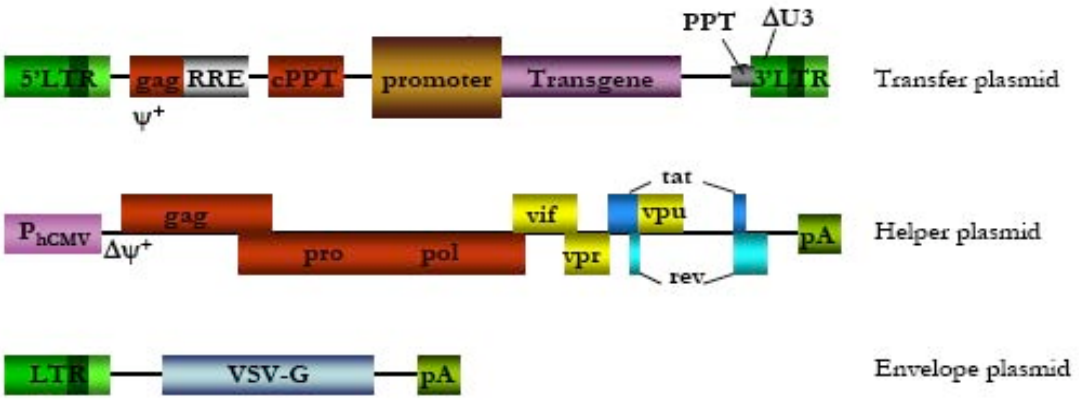

Figure 5: Schematic representation of the HIV-derived lentiviral vectors. In the transfer plasmid viral LTR regions flank the promoter and the transgene. Packaging the viral RNA genome is ensured by the presence of the packaging signal (ψ+) comprised of the 5' untranslated region of the 5' sequence of the *gag* ORF. In addition the vector contains two additional *cis*-acting sequences, the RRE and the PPTs. The helper plasmid supplies the structural matrix and capsid proteins encoded in *gag* ORF and the integrase and the reverse transcriptase encoded in *pro/pol* ORF. Other accessory proteins are provided by the helper plasmid (*tat*,

rev, *vif*, *vpr*, *vpu*) and activate RNA transcription or increase viral tropism. Finally, the envelope plasmid encodes the vesicular stomatitis virus G protein (VSV-G), which pseudotyped the lentiviral particles.

Overall, lentiviral vectors integrate into the host genome and promote long-term transgene expression without eliciting a host immune response. Moreover lentiviral vectors can transduce non-dividing cells with high gene transfer efficiency and can be pseudotyped with different surface proteins, thus enlarging the virus tropism and the utilization of these viral vectors for gene therapy purposes [54, 64, 69, 70].

Lentiviral Regulable Gene Delivery

Regulation systems allow the adjustable expression of heterologous genes in response to extracellular stimuli (temperature), small molecules (antibiotics, hormones, isopropyl β-D-1-thiogalactopyranoside [IPTG]) or metals (copper, cadmium) [71]. A satisfactory artificial gene regulation system must fulfill the following criteria: (i) the system does not interfere with endogenous regulatory networks and it is activated exclusively by exogenous nontoxic drug (*specificity*), (ii) high *inducibility*, that is a low base line and a high induction ratio, (iii) *bioavailability* of the inducer agents in all cells and tissues of animals and humans, (iv) high *reversibility*, (v) low potential for eliciting host immune responses (*immunogenicity*), (vi) high modularity of the regulating components (*flexibility*), (vii) correlation between the response of the system and the concentration of the inducer (*dose-dependence*) [71]. Regulated gene expression has influenced a wide variety of basic and applied biological research strategies. Therefore, lentiviral vectors engineered to regulate transgene expression [72-74] provide a powerful tool for tissue engineering, gene therapy, biopharmaceutical production and functional genomics strategies [75-81]. Many mammalian gene regulation systems have been developed in order to increase the window of applications [82-84].

Streptrogramin-Responsive Expression System (Pip System)

Bacterial antibiotic resistance regulons (collection of genes under control of the same antibiotic) represents an ideal source for mammalian gene regulation concepts. They show an extremely high binding affinity between the antibiotic and the

corresponding repressor and they are often compatible for human therapies since the inducer antibiotic is clinically licensed and has minimal to no side-effects within the dose responsive range.

Streptomyces have developed many resistance mechanisms to tolerate their own antibiotic products [85]. *S. pristinaespiralis* was shown to contain a pristinamycin resistance determinant (*ptr*) whose expression is induced by the streptogramin pristinamycin I (PI). Like other streptogramins, pristinamycin is a mixture of two structurally dissimilar molecules, the streptogramin A component pristinamycin II (PII) and the streptogramin B component pristinamycin I (PI). The regulation of the *ptr* promoter (P_{PTR}) requires a DNA sequence motif (GTACRSYGTAY), which forms the binding site for Pip (pristinamycin-induced protein). Pip was purified and its gene was cloned from *S.coelicolor*. PI was demonstrated to reverse biding of Pip to P_{PTR}. The streptogramin-repressible gene regulation system (Pip_{OFF}) is based on the PI-dependent transactivator (PIT: Pip fused to VP16, transactivator domain) which binds and activates PI-repressible promoter derivatives (P_{PIR}) in the absence of PI, whereas in the presence, PIT binding is prevented and P_{PIR} activity is repressed [86, 87] (Figure 6).

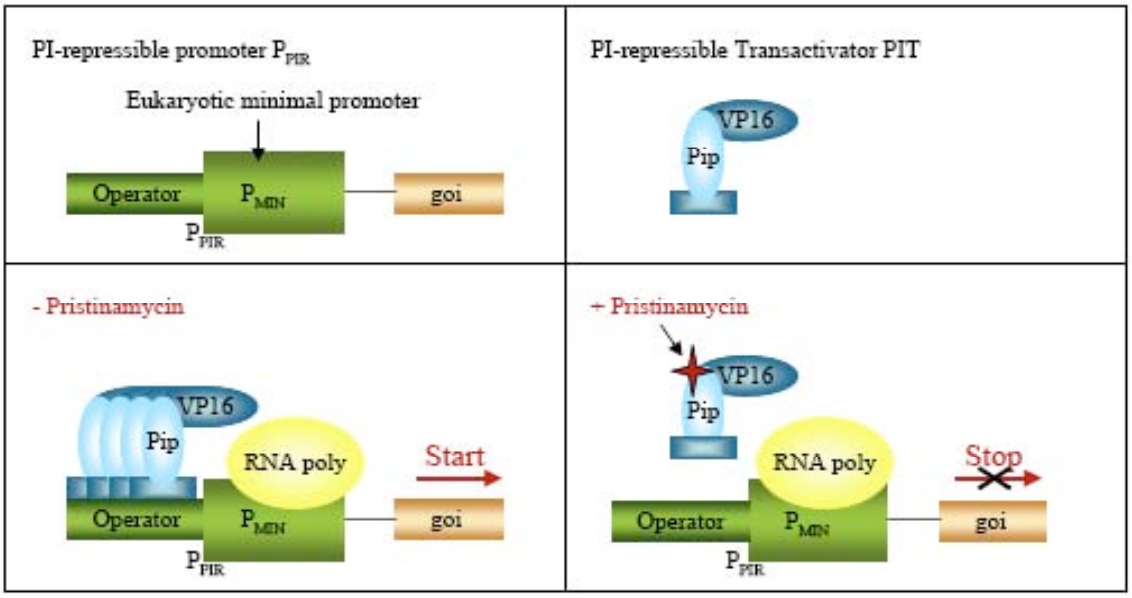

Figure 6: The Pip_{OFF} System [83].

Acetaldehyde-Inducible Expression System (Air System)

The fungus *A.nidulans* harbors a specific regulon responsible for coordinating the utilization of ethanol as its sole carbon source. Alcohol is oxidized via acetaldehyde into acetate, which enters mainstream metabolism in its activated form, acetyl-CoA. In the presence of acetaldehyde, a Zn_2Cys_6-type AlcR transactivator bind to a specific operator module and induces transcription of its own cistron as well as those encoding the alcohol (alcA) and aldehyde dehydrogenases (aldA). The alcA promoter (P_{alcA}) harbors seven AlcR-specific operators (O_{alcA}) each of which interacts with AlcR at high affinity [88].

P_{AIR} (acetaldehyde-adjustable promoter) was designed by placing an *A.nidulans* P_{alcA}-derived heptameric operator module 5' of a minimal version of the human cytomegalovirus immediate early promoter ($P_{hCMVmin}$). AlcR activated P_{AIR} in an acetaldehyde-inducible manner. Acetaldehyde enters into the gas phase and dissolves into the media and is a FDA-approved compound used as a food additive [72, 89].

Applications of Artificial Microtissues

Strategies based on the assembly of single/monodispersed cells by natural reaggregation have already provided insight into cell-cell interactions, tissue function and regulatory networks. Gravity-mediated self-assembly by the hanging drop technique has been used for the aggregation of several cell types in which cell-specific phenotype and functionality has been maintained. This technology has subsequently been widely used to study the differentiation potential of stem cells and to model tumor behavior *in vitro* by providing a surrounding microenvironment capable of promoting tumor initiation and progression. Scaffold-free microtissues represent an alternative to existing tissue engineering strategies and they might have a strong potential in cell-based studies.

In Physiological-based Studies

To this end, a cell embedded within a three-dimensional configuration more closely reproduces its *in vivo* physiology than when it is cultured by means of standard culture technologies (two-dimensional monolayer cultures) [12, 15].

(Electro)Physiological Studies

To date, electrophysiological studies have been performed by fundamentally two different techniques; (i) intracellular recordings, which impales a cell with a fine electrode, also called "patch-clamp" technique [90, 91] and (ii) extracellular recordings, in which the electrode is in tight contact with the cell/tissue [92-97]. Although the "patch clamp" technique yields very accurate information on the electrophysiological properties of the cell, is an invasive method that reduces cell viability and limits the number of possible cell recordings. This can be circumvented by extracellular recordings, where the cells are cultured directly on to an array of transducers, typically known as microelectrode arrays (MEAs), thus recording ion flow across the membrane of a cell/tissue during excitation. Besides the detection of the origin of excitation, the direction and velocity of the excitation spread, the contractility rate can also be measured [98, 99]. MEAs have been recently shown to be able to characterize further properties of the extracellularly recorded field potential, such as action potential upstroke velocity and duration [100].

The standard model used to understand cardiac action potentials are ventricular cardiomyocytes. Cardiac myocyte excitability results from action potentials. When one cell is electrically stimulated, typically by an electric current from an adjacent cell, an increase in the cell permeability allow the Na^+-gated channels to initiate a rapid opening producing a fast depolarization due the rapid entrance of Na^+ ions. The next phase occurs immediately after the maximum peak of Na^+ flow and is recognized as a partial repolarization of the membrane (I_{to}). The following phase, plateau phase, is unique to ventricular and purkinje fiber myocytes. An electrical plateau is generated due to the opening of Ca^{2+} channels (L-type calcium channels) allowing inward Ca^{2+} flow, and outward potassium flow through several types of potassium channels. Some Ca^{2+} ions originate from the extracellular fluid and others from the endoplasmatic reticulum. The total amount of current during the plateau phase of the cardiac action potential is small and can be maintained for 0.3 sec. Ca^{2+} ions subsequently bind to troponin, allowing the actin and myosin filaments to slide against each other, producing tension (strength of contraction). In the last phase the repolarization of the membrane is mediated by outward potassium currents, in which K^+ channels allow dissipation of K^+ ions down their

concentration. There are two main repolarizing potassium currents I_{Kr} and I_{Ks} involved in the final repolarization. Concurrently Na^+ and Ca^{2+} channels start closing, re-establishing the resting/basal potential (-90mV) [101] (Figure 9).

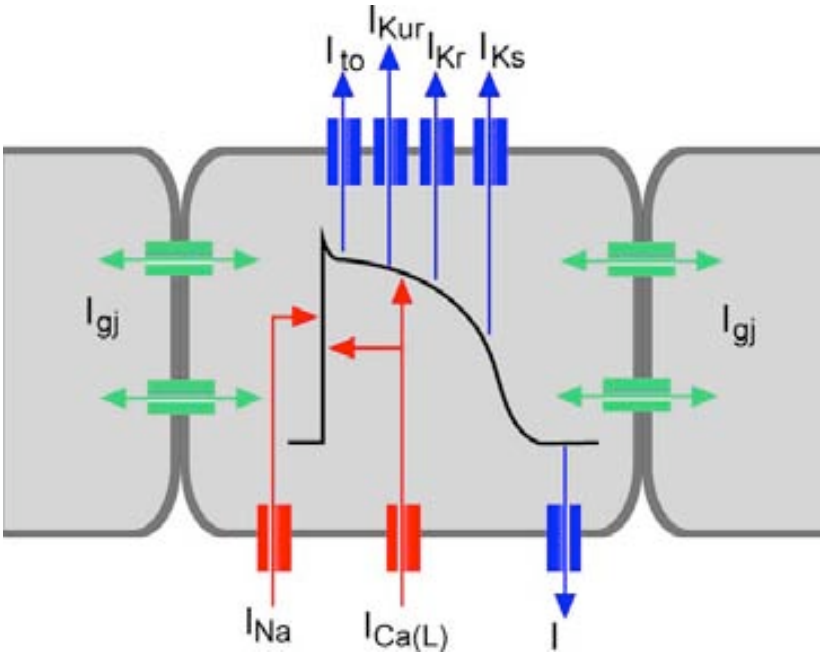

Figure 9: Schematic representation of a cardiac action potential with voltage on the Inward sodium current (1_{Na}) mediates the rapid depolarization phase. Transient outward potassium (K+) current (I_{to}) mediate rapid repolarization phase. The L-type inward calcium current contributes to the long plateau duration. Many outward K+ currents are responsible for repolarization of the cardiac action potential, including rapidly activating delayed rectifying $I_{Kr'}$ slowly activating delayed rectifying $I_{Ks'}$ and inward rectifying I_{K1}. Thus the coordinated opening and closing of caridac ion channels is responsible for cardiac excitability. Adapted from [102].

Artificial Myocardial Microtissues

Primary cardiomyocyte cultures from fetal, neonatal, or adult vertebrate hearts present a reliable source for pioneering cardiac tissue engineering. Even though cardiomyocytes maintained in monolayer cultures have enabled detailed insight for major structure and gene-function studies [103], they are less responsive to growth and differentiation factors compared to cardiomyocytes assembled into 3D cultures [104]. Moreover, while the latest generation of biocompatible scaffolds combine shape-supporting capacity with functional and bioactive properties [105, 106], some have been

associated with post implantation side-effects resulting from toxic degradation products, inflammatory reaction, and poor resorption [107]. In contrast, myocardial microtissues produced in hanging drops show (i) inter-microtissue superstructures, (ii) retention of cardiomyocyte-specific cell qualities, (iii) ECM development, (iv) high-lentiviral transduction rates, and (v) strong potential for regenerative medicine, with the successful integration of myocardial microtissues implanted into the pericardial cavity of adult rats maintaining cardiomyocyte specific phenotype [46, 50]. However, myocardial microtissue functionality hasn't been yet evaluated. In order to study cardiac electrophysiology we tested the BMP-2 gene, known to be related in cardiac functionality.

BMP Signaling Pathway (BMP-2)

Bone morphogenetic proteins (BMPs) are members of the transforming growth factor-β (TGF-β) superfamily. The BMP signaling pathway, like the TGF-β signaling pathway, modifies target gene transcription by receptor-mediated intracellular signaling [108]. There are two types of BMP receptors; type I (BMPR1A and BMPR1B) and type II (BMPR2). In the common BMP pathway, type I BMP receptors activate SMAD1/5/8 by phosphorylation [109]. A dimer of phosphorylated R-SMADs then forms a complex with SMAD4. This heterodimic complex translocates into the nucleus and binds to transcription factors regulating the expression of target genes [110, 111]. In the uncommon BMP pathway, activated BMP receptors interact with a X-linked inhibitor of apoptosis (XIAP), which activates the MAPK (mitogen activated protein kinase) pathway. XIAP links the BMP receptor signal to TAK1, and TAK1 binding proteins (TAB1/2/3) can trigger Jun N-terminal kinase (JNK) and NF-kB. In the common BMP pathway, SMAD function can be inhibited through blocking its translocation to the nucleus by Erk, in response to GF/CK signaling through Ras/Raf/Mek (Figure 7).

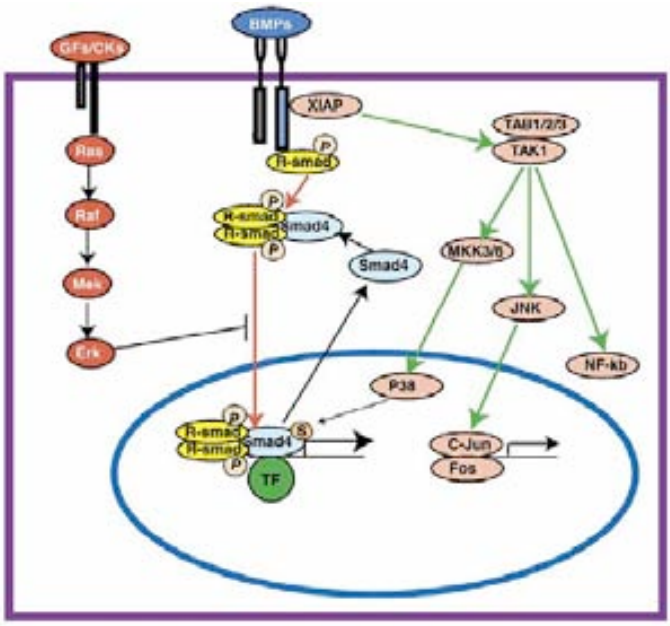

Figure 7. The BMP signaling transduction pathway. Adapted from [108].

BMPs were originally identified as growth and differentiation factors for the skeletal development but are now considered multifunctional cytokines, which play important roles in the development of many organs, including lung, kidney, gut, skin, teeth, and heart [112]. BMP-2, a member of this family of proteins, is expressed during mouse embryonic heart development [113]. It also directs the development of neural crest cells into neuronal phenotypes [114] and is able to induce *de novo* formation of bone at no bony sites in adult animal [115]. Preclinical and clinical studies have shown that BMP-2 can be applied in various therapeutic interventions such as bone defects, non-union fractures, spinal fusion, osteoporosis and root canal surgery [116]. In addition, BMP-2 has been recently associated with cardiac functionality via MEF-2A (myocyte enhancer factor 2A) through the PI3K (Phosphatidylinositol 3-Kinase) pathway [117], suggesting BMP-2/MEF-2A pathway as an alternative for the heart failure treatment (Figure 8).

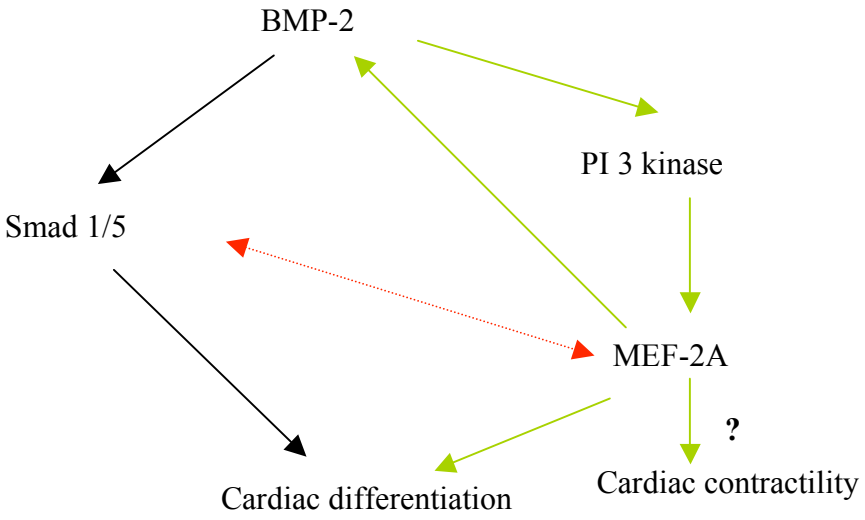

Figure 8: Scheme of BMP-2-induced MEF-2A-dependent BMP-2 expression and cardiac differentiation. BMP-2 stimulates BMP-specific Smads to regulate cardiac differentiation. BMP-2 increases PI 3-kinase activity, which regulates MEF-2A-dependent transcription of BMP-2 suggesting a plausible mechanism of autoregulation of BMP-2 expression. Also, increased MEF-2A expression regulates MHC expression, a marker for cardiac differentiation. The *dotted red arrow* indicates a plausible interaction between BMP-specific Smad and MEF-2A (yet to be identified). MEF-2A is suggested to control cardiac contractility. Adapted from Ghosh-Choudhury *et.al* [118].

In Differentiation- and Transdifferentiation-based Studies

Differentiation processes are determined by cellular environment via cell-to-cell, cell-to-cellular matrix, and ECM interactions. Critically, this matrix is reduced and modified when cells are cultivated in conventional two-dimensional cultures [12, 15].

Mesenchymal Stem Cells Differentiation and Transdifferentiation

Mesenchymal Stem Cells (MSCs) differentiate and transdifferentiate in response to changes in the microenvironment and to signals in the ECM [119]. Mesenchymal stem cells (MSCs) are multipotent stem cells that can differentiate into myocytes, adipocytes, condrocytes, or osteoblasts [120] (Figure 10). Differentiated cells (adult cells) are those that express the phenotypic properties characteristic of the functionally mature cell *in vivo* and beyond which the cell cannot progress. Such cells can change their phenotypes into another differentiated cell type, in a process named transdifferentiation. Transdifferentiation belongs to a wider class of cell type conversions referred to as

'metaplasias' [121]. There is still controversy about whether transdifferentiation processes are a direct switch from an already differentiated cell to another differentiated cell or if dedifferentiation takes also place [122].

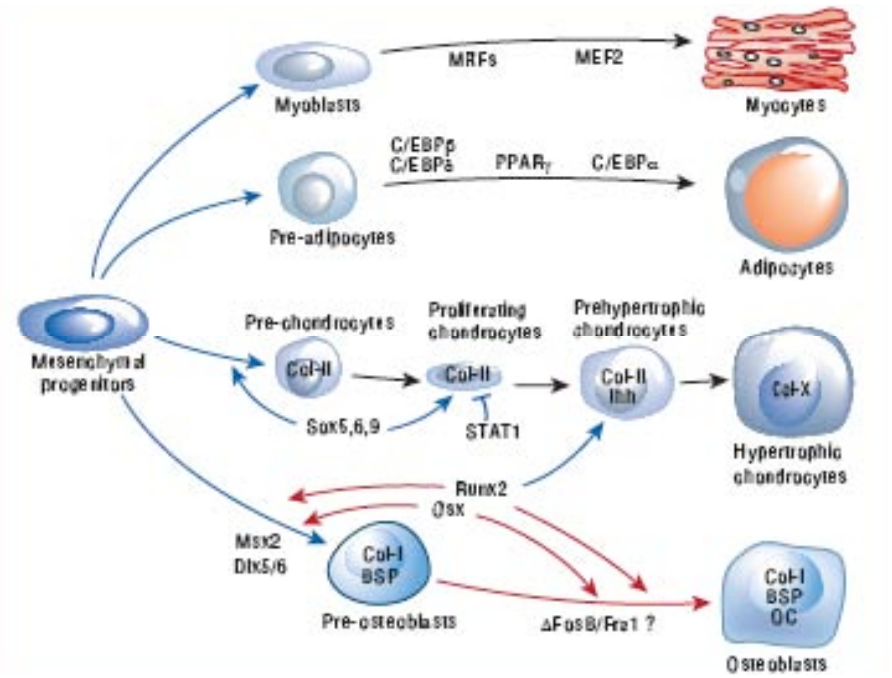

Figure 10: Overview of the mesenchymal stem cell differentiation. Adapted from [123].

However, mesenchymal-derived differentiated cells have been shown to directly transdifferentiate from myoblasts to adipocytes [124, 125] and from osteoblast to adipocytes [126]. Adipocytes and osteoblasts represent two morphologically and functionally distinct cell types. While adipose tissue is a soft tissue able of storing large amounts of fat, which serve as an energy reserve, bone tissue is a stiff tissue formed by a mineralized ECM, which serves as a tissue support. Adipocyte differentiates from preadipocyte in a process named adipogenesis. Adipogenesis is regulated by an elaborate network of transcription factors. The two principal adipogenic factors are PPARγ and C/EBPα [127, 128] (Figure 11).

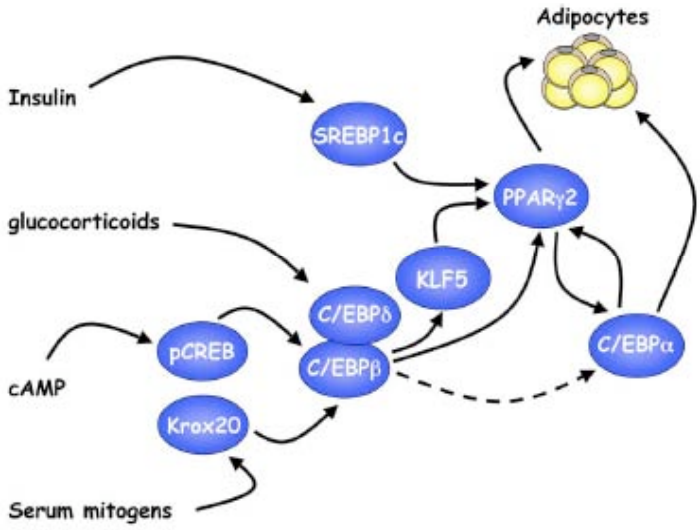

Figure 11: Adipogenesis. Exposure of preadipocytes to a cocktail of adipogenic inducers comprised of insulin, glucocorticoids, agents that elevate cAMP (isobutylmethylxanthine), and fetal bovine serum activates expression of several transcription factors that converge on PPARγ. PPARγ then induces C/EBPα expression, and together, these factors oversee terminal adipogenesis. Adapted from [127].

On the other hand, osteoblasts differ from their precursors fibroblasts (pre-osteoblasts) through a process named osteogenesis, in which the expression of the Cbfa1/Runx2 transcription factor is essential. Cbfa1/Runx2 regulates the expression of all known marker genes expressed during osteogenesis, such as osteocalcin, and is required for bone ECM production [123, 129, 130]. The primary function of osteoblasts is to synthesize and secrete ECM which results in the deposition of new bone (Figure 12).

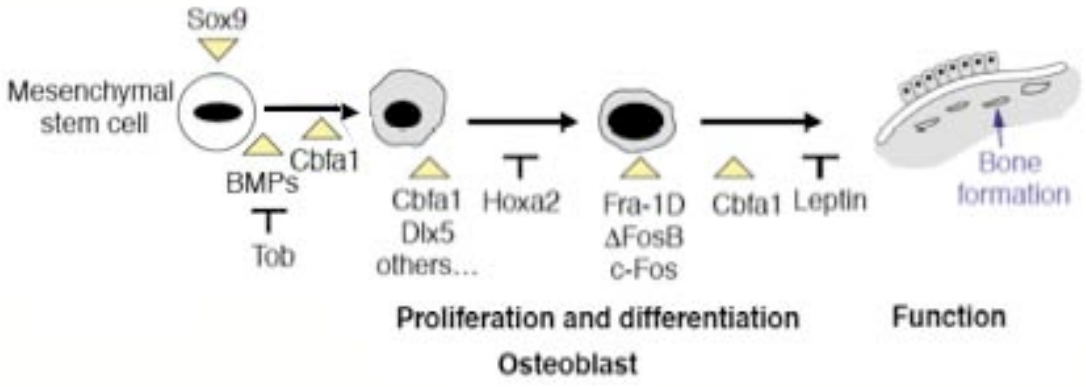

Figure 12: Osteogenesis. Some of the known molecules affecting the differentiation of pre-osteoblasts into osteoblasts as well as some of the inhibitory proteins such as Hoxa2 and Leptin. Adapted from [130].

3D Cell Culture Systems of Adipose Tissue

Adipose tissue has recently become a focus area for tissue engineering, encouraged by the large number of reconstructive, cosmetic and correctional indications that could be addressed with clinically translatable adipose tissue engineering strategies [131]. Adipose tissue is the largest tissue in the body which is often carried in excess and can therefore be harvested without creating contour deformities. Until now, 3D scaffolds have been predominantly used to replace adipose volume but not function [132], but complete adipose tissue engineering meant to restore both volume and function [133]. 3D scaffolds systems have been demonstrated to direct cell differentiation and organization into multicellular communities that approximate the *in vivo* architecture and function, in particular the specific secretory functions of adiopocytes [1]. Therefore, 3D cell cultures systems of adipose tissue are a promising tool to study/understand the cellular and the molecular basis of adipocyte differentiation and metabolism in physiological and pathological states in order to prevent and to treat obesity and its complications [134, 135].

3D Cell Culture Systems of Bone Tissue

Bone tissue repair is one of the major concerns of regenerative medicine. The current need for tissue replacements has necessitated the development of a new science termed 'bone tissue engineering'. Bone development requires the concentrated action of several microenvironmental signals such as cytoquines/growth factors, ECM molecules and cell/cell interactions [136]. During osteogenesis, cells differentiate into pre-osteoblasts and then undergo cellular condensation, a process that precedes osteoblast differentiation and matrix mineralization [137, 138]. Cellular condensation is mimicked in high-density cultures, such as scaffold-free reaggregation where up-regulation of the ECM components and ECM mineralization takes place [34]. 3D porous scaffolds formulated from biocompatible and osteoconductive materials that are not immunoreative are intended to mimic the native *in vivo* microenvironment. This demands construction of bioactive scaffolds that are also capable of supporting vascularization as well as cell proliferation and osteogenic differentiation. 3D cell cultures for bone regeneration provide a surgical tool for bone tissue engineering directed to enhance bone repair and wounding for orthopedic and cranio-maxillofacial clinical applications [139].

Transdifferentiation of adipose tissue to bone tissue

Obesity (fat tissue disease) and osteoporosis (bone tissue disease), two disorders of body composition, share several features including a genetic predisposition as well as a hormonal or environmental disorder. Bone remodeling is centrally regulated through the hypothalamus and sympathetic nervous system, a pathway that also regulates the metabolic fate and distribution of adipose tissue. With aging, the composition of bone marrow shifts to favor the presence of adipocytes with a corresponding decline in osteoblast function, resulting in osteoporosis. The relationship between bone and fat formation within the bone marrow microenvironment is suggested to be one of the causes of osteoporosis, and is accordingly an active area of investigation [140, 141]. Transdifferentiation provides an alternative method for osteoporosis and cell based-therapies in order to replace sick or damaged cells or tissue using patient's own cells [119, 142]. In order to induce transdifferention from adipse tissue to bone tissue we evaluate the effect of BMP-2 (see above) and ΔFosB.

AP-1 Transcription Factors Family (ΔFosB)

The AP-1 (activator protein 1) family of transcription factors consist of dimeric complexes of Fos (c-Fos, FosB, ΔFosB, Fra-1 and Fra-2) and Jun-related (cJun, JunB and JunD) proteins [143]. Some members of the ATF and CREB families of proteins are also part of the AP-1 complexes [144]. These are basic leucine zipper proteins that modulate the transcription of a variety of genes through interactions with specific sequences on the target gene promoters. Members of the AP-1 family participate in a large variety of biological processes including cell differentiation, proliferation, apoptosis and oncogenic transformation [145].

AP-1 components, mainly members of the Fos family, are involved in the regulation of bone cell proliferation and differentiation, and the promoters of several genes related to bone formation contain AP-1 consensus sequences. In addition several regulators of bone formation (TGF-β, parathyroid hormone and 1,25-dihydroxy vitamin D) induce AP-1 expression [146, 147]. The various components of the AP-1 complex are differentially expressed during osteoblast maturation *in vitro* [148]. During osteoblast proliferation, the levels of all Fos and Jun proteins are high. Subsequently, during the

period of ECM production and mineralization, their levels decrease, and Fra-2 and JunD become the principal components of the AP-1 complex in fully differentiated osteoblasts.

Fra-1 overexpression results in increased bone formation and osteosclerosis developement of the entire skeleton [149]. However, Fra-1 deficient mice display no skeletal abnormalities. Furthermore mice overexpressing c-Fos develop osteosarcomas [150], whereas *c-fos* knockout mice lack osteoclasts and develop osteopetrosis [151, 152]. In contrast no bone abnormalities have been described in *fosB* knockout mice, or in mice where FosB [153], Fra-2, c-Jun or JunB alone were overexpressed [147]. Transgenic mice expressing ΔFosB show not only an osteosclerotic phenotype in osteoblasts, but also a pronounced decrease in adipogenesis by altering the DNA-binding of C/EBPβ [154, 155].

ΔFosB is a C-terminally truncated splice variant of FosB that lacks the proline-rich transactivation domain but has maintained the ability to bind DNA and heterodimerize with other AP-1 factors [156-158]. It can be induced in a region-specific manner in the brain in response to several types of chronic perturbation, including drug abuse, antipsychotic drugs, antidepressant drugs, seizures and lesions [159]. Transgenic expression of ΔFosB, widely expressed in many tissues in addition to bone, stimulates bone formation and increases bone mass in mice, but it is not known how this protein, which lacks a transactivation domain, increases bone formation [123].

In Productivity-based Studies

Three-dimensional (3D) cell cultures differ form the two-dimensional (2D) ones not only in specific tissue functionality, but also in their metabolic activity. In contrast to 2D cell cultures, cells assembled within microtissues typically showed lower proliferation rates [24]. Proliferation-controlled cell cultures showed to increase cell specific productivity [75], suggesting that cells growing in a three-dimensional system could optimize the performance of production cell lines.

Heterelogous Protein Production

Biopharmaceutical manufacturing is the science of producing large amounts of high-quality recombinant protein pharmaceuticals [160]. During recent years, biopharmaceutical products manufactured by processes that use mammalian cell cultures

have gained increasing importance [161]. The basis of production processes with mammalian cells was commended in 1949 by Enders who infected cultured HeLa cells with poliomyelitis virus to create a vaccine [162]. In the late 1970's, Kholer and Millstein's work using fused lymphocyte-myeloma mouse cell line was another milestone in the development of animal cell culture [163]. Besides the production of antibodies and vaccines, the 1980's saw significant advances in genetic engineering leading to mammalian cell culture processes in which major pharmaceutical recombinant proteins were produced at large scale, including tissue plasminogen activator (tPA, Activase; produced for the first time in CHO cells in 1987 by Genentech), erythropoietin (EPO; produced for the first time in a mammalian cell line in 1989 by Amgen) and Factor VIII (produced for the first time in a mammalian cell line in 1992 by Baxter Healthcare/Genetics Institute).

Improving cell productivity in bioprocesses has long a major effort within the biotechnological industry to reduce costs of manufacturing and increase product quality [164]. High cell density is particularly desirable as product concentration is directly proportional to viable cell concentration over the time. For maximizing product concentration it is necessary to use cell lines with the ability to proliferate indefinitely to maintain the cells in their productive stage by supplying them with the essential nutrients. However, an uncontrolled proliferation of the cells in a batch mode results in nutrient and oxygen depletion, accumulation of lactate, ammonia and other toxic subproducts, which can lead to the deterioration of the target product. It is therefore useful to maintain cells in a static productive state. Also the development of defined medium (serum-free media) for mammalian cell culture has been relevant for the quality and biosafety of the desired product.

Different strategies for increasing specific productivity of mammalian production cell lines have been performed. Increased productivity by reducing specific growth rates was observed for the first time in hybridoma cells [165, 166]. Jenkin's and coworkers demonstrated that the high requirements for nucleotides and protein during DNA synthesis and mitosis might limit availability of substrates for recombinant RNA and protein synthesis. Their statement is based on Miller's kinetic analysis, which demonstrated that cells with small specific growth rate spend proportionally less time in mitosis. Several approaches, such as low temperature cultivation, chemicals addition and

genetic engineered cells, have achieved a G_1 phase arrest during the cultivation period to improve cell productivity [75, 167-172]. This correlation is supported with in nature whereby many cells of a mature mammal display no further growth after terminal differentiation yet continue to produce and often secret proteins during the lifetime of the organism.

The productivity of recombinant mammalian cell lines is often limited by the rapidity with which cells entry into the decline phase (apoptosis), the period of culture after maximum cell density is reached, and where cell viability starts to decrease. Heterologous protein production by itself is a stimulus of apoptosis. Therefore obviation of apoptosis is essential to prolong the production phase but also important during the adaptation to serum-free media conditions [173]. Apoptosis is triggered by several stimuli, such as serum deprivation, nutrient limitation, oxygen limitation and mechanical stress [174]. Indeed, spatial organization of the cells within a tissue and factors associated with the tissue microenvironment are implicated in programmed cell death in lower organisms [175].

Viability of Artificial Microtissues (vascularization)

Cells within the microtissue suffer nutrient and oxygen limitation. Endothelial cells are the central organizational unit of the vascular structure [176], which is responsible of supplying oxygen and nutrients to the tissues.

Monodispersed human umbilical vein endothelial cells (HUVEC), co-cultured onto microtissue forming human primary fibroblasts produced in hanging drops, show high angiogenic potential [49]. By controlling microtissue size, and without administration of any growth factor, 6-day old HUVEC coated human aortic fibroblast (HAF) microtissues establish a dense microvessel network (Figure 3).

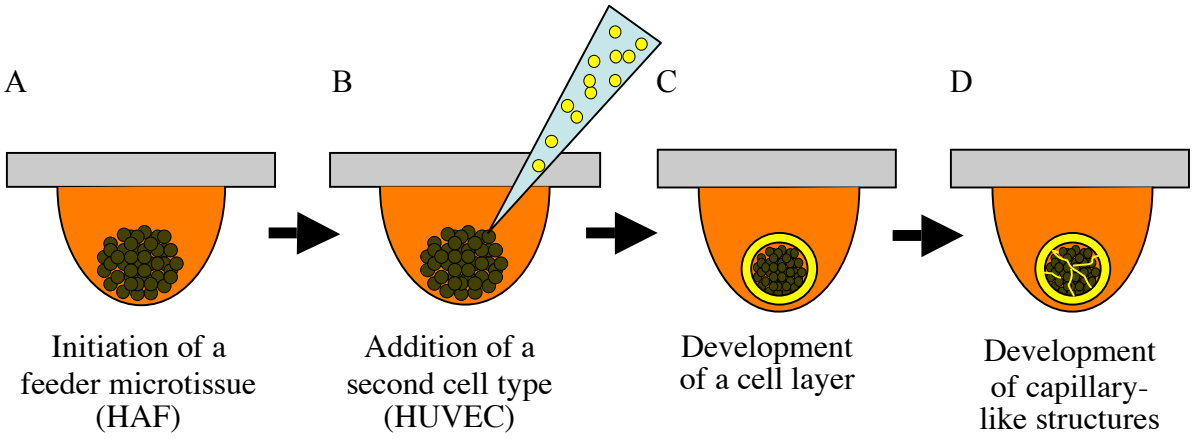

Figure 3: Endothelial-mediated vascularization of microtissues formed in hanging drops. (A) Single cell suspension is aliquoted into 60-well plates and cultivated upside down. After 2-6 days, depending on the cell type and the media composition, cells form a cellular aggregate (microtissues). (B) Generation of a multilayer microtissues by adding a second cell type into the hanging drop. (C) The added cells from an addition cell layer around the feeder spheroid. (D) Development of a capillary network through the microtissues after 6 days of co-cultivation.

Size-controlled microtissues exhibit size-dependent expression of vascular endothelial growth factor (VEGF), which indicated the oxygen levels within the microtissue. Capillary-like filled microtissues reduce VEGF expression thus increasing oxygenation within the tissue and demonstrating functional angiogenesis [49]. Moreover, macrotissues, assembled from HUVEC-coated fibroblasts microtissues, develope a vascular system, which functionally connects to the chicken embryo's vasculature after implantation. This collectively demonstrates that scaffold-free vascularized microtissues could be used for the scale-up and production of artificial tissue implants for future tissue engineering strategies [45, 50]. Moreover, vascularized microtissues optimized the microtissue yield representing an advantage in further biotechnological applications.

References

1. Langer, R. and Vacanti, J.P. Tissue engineering. Science (New York, N.Y **260**, 920, 1993.
2. Lysaght, M.J. and Reyes, J. The growth of tissue engineering. Tissue engineering **7**, 485, 2001.
3. Juliano, R.L. Signal transduction by cell adhesion receptors and the cytoskeleton: functions of integrins, cadherins, selectins, and immunoglobulin-superfamily members. Annual review of pharmacology and toxicology **42**, 283, 2002.
4. Goldmann, W.H. Mechanical aspects of cell shape regulation and signaling. Cell Biol Int **26**, 313, 2002.
5. Boudreau, N.J. Organized living: from cell surfaces to basement membranes. Sci STKE **2003**, pe34, 2003.
6. Tarone, G., Hirsch, E., Brancaccio, M., De Acetis, M., Barberis, L., Balzac, F., Retta, S.F., Botta, C., Altruda, F. and Silengo, L. Integrin function and regulation in development. Int J Dev Biol **44**, 725, 2000.
7. Sechler, J.L. and Schwarzbauer, J.E. Control of cell cycle progression by fibronectin matrix architecture. J Biol Chem **273**, 25533, 1998.
8. Bokel, C. and Brown, N.H. Integrins in development: moving on, responding to, and sticking to the extracellular matrix. Dev Cell **3**, 311, 2002.

9. Schenk, S. and Quaranta, V. Tales from the crypt[ic] sites of the extracellular matrix. Trends Cell Biol **13**, 366, 2003.
10. Boudreau, N., Sympson, C.J., Werb, Z. and Bissell, M.J. Suppression of ICE and apoptosis in mammary epithelial cells by extracellular matrix. Science (New York, N.Y **267**, 891, 1995.
11. Weaver, V.M., Lelievre, S., Lakins, J.N., Chrenek, M.A., Jones, J.C., Giancotti, F., Werb, Z. and Bissell, M.J. beta4 integrin-dependent formation of polarized three-dimensional architecture confers resistance to apoptosis in normal and malignant mammary epithelium. Cancer Cell **2**, 205, 2002.
12. Abbott, A. Cell culture: biology's new dimension. Nature **424**, 870, 2003.
13. Vogel, V. and Baneyx, G. The tissue engineeting puzzle: a molecular perspective. Annu Rev Biomed Eng **5**, 441, 2003.
14. Mathis, L. and Nicolas, J.F. Cellular patterning of the vertebrate embryo. Trends Genet **18**, 627, 2002.
15. Zhang, S. Beyond the Petri dish. Nature biotechnology **22**, 151, 2004.
16. Khalil, M., Shariat-Panahi, A., Tootle, R., Ryder, T., McCloskey, P., Roberts, E., Hodgson, H. and Selden, C. Human hepatocyte cell lines proliferating as cohesive spheroid colonies in alginate markedly upregulate both synthetic and detoxificatory liver function. J Hepatol **34**, 68, 2001.
17. Schmeichel, K.L. and Bissell, M.J. Modeling tissue-specific signaling and organ function in three dimensions. Journal of cell science **116**, 2377, 2003.
18. Duguay, D., Foty, R.A. and Steinberg, M.S. Cadherin-mediated cell adhesion and tissue segregation: qualitative and quantitative determinants. Developmental biology **253**, 309, 2003.
19. Desoize, B. and Jardillier, J. Multicellular resistance: a paradigm for clinical resistance? Crit Rev Oncol Hematol **36**, 193, 2000.
20. Yamada, K.M., Pankov, R. and Cukierman, E. Dimensions and dynamics in integrin function. Braz J Med Biol Res **36**, 959, 2003.
21. Ingber, D.E. Cancer as a disease of epithelial-mesenchymal interactions and extracellular matrix regulation. Differentiation **70**, 547, 2002.
22. Jacks, T. and Weinberg, R.A. Taking the study of cancer cell survival to a new dimension. Cell **111**, 923, 2002.
23. Zahir, N. and Weaver, V.M. Death in the third dimension: apoptosis regulation and tissue architecture. Curr Opin Genet Dev **14**, 71, 2004.
24. Bissell, M.J., Radisky, D.C., Rizki, A., Weaver, V.M. and Petersen, O.W. The organizing principle: microenvironmental influences in the normal and malignant breast. Differentiation **70**, 537, 2002.
25. Elisseeff, J., McIntosh, W., Fu, K., Blunk, B.T. and Langer, R. Controlled-release of IGF-I and TGF-beta1 in a photopolymerizing hydrogel for cartilage tissue engineering. J Orthop Res **19**, 1098, 2001.
26. Richardson, T.P., Peters, M.C., Ennett, A.B. and Mooney, D.J. Polymeric system for dual growth factor delivery. Nature biotechnology **19**, 1029, 2001.
27. Griffith, L.G. and Naughton, G. Tissue engineering--current challenges and expanding opportunities. Science (New York, N.Y **295**, 1009, 2002.
28. Lavik, E. and Langer, R. Tissue engineering: current state and perspectives. Appl Microbiol Biotechnol **65**, 1, 2004.

29. Hunziker, E.B. Articular cartilage repair: are the intrinsic biological constraints undermining this process insuperable? Osteoarthritis Cartilage **7**, 15, 1999.
30. Hench, L.L. and Polak, J.M. Third-generation biomedical materials. Science (New York, N.Y **295**, 1014, 2002.
31. Whitesides, G.M. and Grzybowski, B. Self-assembly at all scales. Science (New York, N.Y **295**, 2418, 2002.
32. Jakab, K., Neagu, A., Mironov, V., Markwald, R.R. and Forgacs, G. Engineering biological structures of prescribed shape using self-assembling multicellular systems. Proc Natl Acad Sci U S A **101**, 2864, 2004.
33. Furukawa, K.S., Ushida, T., Sakai, Y., Suzuki, M., Tanaka, J. and Tateishi, T. Formation of human fibroblast aggregates (spheroids) by rotational culture. Cell transplantation **10**, 441, 2001.
34. Kale, S., Biermann, S., Edwards, C., Tarnowski, C., Morris, M. and Long, M.W. Three-dimensional cellular development is essential for ex vivo formation of human bone. Nature biotechnology **18**, 954, 2000.
35. Muraglia, A., Corsi, A., Riminucci, M., Mastrogiacomo, M., Cancedda, R., Bianco, P. and Quarto, R. Formation of a chondro-osseous rudiment in micromass cultures of human bone-marrow stromal cells. Journal of cell science **116**, 2949, 2003.
36. Watzka, S.B., Lucien, J., Shimada, M., Edwards, V., Yeger, H., Hannigan, G. and Coles, J.G. Selection of viable cardiomyocytes for cell transplantation using three-dimensional tissue culture. Transplantation **70**, 1310, 2000.
37. Kelm, J.M., Timmins, N.E., Brown, C.J., Fussenegger, M. and Nielsen, L.K. Method for generation of homogeneous multicellular tumor spheroids applicable to a wide variety of cell types. Biotechnol Bioeng **83**, 173, 2003.
38. Wobus, A.M., Wolf, E. and Beier, H.M. Embryonic stem cells and nuclear transfer strategies. Present state and future prospects. Cells, tissues, organs **166**, 1, 2000.
39. Kelm, J.M. and Fussenegger, M. Microscale tissue engineering using gravity-enforced cell assembly. Trends Biotechnol **22**, 195, 2004.
40. Radisky, D., Muschler, J. and Bissell, M.J. Order and disorder: the role of extracellular matrix in epithelial cancer. Cancer Invest **20**, 139, 2002.
41. Santini, M.T., Rainaldi, G. and Indovina, P.L. Apoptosis, cell adhesion and the extracellular matrix in the three-dimensional growth of multicellular tumor spheroids. Crit Rev Oncol Hematol **36**, 75, 2000.
42. Weaver, V.M., Petersen, O.W., Wang, F., Larabell, C.A., Briand, P., Damsky, C. and Bissell, M.J. Reversion of the malignant phenotype of human breast cells in three-dimensional culture and in vivo by integrin blocking antibodies. J Cell Biol **137**, 231, 1997.
43. Timmins, N.E., Dietmair, S. and Nielsen, L.K. Hanging-drop multicellular spheroids as a model of tumour angiogenesis. Angiogenesis **7**, 97, 2004.
44. Itskovitz-Eldor, J., Schuldiner, M., Karsenti, D., Eden, A., Yanuka, O., Amit, M., Soreq, H. and Benvenisty, N. Differentiation of human embryonic stem cells into embryoid bodies compromising the three embryonic germ layers. Molecular medicine (Cambridge, Mass **6**, 88, 2000.

45. Kelm, J.M., Djonov, V., Ittner, L.M., Fluri, D., Born, W., Hoerstrup, S.P. and Fussenegger, M. Design of custom-shaped vascularized tissues using microtissue spheroids as minimal building units. Tissue engineering **12**, 2151, 2006.
46. Kelm, J.M., Ehler, E., Nielsen, L.K., Schlatter, S., Perriard, J.C. and Fussenegger, M. Design of artificial myocardial microtissues. Tissue engineering **10**, 201, 2004.
47. Anderer, U. and Libera, J. In vitro engineering of human autogenous cartilage. J Bone Miner Res **17**, 1420, 2002.
48. Kelm, J.M., Ittner, L.M., Born, W., Djonov, V. and Fussenegger, M. Self-assembly of sensory neurons into ganglia-like microtissues. Journal of biotechnology **121**, 86, 2006.
49. Kelm, J.M., Diaz Sanchez-Bustamante, C., Ehler, E., Hoerstrup, S.P., Djonov, V., Ittner, L. and Fussenegger, M. VEGF profiling and angiogenesis in human microtissues. Journal of biotechnology **118**, 213, 2005.
50. Kelm, J.M., Djonov, V., Hoerstrup, S.P., Guenter, C.I., Ittner, L.M., Greve, F., Hierlemann, A., Sanchez-Bustamante, C.D., Perriard, J.C., Ehler, E. and Fussenegger, M. Tissue-transplant fusion and vascularization of myocardial microtissues and macrotissues implanted into chicken embryos and rats. Tissue engineering **12**, 2541, 2006.
51. Kunz-Schughart, L.A., Freyer, J.P., Hofstaedter, F. and Ebner, R. The use of 3-D cultures for high-throughput screening: the multicellular spheroid model. J Biomol Screen **9**, 273, 2004.
52. Layer, P.G., Weikert, T. and Willbold, E. Chicken retinospheroids as developmental and pharmacological in vitro models: acetylcholinesterase is regulated by its own and by butyrylcholinesterase activity. Cell and tissue research **268**, 409, 1992.
53. Kootstra, N.A. and Verma, I.M. Gene therapy with viral vectors. Annual review of pharmacology and toxicology **43**, 413, 2003.
54. Walther, W. and Stein, U. Viral vectors for gene transfer: a review of their use in the treatment of human diseases. Drugs **60**, 249, 2000.
55. Gomez-Vargas, A. and Hortelano, G. Nonviral gene therapy approaches to hemophilia. Seminars in thrombosis and hemostasis **30**, 197, 2004.
56. Pfeifer, A. and Verma, I.M. Gene therapy: promises and problems. Annual review of genomics and human genetics **2**, 177, 2001.
57. Wells, D.J. Gene therapy progress and prospects: electroporation and other physical methods. Gene therapy **11**, 1363, 2004.
58. Fields, B.N., Knipe, D.M., Howley, P.M. and Al, E. Fields Virology. Philadelphia: Lippincott-Raven Publishers, 1996.
59. Tang, H., Kuhen, K.L. and Wong-Staal, F. Lentivirus replication and regulation. Annual review of genetics **33**, 133, 1999.
60. Coffin, J.M., Hughes, S.H. and Varmus, H.E. Retroviruses. New York: Cold Spring Harbor Laboratory Press, 1997.
61. Naldini, L. and Verma, I.M. Lentiviral vectors. Advances in virus research **55**, 599, 2000.
62. Trono, D. Lentiviral vectors: turning a deadly foe into a therapeutic agent. Gene therapy **7**, 20, 2000.

63. Amado, R.G. and Chen, I.S. Lentiviral vectors--the promise of gene therapy within reach? Science (New York, N.Y **285**, 674, 1999.
64. Buchschacher, G.L., Jr. and Wong-Staal, F. Development of lentiviral vectors for gene therapy for human diseases. Blood **95**, 2499, 2000.
65. Hansen, A.C. and Pedersen, F.S. Safety features of retroviral vectors. Current opinion in molecular therapeutics **4**, 324, 2002.
66. Hu, W.S. and Pathak, V.K. Design of retroviral vectors and helper cells for gene therapy. Pharmacological reviews **52**, 493, 2000.
67. Kay, M.A., Glorioso, J.C. and Naldini, L. Viral vectors for gene therapy: the art of turning infectious agents into vehicles of therapeutics. Nature medicine **7**, 33, 2001.
68. Miyoshi, H., Blomer, U., Takahashi, M., Gage, F.H. and Verma, I.M. Development of a self-inactivating lentivirus vector. Journal of virology **72**, 8150, 1998.
69. Lever, A.M., Strappe, P.M. and Zhao, J. Lentiviral vectors. Journal of biomedical science **11**, 439, 2004.
70. Quinonez, R. and Sutton, R.E. Lentiviral vectors for gene delivery into cells. DNA and cell biology **21**, 937, 2002.
71. Fussenegger, M. The impact of mammalian gene regulation concepts on functional genomic research, metabolic engineering, and advanced gene therapies. Biotechnology progress **17**, 1, 2001.
72. Hartenbach, S. and Fussenegger, M. Autoregulated, bidirectional and multicistronic gas-inducible mammalian as well as lentiviral expression vectors. Journal of biotechnology **120**, 83, 2005.
73. Mitta, B., Weber, C.C. and Fussenegger, M. In vivo transduction of HIV-1-derived lentiviral particles engineered for macrolide-adjustable transgene expression. The journal of gene medicine **7**, 1400, 2005.
74. Mitta, B., Weber, C.C., Rimann, M. and Fussenegger, M. Design and in vivo characterization of self-inactivating human and non-human lentiviral expression vectors engineered for streptogramin-adjustable transgene expression. Nucleic acids research **32**, e106, 2004.
75. Fussenegger, M., Schlatter, S., Datwyler, D., Mazur, X. and Bailey, J.E. Controlled proliferation by multigene metabolic engineering enhances the productivity of Chinese hamster ovary cells. Nature biotechnology **16**, 468, 1998.
76. Fux, C., Langer, D. and Fussenegger, M. Dual-regulated myoD- and msx1-based interventions in C2C12-derived cells enable precise myogenic/osteogenic/adipogenic lineage control. The journal of gene medicine **6**, 1159, 2004.
77. Fux, C., Mitta, B., Kramer, B.P. and Fussenegger, M. Dual-regulated expression of C/EBP-alpha and BMP-2 enables differential differentiation of C2C12 cells into adipocytes and osteoblasts. Nucleic acids research **32**, e1, 2004.
78. Koponen, J.K., Kankkonen, H., Kannasto, J., Wirth, T., Hillen, W., Bujard, H. and Yla-Herttuala, S. Doxycycline-regulated lentiviral vector system with a novel reverse transactivator rtTA2S-M2 shows a tight control of gene expression in vitro and in vivo. Gene therapy **10**, 459, 2003.

79. Regulier, E., Trottier, Y., Perrin, V., Aebischer, P. and Deglon, N. Early and reversible neuropathology induced by tetracycline-regulated lentiviral overexpression of mutant huntingtin in rat striatum. Human molecular genetics **12**, 2827, 2003.
80. Vigna, E., Cavalieri, S., Ailles, L., Geuna, M., Loew, R., Bujard, H. and Naldini, L. Robust and efficient regulation of transgene expression in vivo by improved tetracycline-dependent lentiviral vectors. Mol Ther **5**, 252, 2002.
81. Vogel, R., Amar, L., Thi, A.D., Saillour, P. and Mallet, J. A single lentivirus vector mediates doxycycline-regulated expression of transgenes in the brain. Human gene therapy **15**, 157, 2004.
82. Weber, W. and Fussenegger, M. Artificial mammalian gene regulation networks-novel approaches for gene therapy and bioengineering. Journal of biotechnology **98**, 161, 2002.
83. Weber, W. and Fussenegger, M. Approaches for trigger-inducible viral transgene regulation in gene-based tissue engineering. Current opinion in biotechnology **15**, 383, 2004.
84. Weber, W. and Fussenegger, M. Pharmacologic transgene control systems for gene therapy. The journal of gene medicine **8**, 535, 2006.
85. Cundliffe, E. How antibiotic-producing organisms avoid suicide. Annual review of microbiology **43**, 207, 1989.
86. Fussenegger, M., Morris, R.P., Fux, C., Rimann, M., von Stockar, B., Thompson, C.J. and Bailey, J.E. Streptogramin-based gene regulation systems for mammalian cells. Nature biotechnology **18**, 1203, 2000.
87. Weber, W., Kramer, B.P., Fux, C., Keller, B. and Fussenegger, M. Novel promoter/transactivator configurations for macrolide- and streptogramin-responsive transgene expression in mammalian cells. The journal of gene medicine **4**, 676, 2002.
88. Flipphi, M., Kocialkowska, J. and Felenbok, B. Characteristics of physiological inducers of the ethanol utilization (alc) pathway in Aspergillus nidulans. The Biochemical journal **364**, 25, 2002.
89. Weber, W., Rimann, M., Spielmann, M., Keller, B., Daoud-El Baba, M., Aubel, D., Weber, C.C. and Fussenegger, M. Gas-inducible transgene expression in mammalian cells and mice. Nature biotechnology **22**, 1440, 2004.
90. Neher, E. and Sakmann, B. Single-channel currents recorded from membrane of denervated frog muscle fibres. Nature **260**, 799, 1976.
91. Cole, K.S. Some physical aspects of bioelectric phenomena. Proceedings of the National Academy of Sciences of the United States of America **35**, 558, 1949.
92. DeBusschere, B.D. and Kovacs, G.T. Portable cell-based biosensor system using integrated CMOS cell-cartridges. Biosens Bioelectron **16**, 543, 2001.
93. Fromherz, P. Electrical interfacing of nerve cells and semiconductor chips. Chemphyschem **3**, 276, 2002.
94. Jimbo, Y. and Robinson, H.P. Propagation of spontaneous synchronized activity in cortical slice cultures recorded by planar electrode arrays. Bioelectrochemistry (Amsterdam, Netherlands) **51**, 107, 2000.

95. Morefield, S.I., Keefer, E.W., Chapman, K.D. and Gross, G.W. Drug evaluations using neuronal networks cultured on microelectrode arrays. Biosens Bioelectron **15**, 383, 2000.
96. Olsson, R.H., 3rd, Buhl, D.L., Sirota, A.M., Buzsaki, G. and Wise, K.D. Band-tunable and multiplexed integrated circuits for simultaneous recording and stimulation with microelectrode arrays. IEEE transactions on bio-medical engineering **52**, 1303, 2005.
97. Pancrazio, J.J., Gray, S.A., Shubin, Y.S., Kulagina, N., Cuttino, D.S., Shaffer, K.M., Eisemann, K., Curran, A., Zim, B., Gross, G.W. and O'Shaughnessy, T.J. A portable microelectrode array recording system incorporating cultured neuronal networks for neurotoxin detection. Biosens Bioelectron **18**, 1339, 2003.
98. Feld, Y., Melamed-Frank, M., Kehat, I., Tal, D., Marom, S. and Gepstein, L. Electrophysiological modulation of cardiomyocytic tissue by transfected fibroblasts expressing potassium channels: a novel strategy to manipulate excitability. Circulation **105**, 522, 2002.
99. Wang, L. and Duff, H.J. Developmental changes in transient outward current in mouse ventricle. Circulation research **81**, 120, 1997.
100. Halbach, M., Egert, U., Hescheler, J. and Banach, K. Estimation of action potential changes from field potential recordings in multicellular mouse cardiac myocyte cultures. Cell Physiol Biochem **13**, 271, 2003.
101. Keating, M.T. and Sanguinetti, M.C. Molecular and cellular mechanisms of cardiac arrhythmias. Cell **104**, 569, 2001.
102. Jongsma, H.J. Sudden cardiac death: a matter of faulty ion channels? Curr Biol **8**, R568, 1998.
103. Severs, N.J. The cardiac muscle cell. Bioessays **22**, 188, 2000.
104. Armstrong, M.T., Lee, D.Y. and Armstrong, P.B. Regulation of proliferation of the fetal myocardium. Dev Dyn **219**, 226, 2000.
105. Hubbell, J.A. Bioactive biomaterials. Current opinion in biotechnology **10**, 123, 1999.
106. Polonchuk, L., Elbel, J., Eckert, L., Blum, J., Wintermantel, E. and Eppenberger, H.M. Titanium dioxide ceramics control the differentiated phenotype of cardiac muscle cells in culture. Biomaterials **21**, 539, 2000.
107. Yang, S., Leong, K.F., Du, Z. and Chua, C.K. The design of scaffolds for use in tissue engineering. Part I. Traditional factors. Tissue engineering **7**, 679, 2001.
108. Zhang, J. and Li, L. BMP signaling and stem cell regulation. Developmental biology **284**, 1, 2005.
109. Zwijsen, A., Verschueren, K. and Huylebroeck, D. New intracellular components of bone morphogenetic protein/Smad signaling cascades. FEBS letters **546**, 133, 2003.
110. Massague, J., Blain, S.W. and Lo, R.S. TGFbeta signaling in growth control, cancer, and heritable disorders. Cell **103**, 295, 2000.
111. Shi, Y. and Massague, J. Mechanisms of TGF-beta signaling from cell membrane to the nucleus. Cell **113**, 685, 2003.
112. Hogan, B.L. Bone morphogenetic proteins in development. Curr Opin Genet Dev **6**, 432, 1996.

113. Zhang, H. and Bradley, A. Mice deficient for BMP2 are nonviable and have defects in amnion/chorion and cardiac development. Development (Cambridge, England) **122**, 2977, 1996.
114. Christiansen, J.H., Coles, E.G. and Wilkinson, D.G. Molecular control of neural crest formation, migration and differentiation. Current opinion in cell biology **12**, 719, 2000.
115. Rosen, V. and Thies, R.S. The BMP proteins in bone formation and repair. Trends Genet **8**, 97, 1992.
116. Chen, D., Zhao, M. and Mundy, G.R. Bone morphogenetic proteins. Growth factors (Chur, Switzerland) **22**, 233, 2004.
117. Wang, Y.X., Qian, L.X., Liu, D., Yao, L.L., Jiang, Q., Yu, Z., Gui, Y.H., Zhong, T.P. and Song, H.Y. Bone morphogenetic protein-2 acts upstream of myocyte-specific enhancer factor 2a to control embryonic cardiac contractility. Cardiovascular research **74**, 290, 2007.
118. Ghosh-Choudhury, N., Abboud, S.L., Mahimainathan, L., Chandrasekar, B. and Choudhury, G.G. Phosphatidylinositol 3-kinase regulates bone morphogenetic protein-2 (BMP-2)-induced myocyte enhancer factor 2A-dependent transcription of BMP-2 gene in cardiomyocyte precursor cells. J Biol Chem **278**, 21998, 2003.
119. Collas, P. and Hakelien, A.M. Teaching cells new tricks. Trends Biotechnol **21**, 354, 2003.
120. Pittenger, M.F., Mackay, A.M., Beck, S.C., Jaiswal, R.K., Douglas, R., Mosca, J.D., Moorman, M.A., Simonetti, D.W., Craig, S. and Marshak, D.R. Multilineage potential of adult human mesenchymal stem cells. Science (New York, N.Y **284**, 143, 1999.
121. Li, W.C., Yu, W.Y., Quinlan, J.M., Burke, Z.D. and Tosh, D. The molecular basis of transdifferentiation. Journal of cellular and molecular medicine **9**, 569, 2005.
122. Slack, J.M. and Tosh, D. Transdifferentiation and metaplasia--switching cell types. Curr Opin Genet Dev **11**, 581, 2001.
123. Harada, S. and Rodan, G.A. Control of osteoblast function and regulation of bone mass. Nature **423**, 349, 2003.
124. Hu, E., Tontonoz, P. and Spiegelman, B.M. Transdifferentiation of myoblasts by the adipogenic transcription factors PPAR gamma and C/EBP alpha. Proc Natl Acad Sci U S A **92**, 9856, 1995.
125. Ross, S.E., Hemati, N., Longo, K.A., Bennett, C.N., Lucas, P.C., Erickson, R.L. and MacDougald, O.A. Inhibition of adipogenesis by Wnt signaling. Science (New York, N.Y **289**, 950, 2000.
126. Nuttall, M.E., Patton, A.J., Olivera, D.L., Nadeau, D.P. and Gowen, M. Human trabecular bone cells are able to express both osteoblastic and adipocytic phenotype: implications for osteopenic disorders. J Bone Miner Res **13**, 371, 1998.
127. Farmer, S.R. Transcriptional control of adipocyte formation. Cell metabolism **4**, 263, 2006.
128. Rosen, E.D. and MacDougald, O.A. Adipocyte differentiation from the inside out. Nature reviews **7**, 885, 2006.
129. Ducy, P., Schinke, T. and Karsenty, G. The osteoblast: a sophisticated fibroblast under central surveillance. Science (New York, N.Y **289**, 1501, 2000.

130. Wagner, E.F. and Karsenty, G. Genetic control of skeletal development. Curr Opin Genet Dev **11**, 527, 2001.
131. Patrick, C.W. Breast tissue engineering. Annu Rev Biomed Eng **6**, 109, 2004.
132. Katz, A.J., Llull, R., Hedrick, M.H. and Futrell, J.W. Emerging approaches to the tissue engineering of fat. Clinics in plastic surgery **26**, 587, 1999.
133. Patrick, C.W., Jr. Tissue engineering strategies for adipose tissue repair. The Anatomical record **263**, 361, 2001.
134. Kang, X., Xie, Y. and Kniss, D.A. Adipose tissue model using three-dimensional cultivation of preadipocytes seeded onto fibrous polymer scaffolds. Tissue engineering **11**, 458, 2005.
135. Kopelman, P.G. Obesity as a medical problem. Nature **404**, 635, 2000.
136. Lian, J.B. and Stein, G.S. Concepts of osteoblast growth and differentiation: basis for modulation of bone cell development and tissue formation. Crit Rev Oral Biol Med **3**, 269, 1992.
137. Hall, B.K. and Miyake, T. Divide, accumulate, differentiate: cell condensation in skeletal development revisited. Int J Dev Biol **39**, 881, 1995.
138. Dunlop, L.L. and Hall, B.K. Relationships between cellular condensation, preosteoblast formation and epithelial-mesenchymal interactions in initiation of osteogenesis. Int J Dev Biol **39**, 357, 1995.
139. Srouji, S., Kizhner, T. and Livne, E. 3D scaffolds for bone marrow stem cell support in bone repair. Regenerative medicine **1**, 519, 2006.
140. Gimble, J.M., Zvonic, S., Floyd, Z.E., Kassem, M. and Nuttall, M.E. Playing with bone and fat. Journal of cellular biochemistry **98**, 251, 2006.
141. Rosen, C.J. and Bouxsein, M.L. Mechanisms of disease: is osteoporosis the obesity of bone? Nature clinical practice **2**, 35, 2006.
142. Burke, Z.D. and Tosh, D. Therapeutic potential of transdifferentiated cells. Clin Sci (Lond) **108**, 309, 2005.
143. Angel, P. and Karin, M. The role of Jun, Fos and the AP-1 complex in cell-proliferation and transformation. Biochimica et biophysica acta **1072**, 129, 1991.
144. Shaulian, E. and Karin, M. AP-1 in cell proliferation and survival. Oncogene **20**, 2390, 2001.
145. Jochum, W., Passegue, E. and Wagner, E.F. AP-1 in mouse development and tumorigenesis. Oncogene **20**, 2401, 2001.
146. Karsenty, G. The genetic transformation of bone biology. Genes & development **13**, 3037, 1999.
147. Grigoriadis, A.E., Schellander, K., Wang, Z.Q. and Wagner, E.F. Osteoblasts are target cells for transformation in c-fos transgenic mice. J Cell Biol **122**, 685, 1993.
148. McCabe, L.R., Banerjee, C., Kundu, R., Harrison, R.J., Dobner, P.R., Stein, J.L., Lian, J.B. and Stein, G.S. Developmental expression and activities of specific fos and jun proteins are functionally related to osteoblast maturation: role of Fra-2 and Jun D during differentiation. Endocrinology **137**, 4398, 1996.
149. Jochum, W., David, J.P., Elliott, C., Wutz, A., Plenk, H., Jr., Matsuo, K. and Wagner, E.F. Increased bone formation and osteosclerosis in mice overexpressing the transcription factor Fra-1. Nature medicine **6**, 980, 2000.

150. Wang, Z.Q., Liang, J., Schellander, K., Wagner, E.F. and Grigoriadis, A.E. c-fos-induced osteosarcoma formation in transgenic mice: cooperativity with c-jun and the role of endogenous c-fos. Cancer research **55**, 6244, 1995.
151. Johnson, R.S., Spiegelman, B.M. and Papaioannou, V. Pleiotropic effects of a null mutation in the c-fos proto-oncogene. Cell **71**, 577, 1992.
152. Wang, Z.Q., Ovitt, C., Grigoriadis, A.E., Mohle-Steinlein, U., Ruther, U. and Wagner, E.F. Bone and haematopoietic defects in mice lacking c-fos. Nature **360**, 741, 1992.
153. Gruda, M.C., van Amsterdam, J., Rizzo, C.A., Durham, S.K., Lira, S. and Bravo, R. Expression of FosB during mouse development: normal development of FosB knockout mice. Oncogene **12**, 2177, 1996.
154. Sabatakos, G., Sims, N.A., Chen, J., Aoki, K., Kelz, M.B., Amling, M., Bouali, Y., Mukhopadhyay, K., Ford, K., Nestler, E.J. and Baron, R. Overexpression of DeltaFosB transcription factor(s) increases bone formation and inhibits adipogenesis. Nature medicine **6**, 985, 2000.
155. Kveiborg, M., Sabatakos, G., Chiusaroli, R., Wu, M., Philbrick, W.M., Horne, W.C. and Baron, R. DeltaFosB induces osteosclerosis and decreases adipogenesis by two independent cell-autonomous mechanisms. Molecular and cellular biology **24**, 2820, 2004.
156. Mumberg, D., Lucibello, F.C., Schuermann, M. and Muller, R. Alternative splicing of fosB transcripts results in differentially expressed mRNAs encoding functionally antagonistic proteins. Genes & development **5**, 1212, 1991.
157. Nakabeppu, Y. and Nathans, D. A naturally occurring truncated form of FosB that inhibits Fos/Jun transcriptional activity. Cell **64**, 751, 1991.
158. Yen, J., Wisdom, R.M., Tratner, I. and Verma, I.M. An alternative spliced form of FosB is a negative regulator of transcriptional activation and transformation by Fos proteins. Proc Natl Acad Sci U S A **88**, 5077, 1991.
159. Chen, J., Kelz, M.B., Zeng, G., Sakai, N., Steffen, C., Shockett, P.E., Picciotto, M.R., Duman, R.S. and Nestler, E.J. Transgenic animals with inducible, targeted gene expression in brain. Molecular pharmacology **54**, 495, 1998.
160. Wurm, F.M. Production of recombinant protein therapeutics in cultivated mammalian cells. Nature biotechnology **22**, 1393, 2004.
161. Walsh, G. Biopharmaceutical benchmarks--2003. Nat Biotechnol **21**, 865, 2003.
162. Enders, J.F., Weller, T.H. and Robbins, F.C. Cultivation of Lansing strain of poliomyelitis virus in cultures of various human embryonic tissues Science, 109, 1949.
163. Kohler, G. and Milstein, C. Continuous cultures of fused cells secreting antibody of predefined specificity. Nature **256**, 495, 1975.
164. Hesse, F. and Wagner, R. Developments and improvements in the manufacturing of human therapeutics with mammalian cell cultures. Trends Biotechnol **18**, 173, 2000.
165. al-Rubeai, M., Emery, A.N., Chalder, S. and Jan, D.C. Specific monoclonal antibody productivity and the cell cycle-comparisons of batch, continuous and perfusion cultures. Cytotechnology **9**, 85, 1992.

166. Suzuki, E. and Ollis, D.F. Enhanced antibody production at slowed growth rates: experimental demonstration and a simple structured model. Biotechnology progress **6**, 231, 1990.
167. Carvalhal, A.V., Santos, S.S., Calado, J., Haury, M. and Carrondo, M.J. Cell growth arrest by nucleotides, nucleosides and bases as a tool for improved production of recombinant proteins. Biotechnology progress **19**, 69, 2003.
168. Fox, S.R., Patel, U.A., Yap, M.G. and Wang, D.I. Maximizing interferon-gamma production by Chinese hamster ovary cells through temperature shift optimization: experimental and modeling. Biotechnol Bioeng **85**, 177, 2004.
169. Geserick, C., Bonarius, H.P., Kongerslev, L., Hauser, H. and Mueller, P.P. Enhanced productivity during controlled proliferation of BHK cells in continuously perfused bioreactors. Biotechnol Bioeng **69**, 266, 2000.
170. Kaufmann, H., Mazur, X., Fussenegger, M. and Bailey, J.E. Influence of low temperature on productivity, proteome and protein phosphorylation of CHO cells. Biotechnol Bioeng **63**, 573, 1999.
171. Meents, H., Enenkel, B., Werner, R.G. and Fussenegger, M. p27Kip1-mediated controlled proliferation technology increases constitutive sICAM production in CHO-DUKX adapted for growth in suspension and serum-free media. Biotechnol Bioeng **79**, 619, 2002.
172. Mueller, P.P., Schlenke, P., Nimtz, M., Conradt, H.S. and Hauser, H. Recombinant glycoprotein product quality in proliferation-controlled BHK-21 cells. Biotechnol Bioeng **65**, 529, 1999.
173. Fussenegger, M. and Bailey, J.E. Molecular regulation of cell-cycle progression and apoptosis in mammalian cells: implications for biotechnology. Biotechnology progress **14**, 807, 1998.
174. Vaux, D.L. and Korsmeyer, S.J. Cell death in development. Cell **96**, 245, 1999.
175. Zakeri, Z. and Lockshin, R.A. Cell death during development. J Immunol Methods **265**, 3, 2002.
176. Daniel, T.O. and Abrahamson, D. Endothelial signal integration in vascular assembly. Annual review of physiology **62**, 649, 2000.

Contributions of this work

Chapter 1- Physiology of Artificial Microtissues

Electrical properties such as action potential amplitude, upstroke duration, signal propagation velocity, contraction frequency, and thus the contraction rhythm of cardiomyocytes and myocardial microtissues were characterized and detailed on CMOS-based high-density microelectrode arrays (HD-MEAs). Using gene delivery and gene regulation systems, cardiac electrophysiology was precisely controlled by genetic regulation of BMP-2 in cardiomyocytes cultured on HD-MEA. This enable the development of a model to perform electrophysiological studies of gene related electrical pathologies in real time. It also demonstrated that BMP-2 is involved in the restoration of cardiac electrical activity and rhythm, suggesting that it could be used as a therapeutic molecule for heart failure. Importantly, myocardial microtissues transgenic for BMP-2 that were transplanted onto a cardiomyocyte monolayer were capable of acting as a pacemaker-like device by controlling the contractility rate and strength of the whole cardiomyocyte layer.

Chapter 2- (Trans) Differentiation Capacity of Artificial Microtissues

Pre-adipocyte forming microtissues were differentiated into adipose-like microtissues, creating a model system to study adipose differentiation, adipose physiology and its related pathologies. Adipose-like microtissues more closely reproduced the *in vivo* architecture of adipose tissue compared to adipocytes cultured on 2D standard plates, particularly with respect to the formation of multilocular and unilocular lipid droplets. Adipose-like microtissues genetically engineered for ΔFosB overexpression “partially” de-differentiate into a Pref-1-expressing state while retaining adipocyte-specific Nile red staining and subsequently adopting a bone-like extracellular matrix, characterized by a hybrid tissue state where the three phenotypes were present. Such hybrid cell state has never been reported suggesting ΔFosB-transduced adipocytes forming microtissues do not need to completely de-differentiate into the precursor cell in order to transdifferentiate into bone-like cells. ΔFosB accelerated the transdifferentiation process by inhibiting adipogenesis and inducing osteogenesis. After one week of osteogenic induction, ΔFosB-transduced adipose-like microtissues decreased the number of lipid droplets, increased the tissue calcium concentration, up-regulated Cbfa1 and osteocalcin

genes, and enhanced osteocalcin protein expression. Transdifferentiated osteo-like microtissues showed higher collagen type I, hardness of tissue as evidenced by an increased number of bone nodules and initiation of ECM mineralization. It was also demonstrated that hanging drop technology is a suitable technology for osteoblasts cultivation and maturation as osteoblast-forming microtissues developed a bone-like ECM.

Chapter 3- Productivity of Artificial Microtissues

Three different cell-packing models were engineered and evaluated in order to estimate cell number per layer of artificial microtissues. Histological microtissue sections showed highly packed cells suggesting a Rhomododecahedron geometry as the closest model to calculate cell number per layer. This model was applied to estimate and compare protein productivity of cells cultured in monolayer and in microtissue. Higher heterologous protein productivity and reduced glucose consumption of cells embedded in a three-dimensional (3D) environment was demonstrated. Packaging cells (HEK-293T) forming microtissues also produced a higher number of viral particles, suggesting that 3D cultures could be used in the future for viral production. Moreover, cells-forming microtissues survived following serum removal and still maintained high productivity rates, both of which are advantageous for downstream protein purification strategies.

Chapter 1

Physiology of Artificial Microtissues

"Manipulation of Cardiomyocyte Electrical Properties by Regulated BMP-2 Expression"

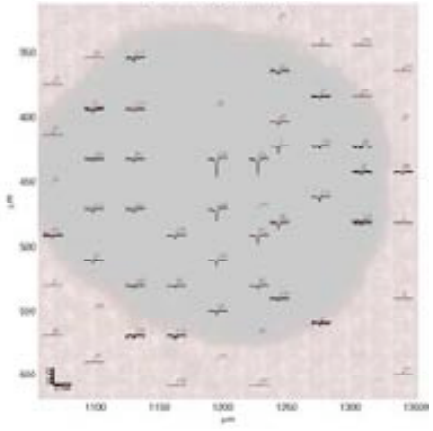

Abstract

Since cardiomyocytes lose their ability to divide after birth, any subsequent cell loss or dysfunction results in pathologic cardiac rhythm initiation or impulse conduction. Strategies to restore and control the electrophysiological activity of the heart may, therefore, have a great impact upon the regeneration of cardiac tissue functionality. Using lentivirus-derived particles to regulate the bone morphogenetic protein-2 (BMP-2) gene expression in a pristinamycin- or gaseous acetaldehyde-inducible manner, we demonstrated the adjustment of cardiomyocyte electrophysiological characteristics. CMOS-based high-density microelectrode arrays (HD-MEAs) were used to monitor the electrophysiological activity of neonatal rat cardiomyocytes (NRCs) cultured either as monolayers (NRCml) or as microtissues (NRCmt). Compared to NRCml, NRCmt more closely resembled heart tissue physiology and could be conveniently monitored using HD-MEAs due to their ability to detect low-signal events and to sub-select the region of interest; namely, areas where the microtissues were placed. Significantly, cardiomyocyte-forming microtissues, transduced with lentiviral vectors encoding BMP-2, were capable of restoring myocardial microtissue electrical activity. We also engineered NRCmt to functionally couple within a cardiomyocyte monolayer thus showing pacemaker-like activity upon local regulation of transgenic BMP-2 expression. The controlled expression of therapeutic transgenes represents a crucial advance for clinical interventions and gene-function analysis.

Introduction

Cardiomyocytes are responsible for heart contractions and are the dominant cell type in the normal heart with respect to volume. Irregularities in the heartbeat, due to cardiac electrical dysfunction, are one of the most frequent causes of mortality and morbidity in todays industrialized society [1]. An increasing number of cardiac electrical diseases have been related to dysfunctional ion channels, such as the long QT syndrome, and to defects in contractile proteins, structural proteins, or signaling molecules [2, 3]. These ion channelopathies or cardiac excitation-coupling disorders lead to cardiac arrhythmias and other cardiomyopathies [4, 5]. There is, accordingly, a compelling need to move clinical

studies toward cardiac regenerative strategies aimed at improving cardiac functionality [6-9]. This will require more complex *in vitro* models that enable the study and assessment of how potent therapeutic genes, related to heart functionality, impact cardiac electrophysiological irregularities [10].

Cardiomyocytes isolated from a neonatal heart adapt readily to culture plates and maintain an intact myofibrillar apparatus, as demonstrated by their beating [11]. Neonatal cardiomyocytes have therefore emerged as the preferred cell type because of their inherent structural, electrophysiological and contractile properties [12], which make them suitable for the study of contractile activities [13-15]. Despite global initiatives to foster advances in cardiomyocyte-related therapies, this cell type has turned out to be refractory to gene transfer technologies, particularly with regard to its terminally differentiated adult phenotype [16]. Based on the ability of pseudotyped lentiviral vectors to transduce a wide variety of cell types and tissues, including quiescent cells, transgenic lentiviral particles have become an attractive gene-transfer tool for cardiac cells [17-19]. Moreover, lentiviral vectors have been recently engineered to regulate transgene expression [20-22], thus providing a powerful tool for (i) functional genomic research [23], (ii) production of transgenes in animal models of human diseases [24], (iii) *in vivo* or *ex vivo* titration of pharmaceutical proteins within a therapeutic range [25-27], and (iv) rational reprogramming of the proliferation, differentiation, or apoptosis pathways to engineer specific cell/tissue phenotypes [20, 28-32]. Capitalizing on the potential of inducible viral transgene expression [33] and on recent advances in novel regulation systems [34], we selected two lentivirus-based gene-regulation systems to genetically manipulate neonatal cardiomyocytes: a streptogramin-responsive expression system [20, 35], in which addition of pristinamycin I switches off transgene expression (OFF system), and a gas-inducible expression system, in which the presence of administered gaseous acetaldehyde switches on transgene expression (ON system) [21, 36].

Controlling physiological changes in cell behavior at the single-cell level remains a major challenge. To this end, a cell embedded within a three-dimensional configuration/extracellular matrix (ECM) more closely reproduces its *in vivo* physiology than standard culture technologies (two-dimensional monolayer cultures) [37, 38]. Therefore, it was sought to validate gene transfer and its impact on myocardial microtissue

electrophysiology by using microtissues (NRCmt) in addition to conventional monolayer cultures (NRCml). To evaluate electrophysiological changes we made use of CMOS (complementary metal oxide semiconductor)-based high-density microelectrode arrays (HD-MEAs) [39-41], which provide a reconfigurable routing for an almost unrestricted set of 126 electrodes to record electrical changes of multicellular cardiac myocytes in real time.

In order to modulate cardiac electrogenic properties we selected the bone morphogenetic protein-2 (BMP-2) gene, which was originally identified as a molecule that induces bone and cartilage formation [42] but is today considered a multifunctional cytokine [43]. It was previously reported to induce myocyte shortening [44], and more recently suggested to control cardiac ventricular contractility upstream of MEF2A (myocyte-specific enhancer factor 2A) [45] via PI3K (phosphatidylinositol 3-kinase) [46, 47]. BMP-2 appears to operate at several temporal points. First, during embryogenesis and differentiation, it was shown that BMP-2 is essential for proper heart tissue formation [48-50]. Secondly, in the adult state, BMP-2 is involved in cardiac functionality [45] as well as in promoting cardiomyocyte survival [51, 52]. For these reasons expression control and a precise fine-tuning of BMP-2 expression could be a potential therapy to alleviate complications in cardiac development and dysfunctional contractility at different developmental stages of the heart.

To date, proof of electrophysiological control of cells through heterologous synthetic regulation systems is lacking. The model system described here may be useful for both basic and applied biological research of electrically active cells. In this case, modulation of cardiac electrogenic activity by regulated BMP-2 expression is demonstrated, which might represent an important therapeutic avenue in the future treatment of heart failure.

Material and methods

CMOS-based high-density microelectrode array (HD-MEA). The HD-MEA consists of 11,016 metal electrodes and 126 channels (Fig. 1A), each of which contains recording and stimulation electronics for bidirectional communication with electrogenic cells, as described by Frey *et al* [53]. Each HD-MEA-based device exhibits a total array area of 1.75x1.97 mm^2 and electrode openings of 8.2x5.8 μm^2 (Fig. 1B). The array was

fabricated in an industrial 0.6 µm CMOS-process that features three metal layers. The electrodes were fabricated in a two-mask post-processing step; Ti:W, as an adhesion promoter (20 nm), and platinum (200 nm), as the electrode material, were sputtered onto a wafer and patterned using a lift-off process. Then, a passivation layer stack, 1.6-µm thick, consisting of alternating SiO_2 and Si_3N_4 layers (1 µm of Si_3N_4 followed by two 100 nm SiO_2 / 200 nm Si_3N_4) was deposited by means of plasma-enhanced chemical vapor deposition (PECVD) to protect the array against corrosion. A glass ring was subsequently mounted and the bond wires encapsulated with epoxy resin (EPOTEK 302-3M). A platinum wire, which represents the counter/reference electrode, was inserted into the culture medium. The recorded cell signals, simultaneously obtained from up to 126 selected electrodes, were first high-pass filtered (0.3 Hz cut off) to remove large DC offsets and fluctuations of the electrode-solution interface; then amplified by a programmable-gain (amplification from 1 to 10,000 in 18 steps), low-pass filter (first to 15 kHz and then to 4 kHz); and digitized using an 8-bit AD converter with 20 KSamples/s per channel (Fig. 1B). All recordings were performed at 37°C for 20 seconds.

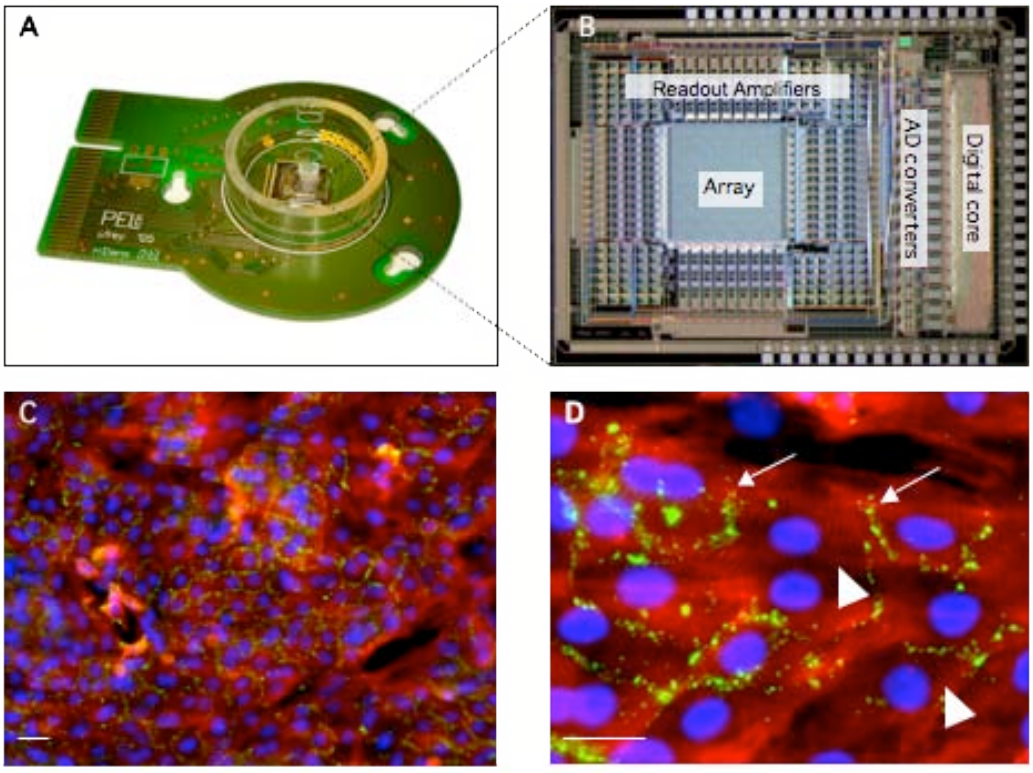

Figure 1. Neonatal rat cardiomyocytes (NRCs) cultured as monolayers (NRCml) on HD-MEAs. (A) Packaged HD-MEA device. (B) Overall HD-MEA micrograph. (C-D) NRCml cultured for a total of 10 days on the HD-MEA. Morphology of NRCml and electrical coupling were visualized by immunohistologic staining specific for sarcomeric α-actinin (red), 4'-6-diamidino-2-phenylindole (DAPI) (blue) and connexin 43 (green, arrows). Intercalated disks are also shown (arrow head). Scale bar 30 μm.

Isolation of neonatal rat cardiomyocytes and culture on HD-MEAs. Neonatal rat cardiomyocytes (NRCs) from both the left and the right ventricles were isolated from newborn rat hearts (Wistar rats; Elevage Janvier, Le Genest Saint Isle, France) by digestion with collagenase (Worthington Biochemical Corp., Freehold, NJ, USA) and pancreatin (Invitrogen, Carlsbad, CA, USA), followed by density gradient purification according to the protocol of Auerbach *et al* [54]. One thousand NRCs were seeded in 1-ml plating media (67% Dulbecco's modified Eagle medium [DMEM; Invitrogen], 17% M199 EBS [AMIMED, Allschwil, Switzerland], 10% horse serum [Cat. No. 16050-122, Lot. No. 336379, Invitrogen], 5% fetal bovine serum [FBS; Cat. No. 3302-P251110, Lot No. P251110, PAN biotech GmbH, Aidenbach, Germany], and 1% penicillin/streptomycin solution [Sigma, St. Louis, MO, USA]), and then placed onto a HD-MEA that had been previously incubated with 20 μg/ml laminin (Sigma) for 2 hours at 37°C. HD-MEA containing cells were cultivated at 37°C in a humidified atmosphere containing 5% CO_2 for up to 10 days. Four hundred thousand freshly isolated cardiomyocytes, seeded in plating media and cultured on tissue culture plates (35 × 10 mm) previously coated with collagen (Sigma) were used as culture controls.

Design, production and transduction of lentiviral particles. pCD10 (5'LTR-ψ^+-ori$_{SV40}$-cPPT-RRE-P$_{PIR8}$-BMP-2-HAtag-3'LTR$_{\Delta U3}$) was constructed by *Eco*RI/*Mlu*I excision of human BMP-2HAtag from pBP253 [30] followed by cloning into identically digested pBM94 [20] (5'LTR-ψ^+-ori$_{SV40}$-cPPT-RRE-P$_{PIR8}$-EYFP-3'LTR$_{\Delta U3}$). pCD20 (5'LTR-ψ^+-ori$_{SV40}$-cPPT-RRE-P$_{AIR}$-BMP-2-HAtag-3'LTR$_{\Delta U3}$) was constructed by *Eco*RI/*Pme*I excision of human BMP-2HAtag from pBP253 [30] followed by cloning into identically digested pSH16 (unpublished) (5'LTR-ψ^+-ori$_{SV40}$-cPPT-RRE-P$_{AIR}$-SEAP-3'LTR$_{\Delta U3}$). pCD22 (5'LTR-ψ^+-ori$_{SV40}$-cPPT-RRE-P$_{hEF1\alpha}$-alcR-3'LTR$_{\Delta U3}$) was constructed by *Eco*RI/*Mlu*I excision of *alcR* from pWW195 [36] followed by cloning into identically digested pBM07 [18] (5'LTR-ψ^+-ori$_{SV40}$-cPPT-RRE-P$_{hEF1\alpha}$-MCS-3'LTR$_{\Delta U3}$).

To produce replication-incompetent, self-inactivating lentiviral particles a mixture containing (i) 0.25 M $CaCl_2$ (Acros Organics), (ii) 1 μg pLTR-G, encoding the pseudotyping envelope protein VSV-G of the vesicular stomatitis virus, (iii) 1 μg of the helper construct pCD/NL-BH*, and (iv) 2 μg of the gene of interest (GOI)-encoding lentiviral expression vector, within a total volume of 100 μl was added drop wise into 100 μl 2x HEPES-buffered saline (HBS, 280 mM NaCl; 100 mM HEPES 1.5 mM Na_2HPO_4; pH 7.1) solution, incubated for 15 minutes, and transfected into 4×10^5 human embryonic kidney cells (HEK-293T), previously seeded into a single well of a 6-well plate. Prior to transfection, 2 μl of a 25-mM chloroquine solution (Bode Chemie, Hamburg, Germany) was added to the cell culture medium. Six hours after transfection the medium was changed; lentiviral particle production continued for another 36 hours prior to filtration-based harvesting of the lentiviral particles from the culture supernatant (0.45 μm pore size FP 030/2 filter; Schleicher & Schuell, Dassel, Germany). Quantification of lentiviral particle titer was determined as described elsewhere [55] but using neonatal rat cardiomyocytes for titration. The following lentivector preparations were used: (i) pMF365 (5'LTR-ψ^+-ori_{SV40}-cPPT-RRE-$P_{hEF1\alpha}$-YFP-3'$LTR_{\Delta U3}$) [18] (virus titer: 1.6×10^4 TU/ml), (ii) pBP253 (5'LTR-ψ^+-ori_{SV40}-cPPT-RRE-$P_{hEF1\alpha}$-BMP-2-HAtag-3'$LTR_{\Delta U3}$) [29] (virus titer: 5.7×10^3 TU/ml), (iii) pMF392 (5'LTR-ψ^+-ori_{SV40}-cPPT-RRE-$P_{hEF1\alpha}$-PIT-3'$LTR_{\Delta U3}$) [20] (virus titer: 2.3×10^3 TU/ml), (iv) pCD10 (virus titer: 1.3×10^4 TU/ml), (v) pCD22 (virus titer: 1.2×10^4 TU/ml) and (vi) pCD20 (virus titer: 8×10^3 TU/ml).

Twenty-four hours after seeding NRCs onto HD-MEAs, the media was exchanged and cells transduced with 5×10^3 TU of total lentiviral-particle-containing supernatant, supplemented with pristinamycin I (PI) or acetaldehyde (AcAl) where indicated. Two-days post-transduction, fresh plating media was added, and the NRCs were again exposed to PI or AcAl, as required, for at least 24 hours (total of four days in culture) before measuring cell electrophysiological properties. PI was added directly to the culture media, while AcAl liquid was added to an airtight polypropylene box, previously balanced for CO_2 at 37°C and, containing NRCs cultured on HD-MEAs, in which gaseous AcAl could diffuse into the culture media [21, 36]. As a control, non-

transduced NRCs (negative control, NC) were cultured for four days prior to electrical recordings, which corresponded to their spontaneous beating activity. Electrogenic signals from NRCs cultured as monoloyers (NRCml) were recorded for up to one week.

Microtissue production. In order to enable gravity-enforced microtissue production in hanging drops [56], freshly isolated monodispersed NRCs were seeded at 2,500 cells/well (1×10^5 cells/ml) into 60-well plates (Microtest-Platten Terasaki, Cat. No. 635161, Greiner Bio-One GmbH, Frickenhausen, Germany) and cultivated with plating media for four days. For large-scale microtissue production in hanging drops, 96-well IMPACT plates (Greiner Bio-One Inc.USA) were handled by a novel custom-designed robotic assembly module, which precisely and automatically turned loaded cell culture plates upside down. This assembly module consists of (i) a turning system, which comprises a Servomotor with a Servodrive (Minimotor SA, Croglio, Switzerland) programmed for soft start and soft stop and (ii) standard SERVOmotors (Miniatur-Servo Ultra, Topmodel, Oberkirch, Switzerland) as plate holders. The assembly module was incorporated into a fully automatic multi-pipette robot (Xiril AG, Switzerland). After four days, NRC microtissues (NRCmt) in hanging drops (25 μl) were transduced with 2.5×10^2 TU of lentiviral particle-containing supernatant and incubated with 2 μg/ml PI or 1.8 mg/l AcAl as required. Two days post-transduction, transduced and non-transduced NRCmt were harvested and placed into 96 × 16 mm suspension tissue culture flasks (Cat. No. 622180, Greiner Bio-One GmbH) containing fresh plating media. Subsequently, they were seeded onto a HD-MEA previously coated with 20 μg/ml laminin. Within two hours, myocardial microtissues attached to the array surface and after six hours electrogenic recordings were performed.

Western Blot. Prior to resolution on a 10% (wt/vol) SDS-PAGE gel, the cell culture media was denaturated by boiling for five minutes in loading buffer (10% glycerol, 50 mM Tris-HCl, 1 % SDS and 0.005% bromophenol blue). Proteins were then blotted onto polyvinylidene difluoride (PVDF) membranes (Millipore, Bedford, MA, USA), which were subsequently blocked using 5% non-fat powdered milk and probed with specific primary antibodies (HAtag-probe: rabbit polyclonal, Cat. No. sc-805, Lot No. 2405, Santa Cruz Biotechnology Inc., Santa Cruz, CA, USA; Tubulin-α Ab-2: mouse monoclonal, Cat. No. MS-581-P1, Neomarkers, Fremont, CA) followed by the

appropriate horseradish peroxidase-coupled secondary antibodies (Cat. No. NA934V (anti-rabbit) or NA931V (anti-mouse), Amersham Bioscience, Otelfingen, Switzerland). Visualization was performed using an ECL detection kit (Cat. No. RPN 2132, Amersham Bioscience) and a ChemieLux imager (Intas Science Imaging Instruments GmbH, Göttingen, Germany).

Immunofluorescence microscopy. NRCml seeded on HD-MEAs were washed twice in phosphate-buffered saline solution (PBS; 150 mM NaCl, 6.5 mM Na_2HPO_4 x 2 H_2O, 2.7 mM KCl, 1.5 mM KH_2PO_4, pH 7.4; Sigma Chemicals), fixed at room temperature (RT) for 30 min. in PBS containing 2% paraformaldehyde (PFA, Sigma Chemicals), washed three times for 5 min. in PBS, and permeated for 10 min. in PBS containing 0.2% Triton X-100. Primary antibodies, specific for desired proteins, as well as fluorescence-labeled secondary antibodies were diluted in 1% BSA-containing Tris-buffered saline (TBS, 20 mM Tris base, 155 mM NaCl, 2 mM EGTA, 2 mM $MgCl_2$) and sequentially incubated for 1 hr. at RT. Finally, the NRCml on the HD-MEAs were washed in PBS and embedded on Tris-buffered glycerol (a 3:7 mixture of 0.1 M Tris-HCl (pH 9.5) and glycerol supplemented with 50 mg/ml n-propyl-gallat). Immunofluorescence-based analysis of NRCmt was performed as described elsewhere [57]. Briefly, NRCmt were fixed at RT for 1 hr. in PBS containing 4% PFA, washed three times in PBS and then made permeable by incubation for 1 hr. in PBS containing 0.5% Triton X-100. Primary antibodies as well as fluorescence-labeled secondary antibodies were diluted in 1% BSA-containing TBS and sequentially incubated for 12 hr. at 4°C. NRCml plated on HD-MEAs as well as NRCmt required specific antibodies for sarcomeric-α-actinin (mouse monoclonal, clone EA53, Sigma Chemicals) and connexin 43 (rabbit polyclonal, sc-9059, Santa Cruz Biotechnology, Inc.), and staining with Cy3-coupled secondary anti-mouse antibodies (Jackson Immunochemicals, West Grove, PA, USA) and Cy2-coupled anti-rabbit antibodies (Jackson Immunochemicals). All samples were co-stained with 4',6-diamidino-2-phenylindole (DAPI; Molecular Probes Inc., Eugene, OR, USA) for nuclear localization.

Confocal imaging was performed with a fluorescence microscope equipped with oil immersion objectives (40×/63×) and a confocal scanner (Zeiss LSM 510; Carl Zeiss AG, Feldbach, Switzerland) with a two-photon laser featuring a chameleon, argon, and

helium-neon laser. Images were obtained with a BP 565-615 filter for Cy3 dye or BP 490-520 filter for Cy2 fluorescence. A BP 390-465 filter was used for DAPI detection. Image acquisition was performed by multitracking the different filters with data processed by Zeiss LSM software and a 3D multichannel image processor (Bitplane, AG, Zurich, Switzerland (Messerli et al. 1993)). Fluorescent micrographs from NRCml on HD-MEAs were obtained using an upright microscope (DM IL, Leica Microsystems AG, Glattbrugg, Switzerland) equipped with a digital camera (DC300FX, Leica Microsystems), and filters for Cy2, Cy3, and UV light (Leica Microsystems). Fluorescent images from tissue culture plates were taken using a Leica AF6000 system equipped with a DMI 6000B microscope and a DFC350 FX digital camera (Leica Microsystems). Videos were taken by standard Leica light microscopy (Leica DMIL, Leica Microsystems) and a digital camera (Canon, Power shot S50).

Drugs. The following drugs were used. Phenylephrine hydrochloride (PE, 10^{-2}mM) and isoproterenol hydrochloride (ISO, 0.1μM) were obtained from Sigma. Lidocain (LID, 20μM) was produced by Streuli (G. Streuli & Co. AG, Uznach, Switzerland) and 4-aminopyridine (4AP, 5mM) by Fluka-Chemie AG (Buchs, Switzerland). The pristinamycin I antibiotic Pyostacin® (PI, Lot. No. 27404) was purchased from Sanofi-Aventis (Sanofi-Aventis Inc., Paris, France) and acetaldehyde from Acros Organics (Cat. No. 149510010, Acros Organics, Geel, Belgium).

Data analysis. Data analysis was performed using MATLAB software (2007a, MathWorks, Natick, MA). The digitized data was further high pass filtered at 10 Hz. RMS noise was estimated as described in Quiroga 2004 [58]. Nonviable channels, such as channels providing values at the rails, were discarded. Events were detected using a threshold set to 4.5 times the RMS noise level. Events were up sampled to 100 kHz and then aligned with regard to the center between the first positive peak (maximum) and the following negative peak (minimum). Where the first positive peak was missing, the events were aligned with regard to the negative peak. As an accurate timestamp is pivotal in determining wave propagation characteristics, the timestamps were obtained in the following way: an overall spike shape template was calculated as the average of all aligned events. The peak of the normalized cross-correlation between the events and the template was then used as a timestamp, which was less sensitive to noise and showed

improved accuracy over the peak-based timestamp described above. Next waves (bursts) were detected if the inter spike interval (ISI) fell below a threshold based on total activity and at least 25% of all viable channels participated in the wave.

Four parameters were then used: two parameters characterizing the culture (frequency and propagation velocity) and two describing the signal shape (signal amplitude and upstroke duration). The frequency was taken as one over the mean inter burst interval (IBI), which represents the rhythm of the culture (Fig. 2A). Rhythm variability corresponds to the coefficient of variation of the IBI. The propagation velocity was averaged over all bursts within one recording (an example of one burst in Fig. 2B) and calculated in the following way: a two–dimensional map of the time difference between the first event within a burst and the subsequent events on each channel was generated and then interpolated using a regular grid. A contour plot of such a map is shown in Figure 2C. The propagation velocity was then determined from the mean gradient of this map. Signal amplitude and upstroke duration were calculated from the signal shape averaged over all channels and all detected events, as shown in Figure 2DE. The signal amplitude was taken as the difference between the maximum and the minimum of the averaged signal value. The upstroke duration was taken as the time difference between those two values.

Statistical analysis. Statistical significance was assessed by one-way analysis of variance (ANOVA) followed by a Tukey post hoc test (Software: Systat 12 for Windows). Data are presented as means ± standard deviation (SD) and $p < 0.05$ was considered significant. The SD represent the variation of the mean values obtained from separate HD-MEA with cells cultured under the same conditions to obtain an estimate for the reproducibility of culture-to-culture and HD-MEA-to-HD-MEA variability.

Results

HD-MEA-based electrophysiological analysis of neonatal rat cardiomyocytes.

To monitor the electrophysiological properties of cardiomyocytes and to characterize HD-MEA-based electrophysiological results, we used NRCml placed on HD-MEAs (Fig. 1AB). NRCml were positive for sarcomeric α-actinin and connexin 43 which is required for electrical coupling between the cells (Fig. 1CD). A typical HD-

MEA-based electrogram plot, generated during the spontaneous rhythm of contracting NRCml for four days in plating media, demonstrated tight temporal coupling over the culture at a frequency of 1.4±0.05 Hz (Fig. 2A) as can be seen at http://mf-229-serv.ethz.ch/fussi_download/carlota/NRCml_wt.mpg. As HD-MEAs simultaneously record extracellular potentials (field potentials) from 126 electrodes, it is possible to generate activation maps that show the direction of the excitation spread and propagation velocity (322±8 mm/s) within the cultures (Fig. 2C). Figure 2D shows the average signal shape per channel aligned in time. As described by Halbach *et. al.* the action potential (AP) parameters can be estimated from the field potential (FP) [59]. Based on these parameters, the average peak-to-peak amplitude was determined at 2.8±1.3 mV (Fig. 2E). A similar correlation was obtained by Spach *et. al.* [60], where the duration of the AP upstroke (depolarization time) matched the time from maximum to minimum peak, which here corresponds to 0.35±0.05 ms (Fig. 2E). Hence, AP upstroke voltage gradient can be calculated as 8 V/s. Although electrogenic signals, recorded by extracellular electrodes, rely on local changes in the membrane potential of individual cardiomyocytes, the observed signal is modulated by the electrically coupled neighboring cells, so that local field potentials are recorded [59, 61].

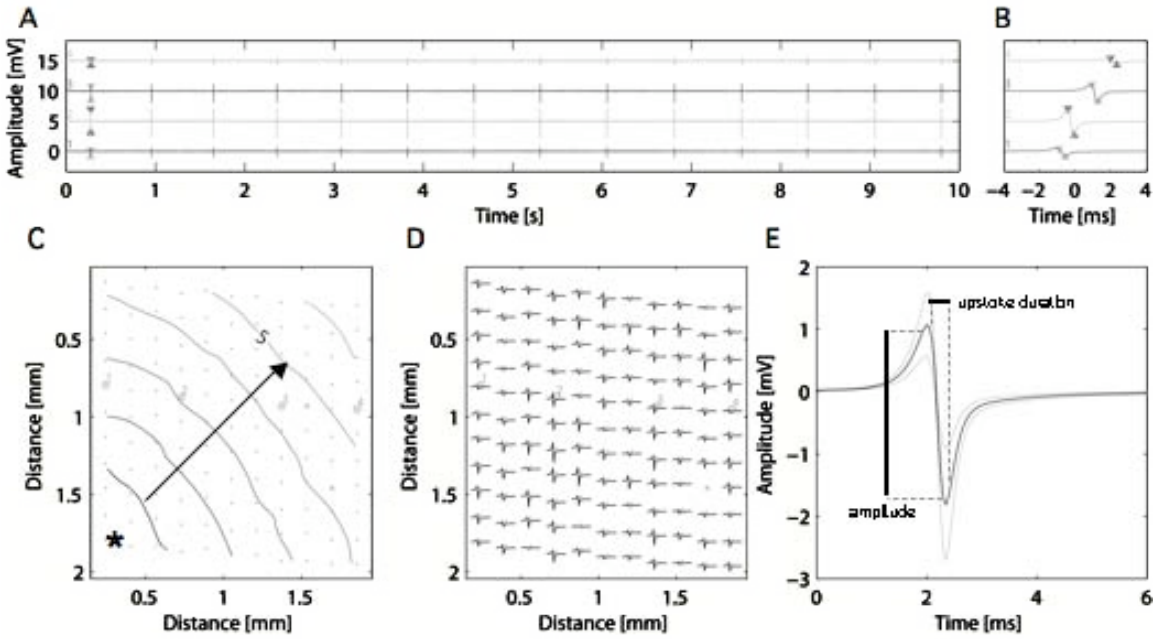

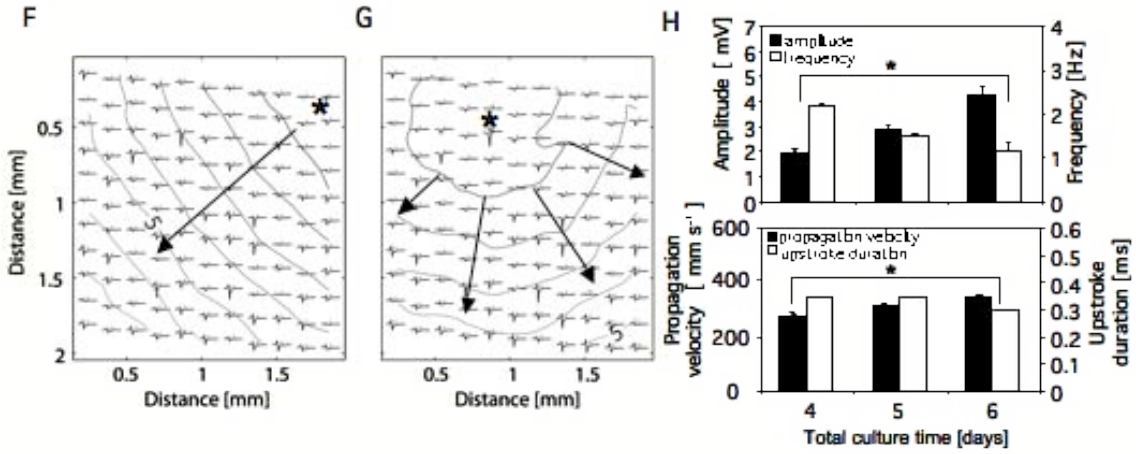

Figure 2. Electrogenic recordings of NRCml cultured for 5 days on HD-MEAs. (A) Long signal trace showing the synchronized contraction frequency and the field potential amplitude of NRCml for 10 seconds and (B) zoom-in of one burst. (C) Propagation pattern of an electrical wave showing the electrical activation origin (asterisk), the direction of the wave (arrow), and the location of the 126 electrodes (dots). The contour lines are in milliseconds. The location of the four channels shown in (A-B) is marked on (C). (D) Detailed activation map illustrating the average signal shape of the 126 electrodes for 10 seconds. (E) Average signal shape over all 126 channels. (F-G) Propagation pattern and average signal shape of an electrical wave showing the different electrical activation origins (asterisk) and the direction of the waves (arrows). (H) Electrophysiological properties of wild-type NRCml over time. In this case the error bars represent the average from different recordings on one HD-MEA; * $p<0.01$.

Figures 2F and 2G show activation maps of the same batch of cells recorded at a 10 min intervall and reveal different propagation patterns and excitation origins. While the origin of excitation shows an action potential with an exclusive negative peak (asterisk in Fig. 2G), action potentials in which a negative peak is preceded by a positive one indicate previously excited cells. After four days in culture, NRCml started spontaneous beating. The average of the electrogenic signals recorded over the culture period is plotted and shown in Fig. 2H. An increase in the amplitude of the electrical signal and in the velocity of the wave propagation was monitored ($p< 0.01$), indicating that membrane depolarization rises over time (Fig. 2H).

In order to evaluate the reliability of recorded signals from HD-MEAs, we applied standard stimulators of the α- and β-adrenergic signaling cascade (phenylephrine and isoprenaline) and cardioactive drugs (lidocain and 4-aminopyridine). Although the

responsiveness of cardiomyocytes to adrenergic drugs, such as adrenalin is controversial, they are known to increase the strength of cardiac contraction and heart rate [62]. When 10 μM phenylephrine (PE), an α1-adrenergic drug, was added to NRCml cultured on HD-MEA-based devices, a 2.5-fold increase in the beating frequency (positive chronotropic effect) was monitored 10 minutes after addition ($p< 0.01$). This effect was temporary and lost after 30 minutes in culture (Fig. 3A). Furthermore, upstroke duration increased ($p< 0.01$), which could be attributed to the inhibition of a variety of K^+ currents [63, 64]. In contrast to PE, 10 nM isoprenaline (ISO), a β-adrenergic drug responsible for cAMP responses [65], enhanced the signal propagation velocity up to 2-fold, thus decreasing the upstroke duration ($p< 0.01$, Fig. 3B). The field potential amplitude increased up to 2.5-fold (positive inotropic effect) and beating frequency up to 2-fold($p< 0.01$). Application of the Na^+ channel blocker, lidocain (21 μM) [66]led to a 7-fold decrease in field potential amplitude (negative inotropic effect), a 4-fold reduction in propagation velocity, and an increase up to nine times in upstroke duration after two hours in culture ($p< 0.01$, Fig. 3C). After adding 5mM 4-aminopyridine, an unselective blocker of voltage-dependent K^+ channels [67], the upstroke duration was nine times longer and contractility was enhanced after 10 minutes in culture ($p< 0.01$, Fig. 3D). These data suggest that HD-MEA-based analysis could be used to quantify specific electrophysiological effecs of some drugs and genes.

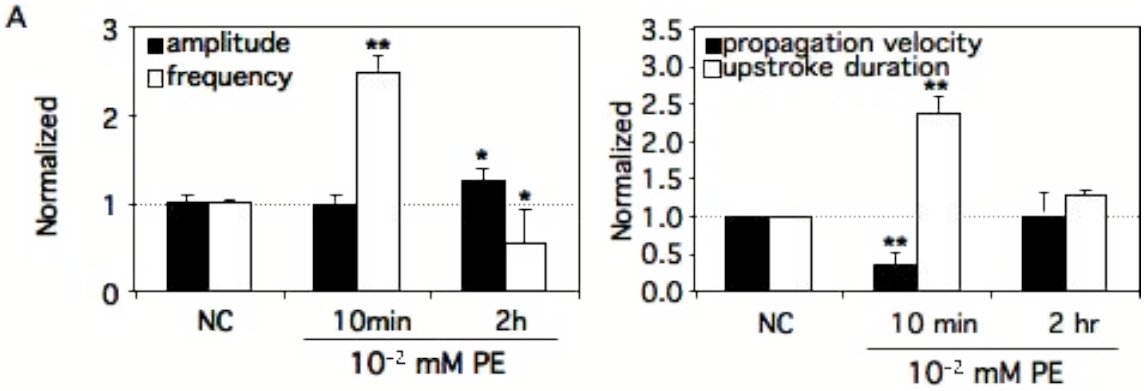

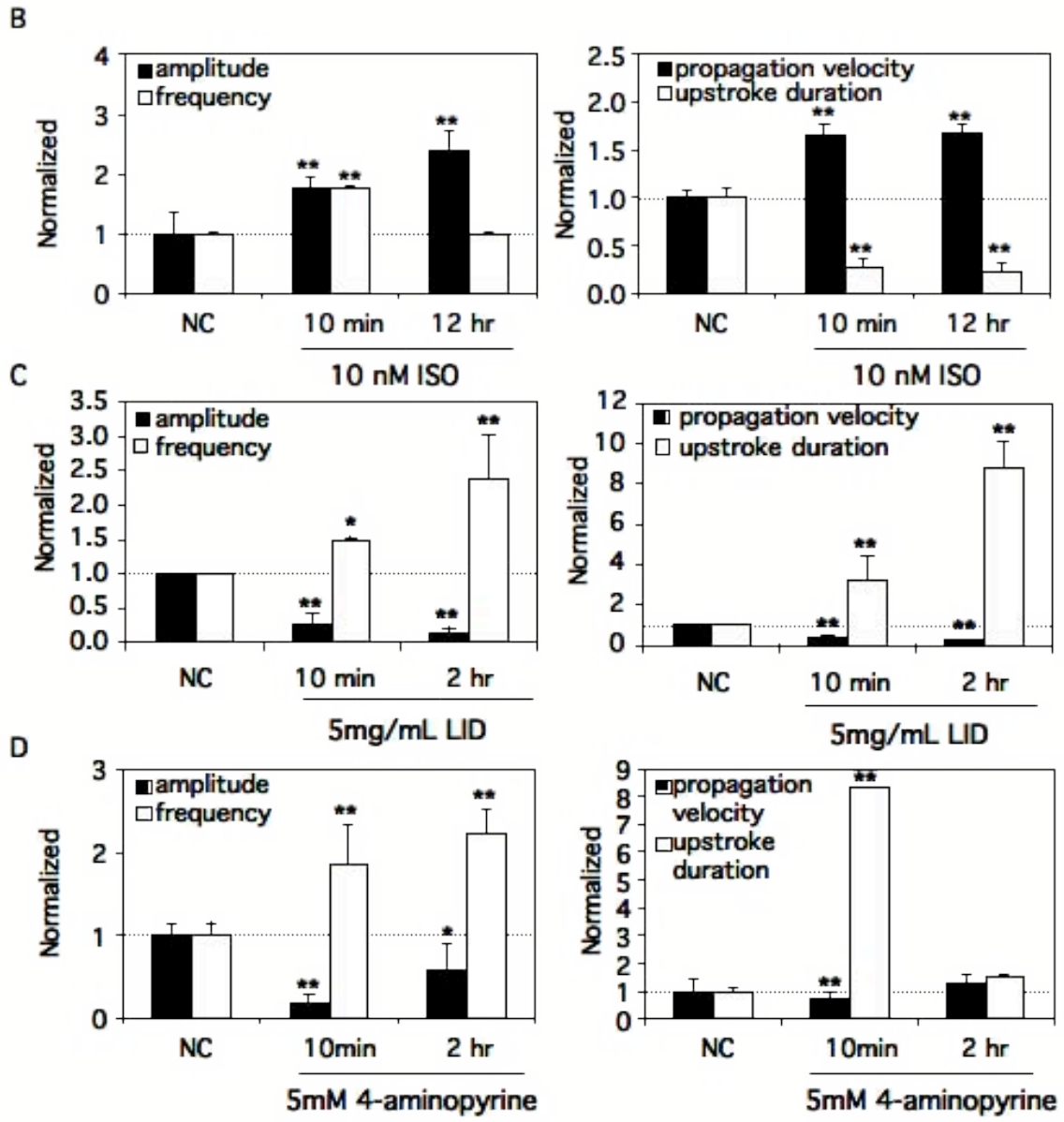

Figure 3. Electrophysiological reaction of wild-type NRCml (negative control, NC) incubated with (A) phenylephrine (PE, α1-adrenergic agonist), (B) isoprenaline (ISO, β-adrenergic agonist), (C) lidocain (LID, blocker of Na+ channels), and (D) 4-aminopyridine (blocker of the K+ channels) for 10 minutes and two hours. Error bars represent the average from three independent measurements (HD-MEA-to-HD-MEA and NRC batch variability). Statistically significant differences relative to NC are denoted by *p<0.05 and ** p<0.01.

Modulation of neonatal rat cardiomyocyte electrophysiology by genetic manipulation

Capitalizing on the ability of HD-MEAs to characterize cardiac electrical signals we modulated cardiac electrophysiology and validated this system for gene/cell therapeutic applications. Therefore, freshly isolated cardiomyocytes were seeded on HD-MEAs and transduced with third-generation self-inactivating lentiviral particles encoding either the enhanced yellow fluorescence protein (EYFP) under a constitutive promoter (P_{hCMV}; human immediate early cytomegalovirus promoter) (pMF365; 5'LTR-ψ^+-ori_{SV40}-cPPT-RRE-P_{hCMV}-EYFP-3'$LTR_{\Delta U3}$ [18]) or the bone morphogenetic protein-2 (BMP-2) driven by: (i) a strong constitutive human elongation factor 1α promoter ($P_{hEF1\alpha}$) (pBP253; 5'LTR-ψ^+-ori_{SV40}-cPPT-RRE-$P_{hEF1\alpha}$-BMP-2-HAtag-3'$LTR_{\Delta U3}$ [30]), (ii) an optimized streptogramin-responsive promoter (P_{PIR8}; [68]) (pCD10; 5'LTR-ψ^+-ori_{SV40}-cPPT-RRE-P_{PIR8}-BMP-2-HAtag-3'$LTR_{\Delta U3}$), or (iii) an acetaldehyde-adjustable promoter (P_{AIR}; [36]) (pCD20; 5'LTR-ψ^+-ori_{SV40}-cPPT-RRE-P_{AIR}-BMP-2-HAtag-3'$LTR_{\Delta U3}$) (Fig. 4A). Lentiviral transduction efficiency was assessed on NRCml by lentiviral particles encoding EYFP three days after transduction (Fig. 4B). Lentiviral particles were able to transduce cardiomyocytes (positive for sarcomeric α-actinin) (Fig. 4B). Two days post-transduction, BMP-2 expression in transduced NRCml was demonstrated by Western blot analysis (Fig. 4C). Negative controls are represented by non-transduced NRCml (NC, Fig. 4C). NRCml, co-transduced with (i) pMF392- (encoding constitutive streptogramin-dependent transactivator [PIT] expression) and pCD10-derived lentiviral particles (Fig. 4A) or (ii) pCD22- (encoding constitutive acetaldehyde-dependent transactivator [AlcR] expression), and pCD20-derived lentiviral particles (Fig. 4A) showed regulation of BMP-2 expression following two days of cultivation in media supplemented with (i) pristinamycin I (PI) (Fig. 4D) or (ii) acetaldehyde (AcAl) (Fig. 4E), respectively.

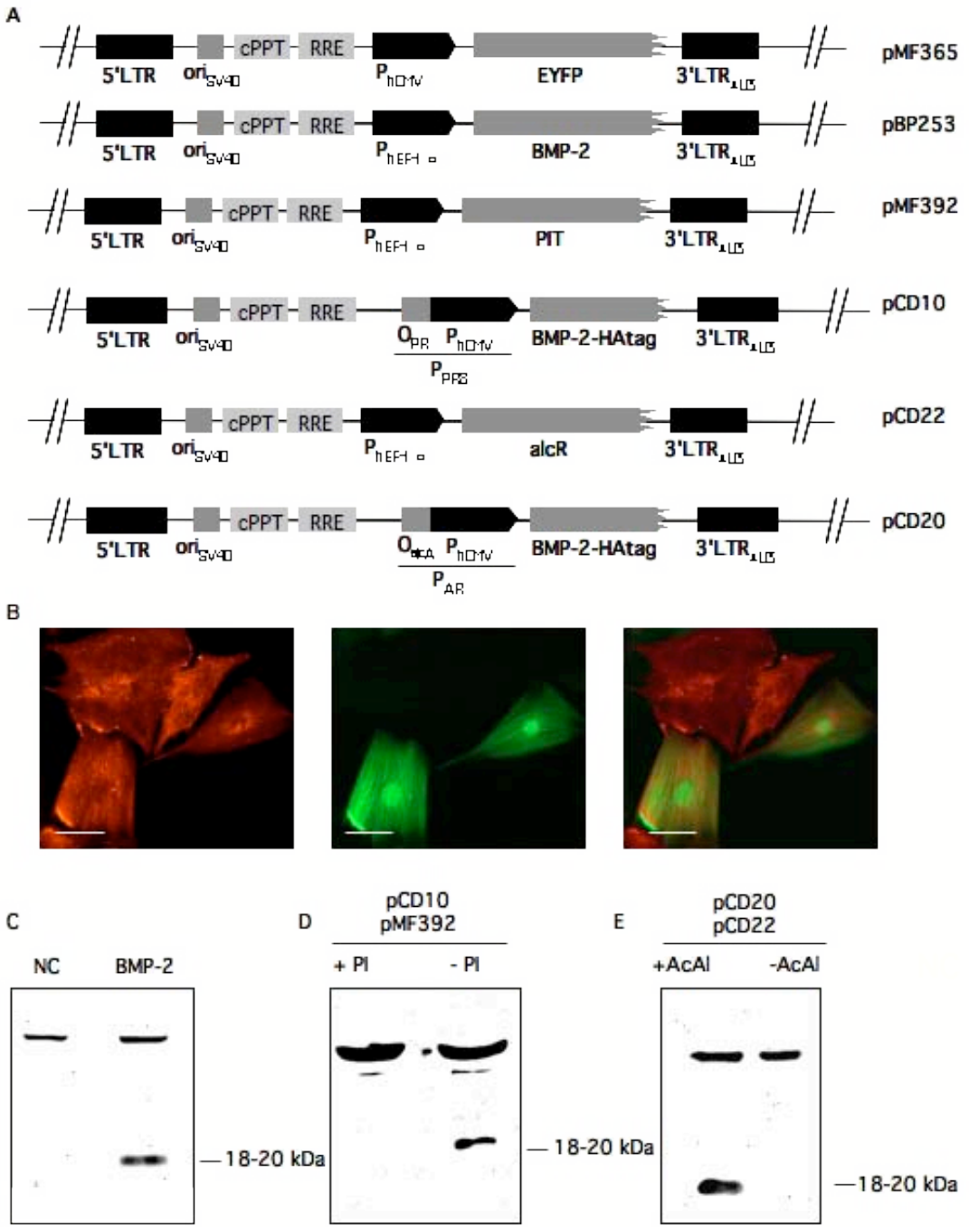

Figure 4. (A) Schematic diagram of pMF365-, pBP253-, pMF392-, pCD10-, pCD20 and pCD22-derived lentiviral vectors encoding EYFP under the human immediate early cytomegalovirus promoter (P_{hCMV}), BMP-2 driven by a strong constitutive human elongation factor 1α promoter ($P_{hEF1\alpha}$), PIT and alcR driven by $P_{hEF1\alpha}$, BMP-2 under streptogramin-responsive promoter (P_{PIR8}) and BMP-2 under control of the acetaldehyde-inducible promoter (P_{AIR}). (B) Immunofluorescence of NRCml transduced with pMF365-derived lentiviral particles. (C-E) Western blot analysis of culture supernatants from (C) native, non-transduced NRCml (negative control, NC) or NRCml transduced with pBP253-, (D) pCD10- and pMF392-,

(E) pCD20- and pCD22-(co)transduced lentiviral particles and cultivated in the presence or absence of 2 μg/ml pristinamycin I (PI) (D) or 1.8 μg/ml acetaldehyde (AcAl) (E). As endogenous control, Tubulin-α is shown at 55kDa. Scale bar 5 μm.

After BMP-2 was expressed for 24 hours in NRCml, a higher contraction frequency and a lower action potential amplitude were recorded and confirmed using HD-MEA (Fig. 5A). The activation map showed a clear decrease in the signal propagation velocity when BMP-2 was expressed and the upstroke duration increased in the presence of BMP-2 (Fig. 5A). In order to compare and quantify electrophysiological changes during BMP-2 expression, the average value measured of three independent cultures was normalized to that of a control HD-MEA containing non-transduced NRCml as negative control (NC). NRCml were recorded under equivalent conditions. Whereas contraction frequency was up-regulated 4-fold in BMP-2-transduced NRCml, peak-to-peak amplitude was down-regulated 6-fold ($p< 0.01$, Fig. 5B). Rhythm variability decreased in the presence of BMP-2 (NC; 25%, BMP-2; 8%). In addition, the signal propagation velocity was 3.5 times lower and the upstroke duration 12 times higher. EYFP-transduced cells showed no significant differences in basal contractility, suggesting that the electrophysiological changes were not due to transfection with the lentiviral particles (Fig. 5B). Moreover, BMP-2-transduced cells responded to the α-adrenergic stimulus of PE, thus leading to a three-fold increase in beating frequency and up to a 5-fold increase compared to PE alone ($p< 0.01$, Fig. 5B). Electrophysiological characteristics over time were also monitored in order to evaluate the durability of the BMP-2-electrogenic effect (Fig. 5C). These results showed that an enhanced frequency and a reduced propagation velocity were maintained for up to five days. Importantly, after 48 hours of BMP-2 expression, peak-to-peak amplitude and upstroke duration returned to the values measured in non-transduced NRCml used as negative controls (NC) (Fig. 5C). This resulted in a slight reduction in the beating frequency and an increase in the velocity of signal propagation, which is comparable with the electrophysiological properties of non-transduced NRCml used as negative controls (Fig. 2E). After one week of BMP-2 expression, and a total of 10 days in culture, NRCml started to detach from the array surface, and recordings were stopped (Fig. 5C).

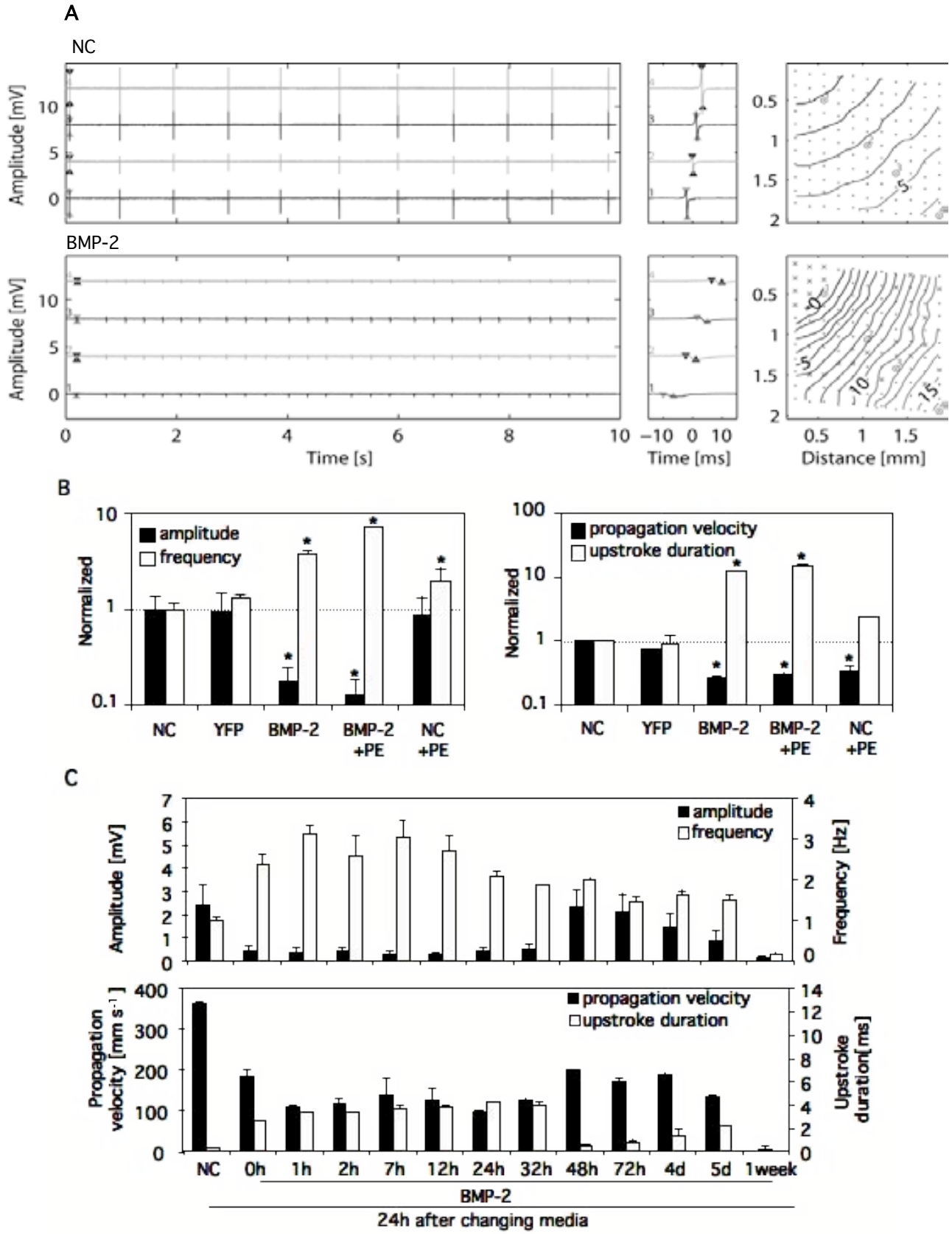
A
NC
BMP-2
Amplitude [mV]
Time [s]
Time [ms]
Distance [mm]
B
amplitude
frequency
Normalized
propagation velocity
upstroke duration
NC
YFP
BMP-2
BMP-2 +PE
NC +PE
C
amplitude
frequency
Amplitude [mV]
Frequency [Hz]
propagation velocity
upstroke duration
Propagation velocity [mm s-1]
Upstroke duration[ms]
NC
0h
1h
2h
7h
12h
24h
32h
48h
72h
4d
5d
1week
BMP-2
24h after changing media

Figure 5. Electrophysiological characterization of genetically engineered NRCml for constitutive BMP-2 expression. (A) Long signal traces and wave propagation maps for wild-type (NC) and NRCml transduced with pBP253-derived lentiviral particles (BMP-2). (B) Plots of the field potential amplitude, frequency, signal propagation velocity and upstroke duration of NRCml transduced with pMF365-(YFP) or pBP253-(BMP-2) derived lentiviral particles. The data were normalized to non-transduced NRCml used as negative control (NC). The y-axis is plotted on a logarithmic scale in order to visualize all values. (C) Plots showing the electrophysiological characteristics of cardiomyocytes constitutively expressing BMP-2 for 24 hr (0 hr) over time. Y-axes showing the recorded absolute values. Error bars represent the average of three independent measurements (HD-MEA-to-HD-MEA and NRC batch variability). Statistically significant differences relative to NC are denoted by * $p<0.01$.

We next assessed the ability of (i) an antibiotic (pristinamycin I [PI]; streptogramin-responsive expression system) and (ii) a gas (acetaldehyde [AcAl]; acetaldehyde-responsive expression system) regulation system to modulate the expression of BMP-2 and thus to control cardiac electrophysiology. Co-transduction of pCD10- and pMF392-derived lentiviral particles in NRCml cultivated under PI-free conditions exhibited a 3-fold increase in frequency compared to non-transduced NRCml used as negative control (NC) ($p< 0.01$, Fig. 6AB). Signal amplitude, signal propagation velocity, and upstroke duration under PI-free conditions showed equivalent variations as with constitutively expressed BMP-2 ($p< 0.01$, Fig. 6A). Co-transduced NRCml, cultivated in the presence of 2 μg/ml PI, reproduced basal electrogenic profiles, while PI did not show a significant electrogenic effect when added to wild-type cardiomyocytes (NC) (Fig. 6A). This demonstrated the complete repression of the BMP-2 electrophysiological effect in the presence of PI (Fig. 6AB). Streptogramin-responsive BMP-2 expression could also be titrated to induce the desired levels of cardiac electrical activity by defined PI dosing (Fig. 6AB). Moreover, rhythm variability increased when BMP-2 expression was switched off (0 μg/ml; 1.6%, 0.5 μg/ml: 12% and 2 μg/ml; 48%).

A

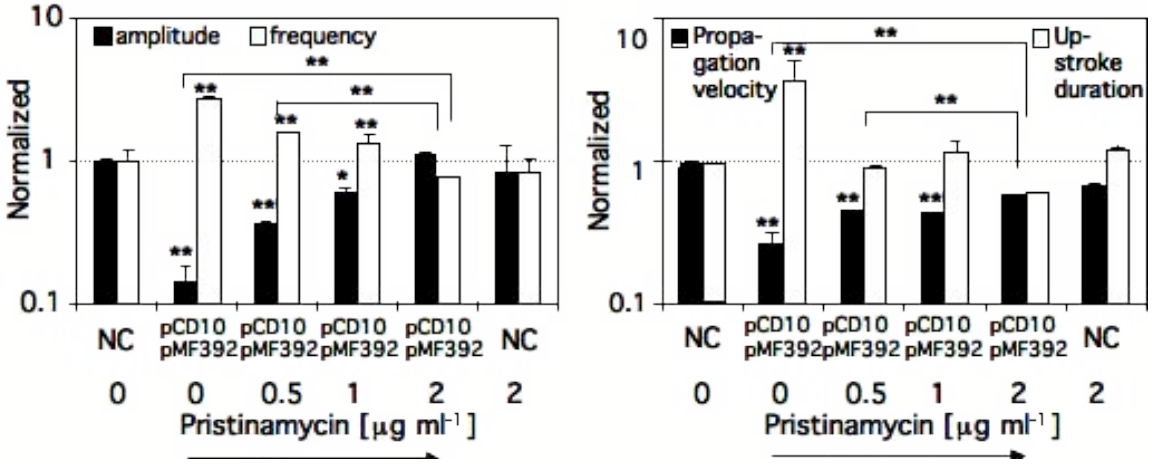

B

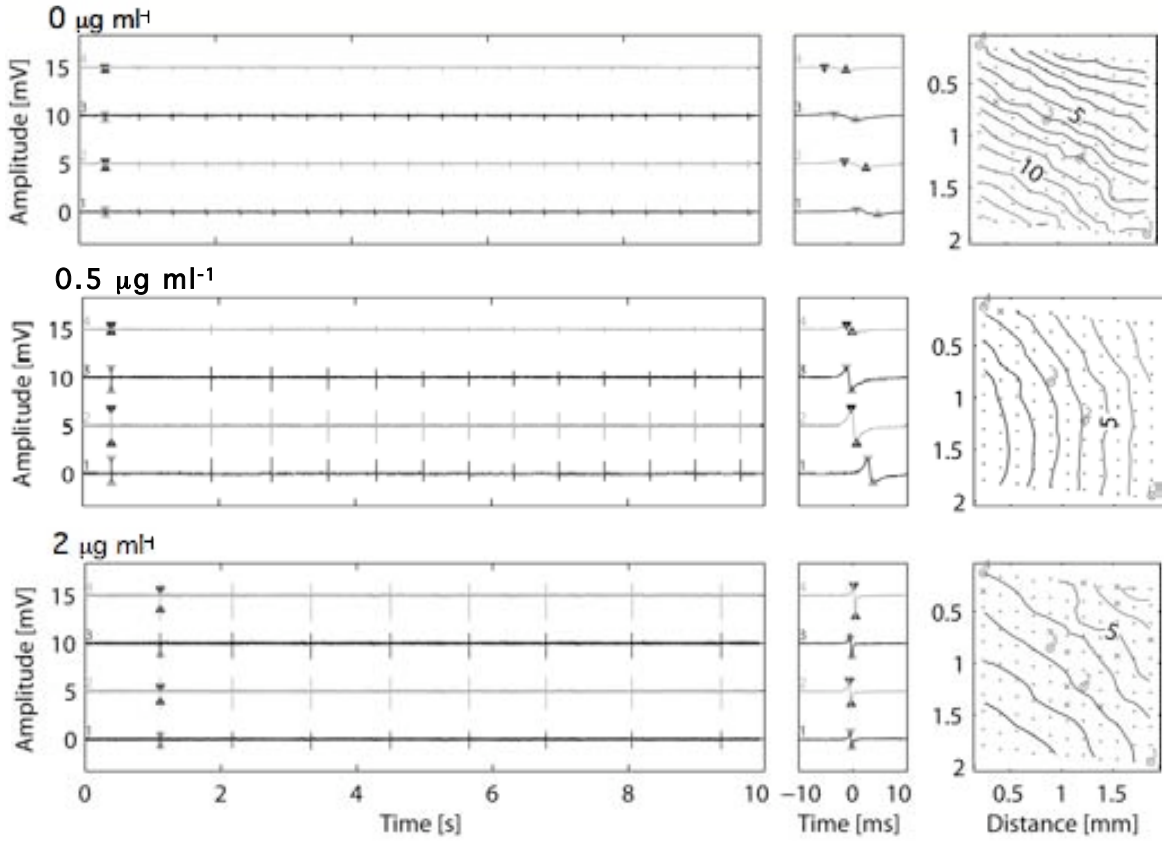

Figure 6. Electrophysiological characterization of genetically engineered NRCml for streptogramin-inducible BMP-2 expression. (A) Plots showing adjustable electrophysiological properties of NRCml co-transduced with pCD10- and pMF392-derived lentiviral particles and incubated in medium supplemented with indicated pristinamycin I concentrations. Values normalized to native NRCml used as negative control (NC). The y-axis is plotted on a logarithmic scale in order to visualize all values. (B) Long signal traces and wave propagation maps of NRCml co-transduced with pCD10- and pMF392-derived lentiviral particles and cultured in media supplemented without PI (0 µg/ml) or with 0.5 or 2 µg/ml PI. Error bars represent the average from three independent measurements (HD-MEA-to-HD-MEA and NRC batch variability). Statistically significant differences relative to NC and between groups are denoted by $p<0.05$ (*) or $p<0.01$ (**).

The gas-inducible system was also able to control cardiac electrophysiology by regulated BMP-2 expression fine-tuned by different AcAI doses. The beating frequency increased 4-fold, when the cells were exposed to 1.8 mg/l (5 ppm) of AcAl for 48 hours, while the beating amplitude decreased 2.3-fold compared to non-induced cells (0 ppm) ($p< 0.01$, Fig. 7AB). The rhythm variability was also decreased in the presence of BMP-2

(0 ppm; 8%, 5ppm; 0.3%). NRCml, co-transduced with pCD20- and pCD22-derived lentiviral particles in an AcAl-free atmosphere, and also cultivated in airtight polypropylene boxes for 48 hours, showed electrogenic patterns similar to those of non-transduced NRCml used as negative control (NC; Fig. 7A). Native NRCml exposed to 5 ppm acetaldehyde did not show any relevant electrogenic effects. Signal propagation velocity and, hence, upstroke duration changed insignificantly after acetaldehyde-induced BMP-2 expression (Fig. 7A) compared to PI-induced BMP-2 expression (see Figs. 5 and 6).. To evaluate this, we analyzed the electrogenic influence of 5 ppm AcAl in NRCml constitutively expressing BMP-2. In this case, signal propagation velocity did not decrease as previously shown in Fig. 5, suggesting that AcAl might by itself maintain high propagation velocities (Fig. 7A).

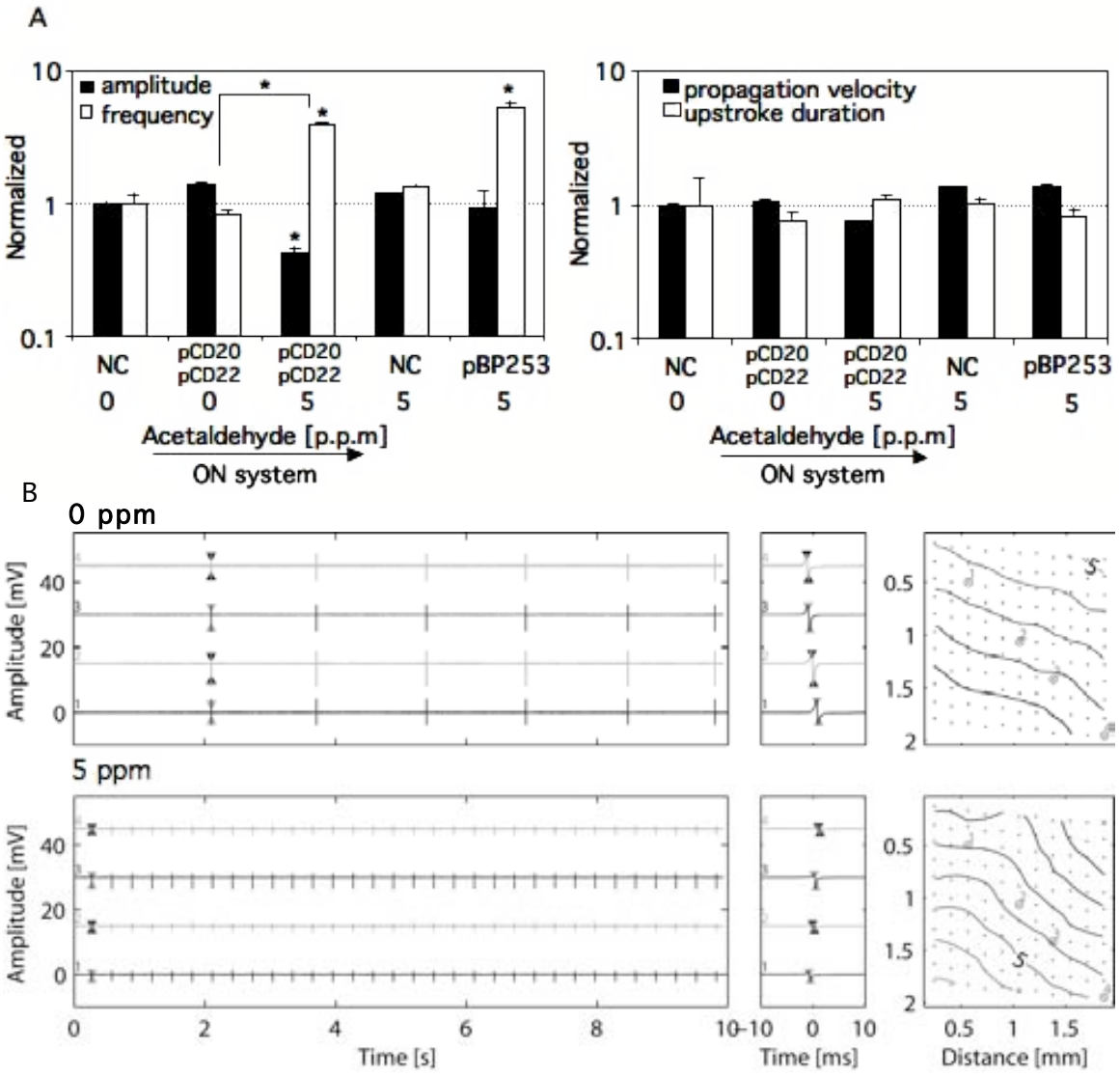

Figure 7. Electrophysiological characterization of NRCml engineered for acetaldehyde-inducible BMP-2 expression. (A) Plots representing the regulable electrophysiological properties of NRCml co-transduced with pCD20- and pCD22-derived lentiviral particles and incubated in the absence (0 ppm) or presence (5 ppm) of acetaldehyde. Values normalized to non-transduced NRCml used as negative control (NC). The y-axis is plotted on a logarithmic scale in order to visualize all values. (B) Long signal traces and wave propagation maps of NRCml co-transduced with pCD20- and pCD22-derived lentiviral particles and cultivated in the absence (0 ppm) or presence (5 ppm) of acetaldehyde. Error bars represent the average from three independent measurements (HD-MEA-to-HD-MEA and NRC batch variability). Statistically significant differences relative to NC and between groups are denoted by $p<0.01$ (*).

Electrophysiological regulation of cardiac-like microtissue

Although thus far we have used monolayer cultures as *in vitro* models to characterize the electrophysiology of cardiomyocytes, this culture type does not precisely replicate an *in vivo* structure. Previous experiments demonstrated that monodisperse cardiomyocytes, self-assembled in hanging drops, preserved their cardiomyocyte-specific cell phenotype, intramicrotissue superstructures, and extracellular matrix [69]. In this study we used myocardial microtissues (NRCmt) to monitor the electrophysiology of cardiac-like tissues and the BMP-2 cardiogenic effect in the whole tissue. For future high-throughput drug/gene screening applications using 3D cultures, we scaled up NRCmt production using a novel robotic microtissue assembly module enabling serial formation of scaffold-free microtissues. Four-day old NRCmt were cultured in plating media supplemented with PE on HD-MEAs, previously coated with laminin. After five minutes, NRCmt started rhythmic contraction as can be seen on the video http://mf-229-serv.ethz.ch/fussi_download/carlota/NRCmt_PE.mpg, and after six hours the beating frequencies reached 100±40 bpm (beatings per minute) (Fig 8A). NRCmt did not initiate contraction or rhythmic beats in the absence of hormonal stimuli. Field potential signal shape was represented by one negative peak (negative voltage), suggesting that the origin of excitation was close to the recorded area (Fig. 8B). Such electrogenic signals enabled us to plot the two-dimensional wave propagation of cardiac microtissues (Fig. 8C). Activation maps show the location and the field potential shape of electrically active cells that were integrated into a three-dimensional cardiac extracellular matrix (Fig. 8D). Along with the synchronized beating, the activation maps confirmed electrophysiological coupling among the cardiomyocytes embedded in an artificial microtissue structure,

which correlates with the high number of gap junctions visualized by confocal microscopy (Fig. 8E). In order to validate the effect of known cardiogenic hormones/drugs on NRCmt, we first added 10^{-2} mM PE and one hour after we applied (i) ISO or (ii) LID for 10 minutes. We analyzed contraction frequency and signal propagation velocity from different NRCmt. Field potential amplitude and upstroke duration were not considered due to the variability in the adherence of the microtissues to the array surface, which directly influences the electrical potential values. Addition of 10 nM ISO increased the beating frequency of the microtissue and enhanced signal propagation velocity throughout the tissue ($p< 0.01$, Fig. 8F). In contrast, application of 5 mg/ml LID decreased field potential propagation velocity ($p< 0.05$, Fig. 8G). This demonstrated that 3D cultures reproduced the drug-induced effect, and that corresponding changes in electrical activity could be assessed using HD-MEAs.

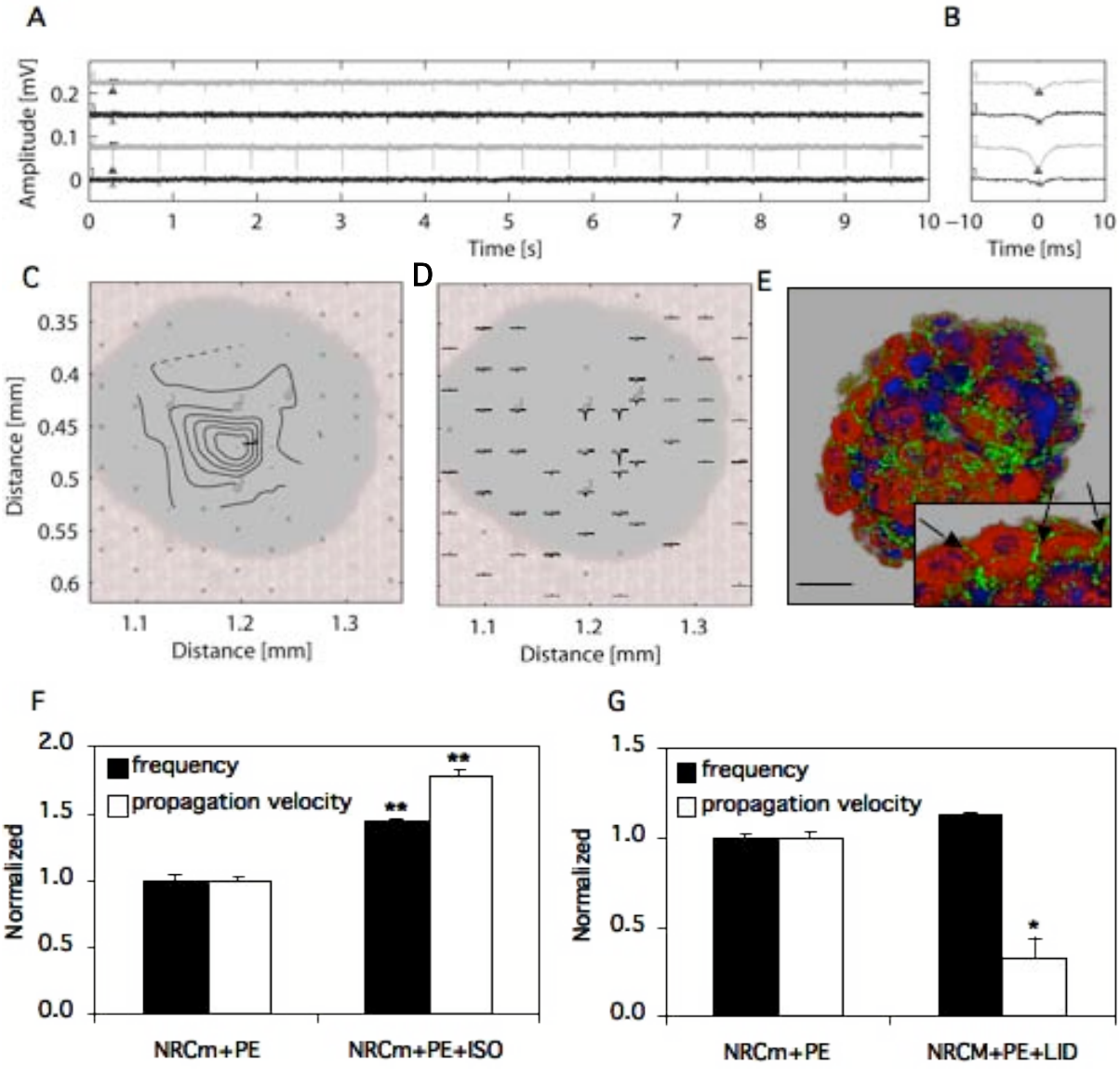

Figure 8. Electrophysiological characterization of neonatal rat cardiomyocyte-forming microtissues (NRCmt). (A) Long signal traces showing synchronized beating frequency and the field potential amplitude recorded from different electrodes located under the NRCmt. (B) Zoom-in into a wave. (C) Propagation pattern of an electrical wave within the NRCmt. The contour lines are in 0.2 milliseconds. (D) Average signal shape of each electrode adjacent to the NRCmt. (E) Immunofluorescence-based characterization of 5-day old NRCmt. Morphology and electrical coupling within the NRCmt was visualized by immunohistologic staining specific for sarcomeric α-actinin (red), 4'-6-diamidino-2-phenylindole (DAPI) (blue) and connexin 43 (green, arrows). Scale bar 50 μm. (F-G) Electrophysiological reaction of NRCmt cultured in media supplemented with 10^{-2} M phenylephrine (PE) and incubated for 10 minutes with (F) 10 nM isoprenaline (ISO) or (G) 5 mg/ml lidocain (LID). Error bars represent the average from a minimum of three independent measurements (NRCmt-to-NRCmt variability). Statistically significant differences relative to NRCm+PE are denoted by *p<0.05 and ** p<0.01.

To examine BMP-2 activity, 4-day old cardiomyocyte forming microtissues were transduced with (i) pBP253-derived lentiviral particles or co-transduced with (ii) pCD10- and pMF392- or (iii) pCD20- and pCD22-derived lentiviral particles in the presence or absence of PI or AcAl, respectively. Two days post-transduction, engineered cells were found at the periphery of the microtissues as previously shown by Kelm, et al. [69] (Fig. 9A). Therefore, transgenic cardiomyocytes, located at the periphery and producing BMP-2 modulate the spontaneous activity of the entire microtissue, as shown in the video http://mf-229-serv.ethz.ch/fussi_download/carlota/NRCmt_BMP-2.AVI. Such electrical activity, in the absence of hormonal stimulus, could be recorded by HD-MEAs showing a beating frequency of 60±12 bpm (Fig. 9B). Signal propagation throughout the BMP-2-transduced NRCmt was also monitored (Fig. 9B). Transduced NRCmt expressing BMP-2 (pBP253, -PI or +AcAl) showed frequency rates of approximately 60±20 bpm and signal propagation velocities of 40±20 mm/s. However, in the absence of BMP-2 (NC, + PI or -AcAl) NRCmt did not initiate contraction and therefore was undetectable by HD-MEA (Fig. 9C).

A

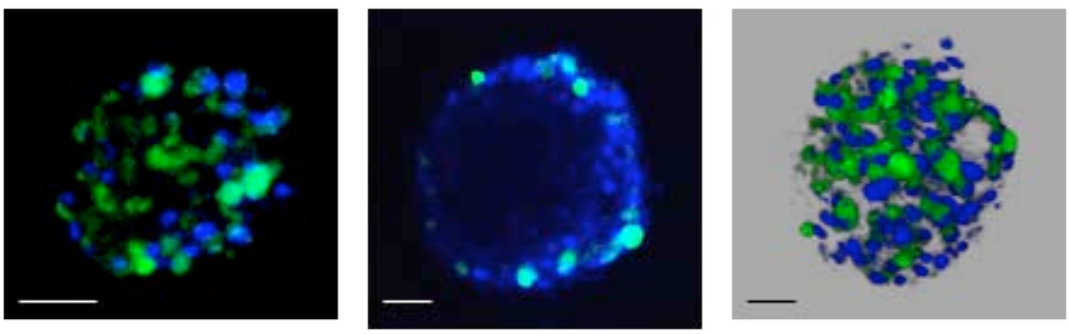

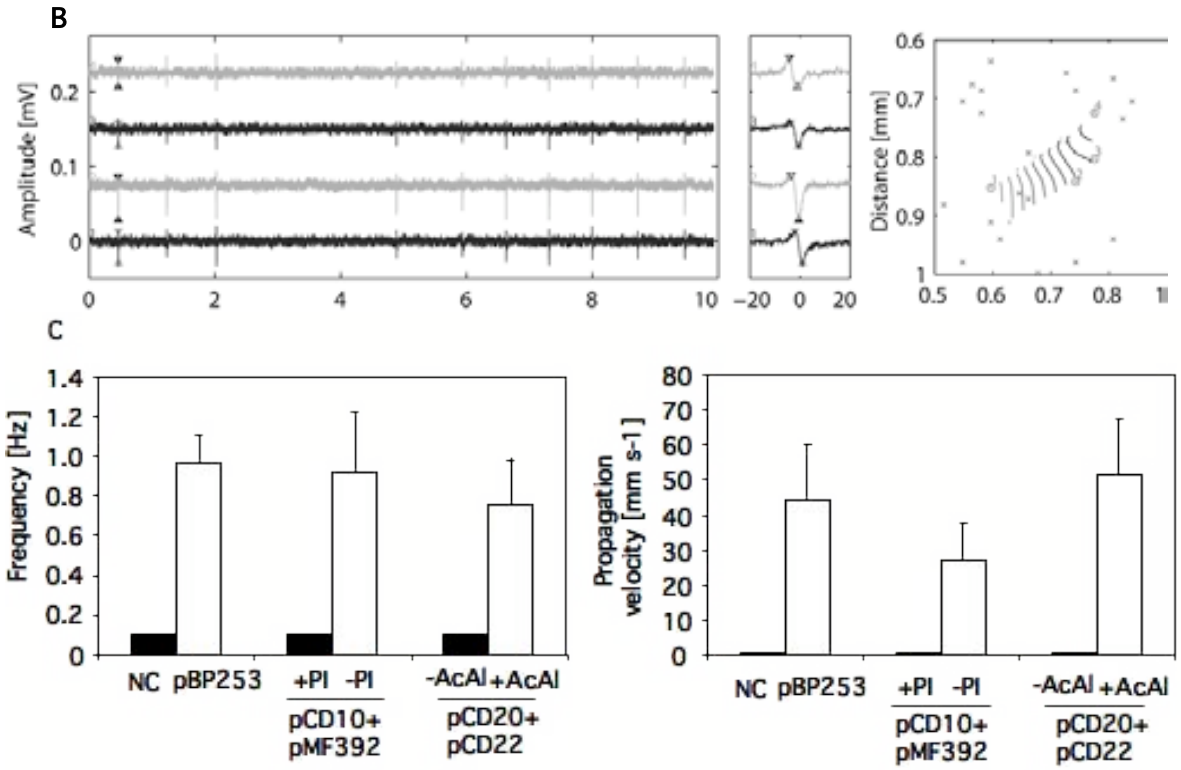

Figure 9. Electrophysiological characterization of genetically engineered NRCmt for BMP-2 expression. (A) Confocal fluorescence micrographs of NRCmt with EYFP-encoding pMF365-derived lentiviral particles. The left panel shows YFP expressing cells at the top of the microtissue, middle panel at the midpoint of the microtissue and right panel overlay of all confocal sections. Scale bar 50 μm. (B) Long signal traces and wave propagation maps of NRCmt transduced with pBP253-derived lentiviral particles transgenic for constitutive BMP-2-expression. Each contour line represents 0.2 milliseconds. (C) Contractility rate (frequency) and signal propagation velocity of non-transduced 6-day old NRCmt used as negative control (NC) or 4-day old NRCmt transduced for two days with pBP253-, pCD10- and pMF392- or pCD20- and pCD22-derived lentiviral particles. Error bars represent the average from a minimum of three independent measurements (NRCmt-to-NRCmt variability).

Pacemaker-like activity of myocardial microtissues

In order to spatially and genetically control the spontaneous electrical activity of a multicellular layer of cardiomyocytes, we adopted an *in vitro* transplantation model to analyze the electrophysiology of microtissue implants. 4-day old NRCmt transduced with pCD10- and pMF392-derived lentiviral particles were transplanted onto a NRCml, which had a stable beating frequency of 80±10 bpm. After six hours, a synchronous rhythmic

beating of transgenic NRCmt and NRCml was observed, as shown http://mf-229-serv.ethz.ch/fussi_download/carlota/NRCmt_NRCml.mpg. Immunostaining of the gap junction protein connexin 43 showed connexin-mediated coupling between the NRCml and the NRCmt (Fig. 10AB). Indeed, extracellular field potentials, recorded by the HD-MEAs, revealed a coordinated pattern of electrical activity (Fig. 10C). Implantation of myocardial microtissues transgenic for streptogramin-responsive BMP-2 expression doubled the beating frequency of NRCml, thus decreasing the average amplitudes when PI was absent ($p< 0.01$, Fig. 10DE). The field potential propagation velocity diminished, while upstroke duration was twice as long as that of the non-cocultured NRCml ($p< 0.01$, Fig. 10DE), demonstrating that transgenic BMP-2 microtissues influenced the electrophysiological characteristics of the NRCml. Moreover, when PI was present the electrophysiological modulation was restored to control conditions (NRCml, Fig. 10DE).

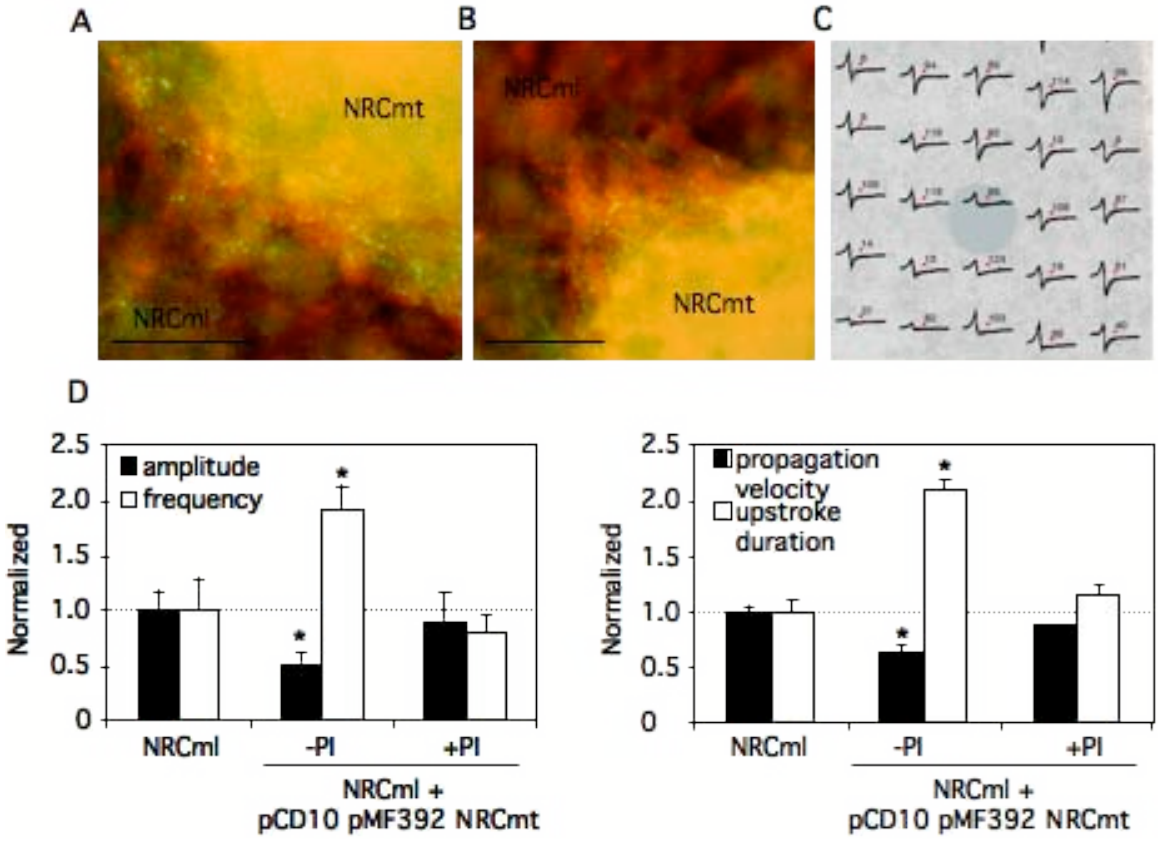

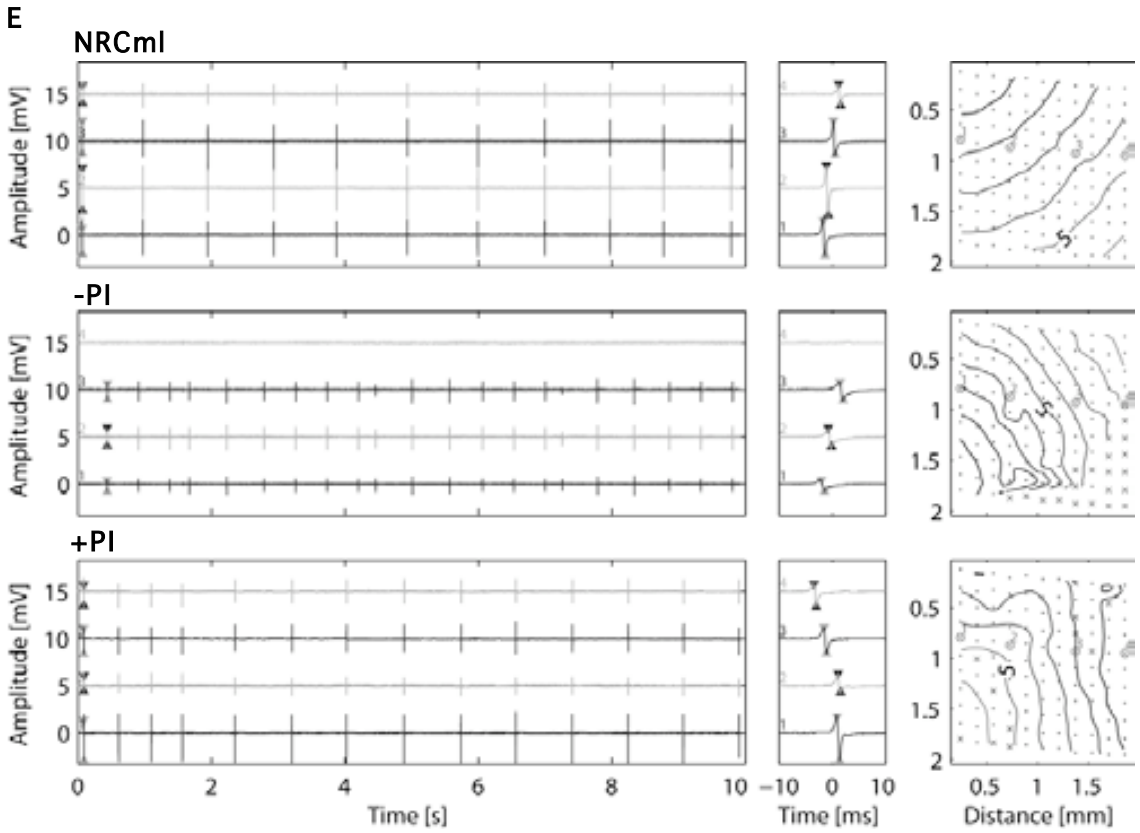

Figure 10. Electrophysiological characterization of NRCml co-cultured with NRCmt co-transduced with pCD10- and pMF392-derived lentiviral particles. (AB) Immunofluorescence image of a NRCmt cultivated on top of NRCml plated on a HD-MEA indicating the presence of connexin 43 (green, arrows) at the boundary between the NRCmt and NRCml. Sarcomeric α-actinin is shown in red. Scale bar 50 μm. (C) Average signal shape of all electrically active NRCs adjacent to the NRCmt. (D) Electrophysiological influence of NRCmt co-transduced with pCD10- and pMF392-derived lentiviral particles integrated on the NRCml in media supplemented with or without PI. (E) Long signal traces and wave propagation maps of NRCml alone (NRCml) or with a transplanted NRCmt co-transduced with pCD10- and pMF392-derived lentiviral particles cultivated in the absence (-PI) or presence of (+PI) pristinamycin I. Error bars represent the average of three independent measurements (HD-MEA-to-HD-MEA, NRC batch and NRCmt-to-NRCmt variability). Statistically significant differences are denotey by * $p<0.01$.

Discussion

The physiological control of cells and tissues remains one of the greatest challenges for molecular and cellular biologists which, if overcome, promises a wide variety of therapeutic applications. To this end, the control and restoration of the electrophysiological functions of cardiac tissue is today one of the central aims of

cardiovascular medicine and research [70]. We have shown here, for the first time, the ability to regulate cardiac electrophysiology by means of synthetic gene control systems responsive to external factors such as antibiotics and gaseous acetaldehyde. We have explored this approach by extensively analyzing electrophysiological changes in freshly isolated neonatal rat cardiomyocytes cultured on HD-MEAs. We also established HD-MEA-based devices to evaluate field potential properties, such as upstroke duration and depolarization amplitude, which were previously demonstrated to correlate with changes in action potential [59]. Moreover the field potential signal shape indicated the presence of previously excited cells and thus the origin of excitation [59, 60]. The first positive peak (positive voltage) represents a passive signal caused by previously excited neighboring cells, while the following negative peak (negative voltage) shows the rapid depolarization phase (entry of Na^+ ions into the cell) occurring during the contraction of the cell. Signal propagation velocities, contraction rate, and rhythm variability were also assessed. Overall, the electrophysiological control of cardiac cells in HD-MEAs offers the possibility to measure functional effects in real time, thus providing insights and a ready-to-use tool for gene-function studies and for the future discovery and preclinical evaluation of novel genes with potential therapeutic effects.

At present, tissue transplantation and insertion of electrical pacemakers are the clinical solutions offered to treat cardiac dysfunction. As cardiac-related insufficiencies are the major cause of death in industrialized countries [71], new technologies are required to regenerate cardiac tissue functionality [72], such as (i) stem cell transplantation [73], (ii) active myogenic cell transplantation [74], or (iii) implantation of biologic pacemakers [75, 76]. The efficient delivery and adjustable expression of therapeutic genes might also be required to cure common disorders. Therefore, regulation systems, in which the expression of one or more selected therapeutic transgenes can be controlled, present an attractive approach to improve/restore cardiac tissue functionality. We have been able to control cardiac electrical activity of cardiomyocytes by using lentivectors engineered for streptogramin-responsive [20, 35] and for acetaldehyde-responsive [21, 36] BMP-2 expression. Lentiviral particles successfully transduced non-dividing cardiomyocytes without disturbing the electrophysiological behavior of the cells. In relation to the two systems, the pristinamycin I (PI) regulable system exhibited (i) a change of up to 12-fold in

electrophysiological activity (upstroke duration) in the induced (absence of PI) state, (ii) a side-effect-free state (no effect seen in negative controls) under repressed conditions, (iii) tuning of electrophysiological changes through intermediate PI dosing, and (iv) a design compatible with lentiviral delivery systems, thus meeting the requirements of future clinical implementation. The gaseous acetaldehyde system also functioned to inducibly enable controlled BMP-2 expression. However, acetaldehyde was not completely side-effect-free showing a significant influence on signal propagation velocity. This is possibly due to an interaction between acetaldehyde and endogenous Na^+ channels, as described by Brodie and Sampson [77].

The role of BMP-2 in cardiac development and cardiomyocyte differentiation *in vitro* has been described [49, 78], but its role in the functioning of cardiomyocytes has not been extensively investigated. Although there is evidence that BMP-2 induces myocyte contractility by PI3K (phosphatidyl inositol 3-kinase) [44, 47], its electrophysiological effect and the mechanisms involved in the increase of the contraction frequency have not yet been resolved. We have shown that BMP-2 expression not only increases cardiomyocyte beating frequency up to 4-fold, but also reduces signal propagation velocity up to 3.5-fold, which is not only a normal physiological phenomenon in the pacemaker region of the heart, but is also related to many pathophysiological conditions, such as arrhythmia [79, 80]. However, BMP-2-treated cells not only showed a synchronized beating frequency over time, but also a decrease in the rhythm variability compared to spontaneously beating wild-type cardiomyocytes. BMP-2-transduced cardiomyocytes also showed a six-fold decrease in their action potential amplitudes and extended action potential duration up to 12 times, suggesting an affect on K^+ channels [81]. Interestingly, the electrophysiological characteristics induced after BMP-2 expression were similar compared to addition of α1-adrenergic drugs. Although there is some discrepancy in the α1-adrenergic responses, Capogrossi and colleagues indicated that at high Ca^{2+} concentrations, α1-adrenergic stimulation leads to a negative inotropic effect and subsequently enhanced myocardial contractility [62, 82]. Moreover, α1-adrenergic drugs, such as phenylephrine, reduce outward K^+ currents, thus increasing the action potential upstroke duration [63, 64]. As mentioned above, BMP-2 activates PI3K, a kinase that is involved in the β2-adrenergic signaling cascade [62, 83], which shows a cardioprotective

effect via Akt [65], thereby functionally linking BMP-2 with cell survival [51, 52]. This effect was confirmed by restoring the electrical activity from electrically inactive cardiomyocyte-forming microtissues, supporting a previous statement, which associates BMP-2 signaling pathway with the recovery of cardiomyocyte function [45]. In addition, PI3K regulates MEF-2A (myocyte enhancer factor-2A) [46], which has been shown to control cardiac contractility [45]. Concurrently, MEF-2 is known to regulate α-MHC (α-cardiac myosin heavy chain) [84, 85], which appears to be directly related to the mechanical performance of the heart [86], being highly expressed in species with fast-contractile ventricles [87]. This suggests that BMP-2 increases the expression of α-MHC inducing an incremental change in cardiac contractility, which implies that BMP-2 could also act as a potential molecule for the treatment of heart failure [88]. Overall, these findings support BMP-2's role as a multifunctional cytokine involved in several physiological pathways, for which adjustable expression might be useful in future therapeutic interventions.

Todays strategies for drug/gene discovery also require easy test methods that mimic the human tissue environment in order to optimize preclinical selection of the most active molecules from a large pool of potential effectors. Although 3D cultures better reflect the *in vivo* behavior of most cell types, these 3D test systems have not yet been incorporated into mainstream drug development operations [89]. We have recorded electrogenic activity in myocardial microtissues, reproducing the *in vivo* electrogenic effect of known cardioactive drugs. This suggests that they might provide an *ex-vivo* feasible assay to determine cardiac excitation patterns for the screening of potential therapeutic molecules and as a pre-implantation quality control. The feasibility of the 3D platform to assess cardiac functionality was shown by the impact of regulable BMP-2 expression. BMP-2-transduced NRCmt showed coordinated beating. Microtissues transgenic for BMP-2 did not require a hormonal stimulus compared to wild-type microtissues, demonstrating that BMP-2 is able to restore cardiac electrical activity. Controlled production of BMP-2 using either the pristinamycin-repressible or the acetaldehyde-inducible gene regulation systems restored the electrical activity of NRCmt. This demonstrates the functionality of these inducible systems for a 3D culture, which inherently reflects *in vivo* functioning more accurately. Moreover, genetically engineered NRCmt, integrated into the NRCml and locally expressing BMP-2, affected the

electrophysiological activity of the entire monolayer. This configuration presents an opportunity for *in vivo* transplantation [90] of a biological pacemaker-like device, which responds to external signals in order to control total cardiac activity.

The ability to engineer cell and tissue electrophysiology will foster great advances in the understanding of cardiac cell behavior and in the development of novel therapies to treat cardiac beating disorders. In particular, BMP-2 might be of therapeutic use when insufficient beating frequency compromises heart function. We have shown, for the first time, the ability to regulate cardiac electrophysiology by biocompatible inducers, which can tightly adjust the therapeutic transgene expression level, thus tuning the electrical activity of cardiac cells. Moreover, we have been able to restore the contractility of cardiomyocytes in myocardial-like microtissues. Finally, this system provides us with an *ex-vivo* assay to determine cardiac excitation patterns for (i) pre-clinical and experimental electrophysiological tests and (ii) novel gene function studies.

Acknowledgements

We thank Evelyne Perriard, Anna Bogdanova and Nikolai Bogdanov for providing neonatal rat cardiomyocytes and advice, Francesca Faraci for help with the data analysis, Frauke Greve for technical support, Shizuka Hartenbach for providing pSH16 prior to publication, David Greber for critical comments on the manuscript and Juerg Schelldorfer for statistical analysis. This work was supported by the Swiss National Science foundation (grant no. 3100A0-112549), the ETH-internal grant TH-1-03-1 and the EC Framework 6 (COBIOS).

References

1. Cohn, J.N., Bristow, M.R., Chien, K.R., Colucci, W.S., Frazier, O.H., Leinwand, L.A., Lorell, B.H., Moss, A.J., Sonnenblick, E.H., Walsh, R.A., Mockrin, S.C. and Reinlib, L. Report of the National Heart, Lung, and Blood Institute Special Emphasis Panel on Heart Failure Research. Circulation **95**, 766, 1997.
2. Lehmann-Horn, F. and Jurkat-Rott, K. Voltage-gated ion channels and hereditary disease. Physiological reviews **79**, 1317, 1999.
3. Keating, M.T. and Sanguinetti, M.C. Molecular genetic insights into cardiovascular disease. Science (New York, N.Y **272**, 681, 1996.

4. Gambit, S. New approaches to antiarrhythmic therapy: emerging therapeutic applications of the cell biology of cardiac arrhythmias(1). Cardiovascular research **52**, 345, 2001.
5. Priori, S.G. and Napolitano, C. Role of genetic analyses in cardiology: part I: mendelian diseases: cardiac channelopathies. Circulation **113**, 1130, 2006.
6. Chien, K. Making a Play at Regrowing Hearts. The Scientist **20**, 2006.
7. Kehat, I., Khimovich, L., Caspi, O., Gepstein, A., Shofti, R., Arbel, G., Huber, I., Satin, J., Itskovitz-Eldor, J. and Gepstein, L. Electromechanical integration of cardiomyocytes derived from human embryonic stem cells. Nature biotechnology **22**, 1282, 2004.
8. Rubart, M. and Field, L.J. Cardiac regeneration: repopulating the heart. Annual review of physiology **68**, 29, 2006.
9. Rubart, M., Pasumarthi, K.B., Nakajima, H., Soonpaa, M.H., Nakajima, H.O. and Field, L.J. Physiological coupling of donor and host cardiomyocytes after cellular transplantation. Circulation research **92**, 1217, 2003.
10. Stett, A., Egert, U., Guenther, E., Hofmann, F., Meyer, T., Nisch, W. and Haemmerle, H. Biological application of microelectrode arrays in drug discovery and basic research. Analytical and bioanalytical chemistry **377**, 486, 2003.
11. Atherton, B.T., Meyer, D.M. and Simpson, D.G. Assembly and remodelling of myofibrils and intercalated discs in cultured neonatal rat heart cells. Journal of cell science **86**, 233, 1986.
12. Chlopcikova, S., Psotova, J. and Miketova, P. Neonatal rat cardiomyocytes--a model for the study of morphological, biochemical and electrophysiological characteristics of the heart. Biomed Pap Med Fac Univ Palacky Olomouc Czech Repub **145**, 49, 2001.
13. Galaris, D., Hoijer, B. and Rydstrom, J. Improved methods for automatic monitoring of contracting heart cells in culture. Journal of biochemical and biophysical methods **2**, 213, 1980.
14. Harary, I. and Farley, B. In vitro studies on single beating rat heart cells. I. Growth and organization. Experimental cell research **29**, 451, 1963.
15. Harary, I. and Farley, B. In vitro studies on single beating rat heart cells. II. Intercellular communication. Experimental cell research **29**, 466, 1963.
16. Datwyler, D.A., Magyar, J.P., Busceti, V., Hirschy, A., Perriard, J.C., Bailey, J.E. and Eppenberger, H.M. Recombinant Sindbis virus allows expression and precise targeting of proteins of the contractile apparatus in cultured cardiomyocytes. Basic research in cardiology **96**, 630, 2001.
17. Sakoda, T., Kasahara, N., Hamamori, Y. and Kedes, L. A high-titer lentiviral production system mediates efficient transduction of differentiated cells including beating cardiac myocytes. Journal of molecular and cellular cardiology **31**, 2037, 1999.
18. Mitta, B., Rimann, M., Ehrengruber, M.U., Ehrbar, M., Djonov, V., Kelm, J. and Fussenegger, M. Advanced modular self-inactivating lentiviral expression vectors for multigene interventions in mammalian cells and in vivo transduction. Nucleic acids research **30**, e113, 2002.
19. Zhao, J., Pettigrew, G.J., Thomas, J., Vandenberg, J.I., Delriviere, L., Bolton, E.M., Carmichael, A., Martin, J.L., Marber, M.S. and Lever, A.M. Lentiviral

vectors for delivery of genes into neonatal and adult ventricular cardiac myocytes in vitro and in vivo. Basic research in cardiology **97**, 348, 2002.

20. Mitta, B., Weber, C.C., Rimann, M. and Fussenegger, M. Design and in vivo characterization of self-inactivating human and non-human lentiviral expression vectors engineered for streptogramin-adjustable transgene expression. Nucleic acids research **32**, e106, 2004.
21. Hartenbach, S. and Fussenegger, M. Autoregulated, bidirectional and multicistronic gas-inducible mammalian as well as lentiviral expression vectors. Journal of biotechnology **120**, 83, 2005.
22. Mitta, B., Weber, C.C. and Fussenegger, M. In vivo transduction of HIV-1-derived lentiviral particles engineered for macrolide-adjustable transgene expression. The journal of gene medicine **7**, 1400, 2005.
23. Vogel, R., Amar, L., Thi, A.D., Saillour, P. and Mallet, J. A single lentivirus vector mediates doxycycline-regulated expression of transgenes in the brain. Human gene therapy **15**, 157, 2004.
24. Regulier, E., Trottier, Y., Perrin, V., Aebischer, P. and Deglon, N. Early and reversible neuropathology induced by tetracycline-regulated lentiviral overexpression of mutant huntingtin in rat striatum. Human molecular genetics **12**, 2827, 2003.
25. Vigna, E., Cavalieri, S., Ailles, L., Geuna, M., Loew, R., Bujard, H. and Naldini, L. Robust and efficient regulation of transgene expression in vivo by improved tetracycline-dependent lentiviral vectors. Mol Ther **5**, 252, 2002.
26. Koponen, J.K., Kankkonen, H., Kannasto, J., Wirth, T., Hillen, W., Bujard, H. and Yla-Herttuala, S. Doxycycline-regulated lentiviral vector system with a novel reverse transactivator rtTA2S-M2 shows a tight control of gene expression in vitro and in vivo. Gene therapy **10**, 459, 2003.
27. Johansen, J., Rosenblad, C., Andsberg, K., Moller, A., Lundberg, C., Bjorlund, A. and Johansen, T.E. Evaluation of Tet-on system to avoid transgene down-regulation in ex vivo gene transfer to the CNS. Gene therapy **9**, 1291, 2002.
28. Fussenegger, M., Schlatter, S., Datwyler, D., Mazur, X. and Bailey, J.E. Controlled proliferation by multigene metabolic engineering enhances the productivity of Chinese hamster ovary cells. Nature biotechnology **16**, 468, 1998.
29. Fux, C., Langer, D. and Fussenegger, M. Dual-regulated myoD- and msx1-based interventions in C2C12-derived cells enable precise myogenic/osteogenic/adipogenic lineage control. The journal of gene medicine **6**, 1159, 2004.
30. Fux, C., Mitta, B., Kramer, B.P. and Fussenegger, M. Dual-regulated expression of C/EBP-alpha and BMP-2 enables differential differentiation of C2C12 cells into adipocytes and osteoblasts. Nucleic acids research **32**, e1, 2004.
31. Fussenegger, M. The impact of mammalian gene regulation concepts on functional genomic research, metabolic engineering, and advanced gene therapies. Biotechnology progress **17**, 1, 2001.
32. Kelm, J.M., Kramer, B.P., Gonzalez-Nicolini, V., Ley, B. and Fussenegger, M. Synergies of microtissue design, viral transduction and adjustable transgene expression for regenerative medicine. Biotechnology and applied biochemistry **39**, 3, 2004.

33. Weber, W. and Fussenegger, M. Approaches for trigger-inducible viral transgene regulation in gene-based tissue engineering. Current opinion in biotechnology **15**, 383, 2004.
34. Weber, W. and Fussenegger, M. Novel gene switches. Handbook of experimental pharmacology, 73, 2007.
35. Fussenegger, M., Morris, R.P., Fux, C., Rimann, M., von Stockar, B., Thompson, C.J. and Bailey, J.E. Streptogramin-based gene regulation systems for mammalian cells. Nature biotechnology **18**, 1203, 2000.
36. Weber, W., Rimann, M., Spielmann, M., Keller, B., Daoud-El Baba, M., Aubel, D., Weber, C.C. and Fussenegger, M. Gas-inducible transgene expression in mammalian cells and mice. Nature biotechnology **22**, 1440, 2004.
37. Abbott, A. Cell culture: biology's new dimension. Nature **424**, 870, 2003.
38. Zhang, S. Beyond the Petri dish. Nature biotechnology **22**, 151, 2004.
39. Heer, F., Hafizovic, S., Ugniwenko, T., Frey, U., Franks, W., Perriard, E., Perriard, J.C., Blau, A., Ziegler, C. and Hierlemann, A. Single-chip microelectronic system to interface with living cells. Biosens Bioelectron, 2006.
40. Frey, U., Heer, F., Pedron, R., Greve, F., Hafizovic, S., Kirstein, K.-U. and Hierlemann, A. 11'000 electrode-, 126 channel-CMOS microelectrode array for electrogenic cells. in Proceedings of the IEEE MEMS 2007, Kobe, Japan, 541, 2007.
41. Frey, U., Heer, F., Pedron, R., Hafizovic, S., Greve, F., Sedivy, J., Kirstein, K.-U. and Hierlemann, A. An 11k-electrode 126-channel highdensity microelectrode array to interact with electrogenic cells. in Proceedings of the IEEE ISSCC 2007, San Francisco USA, 158, 2007.
42. Wozney, J.M., Rosen, V., Celeste, A.J., Mitsock, L.M., Whitters, M.J., Kriz, R.W., Hewick, R.M. and Wang, E.A. Novel regulators of bone formation: molecular clones and activities. Science (New York, N.Y **242**, 1528, 1988.
43. Hogan, B.L. Bone morphogenetic proteins: multifunctional regulators of vertebrate development. Genes & development **10**, 1580, 1996.
44. Ghosh-Choudhury, N., Abboud, S.L., Chandrasekar, B. and Ghosh Choudhury, G. BMP-2 regulates cardiomyocyte contractility in a phosphatidylinositol 3 kinase-dependent manner. FEBS Lett **544**, 181, 2003.
45. Wang, Y.X., Qian, L.X., Liu, D., Yao, L.L., Jiang, Q., Yu, Z., Gui, Y.H., Zhong, T.P. and Song, H.Y. Bone morphogenetic protein-2 acts upstream of myocyte-specific enhancer factor 2a to control embryonic cardiac contractility. Cardiovascular research **74**, 290, 2007.
46. Ghosh-Choudhury, N., Abboud, S.L., Mahimainathan, L., Chandrasekar, B. and Choudhury, G.G. Phosphatidylinositol 3-kinase regulates bone morphogenetic protein-2 (BMP-2)-induced myocyte enhancer factor 2A-dependent transcription of BMP-2 gene in cardiomyocyte precursor cells. J Biol Chem **278**, 21998, 2003.
47. Crackower, M.A., Oudit, G.Y., Kozieradzki, I., Sarao, R., Sun, H., Sasaki, T., Hirsch, E., Suzuki, A., Shioi, T., Irie-Sasaki, J., Sah, R., Cheng, H.Y., Rybin, V.O., Lembo, G., Fratta, L., Oliveira-dos-Santos, A.J., Benovic, J.L., Kahn, C.R., Izumo, S., Steinberg, S.F., Wymann, M.P., Backx, P.H. and Penninger, J.M. Regulation of myocardial contractility and cell size by distinct PI3K-PTEN signaling pathways. Cell **110**, 737, 2002.

48. Zhang, H. and Bradley, A. Mice deficient for BMP2 are nonviable and have defects in amnion/chorion and cardiac development. Development (Cambridge, England) **122**, 2977, 1996.
49. Monzen, K., Nagai, R. and Komuro, I. A role for bone morphogenetic protein signaling in cardiomyocyte differentiation. Trends in cardiovascular medicine **12**, 263, 2002.
50. Abdelwahid, E., Rice, D., Pelliniemi, L.J. and Jokinen, E. Overlapping and differential localization of Bmp-2, Bmp-4, Msx-2 and apoptosis in the endocardial cushion and adjacent tissues of the developing mouse heart. Cell and tissue research **305**, 67, 2001.
51. Masaki, M., Izumi, M., Oshima, Y., Nakaoka, Y., Kuroda, T., Kimura, R., Sugiyama, S., Terai, K., Kitakaze, M., Yamauchi-Takihara, K., Kawase, I. and Hirota, H. Smad1 protects cardiomyocytes from ischemia-reperfusion injury. Circulation **111**, 2752, 2005.
52. Izumi, M., Fujio, Y., Kunisada, K., Negoro, S., Tone, E., Funamoto, M., Osugi, T., Oshima, Y., Nakaoka, Y., Kishimoto, T., Yamauchi-Takihara, K. and Hirota, H. Bone morphogenetic protein-2 inhibits serum deprivation-induced apoptosis of neonatal cardiac myocytes through activation of the Smad1 pathway. J Biol Chem **276**, 31133, 2001.
53. Frey, U., Sanchez-Bustamante, C.D., Ugniwenko, T., Heer, F., Sedivy, J., Hafizovic, S., Roscic, B., Fussenegger, M., Blau, A., Egert, U. and Hierlemann, A. Cell Recordings with a CMOS High-density Microelectrode Array. IEEE Engineering in Medicine and Biology Society **In press**, 2007.
54. Auerbach, D., Bantle, S., Keller, S., Hinderling, V., Leu, M., Ehler, E. and Perriard, J.C. Different domains of the M-band protein myomesin are involved in myosin binding and M-band targeting. Molecular biology of the cell **10**, 1297, 1999.
55. Mitta, B., Rimann, M. and Fussenegger, M. Detailed design and comparative analysis of protocols for optimized production of high-performance HIV-1-derived lentiviral particles. Metabolic engineering **7**, 426, 2005.
56. Kelm, J.M., Timmins, N.E., Brown, C.J., Fussenegger, M. and Nielsen, L.K. Method for generation of homogeneous multicellular tumor spheroids applicable to a wide variety of cell types. Biotechnology and bioengineering **83**, 173, 2003.
57. Sanchez-Bustamante, C.D., Kelm, J.M., Mitta, B. and Fussenegger, M. Heterologous protein production capacity of mammalian cells cultivated as monolayers and microtissues. Biotechnology and bioengineering **93**, 169, 2006.
58. Quiroga, R.Q., Nadasdy, Z. and Ben-Shaul, Y. Unsupervised spike detection and sorting with wavelets and superparamagnetic clustering. Neural computation **16**, 1661, 2004.
59. Halbach, M., Egert, U., Hescheler, J. and Banach, K. Estimation of action potential changes from field potential recordings in multicellular mouse cardiac myocyte cultures. Cell Physiol Biochem **13**, 271, 2003.
60. Spach, M.S., Miller, W.T., 3rd, Miller-Jones, E., Warren, R.B. and Barr, R.C. Extracellular potentials related to intracellular action potentials during impulse conduction in anisotropic canine cardiac muscle. Circulation research **45**, 188, 1979.

61. Hescheler, J., Halbach, M., Egert, U., Lu, Z.J., Bohlen, H., Fleischmann, B.K. and Reppel, M. Determination of electrical properties of ES cell-derived cardiomyocytes using MEAs. Journal of electrocardiology **37 Suppl**, 110, 2004.
62. Xiao, R.P., Zhu, W., Zheng, M., Cao, C., Zhang, Y., Lakatta, E.G. and Han, Q. Subtype-specific alpha1- and beta-adrenoceptor signaling in the heart. Trends in pharmacological sciences **27**, 330, 2006.
63. Fedida, D., Braun, A.P. and Giles, W.R. Alpha 1-adrenoceptors reduce background K+ current in rabbit ventricular myocytes. The Journal of physiology **441**, 673, 1991.
64. Van Wagoner, D.R., Kirian, M. and Lamorgese, M. Phenylephrine suppresses outward K+ currents in rat atrial myocytes. The American journal of physiology **271**, H937, 1996.
65. Xiao, R.P., Zhu, W., Zheng, M., Chakir, K., Bond, R., Lakatta, E.G. and Cheng, H. Subtype-specific beta-adrenoceptor signaling pathways in the heart and their potential clinical implications. Trends in pharmacological sciences **25**, 358, 2004.
66. Xiao, Y.F., Ke, Q., Wang, S.Y., Yang, Y., Chen, Y., Wang, G.K., Morgan, J.P., Cox, B. and Leaf, A. Electrophysiologic properties of lidocaine, cocaine, and n-3 fatty-acids block of cardiac Na+ channels. Eur J Pharmacol **485**, 31, 2004.
67. Ridley, J.M., Milnes, J.T., Zhang, Y.H., Witchel, H.J. and Hancox, J.C. Inhibition of HERG K+ current and prolongation of the guinea-pig ventricular action potential by 4-aminopyridine. The Journal of physiology **549**, 667, 2003.
68. Weber, W., Kramer, B.P., Fux, C., Keller, B. and Fussenegger, M. Novel promoter/transactivator configurations for macrolide- and streptogramin-responsive transgene expression in mammalian cells. The journal of gene medicine **4**, 676, 2002.
69. Kelm, J.M., Ehler, E., Nielsen, L.K., Schlatter, S., Perriard, J.C. and Fussenegger, M. Design of artificial myocardial microtissues. Tissue engineering **10**, 201, 2004.
70. Kusumoto, F.M. and Goldschlager, N. Cardiac pacing. The New England journal of medicine **334**, 89, 1996.
71. Hennekens, C.H. Increasing burden of cardiovascular disease: current knowledge and future directions for research on risk factors. Circulation **97**, 1095, 1998.
72. Dowell, J.D., Rubart, M., Pasumarthi, K.B., Soonpaa, M.H. and Field, L.J. Myocyte and myogenic stem cell transplantation in the heart. Cardiovascular research **58**, 336, 2003.
73. Strauer, B.E., Brehm, M., Zeus, T., Kostering, M., Hernandez, A., Sorg, R.V., Kogler, G. and Wernet, P. Repair of infarcted myocardium by autologous intracoronary mononuclear bone marrow cell transplantation in humans. Circulation **106**, 1913, 2002.
74. SoRelle, R. Myoblast transplant to heart attempted. Circulation **102**, E9030, 2000.
75. Robinson, R.B., Brink, P.R., Cohen, I.S. and Rosen, M.R. I(f) and the biological pacemaker. Pharmacol Res **53**, 407, 2006.
76. Rosen, M.R., Brink, P.R., Cohen, I.S. and Robinson, R.B. Genes, stem cells and biological pacemakers. Cardiovascular research **64**, 12, 2004.

77. Brodie, C. and Sampson, S.R. Effects of ethanol on voltage-sensitive Na-channels in cultured skeletal muscle: up-regulation as a result of chronic treatment. The Journal of pharmacology and experimental therapeutics **255**, 1195, 1990.
78. van Wijk, B., Moorman, A.F. and van den Hoff, M.J. Role of bone morphogenetic proteins in cardiac differentiation. Cardiovascular research **74**, 244, 2007.
79. Kleber, A.G. and Rudy, Y. Basic mechanisms of cardiac impulse propagation and associated arrhythmias. Physiological reviews **84**, 431, 2004.
80. Rohr, S., Kucera, J.P. and Kleber, A.G. Slow conduction in cardiac tissue, I: effects of a reduction of excitability versus a reduction of electrical coupling on microconduction. Circulation research **83**, 781, 1998.
81. Kleber, A.G. The shape of the electrical action-potential upstroke: a new aspect from optical measurements on the surface of the heart. Circulation research **97**, 204, 2005.
82. Capogrossi, M.C., Kachadorian, W.A., Gambassi, G., Spurgeon, H.A. and Lakatta, E.G. Ca2+ dependence of alpha-adrenergic effects on the contractile properties and Ca2+ homeostasis of cardiac myocytes. Circulation research **69**, 540, 1991.
83. Kamp, T.J. and Hell, J.W. Regulation of cardiac L-type calcium channels by protein kinase A and protein kinase C. Circulation research **87**, 1095, 2000.
84. Allen, D.L., Weber, J.N., Sycuro, L.K. and Leinwand, L.A. Myocyte enhancer factor-2 and serum response factor binding elements regulate fast Myosin heavy chain transcription in vivo. J Biol Chem **280**, 17126, 2005.
85. Molkentin, J.D. and Markham, B.E. Myocyte-specific enhancer-binding factor (MEF-2) regulates alpha-cardiac myosin heavy chain gene expression in vitro and in vivo. J Biol Chem **268**, 19512, 1993.
86. Morkin, E. Control of cardiac myosin heavy chain gene expression. Microscopy research and technique **50**, 522, 2000.
87. Swynghedauw, B. Developmental and functional adaptation of contractile proteins in cardiac and skeletal muscles. Physiological reviews **66**, 710, 1986.
88. Miyata, S., Minobe, W., Bristow, M.R. and Leinwand, L.A. Myosin heavy chain isoform expression in the failing and nonfailing human heart. Circulation research **86**, 386, 2000.
89. Kunz-Schughart, L.A., Freyer, J.P., Hofstaedter, F. and Ebner, R. The use of 3-D cultures for high-throughput screening: the multicellular spheroid model. J Biomol Screen **9**, 273, 2004.
90. Kelm, J.M., Djonov, V., Hoerstrup, S.P., Guenter, C.I., Ittner, L.M., Greve, F., Hierlemann, A., Sanchez-Bustamante, C.D., Perriard, J.C., Ehler, E. and Fussenegger, M. Tissue-transplant fusion and vascularization of myocardial microtissues and macrotissues implanted into chicken embryos and rats. Tissue engineering **12**, 2541, 2006.

Chapter 2

(Trans-) Differentiation Capacity of Artifical Microtissues

"Ectopic expression of ΔFosB mediates transdifferentiation of Adipose-Like Microtissues Into Osteo-Like Microtissues"

Abstract

Differentiation and transdifferentiation strategies have a great impact on the manipulation of cells in order to replace dysfunctional cells and tissues. We developed adipose-like microtissues by gravity-enforced self-assembly of monodispersed human primary preadipocytes in order to determine their transdifferentiation capacity to form bone-like tissues. Using lentivirus-derived particles to induce ectopic BMP-2 and ΔFosB gene expression, we demonstrated a time-dependent induction of osteoblast-specific genes and properties such as calcium deposits, bone-like extracellular matrix (ECM) and matrix mineralization. ΔFosB was able to trigger partial Pref-1-mediated de-differentiation of adipocytes which also retained their adipocytic cell phenotype. Osteoblast-specific structures could be co-localized in the ECM of lipid-containing cells analyzed by immunofluorescence as well as transmission electron microscopy when BMP-2 and ΔFosB were co-expressed, suggesting that differentiated adipocytes are able to transdifferentiate into osteoblasts via a transient hybrid adipocyte/preadipocyte/osteoblast cell phenotype. Microtissues transgenic for BMP-2 and ΔFosB expression were able to reproduce bone matrix, which occurs to a lesser extent in conventional two-dimensional cultures but which is known to play a decisive role in the development and function of bone *in vivo*. This demonstrates that ECM-inclusive studies are essential for future characterization assays. Therefore, three-dimensional cultures provide a superior *ex vivo* system for the improved characterization of phenotypical and functional alterations resulting from interventions directed toward differentiation processes. Precise control of transdifferentiation of adipocytes into osteoblasts in a three-dimensional culture mimicking *in-vivo* tissue conditions as closely as possible will foster important advances in regenerative medicine and tissue engineering.

Introduction

Adipose tissue is not only a potent endocrine organ key to many obesity-related diseases, it also possesses a population of stem cells with multi-lineage capacity (adipose-derived adult stem cells, ADAS cells) [1]. Furthermore, it is an ubiquitous, uniquely expendable and accessible tissue, thus meeting significant requirements of tissue engineers [2]. Fat tissue has become a main area of interest in soft-tissue engineering, as

proven by the large number of reconstructive and cosmetic strategies that have been developed [3]. Since aspirated adipocytes are easily traumatized by the mechanical forces of liposuction and difficult to handle reliably as they float ontop of any cell culture media [4], preadipocytes (subcutaneous), which expand easily and take up lipids during differentiation into adipocytes, have been used recently in tissue engineering strategies [5].

Despite easy accessibility to adipose tissue and its potential in reconstructive surgery, little is known about its ability to transform its phenotype and functionality into bone tissue for use in the treatment of bone-related diseases. Since adipogenic and osteogenic cells share a part of the early differentiation pathway, much work has focused on elucidating the signals that determine commitment to one of these two lineages [6]. The close connection between these two lineages in adult tissue is emphasized by the inverse relationship between adipocyte and osteoblast differentiation [7], which is typical of bone diseases such as osteoporosis where a smaller population of osteoblasts is accompanied by a greater number of adipocytes [8, 9]. It has been suggested that the conversion of adipocytes into osteoblasts requires an intermediate step to induce the formation of fibroblast-like cells that are morphologically similar to preadipocytes [10]. It has been reported that preadipocytes can differentiate into several cell lineages, including bone-forming osteoblasts [11]. However, the degree of plasticity between mature adipocytes and osteoblasts is still uncertain [10, 12]. An essential step during the differentiation process is the activation or repression of defined transcription factors, thus setting the stage for patterns of gene expression, characteristic of a particular cell type [13, 14]. Adipocyte differentiation can be initiated by a cocktail of adipogenic inducers consisting of insulin, glucocorticoids, agents that elevate cAMP levels and fetal calf serum, all of which activate the expression of several transcription factors that converge on PPARγ (peroxisome proliferators activated receptor γ) [15], the master regulator of adipogenesis [16]. Osteoblast differentiation is characterized by the expression of the transcription factor Cbfa1/Runx2 (core-binding factor-1/runt homeodomain protein 2), the earliest and most specific marker of osteogenesis. Cbfa1/Runx2 enhances expression of osteocalcin and collagen type I, leading to calcification of the ECM [17]. However, little is known about the ability of extracellular signals to induce transdifferentiation from an adipogenic lineage

into an osteoblastic one. Therefore, further work is necessary to determine the optimal conditions and factors required for maximal bone formation from adipose-derived cells.

In spite of the advances made in molecular biology, new cell culture models are necessary to characterize the molecular, morphologic, and functional transdifferentiation level of adipocytes to osteoblasts in a three-dimensional (3D) environment, where the cells are embedded in their natural ECM. Recently, Birk and coworkers [18] demonstrated the osteogenic ability of preadipocyte stromal-like cells with crystalline porous biomatrices. 3D cell cultures are characterized by *in vivo* tissue-inherent factors such as cell-to-cell and cell-to-extracellular matrix (ECM) interactions, which occur to a lesser extent in two-dimensional (2D) cell cultures [19, 20]. Important, growth and differentiation of preadipocytes and osteoblast precursors is determined by the cellular environment via cell-to-cell, cell-to-cellular matrix, and ECM interactions, which exert specific physical forces influencing cellular development [21-23]. Advances in biomaterial sciences have led to the development of artificial scaffolds with optimum adhesion (cellular attachment), efficient transplantation, and high differentiation [24, 25]. However, ideal filler material, able to adapt its mechanical properties to soft and stiff microenvironments [23, 26], typical of transdifferentiation scenarios, has yet to be developed.

In the current study, we have made use of lentiviral particles to overexpress (i) BMP-2 (bone morphogenetic protein 2) and (ii) ΔFosB (alternatively spliced FosB transcript [27]) together with a specific osteo-inductive media in order to stimulate conversion from differentiated primary human adipose-like spheroids to osteo-like microtissues. These factors were selected for the following reasons: (i) When applied locally, BMP-2 induces *de novo* bone formation [28] and Cbfa1 expression *in vitro* [29], although this action seems to be indirect and dependent on the presence of other signaling molecules [16]. (ii) ΔFosB induces osteoblast maturation and inhibits adipogenesis in a transgenic mice model [27, 30] and may, therefore, be an ideal candidate for application in transdifferentiation studies. The assessment of molecular cues and process mechanisms of adipocyte transdifferentiation into osteoblasts in a “more natural” environment will foster advances in regenerative medicine and tissue engineering.

Material and methods

Cell culture and microtissue production. Subcutaneous human preadipocytes (HPA, cat. no. PT-5001, lot. no. 5F0199, Cambrex Bio Science Walkersville, Inc., Walkersville, MD, USA) and normal human osteoblasts (HO, cat. no. CC-2538, lot. no. 5F0335, Cambrex Bio Science Walkersville, Inc.) were expanded in Dulbecco's Modified Eagle's Medium (DMEM, Invitrogen, Carlsbad, CA, USA) supplemented with 10% fetal calf serum (FCS, cat. no. 3302-P251110, lot. no. P251110, PAN biotech GmbH, Aidenbach, Germany) and 1% penicillin/streptomycin solution (Sigma Chemicals, St.Louis, MO, USA). In order to enable the formation of gravity-enforced microtissues in hanging drops, HPA and HO monolayers were trypsinized, seeded at 2,000 cells/well (8×10^4 cells/ml) into 60-well plates (Micotest-Platten Terasaki, cat. no. 635161, Greiner Bio-One GmbH, Frickenhausen, Germany), and cultivated upside down in DMEM supplemented with 10% FCS or in osteoblast-maintenance media (OM; DMEM, 10% FCS, 10mM β-glycerophosphate, 50μM L-ascorbic acid 2-phosphate, 10^{-7}M dexamethasone, 1% penicillin/streptomycin and 50μg/ml gentamycin), respectively.

For production of human adipose microtissues (HAm), HPAs were grown to confluence prior to incubation in preadipocyte differentiation medium (DM, cat. no. C-39437, PromoCell, Heidelberg, Germany) for 72 hours. After three days, human preadipocytes were trypsinized, seeded at 2,000 cells/well into 60-well plates and cultivated in adipocyte-specific medium (AM; DMEM, 3% FCS, 10μg/ml human recombinant insulin, 10^{-4}M dexamethasone, 0.2mg/ml dBiotin, 1M Hepes, 1% penicillin/streptomycin and 50μg/mL gentamycin) for seven days. Human osteoblast-derived microtissues (HOm) were cultured in OM for up to two weeks before characterization, as described by Kale and co-workers [31]. All cells were cultivated at 37°C in a humidified atmosphere containing 5% CO_2. All media components were purchased from Sigma (Sigma Chemicals).

Vector design and lentiviral transduction. pCD4 was constructed according to a two-step procedure: (i) Mouse ΔFosB-HisTag was excised from pCDNA3.1-ΔFosB-HisTag (obtained from Paula G. Ulery [32]) using *Bam*HI/*Xba*I and cloned into the corresponding sites (*Bam*HI/*Xba*I) of pAAV-MCS (Stratagene, La Jolla, CA, USA) to create pCD3. (ii) Mouse ΔFosB-HisTag was excised from pCD3 using *Cla*I/*Eco*RV and

cloned into the corresponding sites (*Bst*BI/*Pme*I) of pMF359 (5'LTR-ψ^+-ori$_{SV40}$-cPPT-RRE-P$_{hEF1\alpha}$-MCS-3'LTR$_{\Delta U3}$) [33] to give pCD4 (5'LTR-ψ^+-ori$_{SV40}$-cPPT-RRE-P$_{hEF1\alpha}$-ΔFosB-HisTag-3'LTR$_{\Delta U3}$).

To produce replication-incompetent, self-inactivating lentiviral particles a mixture containing (i) 0.25M $CaCl_2$ (Acros Organics, Geel, Belgium), (ii) 1μg pLTR-G, encoding the pseudotyping envelope protein VSV-G of the vesicular stomatitis virus, (iii) 1μg of the helper construct pCD/NL-BH*, and (iv) 2μg of the gene of interest (GOI)-encoding lentiviral expression vector in a final volume of 100μl was added drop wise into 100μl 2×HEPES-buffered saline (HBS, 280mM NaCl; 100mM HEPES 1.5mM Na_2HPO_4; pH7.1) solution, incubated for 15 minutes, and transfected into 4×10^5 human embryonic kidney cells (HEK-293T) previously seeded into a single well of a 6-well plate. Prior to transfection, 2μl of a 25mM chloroquine solution (Bode Chemie, Hamburg, Germany) were added to the cell culture medium. Six hours after transfection the medium was changed, and lentiviral particle production continued for another 36 hours prior to filtration-based harvesting of the lentiviral particles from the culture supernatant (0.45μm pore size FP 030/2 filter; Schleicher & Schuell, Dassel, Germany). Lentiviral particle titer was determined as described elsewhere [34]. The following lentivectors were used in the transdifferentiation studies: (i) pBP253 (5'LTR-ψ^+-ori$_{SV40}$-cPPT-RRE-P$_{hEF1\alpha}$-BMP-2-HAtag-3'LTR$_{\Delta U3}$) [35] (virus titer: 4.22×10^4 TU/ml) and (ii) pCD4 (5'LTR-ψ^+-ori$_{SV40}$-cPPT-RRE-P$_{hEF1\alpha}$-ΔFosB-HisTag-3'LTR$_{\Delta U3}$) (virus titer: 3.71×10^4 TU/ml).

Lentivirus transduction and transdifferentiation of adipose-like spheroids into osteo-like microtissues. After seven days in AM, hanging drops (25μl) containing HAm were transduced with 10^2 lentiviral particles (5μl lentiviral particle-containing supernatant). Two days after transduction, HAm were harvested into suspension tissue culture flasks (94 × 16mm) (cat. no. 633180, Greiner Bio-One GmbH) containing 7ml OM (Fig. 1A). Every three days the medium was exchanged and the transdifferentiation capacity assessed for up to one month. Every two weeks transdifferentiation-induced HAm were examined for lipid accumulation, calcium incorporation, and osteoblast-specific protein production by immunofluorescence analysis and every week for tissue-specific gene expression by quantitative real time PCR and mineralization rate (see

below). As a negative control, HAm were incubated in AM for one month. HOm, cultivated in OM, were used as the positive control. To study the time dependence of differentiation dynamics 14- and 21-day-old HAm were transduced with 10^2 BMP-2- and ΔFosB-derived lentiviral particles and then cultivated for 21 days in OM

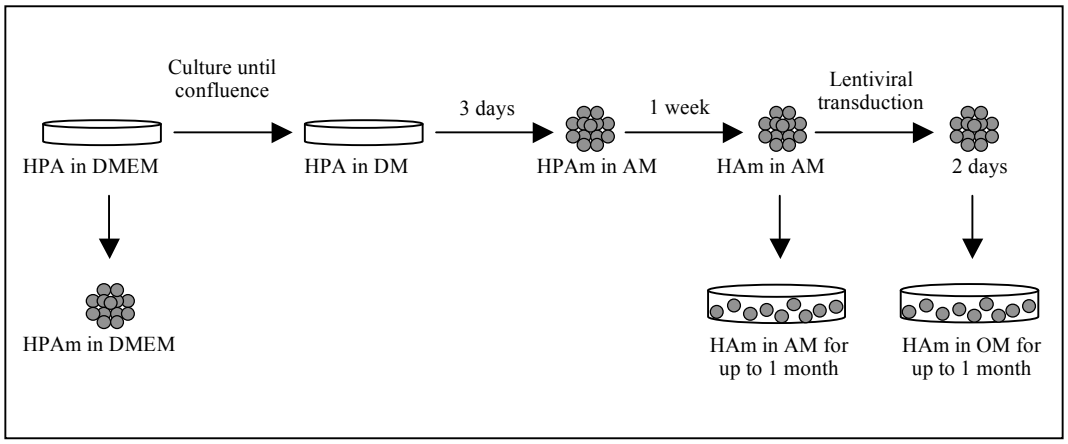

Figure 1: Schematic representation of microtissue production and transdifferentiation induction. Abbreviations: AM (adipocyte-specific media), DM (preadipocyte differentiation media), HAm (human adipocyte-forming microtissues), HPA (human preadipocytes monolayer), HPAm (human preadipocyte-composed microtissues), N (Nuclei), and OM (osteoblast-specific media).

FACS analysis. The number of adipocytes in microtissues was determined by dissociating 1-, 3-, 7-, 14-, 21- and 28-day-old HAm for 5min at 37°C in 0.5% Trypsin-EDTA solution (Invitrogen), passing the cell suspension twice through a 21-gauge needle (Becton Dickinson, Franklin Lakes, NJ), fixing the cells in 2% paraformaldehyde for 20 min at 4°C, staining adipocyte-specific lipid droplets by incubation for 30min in ice-cold PBS containing 1 μg/ml Nile red (stock solution of 1mg/ml Nile red in DMSO) and analyzing the cell population using a Cytomics FC500 flow cytometer with Beckman CXP analysis software (Beckman Coulter, Miami, FL) set to 488 nm (excitation) and 575nm (emission). The mean fluorescence of 5,000 Nile red-stained HAm-derived cells was indicated relative to HPAm-derived control populations.

Western blot analysis. To prepare whole-cell extracts, microtissues were washed twice with ice-cold PBS (Invitrogen) and resuspended in fresh lysis buffer (50mM TrisCl, 150mM NaCl, 0.02% sodium azide, 0.1% SDS, 1mM Phenylmethanesulphonylfluoride [PMSF], 1×Complete EDTA-free [protease inhibitor

cocktail tablets, Roche Diagnostics GmbH, Mannheim, Germany], 1% Triton X-100, 1% sodium deoxycholate, 2mM EDTA, 30mM DTT) pre-cooled to 4°C. Cells were disrupted by gently rocking on an orbital shaker (Thermomixer comfort, Eppendorf, Hamburg, Germany) for 30 minutes at 4°C and by passing the lysate several times through a 20-gauge needle (0.9mm diameter). Finally, the lysate was centrifuged at 14,000×*g* for 15 minutes at 4°C and the supernatant stored at -80°C. Prior to resolution on a 10% (wt/vol) SDS-PAGE, the proteins in the whole-cell extracts or the cell culture supernatants were denaturated by boiling for 5 minutes in loading buffer (10% glycerol, 50mM Tris-HCl, 1% SDS and 0.005% bromophenol blue). Proteins were then blotted onto polyvinylidene difluoride (PVDF) membranes (Millipore, Bedford, MA), which were subsequently blocked using 5% non-fat powdered milk (Bio-Rad Laboratories, Hercules, CA, USA) in PBS for one hour. Blots were probed with specific primary antibodies (HA-probe: rabbit polyclonal, cat. no. sc-805, lot no. 2405, Santa Cruz Biotechnology Inc., Santa Cruz, CA; HisTag: mouse monoclonal, cat. no. 70796-3, lot no. N56036, Novagen, Madison, WI) followed by the appropriate horseradish peroxidase-coupled secondary antibody (cat. no. NA934V (anti-rabbit) or NA931V (anti-mouse), Amersham Bioscience, Piscataway, NJ, USA). Visualization was performed using an ECL detection kit (cat. no. RPN 2132, Amersham Bioscience) and a ChemieLux imager (Intas Science Imaging Instruments GmbH, Goettingen, Germany).

Quantification and visualization of lipid accumulation and calcium incorporation. Following 20 minutes fixation in 2% paraformaldehyde, lipid accumulation was quantified by incubating 10 minutes in 3mg/ml oil red O (Fluka, Buchs, Switzerland). Unincorporated dye was removed by washing once with 60% isopropanol and several times with dH_2O. To extract the oil red O from the lipid droplets, microtissues were incubated in 100% isopropanol and shaken slowly at 800 rpm for 30 min. The concentration of oil red O in the supernatant was determined by quantifying the absorbance at 492 nm. For lipid droplet visualization, the fixed microtissues were stained in 100 μg/ml Nile red (Sigma Chemicals), dissolved in acetone, for 20 minutes. After washing several times in PBS, the microtissues were co-stained with 1μg/ml 4',6-diamidino-2-phenylindole (DAPI; Molecular Probes Inc., Eugene, OR) for 5 min in the dark prior to confocal laser scanning microscopy. To detect calcium formation, alizarin

red (Fluka) staining was carried out on microtissues fixed with 70% ice-cold ethanol. The fixed microtissues were incubated at room temperature for 10 min in 40 mM Alizarin red adjusted to pH 4.2 with 10% ammonium hydroxide. The microtissues were then washed three times with dH_2O and then once with PBS. Positive alizarin red microtissues were visualized by light microscopy. After microscope visualization, microtissues were incubated by gently shaking in 1ml 10% CPC (cetylpyridinium chloride; Sigma-Fine Chemicals) dissolved in 10mM sodium phosphate at pH 7.0 for 1h at room temperature. The dye was then extracted and 200 μl aliquots were transferred to a transparent 96-well plate to quantify absorbance at 492 nm (2 mol of Ca^{2+}/ mol of dye in solution) [36, 37]. Mineralization was visualized by incubating (37°C, 5% CO^2, rocking) microtissues overnight in 60μM Calcein blue (stock solution of 30mM Calcein blue [Sigma] in 100 mM KOH).

Immunofluorescence analysis. Imunofluorescence-based analysis was performed as described elsewhere [38] by using the primary antibodies specific for human osteopontin (mouse monoclonal, Cat. No. MAB1433, R&D Systems Inc., Minneapolis, MN), human osteocalcin (rabbit polyclonal, Cat. No. 7060-0017, AbD Serotec, Duesseldorf, Germany), human collagen type I (mouse monoclonal, Cat. No. C2456, Sigma Chemicals), human Preadipocyte factor 1 (pref-1/DLK, goat polyclonal, Cat. No. sc-8624, Santa Cruz Biotechnology), Tubulin-α Ab-2 (mouse monoclonal, Cat. No. MS-581-P1, Neomarkers, Fremont, CA), His-Tag (mouse monoclonal, Cat. No. 70796-3, Novagen) and HA-Tag (rabbit polyclonal, Cat. No. sc-805, Santa Cruz Biotechnology). For primary antibody detection Cy3-coupled secondary anti-mouse antibodies (Jackson Immunochemicals, West Grove, PA)Cy5-coupled anti-rabbit antibodies and Cy2-coupled anti-goat antibodies (Jackson Immunochemicals) were used. All samples were co-stained with DAPI (Molecular Probes Inc.) for nucleus localization.

Microscopy. Confocal imaging was done with a fluorescence microscope equipped with oil immersion objectives (40×/63×) and a confocal scanner (Zeiss LSM 510; Carl Zeiss AG, Feldbach, Switzerland) with a two-photon laser featuring a chameleon MP, argon and helium-neon laser. Images were obtained with BP 565-615 filter for Cy3 dye or BP 600-710 filter for Cy5 dye; a BP 390-465 filter was used for DAPI and Calcein blue detection. Image acquisition was performed by multitracking the

different filters and processed by Zeiss LSM software with a 3D multichannel image processor (Bitplane, AG, Zurich, Switzerland (Messerli et al. 1993)). Fluorescent images were acquired by means of a Leica AF6000 system equipped with a DMI 6000B microscope and a DFC350 FX digital camera (Leica Microsystems AG, Glattburg, Switzerland). Phase-contrast images were taken by a standard Leica light microscope (Leica DMIL, Leica Microsystems AG) and a Cannon digital camera (Power shot S50).

Quantitative RT-PCR. Total RNA was isolated from one 60-well plate containing microtissues in triplicates with a RNeasy plus mini kit (Qiagen AG, Hombrechtikon, Switzerland), according to the manufacturer's protocol. Reverse transcription and relative quantification of (i) human peroxisome proliferator activated receptor γ (PPARγ; acc. no: NM_138712; forward primer, 5'-GGCTTCATGACAAGGGAGTTTC-3'; reverse primer, 5'-AACTCAAACTTGGGCTCCATAAAG-3'; and a probe labeled with 5'FAM and 3'TAMRA dyes, 5'-AAAGAGCCTGCGAAAGCCTTTTGGTG-3'), (ii) human lipoprotein lipase (LPL; acc. no: NM_000237; forward primer, 5'-TGTGGTGGACTGGCTGTCA-3'; reverse primer, 5'-CTGTCCCACCAGTTTGGTGTAG-3'; and a probe labeled with 5'FAM and 3'TAMRA dyes, 5'-CAGGAGCATTACCCAGTGTCCGCG-3'), (iii) human core-binding factor-1 (Cbfa1; acc. no: NM_001024630; forward primer, 5'-AGTGATTTAGGGCGCATTCCT-3'; reverse primer, 5'-GGAGGGCCGTGGGTTCT-3'; and a probe labeled with 5'FAM and 3'TAMRA dyes, 5'-ATCCCAGTATGAGAGTAGGTGTCCCGCC -3'), (iv) human osteocalcin (OC; acc. no: NM_199173; forward primer, 5'-AGCAAAGGTGCAGCCTTTGT-3'; reverse primer, 5'-GCGCCTGGGTCTCTTCACT-3'; and a probe labeled with 5'FAM and 3'TAMRA, 5'-CCAAGCAGGAGGGCAGCGAGG-3'), and of (v) human preadipocyte factor-1 (pref-1; acc. no: NM_003836; forward primer, 5'-AGAACCTGCTGCTTCAGTACAACA-3'; reverse primer, 5'-TGAAGGTGGTCATGTCGATCTT-3'; add a probe labeled with 5'FAM and 3'TAMRA dyes, 5'-CTGGCCGTCAACATCATCTTCCCC-3') mRNAs were performed in a two-step RT-PCR reaction using TaqMan reverse transcription reagents (cat. no. N808-0234, Applied Biosystems, NJ, USA). Relative quantification was performed with an Applied

Biosystems 7500 real-time PCR device. All samples were standardized using a 18s-RNA specific transcript assay (cat. no. 4308329, Applied Biosystems, CA, USA). All primers were purchased from Sigma Genosys (Sigma).

Quantification of the mineralization rate. To assess matrix mineralization, one 60-well plate containing microtissues was plated in triplicate into one well of a 24-well suspension plates (cat.no, 662102, Greiner Bio-one) and incubated in 46.25KBq/ml of Ca-45 (Amersham Bioscience) for 6 hours. After labeling, the cells were washed three times with PBS and lysed by incubating in 0.5ml 70% formic acid (Fluka) for 60 minutes at 65°C. Cell lysates were transferred to 3.5ml scintillation solution and the radioactivity of the aliquots was scored for 10 minutes in a Beta-Counter (Beta IV, Kontron Instruments, Watford, UK).

Transmission electron microscopy. Tissue samples were fixed by immersion in PBS (Invitrogen) containing 2.5% glutaraldheyde. Tissue blocks were postfixed in osmium tetroxide, block-stained using uranyl acetate, dehydrated by sequential incubation in increasing ethanol concentrations, and embedded in Epon 812 according to the method of Djonov *et. al.* [39](all chemicals from Merck Eurolab AG, Dietikon, Switzerland). Semi-thin 1μm sections were stained with toluidine blue and visualized by an Olympus Vanox BHS light microscope (Olympus AG, Volketswil, Switzerland). Ultra-thin sections of 80-90nm were cut with a diamond knife and picked up on Formvar-coated (polyvinyl formal; Fluka Chemie AG, Buchs, Switzerland) copper grids, double-stained with lead citrate (Merk Eurolab AG) and uranyl acetate, and monitored on a Philips EM 400 electron microscope (FEI AG, Zurich, Switzerland).

Results

Differentiation of human primary preadipocytes into adipocytes in 3D microtissue cultures

Previous experiments with monolayer cultures demonstrated that preadipocytes can differentiate into adipocytes within two weeks when cultivated under specific conditions [24]. To assess the differentiation capacity in a 3D microtissue environment relative to isogenic monolayer cultures, we assembled human primary preadipocytes into microtissues (HPAm) and cultivated them in AM for up to one month (HAm) (Fig. 2A).

Adipocyte-specific differentiation was demonstrated by accumulation of triglyceride-containing lipid droplets (Fig. 2CD). In contrast, control HPAm did not form any lipid vacuoles when cultured in standard cell culture media (Fig. 2B). Ultrastructural analysis of HAm revealed a population of active adipocytes in their adipogenic differentiation process (lipid containing cells) (Fig. 2D) and preadipocytes (fibroblast-like cells) (Fig. 2E).

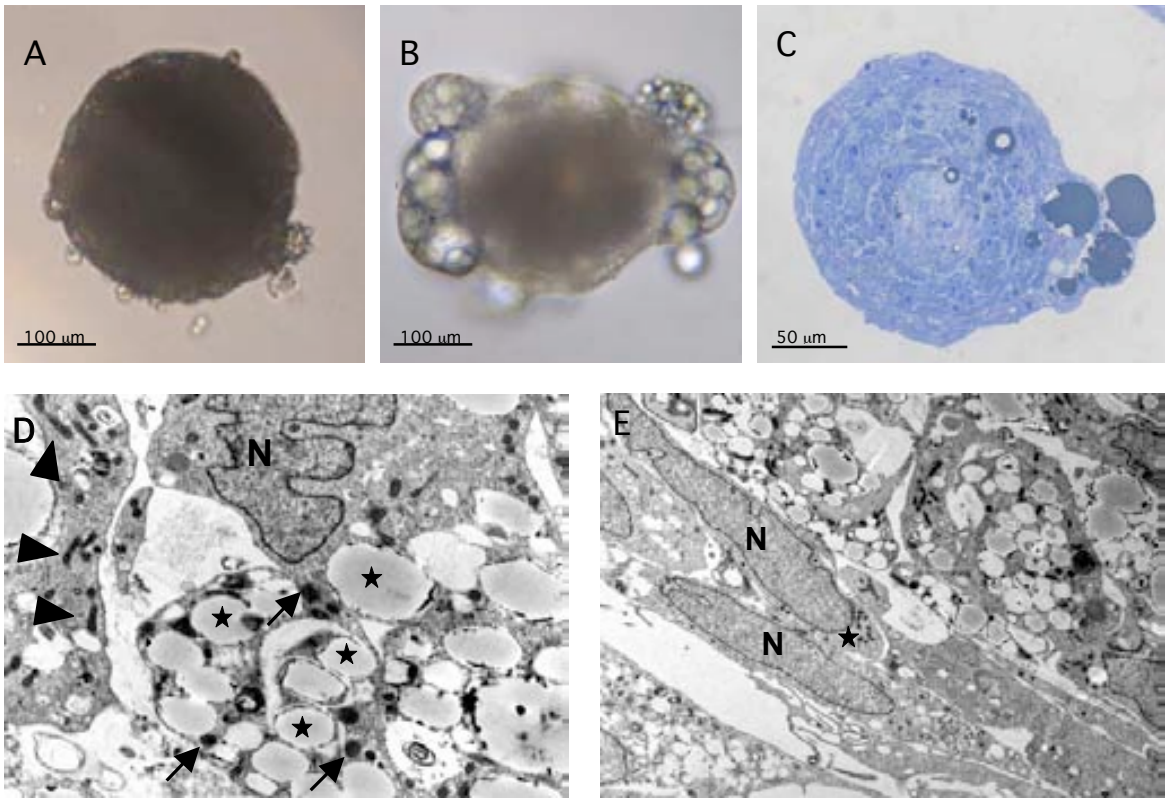

Figure 2: Gravity-enforced self-assembly of 2,000 preadipocytes to microtissues cultured for (A) one week in DMEM (HPAm) and for (B) two weeks in AM (HAm). (C) Toluidine blue-stained semi-thin section of HAm. (D,E) Transmission electron microscopy of HAm reveals (D) multiple lipid droplets (asterisk) characteristic for a developing adipose tissue. High number of lisosomes (arrows) and mitochondria (arrowhead) show an active tissue due to adipogenic differentiation. ×10,000. (E) Fibroblasts like preadipocytes containing many organelles (asterisk) characteristic of active cells. Magnification ×4,600.

After one week in culture, HAm already exhibited considerable lipid accumulation compared to non-differentiated control microtissues (HPAm) (Fig. 3A). The number of adipocytes in HAm was measured, after trypsin-induced dissociation and Nile red-based staining of adipocyte-specific lipid droplets, by FACS-mediated single-

cell analysis revealing 50% adipocytes in 7-day old and 65% in 28-day old HAm, respectively (Fig. 3BC). Adipocyte-specific differentiation was also confirmed by profiling microtissues for expression of adipose-specific genes and transcription factors. The peroxisome proliferator-activated receptor γ (PPARγ), a master switch transcription factor of adipogenesis [16], and lipoprotein lipase (LPL), an adipocyte-specific enzyme hydrolyzing lipids in lipoproteins [40], both increased 8- and 256-fold, respectively in microtissues incubated for seven days in AM compared to HPAm (Fig. 3D). While the PPARγ levels remain 8-fold higher when the microtissues are cultivated beyond 1 week in AM, the expression of LPL gene is partly reduced and levels off at a 32-fold increase compared to HPAm (Fig. 3D).

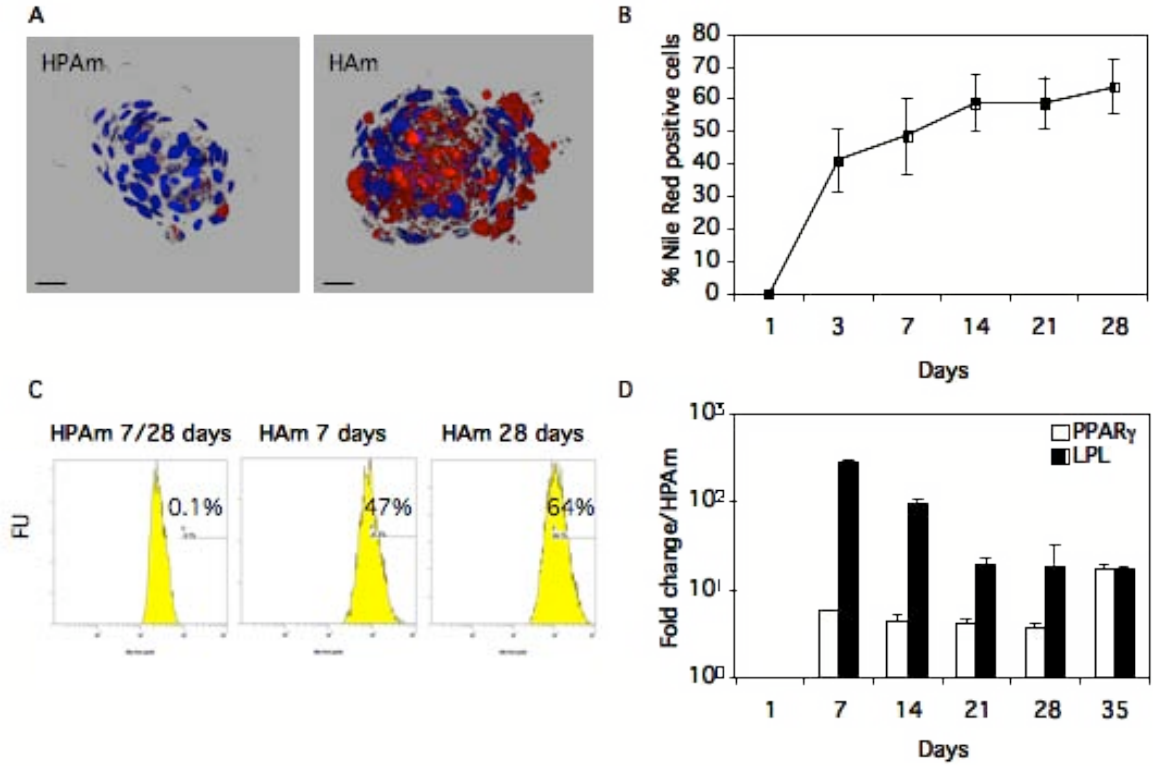

Figure 3: Characterization of adipocyte differentiation. (A) Confocal images with Nile red-specific staining of HPAm and HAm cultivated for 7 days. (B) FACS-based quantification of Nile red-stained adipocytes in HAm cultivated for up to four weeks relative to HPAm (%). (C) FACS-based quantification of Nile red-stained adipocytes in HPAm and HAm cultivated for 7 and 28 days (FU, fluorescence units). (D) Quantification of PPARγ and LPL mRNA expression levels by qRT-PCR. Results are expressed as the fold change variation ($2^{-\Delta\Delta Ct}$) of PPARγ and Lipoprotien Lipase (LPL) gene expression over time in adipose-like microtissues (HAm) compared to microtissues consisting predominantly of preadipocytes (HPAm). For

each sample the results were normalized to the endogenous control 18S (18S of the ribosomal RNA). (scalebar = 100 μm).

Transdifferentiation of human adipose-like spheroids to osteo-like microtissues

Capitalizing on the significant number of adipocytes after one week in culture, we evaluated the transdifferentiation efficiency of seven-day old HAm towards the osteoblastic lineage. HAm were transduced with third-generation self-inactivating lentiviral particles encoding: (i) bone morphogenetic protein 2 (BMP-2; pBP253, 5'LTR-ψ^+-ori_{SV40}-cPPT-RRE-$P_{hEF1\alpha}$-BMP-2-HAtag-3'$LTR_{\Delta U3}$) or (ii) ΔFosB (pCD4, 5'LTR-ψ^+-ori_{SV40}-cPPT-RRE-$P_{hEF1\alpha}$-ΔFosB-HisTag-3'$LTR_{\Delta U3}$) (Fig. 4A). Three days after transduction, BMP-2 and ΔFosB expression in transduced HAm and monolayer preadipocytes was demonstrated by the Western blot analysis (BMP-2 [Fig. 4B]; ΔFosB [Fig. 4E]) and fluorescence imaging (BMP-2 [Fig. 4C]; ΔFosB [Fig. 4F]), respectively. In contrast, neither BMP-2 nor ΔFosB expression could be detected in mock-transduced microtissues (BMP-2 [Fig. 4B and 4D]; ΔFosB [Fig. 4E and 4G].

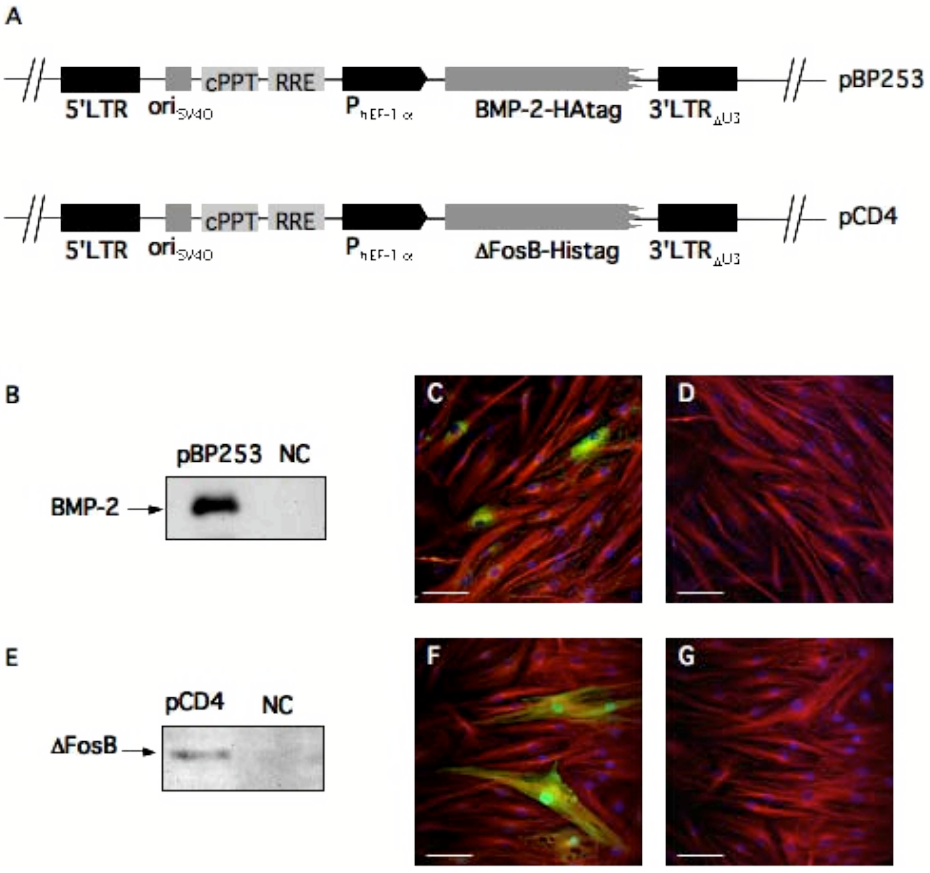

Figure 4: BMP-2 or ΔFosB expression of HAm transduced with pBP253- or pCD4-derived lentiviral particles. (A) Diagram of pBP253- and pCD4-derived lentiviral vectors encoding human BMP-2 and mouse ΔFosB, respectively, driven by a strong constitutive human elongation factor 1α promoter ($P_{hEF\text{-}1\alpha}$) and terminated by an enhancer-free 3' long terminal repeat ($3'LTR_{\Delta U3}$). (B) Western blot analysis of culture supernatant of HAm transduced with pBP253-derived lentiviral particles and (C,D) immunofluorescence of (C) transduced pBP253-derived lentiviral particles and (D) non-transduced confluent HPA. (E) Western blot analysis of whole-cell extracts from HAm transduced with pCD4-derived lentiviral particles and (F,G) immunofluorescence of (F) transduced pCD4-derived lentiviral particles and (G) non-transduced confluent HPA. Experiments were performed 72h post-transduction.

Two days post-transduction with either pBP253- or pCD4-derived lentiviral particles or a combination of both, HAm were harvested and cultivated in OM for up to one month. Since the ability to deposit calcium in the extracellular matrix determines the functional characteristic of osteoblasts, we stained the matrix with alizarin red to detect and quantify calcium accumulation after cultivation in OM for seven and twenty-one days. All combinations (OM, OM BMP-2, OM ΔFosB, and OM BMP-2+ΔFosB) eventually showed a much higher alizarin red concentration compared to microtissues cultured in AM (HAm) (Fig. 5A). However, after seven days, ΔFosB-transduced microtissues exhibited 6-fold higher calcium accumulation, displaying an accelerated differentiation process to osteoblasts compared to non-transduced microtissues maturing in OM. Whereas ΔFosB and BMP-2+ΔFosB were scored as the highest with regard to calcium concentration, OM and BMP-2 were the lowest. After cultivation for twenty-one days in OM, insignificant differences were observed among the five analyzed combinations (OM, OM BMP-2, OM ΔFosB, and OM BMP-2+ΔFosB) (Fig. 5A). Macroscopic imaging of alizarin red staining exhibited an intense red color, while negative micrographs were deep violet in color (Fig. 5B-L).

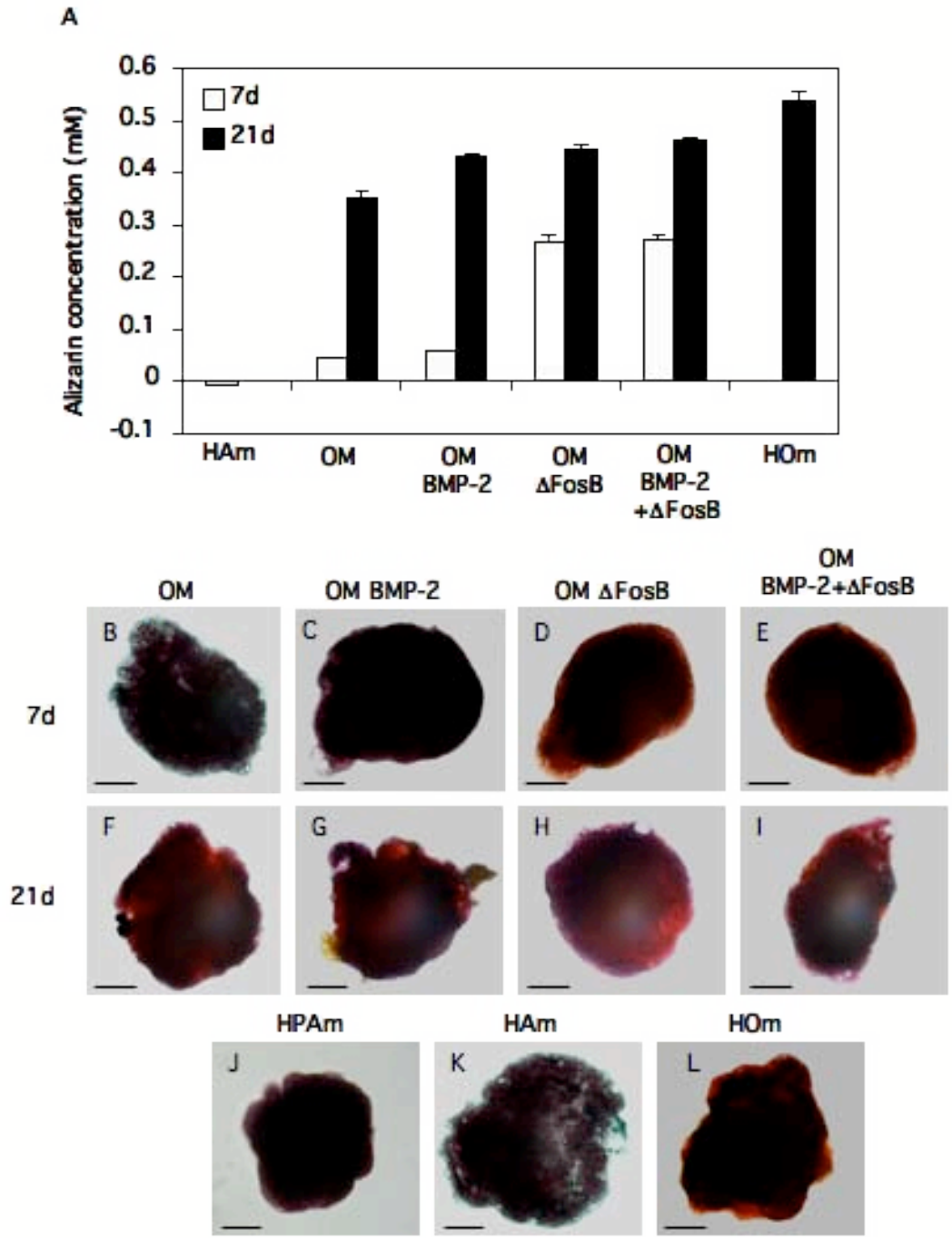

Figure 5: Characterization of calcium deposit formation in transgenic HAm during induction of transdifferentiation. (A) Alizarin red extraction to quantify calcium content of HAm, non-transduced HAm cultivated in OM and transduced HAm cultivated in OM (OM BMP-2, OM ΔFosB, and OM BMP-2+ΔFosB) after 7 and 21 days. The positive control is represented by HOm (human osteoblast-derived microtissues cultivated in OM for two weeks). (B-L) Alizarin red-mediated staining of calcium formation

of non-transduced and transduced HAm cultivated for (B-E) 7 days and (F-I) 21 days in OM. (J,K) Negative controls and (L) positive control. (scalebar = 100 μm).

Quantification of the lipid content of ΔFosB- and BMP-2+ΔFosB-transduced microtissues revealed a reduction of 37%±2 in the number of lipid-containing cells after 21 days in OM from the beginning of the transdifferentiation process (HAm 7days) (Fig. 6A). Whereas BMP-2-transduced microtissues showed a 16% point reduction, non-transduced microtissues displayed a similar number of adipocytes after 21 days in OM than at the beginning of the transdifferentiation (HAm, 7 days) (Fig. 6A). HAm, cultured for a total of 28 days in AM (100% of lipid-containing cells in the microtissues), showed 92% more lipid-containing cells than ΔFosB and BMP-2+ΔFosB-transduced microtissues cultured for 21 days in OM (Fig. 6A). Confocal laser scanning microscopy of Nile red supports the data from the oil red O quantification showing a reduction in the number of lipid droplets but, in some combinations (OM BMP-2 and OM ΔFosB), an increase in the size of the lipid vacuoles over time (Fig. 6B-I).

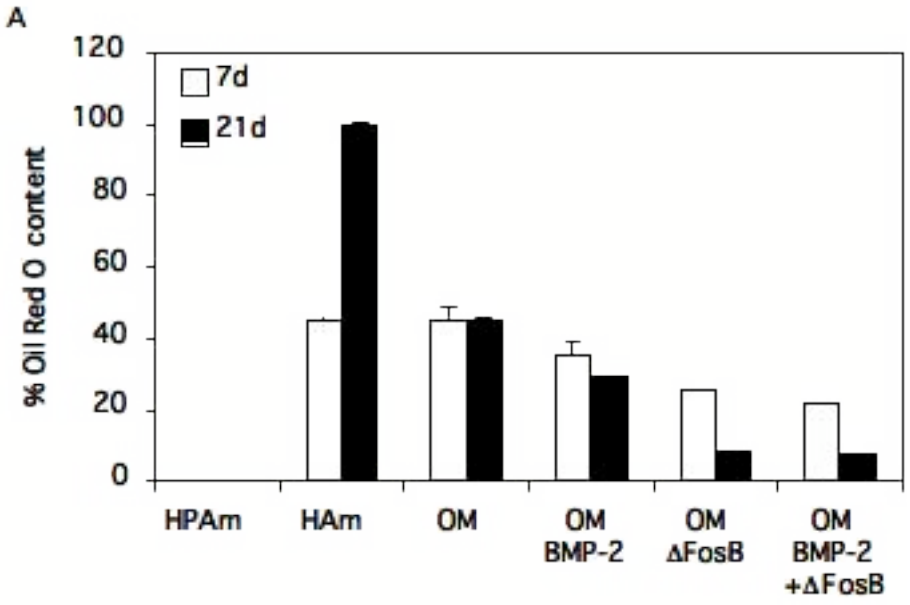

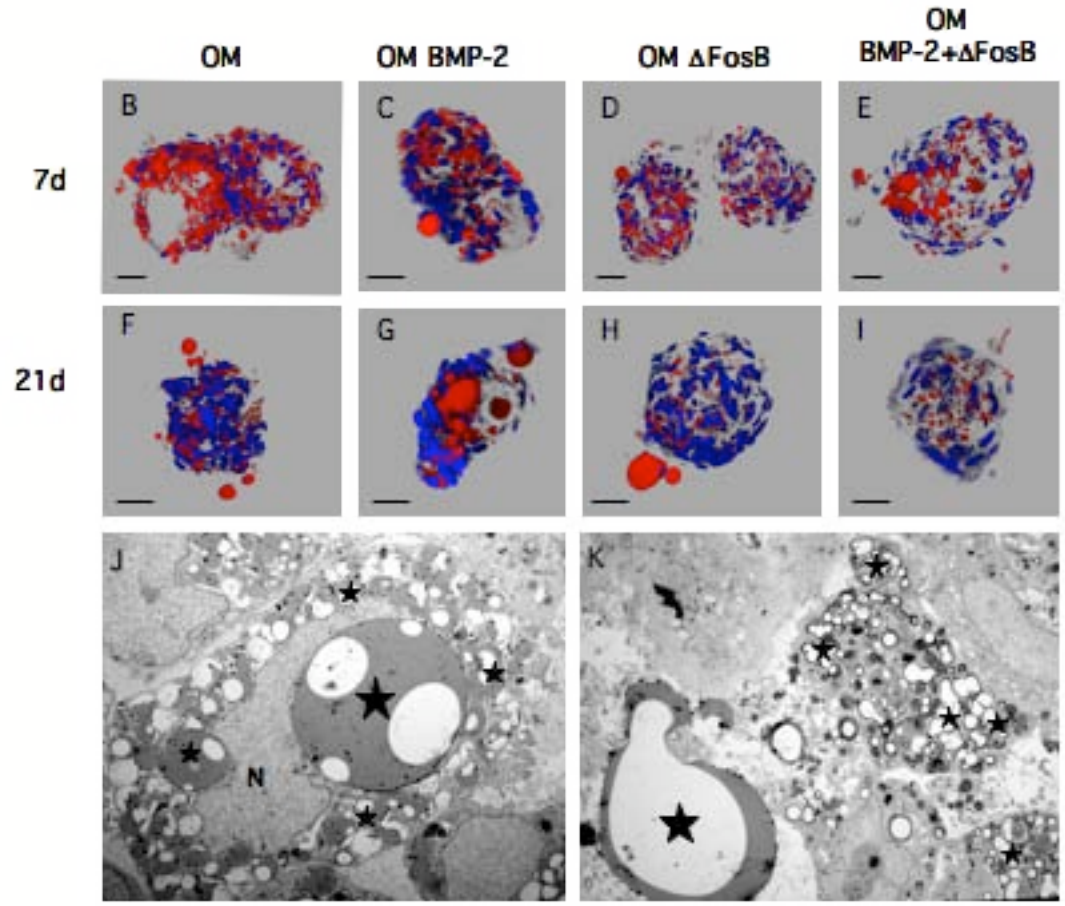

Figure 6: Characterization of lipid accumulation in transgenic HAm during induction of transdifferentiation. (A) Oil red O extraction to quantify lipid-containing cells of non-transduced and transduced HAm cultivated in OM for 7 and 21 days. The positive controls are represented by HAm cultured for one and four weeks in AM. (B-I) Nile red-mediated staining of lipid content of all HAm derivatives cultivated for (B-E) seven and (F-I) 21 days in OM. Triglyceride contained in lipid droplets is shown in red and nuclei are shown in blue. (scalebar = 100 μm).

Gene expression profiling of transdifferentiating human adipose-like microtissues to osteo-like microtissues

The aforementioned experiments demonstrated that microtissues are a functional and adequate environment for the transdifferentiation of adipocytes towards an osteoblastic phenotype, in which ΔFosB appears to play an enhancing role. Throughout the transdifferentiation of our transgenic HAm, we examined the expression level of two genetic markers specific for the adipocyte phenotype, PPARγ and LPL, and two genetic markers specific for the osteoblast phenotype, Cbfa1 and OC. The expression profile of

genes encoding adipose markers were down-regulated during the osteogenic conversion compared with HAm cultured in AM (Fig. 7AB), while the osteoblastic markers were, in general, up-regulated (Fig. 7CD). Seven days after adding OM, ΔFosB-transgenic microtissues showed a two-fold decrease in PPARγ; on the other hand the Cbfa1 transcription factor increased 180-fold, indicating a superior osteogenic activity than adipogenic (Fig. 7AC). The expression profile of the lipoprotein lipase and osteocalcin supported this showing seven-fold decrease and an increase of six-fold, respectively (Fig. 7BD). Furthermore, Cbfa1 mRNA levels were up-regulated up to four times higher (OM and BMP-2+ΔFosB) as early as one day after adding OM (two days after lentiviral transduction) followed by a sharp increase in expression on day 7 of up to 180-fold (ΔFosB) and 32-fold (BMP-2+ΔFosB) (Fig. 7C), consistent with the increase of osteocalcin levels that were up to six times higher (ΔFosB and BMP-2+ΔFosB) (Fig. 7D). After a week in culture the Cbfa1 levels decreased considerably, causing a reduction in the expression of the osteocalcin gene (Fig. 7CD). Down-regulation of PPARγ was up to eight times higher in BMP-2-transduced microtissues after one month in culture (Fig. 7A), while levels of LPL expression were down-regulated by a factor of 8 in ΔFosB-transduced microtissues (Fig. 7B).

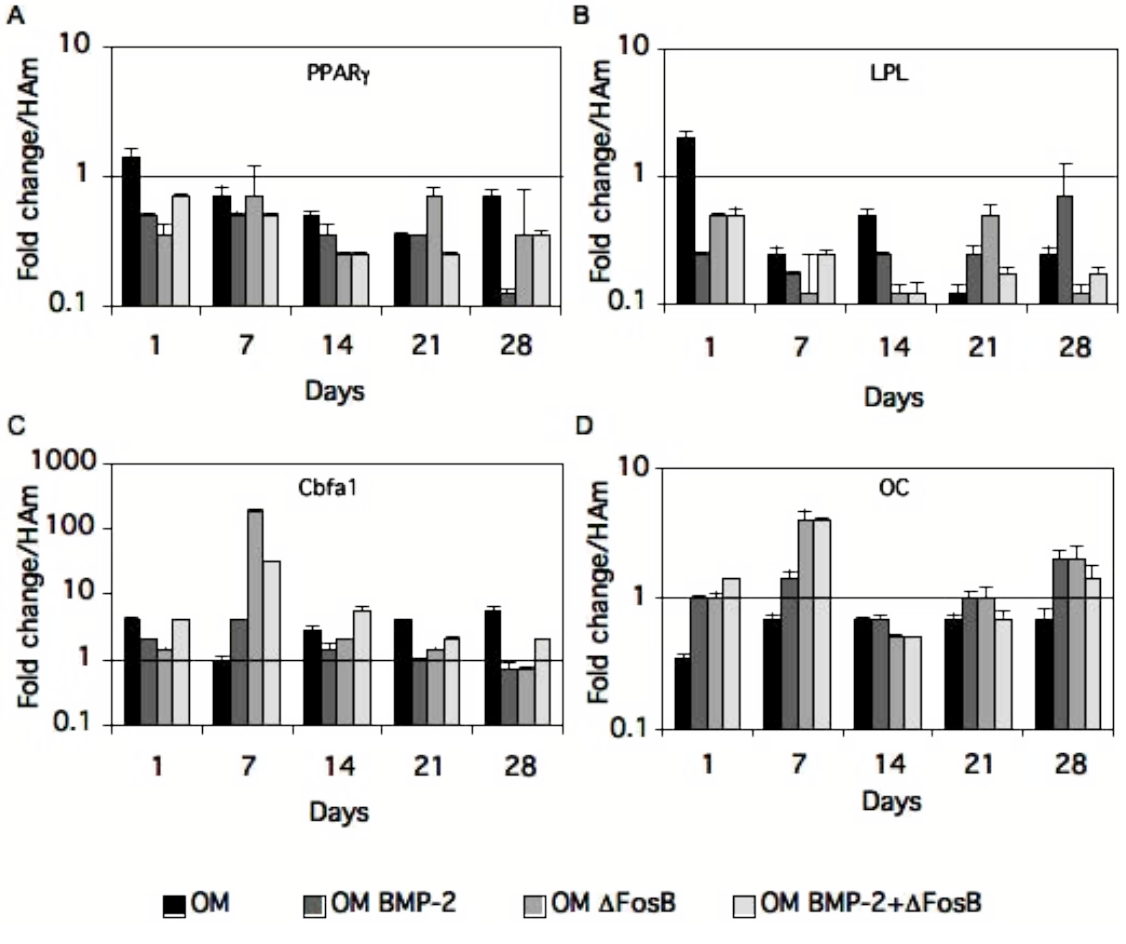

Figure 7: Gene expression profiling during the transdifferentiation process. (A) PPARγ (peroxisome proliferator activated receptor γ), (B) LPL (lipoprotein lipase), (C) Cbfa1 (core-binding factor-1), and (D) OC (osteocalcin) mRNA levels were quantified over the cultivation time by qRT-PCR. mRNA levels are expressed relative to HAm at the equivalent time points with endogenous 18s rRNA used to normalize samples.

Morphological conversion from human adipose-like to osteo-like microtissues

To demonstrate that adipose-like microtissues convert their ECM into a bone-like matrix, we examined the expression of the osteoblast-specific ECM protein osteopontin (also referred to as bone sialoprotein) and osteocalcin, a determinant of bone formation [29, 41] (Fig. 8). Furthermore, collagen type I, the main component of bone extracellular matrix [14, 42], was also assessed (Fig. 9). Detailed analysis of osteopontin, osteocalcin and collagen type I by 3D projection imaging of z-stacks taken with a confocal laser scanning microscope revealed the capability of transgenic BMP-2+ΔFosB-transduced HAm, cultivated for 21 days in OM, to convert even the extracellular matrix environment to an osteoblastic phenotype. All four transduction combinations (OM, OM BMP-2, OM ΔFosB, and OM BMP-2+ΔFosB) showed an increase in osteogenic markers over time. Interestingly, during the first week minute amounts of osteocalcin protein were localized in the basement of lipid droplets (Fig. 8A-D) but none were found in mature HAm (Fig 8J). High production of osteopontin was observed after three weeks in all combinations (OM, OM BMP-2, OM ΔFosB, and OM BMP-2+ΔFosB), whereas osteocalcin production was only enhanced in transgenic microtissues (OM BMP-2, OM ΔFosB, and OM BMP-2+ΔFosB) (Fig. 8E-H) and in HOm (Fig. 8K).

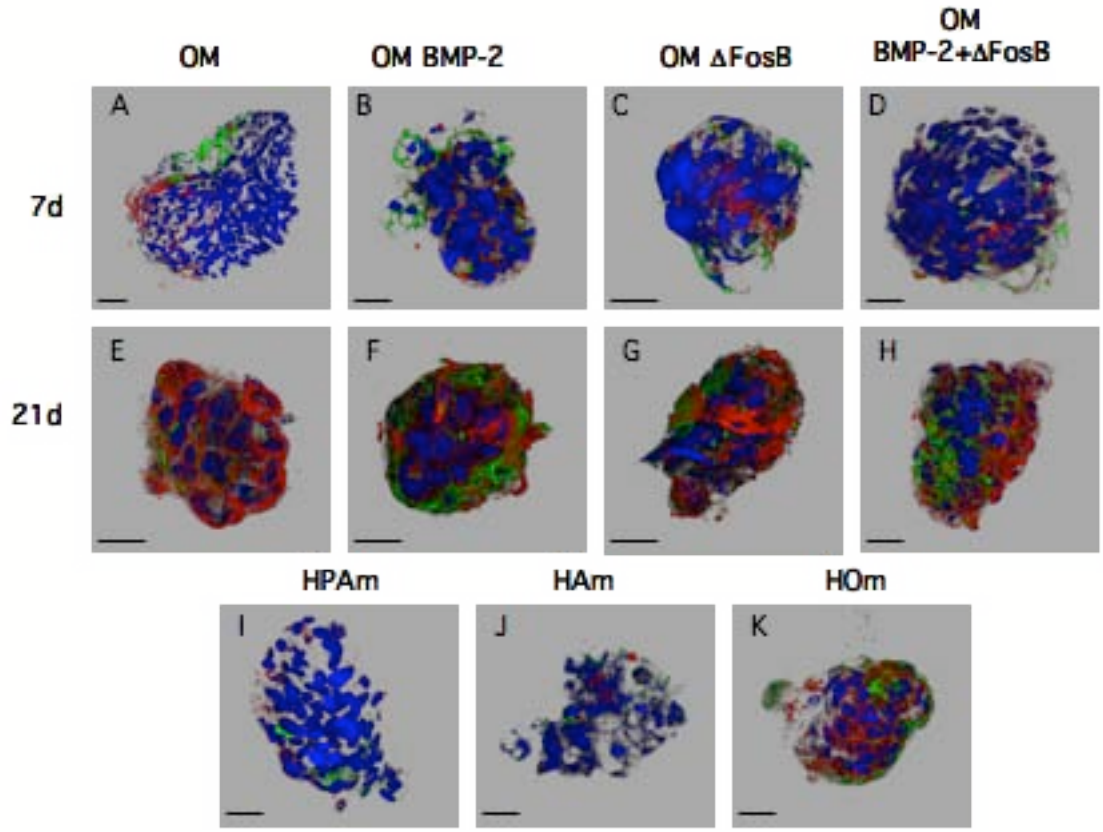

Figure 8: (A-K) Immunofluorescence-based characterization of HAm produced by gravity-enforced self-assembly and induced to transdifferentiate into osteoblast-like microtissues for (A-D) 7 and (E-H) 21 days in OM. Non-transduced HAm cultured in OM for (A) 7 and (E) 21 days. Lentivirus-transduced HAm cultivated in OM for (B-D) 7 and (F-H) 21 days. (I) Non-transduced HPAm cultured in DMEM media for seven days. (J) Non-transduced HAm cultured in AM for 14 days. (K) HOm cultured in OM for 14 days. Osteoblast-specific extracellular matrix proteins were visualized by immunohistologic staining specific for osteopontin (red) and osteocalcin (green). Nuclei were stained with 4',6-diamidino-2-phenylindole (DAPI, blue). (I) Negative controls are represented by HPAm and (J) HAm microtissues. (K) Human osteoblast microtissues are shown as the positive control. (scalebar = 100 μm).

In contrast, collagen type I was highly expressed in HOm [31] (Fig. 9K) but less so in BMP-2+ΔFosB-transgenic microtissues after cultivation for 21 days in OM (Fig. 9H), suggesting that three weeks after initiation of the transdifferentiation process, the adaptation of the ECM to bone-like matrix was still incomplete. Collagen type I production was shown to be less significant among OM, OM BMP-2, and OM ΔFosB microtissues after 21 days in OM (Fig. 9E-G) as well as during the first week of culture

(Fig. 9A-D). A considerable amount of collagen type I was observed in the ECM of HPAm (Fig. 9I), but none was found in HAm (Fig. 9J).

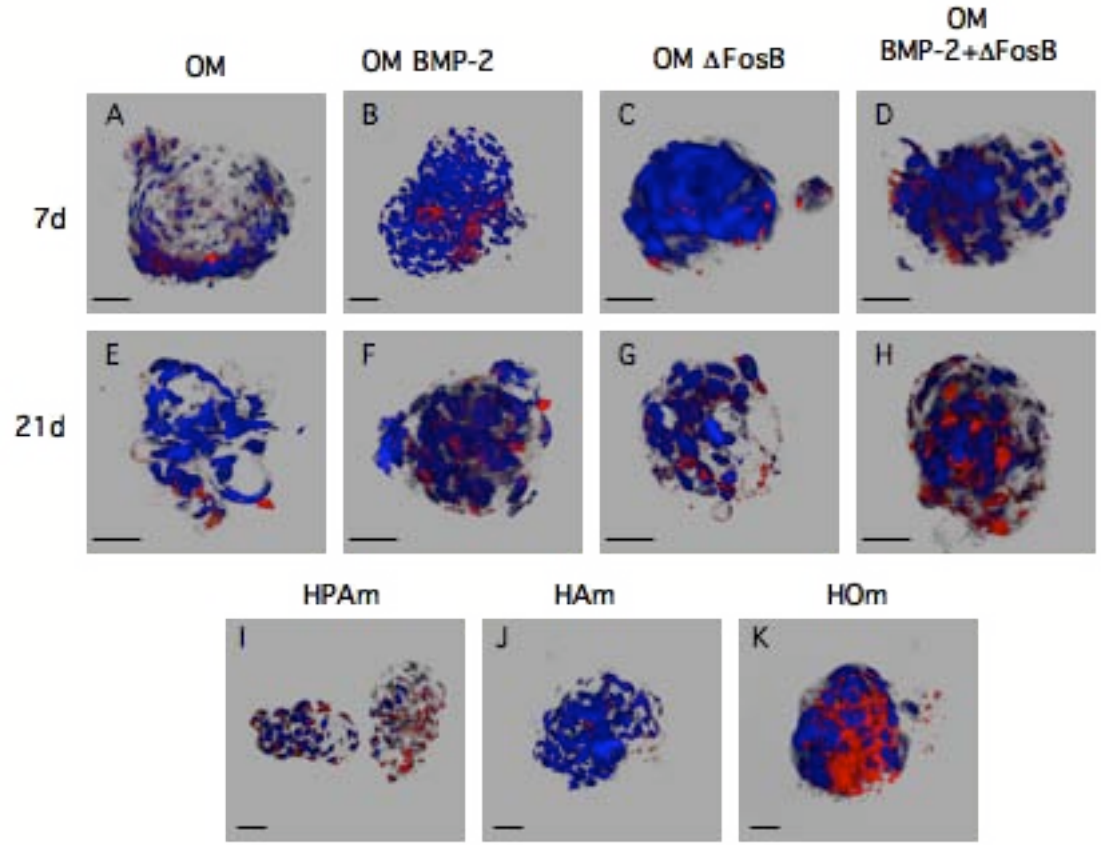

Figure 9: Three-dimensional confocal micrograph projection of HAm induced to transdifferentiate into osteoblast-like microtissues for (A-D) 7 and for (E-H) 21 days in OM. Non-transduced HAm cultured in OM for (A) 7 and (E) 21 days. Lentivirus-transduced HAm cultivated in OM for (B-D) 7 and (E-H) 21 days. (I) Non-transduced HPAm cultured in DMEM for seven days. (J) Non-transduced HAm cultured in AM for 14 days. (K) HOm cultured in OM for 14 days. Osteoblast-specific collagenous matrix was visualized by immunohistologic staining specific for collagen type I (red). Nuclei were stained with 4',6-diamidino-2-phenylindole (DAPI, blue). (scalebar = 100 μm)

Calcium mineralization rate during the transdifferentiation process of adipose-like to osteo-like microtissues

Osteoblast-specific function is characterized by incorporation of calcium during bone maturation, which results in matrix mineralization [14, 31]. Therefore we examined the incorporation of radioactive-labeled calcium (Ca-45) over 28 days in culture normalized

to HAm. A significant increase was observed during the first week in culture (Fig. 10A). Calcium incorporation in BMP-2+ΔFosB-transduced microtissues increased during another 14 days in culture. However, after one month, mineralization was slightly reduced, which could be attributed to a decline in cellular viability (Fig. 10A). ΔFosB- and BMP-2+ΔFosB-transduced microtissues exhibited a 10-fold increase in Ca-45 uptake after three-weeks in culture. BMP-2-transduced and non-transduced microtissues presented a similar, five-fold increase, demonstrating only a minor effect of osteogenesis when BMP-2 is expressed alone in the cells. Light microscopy images already demonstrated a morphological transformation from HAm to HOm (Fig. 10B-G). Osteoblast-mediated mineralized calcium deposition, referred to as bone nodule formation, was observed in BMP-2+ΔFosB-transduced microtissues (Fig. 10F) as well as in HOm (Fig. 10G) [43].

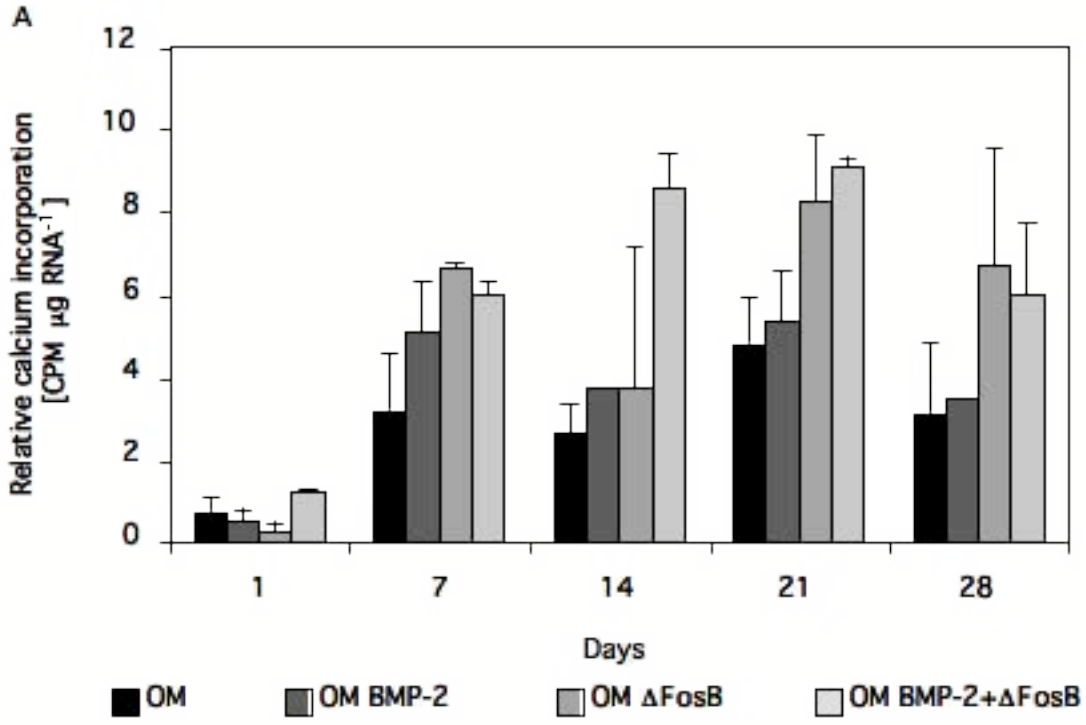

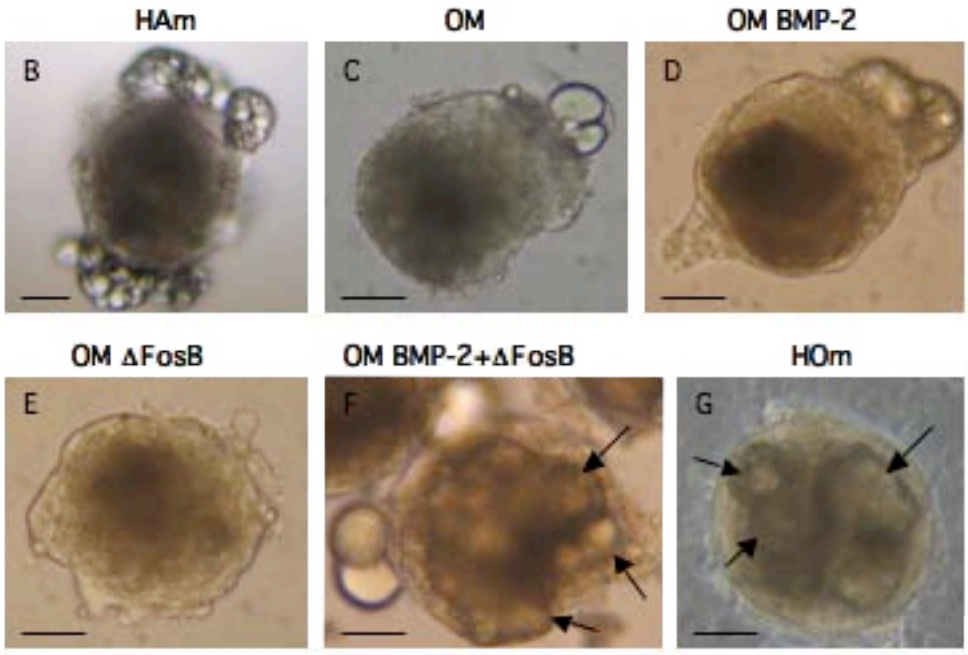

Figure 10: Mineralization quantification of HAm induced to transdifferentiate into osteoblast-like microtissues. (A) Uptake of radioactively labeled calcium (Ca-45) was determined over time in non-transduced and transduced microtissues with lentiviral particles encoding BMP-2 and/or ΔFosB. Ca-45 concentration was measured for 10min and all values were normalized by RNA tissue concentration. The results depict CPM (counts per minute) relative to HAm cultured in AM. Morphological characterization of HAm cultured (B) in AM for 21 days , (C) non-transduced microtissues cultured in OM for 21 days , (C-F) transduced-microtissues (OM BMP-2, OM ΔFosB and OM BMP-2+ΔFosB) cultured in OM for 21 days and (G) HOm cultured in OM for 14 days. Visualization of mineralized bone-like nodule formation (arrows) in (F) BMP-2+ΔFosB-transduced microtissues , similar to (G) the positive control represented by osteoblast-forming microtissues (HOm, G).

Ultrastructural analysis of BMP-2+ΔFosB-transduced microtissues (Fig. 11A) demonstrated bone nodule formation (BN) (Fig. 11B). Bone nodules are surrounded by high number of mitochondria, which supports the energy demanding process required for a transdifferentiation process [43] (Fig. 11B). Remaining lipid droplets showed more unsaturated fatty acid content (grey color) due to their maturation (asterisk, Fig. 11A). A mineralization front can be appreciated (arrows, Fig. 11A) which indicates microspicules (MSp) development [31] (Fig. 11C) and collagen-like fibers formation suggesting the development of a bone-like ECM [44] (Fig. 11D).

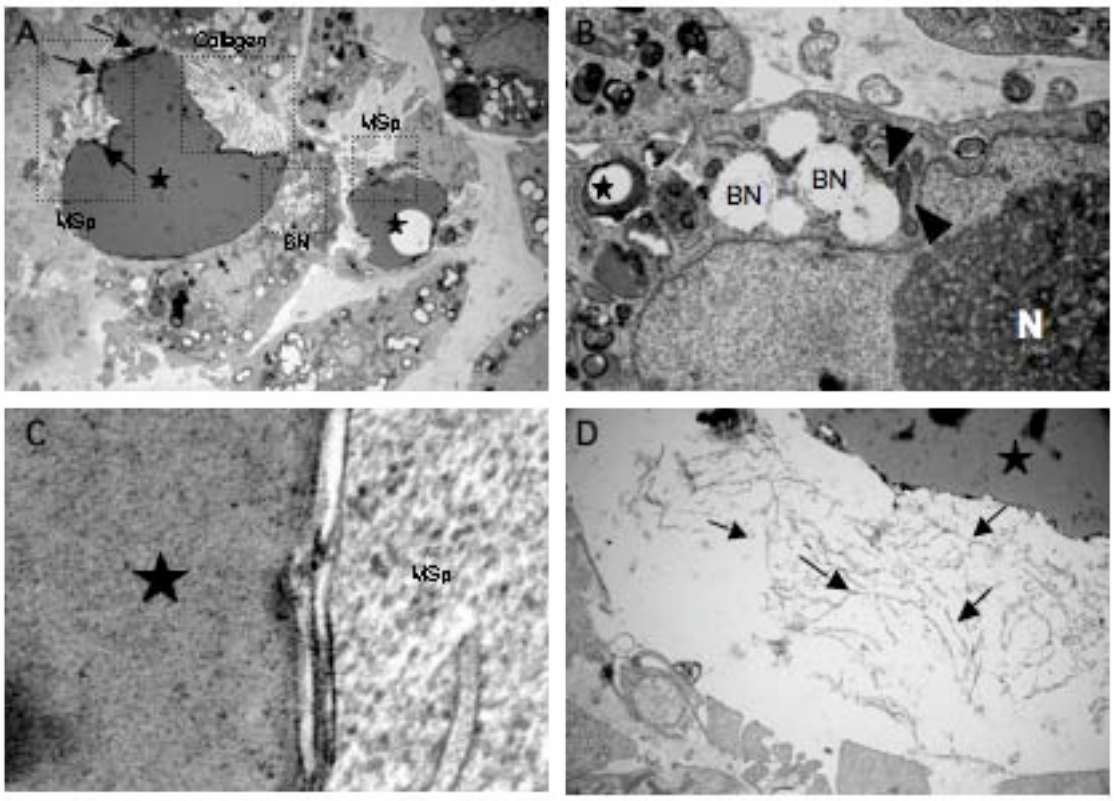

Figure 11: Ultrastructural analysis of BMP-2+ΔFosB-transduced microtissues cultivated for 21 days in OM. (A) Transmission electron micrographs reveal an hybrid tissue, where remaining lipid droplets (asterisks) and osteoblast-specific structures (boxes) are present. Microspicules mineralization front (arrows). Magnification ×7,200. (B) Bone nodule (BN) formation and lipid droplets (asterisk) surrounded by a high number of mitochondria (arrowhead). Magnification ×20,000. (C) Microspicules (MSp) (crystalline structures) surrounding a lipid droplet (asterisk). Magnification ×42,000. (D) Collagen-like fibers. Magnification ×13,600.

In order to assess the time dependency of the transdifferentiation potential of engineered HAm, microtissues were cotransduced with pBP253- and pCD4-derived lentiviral particles after 7, 14 and 21 days of cultivation in AM. After another 21 days of cultivation in OM, analysis of mineralization by Calcein blue staining and adipogenesis by Nile red staining revealed that the ability of BMP-2- and ΔFosB-induced transdifferenetiation was independent of the time point of adipogenic maturation. BMP-2+ΔFosB-transduced microtissues showed higher matrix mineralization and lower lipid formation than non-transduced microtissues whether transduced at days 7, 14 or 21 of adipocyte differentiation (Fig. 12). In some instances, the mineralized matrix was

covering the lipid vesicles (Fig. 12DHL), thereby reducing the size of the the fat droplets (Fig. 12L).

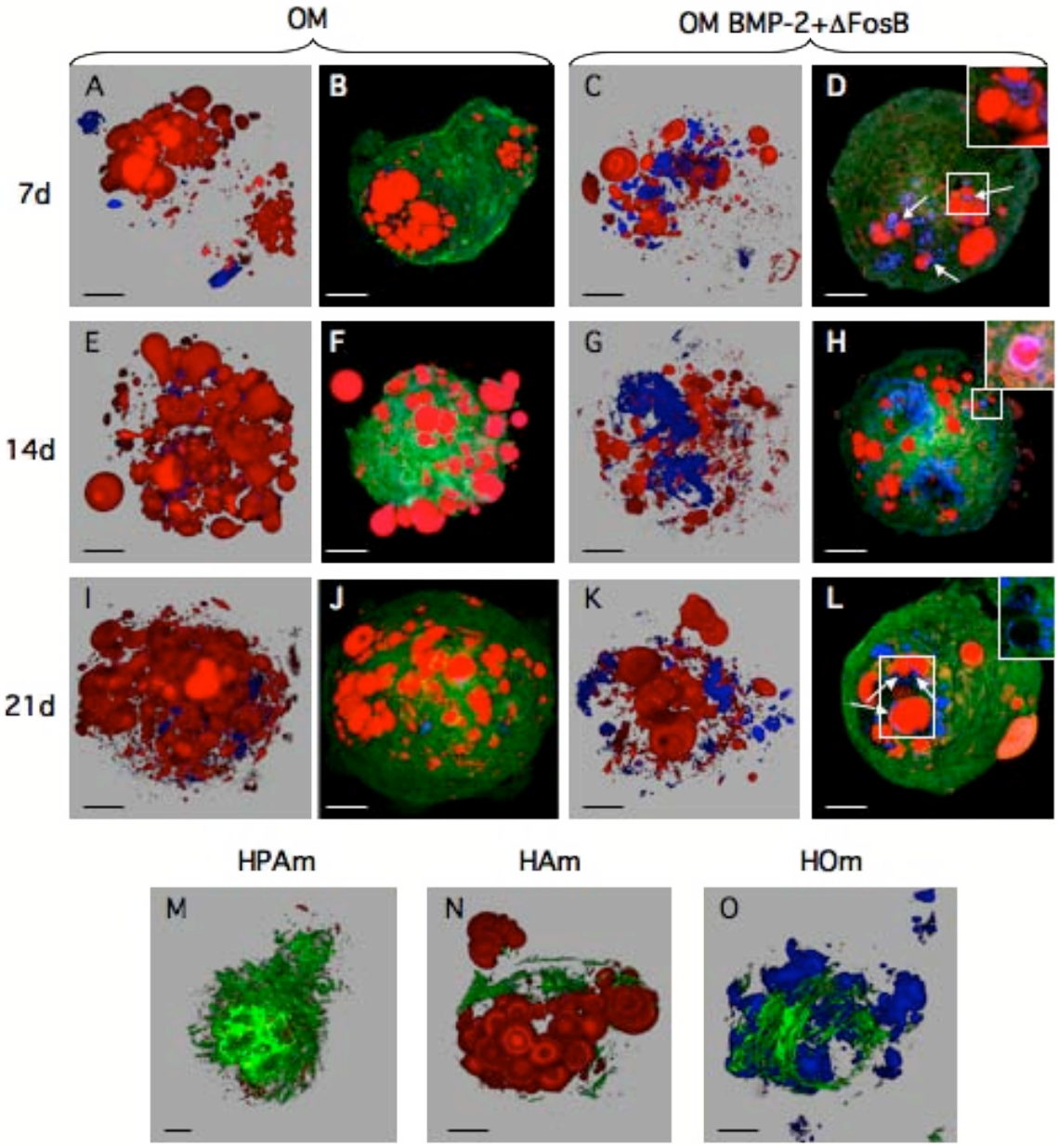

Figure 12: Time dependence studies of the trandifferentiation capacity of (A-D) 7-, (E-H) 14-, (I-L) 21-day-old HAm (AB,EF and IJ) non-transduced and (CD, GH, KL) transduced with BMP-2- and ΔFosB-derived lentiviral particles. (A, C, E, G, I and K) Three-dimensional (B, D, F, H, J and L) and sections of confocal micrographs showing matrix mineralization (Calcein blue; blue), lipid droplets (Nile red; red) and cytoskeleton (F-actin, green). Colocalization of Calcein blue and Nile red (arrows). (M) HPAm and (N) HAm cultivated for 21 and (O) HOm cultivated for 14 days (scalebar= 50 μm).

ΔFosB induces preadipopcyte factor 1 in differentiated adipocytes

In order to better characterize the hybrid cell state containing adipocyte-specific lipid droplets as well as osteblast-specific ECM structures we profiled expression of the preadipocyte factor 1 (pref-1), which was reported to be exclusively expressed in preadipocytes [45]. HAm transduced only with ΔFosB showed 350-fold higher Pref-1 expression after 7 days of transdifferation, while BMP-2 and mock-transduced microtissues did not exhibit a dramatic change in pref-1 expression levels (Fig. 13A). Pref-1-specific confocal micrographs of BMP-2+ΔFosB-transduced HAm confirmed these results (Fig. 13C-E) and showed that pref-1 co-localized with adipocyte-specific Nile red staining (Fig. 13DE). This observation suggests that adipocytes are partially de-differentiated into a hybrid adipocyte/preadipocyte cell state which is then able to also develop osteo-like structures after 21 days (Fig. 13G-I).

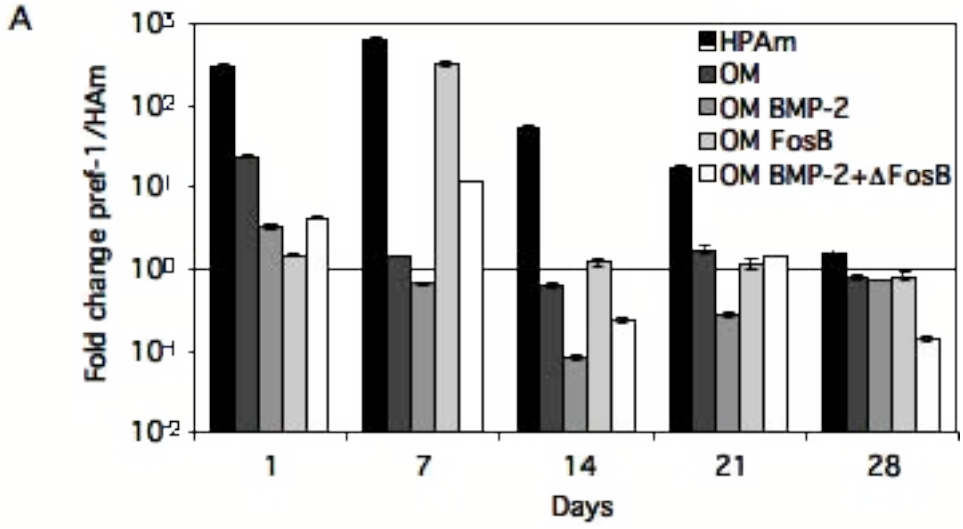

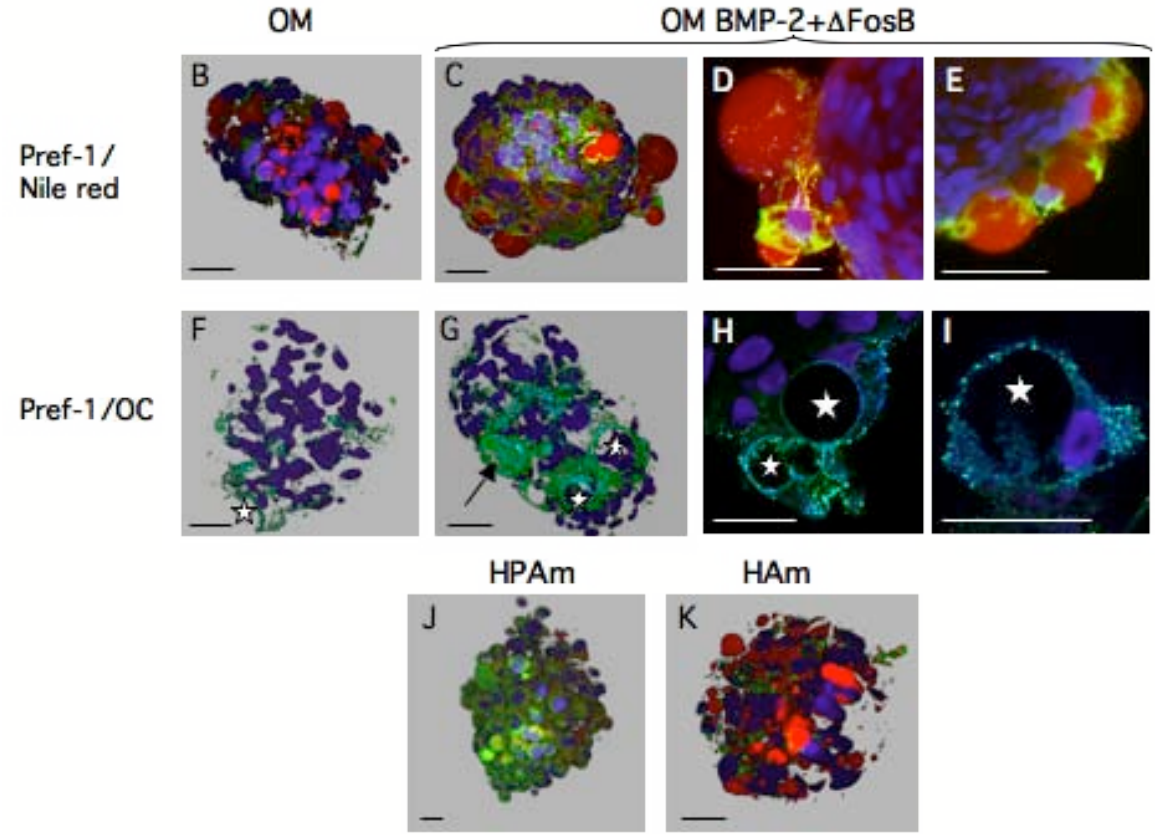

Figure 13: Expression of preadipocyte factor 1 (Pref-1) in differentiating microtissues. (A) qRT-PCR-based profiling of pref-1 in transdifferentiating HAm for up to 4 weeks. Pref-1-specific (green) immunofluorescence micrographs of (B and F) non-tranduced microtissues cultured in OM, (C-E and G-I), BMP-2+ΔFosB-transduced microtissues cultured for 21 days in OM, (J) native HPAm and (K) HAm cultivated for 7 days. (B-E) Pref-1 (green) co-stained with Nile red (red) after 7 days of transdifferentiation. (F-I) Pref-1 (green) co-stained with osteocalcin (blue) after 21 days of transdifferentiation. Lipid droplets (asterisk). (scalebar = 50 μm).

Discussion

Transdifferentiation is the conversion of a differentiated cell type into another mature differentiated cell type. Transdifferentiation is a rare natural event as exemplified by the transdifferentiation of iris cells into lens cells in salamander [46]. *In-vitro* studies have also established the potential of pancreatic AR42J-B13 cells to transdifferentiate into hepatocytes [47] and *vice versa* [48]. Furthermore, mesenchymal cells (MCS), which have started to differentiate into a particular lineage could transdifferentiate into another

mesenchymal lineage, such as myoblasts into adipocytes [49] or osteoblasts into adipocytes [50]. Of particular interest is the transdifferentiation of adipocytes into osteoblasts, which has a potential impact on a number of age-associated diseases, such as osteoporosis [8, 9, 51].

3D cell culture models, which present a platform for studying the molecular signals and the morphogenetic conversion involved in metaplasia, offer new opportunities to evaluate transdifferentiation processes. It is known that the immediate microenvironment and three-dimensional organization are important factors during differentiation in general and, in particular, in osteogenic differentiation, where they produce most of the proteins of the extracellular matrix (ECM) and thus control mineralization [31, 52]. Mesenchymal stem cells differentiate and transdifferentiate in response to changes in the microenvironment and to signals in the ECM [53]. Critically, this matrix is reduced and modified when cells are cultivated in conventional two-dimensional cultures [19, 20]. Furthermore, the ECM plays a crucial role not only during skeletal development, but also in the differentiation of adipose tissue [21]. Therefore, 3D cell culture systems may provide further insight into differentiation and transdifferentiation processes of these connective-tissue cells.

Since terminally differentiated adipocytes float ontop of any cell culture media they are unable to self-assemble into microtissues in hanging drops. However, monodispersed human primary preadipocyte cells, which aggregate into spheroids by gravity-enforced self-assembly in hanging-drops, develop into coherent fat-like tissue *in vitro*, thus indicating that microtissues could be a viable alternative for adipogenic-related studies. 65% of the preadipocytes embedded in the microtissues were able to terminally differentiate into mature fat cells while the rest of the preadipocytes, most of which were located in the core of the microtissue with limited access to differentation inducers, remained uncommitted. Therefore, HAm replicate a more realistic differentiation scenario compared to 2D cultures since they consist of (i) a core feeder microtissue formed by preadipocytes (fibroblasts-like cells) and (ii) a peripheral cell layer/s consisting of multilocular and unilocular adipocytes. 2D cultures lack such mature unilocular adipocytes, most probably because of a reduction of the level of proteins needed for fusion of lipid vacuoles in standard cultures [10]. Consequently, we have made use of differentiated HAm transduced with lentiviral vectors encoding BMP-2 (bone

morphogenetic protein 2) or ΔFosB (alternatively spliced form of the FosB transcript) together with a specific osteo-inductive media, in order to induce transdifferentiation from HAm to osteoblast-like microtissues. This resulted in the formation of bone-like microtissues, which was most successful when ΔFosB was expressed together with BMP-2. This establishes that ΔFosB, the truncated version of the FosB gene, is a promising candidate for osteogenic conversion of adipocytes which is consistent with its known ability to induce osteoblast maturation and to inhibit adipogenesis in transgenic mice [27, 30, 54]. After seven days in OM, ΔFosB-transduced microtissues already exhibited up to a six-fold increase in calcium content, which was not enhanced by the addition of BMP-2. Accordingly, Cbfa1 mRNA levels were up-regulated 180x after one week under osteogenic conditions, which correlated with the higher osteocalcin mRNA levels. Neither of these markers was enhanced in BMP-2 overexpressing adipocytes. In addition, one week after osteogenic-induction, the lipid content was visibly lower in ΔFosB and BMP-2+ΔFosB-transduced microtissues compared with mock and BMP-2-transduced microtissues, signifying a negative adipogenic effect of ΔFosB. Quantification of lipid content by oil red O dye extraction and of a preadipocyte marker (pref-1) by qRT-PCR confirmed these observations, suggesting that adipocytes de-differentiate and then differentiate towards the osteogenic lineage as previously confirmed by Justesen et.al. [10]. However, confocal microscopy of pref-1 on BMP-2+ΔFosB-transduced microtissues indicated a "partial" de-differentiation since pref-1-expressing cells retained adipocyte-specific Nile red staining. Therefore, whether adipocyte-forming microtissues must "completely" de-differentiate (de-lipidate) in order to be able to switch cell type or whether they traverse an intermediate hybrid state on their way to an osteogenic phenotype remains elusive. Transmission electron microscopy (TEM) and confocal microscopy reveals a hybrid phenotype in which fat droplets and osteoblast-specific markers co-exist in the adipocyte/osteoblast. Such a hybrid phenotype could be induced at any time of adipose-like microtissue maturation, suggesting that the ΔFosB-transdifferentation capacity might be independent of adipogenic maturation state. These cells transform their extracellular matrix into a bone-like ECM, suggesting a direct conversion of adipocytes to osteoblasts. However, confocal microscopy also reveals co-localization of pref-1 with lipid droplets and osteocalcin, which indicates that transgenic

HAm partially de-differentiate into a pref-1-expressing state while retaining adipocyte-specific phenotype and subsequently adopting a bone-like extracellular matrix.

As shown by Alizarin red extraction, transgenic microtissues for BMP2 and ΔFosB incorporated similar amounts of dye as human primary osteoblast-composed microtissues (HOm) after cultivation for three weeks in OM medium. This suggests a similar degree of differentiation capacity of transgenic adipocytes and native osteoblasts. ΔFosB expression was also shown to enhance the expression of osteopontin and osteocalcin, the most common non-collagenous proteins of the bone ECM synthesized only by osteoblasts. The presence of osteocalcin appears to be in direct proportion to the calcification process, being located in the area of mineralization [55]. Levels of osteopontin and osteocalcin in the transdifferentiated microtissues were comparable or even higher than in osteoblast-derived microtissues (HOm). After three weeks under osteogenesis-promoting conditions, BMP-2 alone substantially increased osteocalcin expression, which however was not correlating with an increase in calcium mineralization (calcium incorporation), as previously reported by Ducy et al., where an increase of the bone function was found in osteocalcin-deficient mice [29]. Bone ECM is essentially a collagenous matrix, in which the main component is collagen type I [14]. Collagen type I is synthesized by osteoblasts as well as by fibroblasts, although only in bone tissue collagen is mineralized. HOm showed a very rich collagen type I and mineralized matrix, which was not found in transdifferentiated microtissues, suggesting that the previous tests (alizarin red, RT-PCR, and calcium incorporation rate) did not necessarily provide conclusive evidence of morphogenetic transformation. Careful characterization of the ECM is required in transdifferentiation studies. BMP-2+ΔFosB-transduced microtissues illustrated elevated production of collagen type I compared to BMP-2- or ΔFosB-transduced microtissues, signifying that the ability of BMP-2 to induce the formation of osteoblast-specific ECM depends on the presence of other signaling molecules [16] such as ΔFosB. ΔFosB accelerated and improved osteogenesis by increasing the formation of calcium deposits after one week, thus decreasing adipogenic activity, and enhancing matrix mineralization. We suggest that osteo-like cell phenotypes observed in 21-day-old HAm co-transduced with BMP-2- and ΔFosB-derived lentiviral particles may originate either from uncommitted cells (about 50% at day 7 after transduction) directly

differentiating into osteoblasts [11] or partially de-differentiated adipocytes which traverse a hybrid cell state characterized by increased Pref-1 expression and reduced lipid droplet content and eventually develop osteo-specific markers. This does not exclude that some adipocytes may not attain an osteo-like cell phenotype as previously suggested [56].

The ability of engineering cell fate using 3D cell culture models will foster important advances in the understanding of age-related diseases and in the development of regenerative therapies. We were able to show for the first time that differentiated transgenic adipocytes transform their ECM into a bone-like matrix, thereby displaying a hybrid adipocyte/preadipocyte/osteoblast cell phenotype. These results suggested that ΔFosB partially de-differentiates adipocytes into a Pref-1-expressing preadipocyte-like cell phenotype which is sensitive to subsequent ΔFosB- and BMP-2-mediated bone-like differentiation. Therefore, we provide the first evidence that ΔFosB is a transcriptional regulator critical for the commitment of tissues of mesenchymal origin. In addition, we have demonstrated that ECM characterization is required for the in-depth study of functional and morphogenetic tissue-specific properties, thus presenting 3D culture as a key tool to monitor transdifferentiation processes and to gain new insight into processes controlling metaplasia.

Acknowledgments

We thank David Greber for critical comments on the manuscript, Rulsan Hlushchuck for preparation of TEM micrographs and Sonja Hemmi (University Hospital, Zurich) for technical support. This work was supported by the Swiss National Science foundation (grant no. 3100A0-112549), The EC Framework 7 (COBIOS) and Cistronics Cell Technology GmbH, Einsteinstrasse 1-5, P.O.B 145, CH-8093 Zurich, Switzerland.

References

1. Zuk, P.A., Zhu, M., Ashjian, P., De Ugarte, D.A., Huang, J.I., Mizuno, H., Alfonso, Z.C., Fraser, J.K., Benhaim, P. and Hedrick, M.H. Human adipose tissue is a source of multipotent stem cells. Molecular biology of the cell **13**, 4279, 2002.
2. Muschler, G.F., Nakamoto, C. and Griffith, L.G. Engineering principles of clinical cell-based tissue engineering. J Bone Joint Surg Am **86-A**, 1541, 2004.

3. Brey, E.M. and Patrick, C.W., Jr. Tissue engineering applied to reconstructive surgery. IEEE Eng Med Biol Mag **19**, 122, 2000.
4. Hazen, S.A., Rowe, W.A. and Lynch, C.J. Monolayer cell culture of freshly isolated adipocytes using extracellular basement membrane components. Journal of lipid research **36**, 868, 1995.
5. Gomillion, C.T. and Burg, K.J. Stem cells and adipose tissue engineering. Biomaterials **27**, 6052, 2006.
6. Pittenger, M.F., Mackay, A.M., Beck, S.C., Jaiswal, R.K., Douglas, R., Mosca, J.D., Moorman, M.A., Simonetti, D.W., Craig, S. and Marshak, D.R. Multilineage potential of adult human mesenchymal stem cells. Science **284**, 143, 1999.
7. Beresford, J.N., Bennett, J.H., Devlin, C., Leboy, P.S. and Owen, M.E. Evidence for an inverse relationship between the differentiation of adipocytic and osteogenic cells in rat marrow stromal cell cultures. J Cell Sci **102 (Pt 2)**, 341, 1992.
8. Gimble, J.M., Zvonic, S., Floyd, Z.E., Kassem, M. and Nuttall, M.E. Playing with bone and fat. J Cell Biochem **98**, 251, 2006.
9. Rosen, C.J. and Bouxsein, M.L. Mechanisms of disease: is osteoporosis the obesity of bone? Nat Clin Pract Rheumatol **2**, 35, 2006.
10. Justesen, J., Pedersen, S.B., Stenderup, K. and Kassem, M. Subcutaneous adipocytes can differentiate into bone-forming cells in vitro and in vivo. Tissue Eng **10**, 381, 2004.
12. Park, S.R., Oreffo, R.O. and Triffitt, J.T. Interconversion potential of cloned human marrow adipocytes in vitro. Bone **24**, 549, 1999.
13. Rosen, E.D. and Spiegelman, B.M. Molecular regulation of adipogenesis. Annu Rev Cell Dev Biol **16**, 145, 2000.
14. Wagner, E.F. and Karsenty, G. Genetic control of skeletal development. Curr Opin Genet Dev **11**, 527, 2001.
15. Tontonoz, P., Hu, E. and Spiegelman, B.M. Stimulation of adipogenesis in fibroblasts by PPAR gamma 2, a lipid-activated transcription factor. Cell **79**, 1147, 1994.
16. Rosen, E.D. and MacDougald, O.A. Adipocyte differentiation from the inside out. Nat Rev Mol Cell Biol **7**, 885, 2006.
17. Ducy, P., Zhang, R., Geoffroy, V., Ridall, A.L. and Karsenty, G. Osf2/Cbfa1: a transcriptional activator of osteoblast differentiation. Cell **89**, 747, 1997.
18. Birk, R.Z., Abramovitch-Gottlib, L., Margalit, I., Aviv, M., Forti, E., Geresh, S. and Vago, R. Conversion of adipogenic to osteogenic phenotype using crystalline porous biomatrices of marine origin. Tissue Eng **12**, 21, 2006.
19. Abbott, A. Cell culture: biology's new dimension. Nature **424**, 870, 2003.
20. Zhang, S. Beyond the Petri dish. Nat Biotechnol **22**, 151, 2004.
21. Boudreau, N. and Weaver, V. Forcing the third dimension. Cell **125**, 429, 2006.
22. Chun, T.H., Hotary, K.B., Sabeh, F., Saltiel, A.R., Allen, E.D. and Weiss, S.J. A pericellular collagenase directs the 3-dimensional development of white adipose tissue. Cell **125**, 577, 2006.
23. Vogel, V. and Sheetz, M. Local force and geometry sensing regulate cell functions. Nat Rev Mol Cell Biol **7**, 265, 2006.

24. Kang, X., Xie, Y. and Kniss, D.A. Adipose tissue model using three-dimensional cultivation of preadipocytes seeded onto fibrous polymer scaffolds. Tissue Eng **11**, 458, 2005.
25. Service, R.F. Tissue engineers build new bone. Science **289**, 1498, 2000.
26. Georges, P.C. and Janmey, P.A. Cell type-specific response to growth on soft materials. J Appl Physiol **98**, 1547, 2005.
27. Sabatakos, G., Sims, N.A., Chen, J., Aoki, K., Kelz, M.B., Amling, M., Bouali, Y., Mukhopadhyay, K., Ford, K., Nestler, E.J. and Baron, R. Overexpression of DeltaFosB transcription factor(s) increases bone formation and inhibits adipogenesis. Nature medicine **6**, 985, 2000.
28. Heldin, C.H., Miyazono, K. and ten Dijke, P. TGF-beta signalling from cell membrane to nucleus through SMAD proteins. Nature **390**, 465, 1997.
29. Ducy, P., Schinke, T. and Karsenty, G. The osteoblast: a sophisticated fibroblast under central surveillance. Science **289**, 1501, 2000.
30. Kveiborg, M., Sabatakos, G., Chiusaroli, R., Wu, M., Philbrick, W.M., Horne, W.C. and Baron, R. DeltaFosB induces osteosclerosis and decreases adipogenesis by two independent cell-autonomous mechanisms. Molecular and cellular biology **24**, 2820, 2004.
31. Kale, S., Biermann, S., Edwards, C., Tarnowski, C., Morris, M. and Long, M.W. Three-dimensional cellular development is essential for ex vivo formation of human bone. Nat Biotechnol **18**, 954, 2000.
32. Ulery, P.G., Rudenko, G. and Nestler, E.J. Regulation of DeltaFosB stability by phosphorylation. J Neurosci **26**, 5131, 2006.
33. Mitta, B., Rimann, M., Ehrengruber, M.U., Ehrbar, M., Djonov, V., Kelm, J. and Fussenegger, M. Advanced modular self-inactivating lentiviral expression vectors for multigene interventions in mammalian cells and in vivo transduction. Nucleic Acids Res **30**, e113, 2002.
34. Mitta, B., Rimann, M. and Fussenegger, M. Detailed design and comparative analysis of protocols for optimized production of high-performance HIV-1-derived lentiviral particles. Metabolic engineering **7**, 426, 2005.
35. Fux, C., Mitta, B., Kramer, B.P. and Fussenegger, M. Dual-regulated expression of C/EBP-alpha and BMP-2 enables differential differentiation of C2C12 cells into adipocytes and osteoblasts. Nucleic Acids Res **32**, e1, 2004.
36. Gregory, C.A., Gunn, W.G., Peister, A. and Prockop, D.J. An Alizarin red-based assay of mineralization by adherent cells in culture: comparison with cetylpyridinium chloride extraction. Anal Biochem **329**, 77, 2004.
37. Stanford, C.M., Jacobson, P.A., Eanes, E.D., Lembke, L.A. and Midura, R.J. Rapidly forming apatitic mineral in an osteoblastic cell line (UMR 106-01 BSP). J Biol Chem **270**, 9420, 1995.
38. Sanchez-Bustamante, C.D., Kelm, J.M., Mitta, B. and Fussenegger, M. Heterologous protein production capacity of mammalian cells cultivated as monolayers and microtissues. Biotechnol Bioeng **93**, 169, 2006.
39. Djonov, V., Schmid, M., Tschanz, S.A. and Burri, P.H. Intussusceptive angiogenesis: its role in embryonic vascular network formation. Circulation research **86**, 286, 2000.

40. Enerback, S., Ohlsson, B.G., Samuelsson, L. and Bjursell, G. Characterization of the human lipoprotein lipase (LPL) promoter: evidence of two cis-regulatory regions, LP-alpha and LP-beta, of importance for the differentiation-linked induction of the LPL gene during adipogenesis. Molecular and cellular biology **12**, 4622, 1992.
41. Olsen, B.R., Reginato, A.M. and Wang, W. Bone development. Annu Rev Cell Dev Biol **16**, 191, 2000.
42. Yang, X.B., Bhatnagar, R.S., Li, S. and Oreffo, R.O. Biomimetic collagen scaffolds for human bone cell growth and differentiation. Tissue Eng **10**, 1148, 2004.
43. Chaudhry, G.R., Yao, D., Smith, A. and Hussain, A. Osteogenic Cells Derived From Embryonic Stem Cells Produced Bone Nodules in Three-Dimensional Scaffolds. Journal of biomedicine & biotechnology **2004**, 203, 2004.
44. Barragan-Adjemian, C., Nicolella, D., Dusevich, V., Dallas, M.R., Eick, J.D. and Bonewald, L.F. Mechanism by which MLO-A5 late osteoblasts/early osteocytes mineralize in culture: similarities with mineralization of lamellar bone. Calcified tissue international **79**, 340, 2006.
45. Kim, K.A., Kim, J.H., Wang, Y. and Sul, H.S. Pref-1 (preadipocyte factor 1) activates the MEK/extracellular signal-regulated kinase pathway to inhibit adipocyte differentiation. Molecular and cellular biology **27**, 2294, 2007.
46. Okada, T.S. Cellular metaplasia or transdifferentiation as a model for retinal cell differentiation. Current topics in developmental biology **16**, 349, 1980.
47. Shen, C.N., Slack, J.M. and Tosh, D. Molecular basis of transdifferentiation of pancreas to liver. Nature cell biology **2**, 879, 2000.
48. Li, W.C., Horb, M.E., Tosh, D. and Slack, J.M. In vitro transdifferentiation of hepatoma cells into functional pancreatic cells. Mechanisms of development **122**, 835, 2005.
49. Hu, E., Tontonoz, P. and Spiegelman, B.M. Transdifferentiation of myoblasts by the adipogenic transcription factors PPAR gamma and C/EBP alpha. Proc Natl Acad Sci U S A **92**, 9856, 1995.
50. Nuttall, M.E., Patton, A.J., Olivera, D.L., Nadeau, D.P. and Gowen, M. Human trabecular bone cells are able to express both osteoblastic and adipocytic phenotype: implications for osteopenic disorders. J Bone Miner Res **13**, 371, 1998.
51. Rodan, G.A. and Martin, T.J. Therapeutic approaches to bone diseases. Science **289**, 1508, 2000.
52. Petite, H., Viateau, V., Bensaid, W., Meunier, A., de Pollak, C., Bourguignon, M., Oudina, K., Sedel, L. and Guillemin, G. Tissue-engineered bone regeneration. Nat Biotechnol **18**, 959, 2000.
53. Collas, P. and Hakelien, A.M. Teaching cells new tricks. Trends Biotechnol **21**, 354, 2003.
54. Inoue, D., Kido, S. and Matsumoto, T. Transcriptional induction of FosB/DeltaFosB gene by mechanical stress in osteoblasts. J Biol Chem **279**, 49795, 2004.
55. Boivin, G., Morel, G., Lian, J.B., Anthoine-Terrier, C., Dubois, P.M. and Meunier, P.J. Localization of endogenous osteocalcin in neonatal rat bone and its

absence in articular cartilage: effect of warfarin treatment. Virchows Archiv **417**, 505, 1990.

56. Schilling, T., Noth, U., Klein-Hitpass, L., Jakob, F. and Schutze, N. Plasticity in adipogenesis and osteogenesis of human mesenchymal stem cells. Molecular and cellular endocrinology **271**, 1, 2007.

Chapter 3

Productivity of Artifical Microtissues

"Heterologous Protein Production Capacity of Mammalian Cells Cultivated as Monolayers and Microtissues"

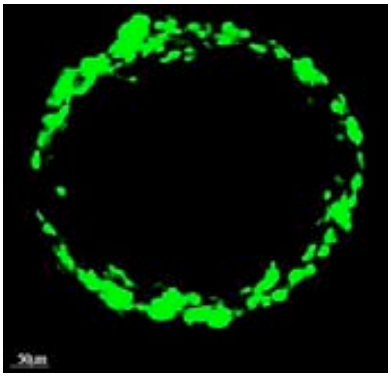

Abstract

A precise understanding of processes managing heterologous protein production *in vitro* and *in vivo* is essential for the manufacture of sophisticated biopharmaceuticals as well as for future gene therapy and tissue engineering initiatives. Capitalizing on the gravity-enforced self-assembly of monodispersed cells into coherent (multicellular) microtissues we studied heterologous protein production of microtissues and monolayers derived from cell lines and primary cells engineered/transduced for (i) constitutive, (ii) proliferation-controlled (iii) macrolide- or (iv) gas-inducible expression of the human placental secreted alkaline phosphatase (SEAP) and of the *Bacillus stearothermophilus*-derived secreted α-amylase (SAMY). Specific productivity of cells assembled in microtissues was up to 20-fold higher than isogenic monolayer cultures. Diffusion across microtissues could be further increased by HUVEC-mediated vascularization. As well as higher specific protein productivities, microtissues were also more efficient than monolayer cultures in assembling transgenic lentiviral particles. Our results showed that mammalian cells embedded in a tissue-like three-dimensional microenvironment exhibit increased production capacity. This observation should be considered for gene therapy and tissue engineering scenarios as well as for biopharmaceutical manufacturing.

Introduction

Biopharmaceutical manufacturing is the science of producing large amounts of high-quality protein pharmaceuticals [1]. Increases in production and quality have been achieved by optimizing the culture media and process parameters or by metabolic engineering of production cell lines for a higher growth rate, enhanced survival, desired glycosylation profiles and increased specific productivity [1-17]. Most of today's available biotechnologically relevant cell lines were derived from their host tissues and engineered and/or selected for indefinite attachment-dependent growth or proliferation in suspension and serum-free media [1]. As a consequence of the missing tissue-specific intercellular crosstalk, the reduction of extracellular matrix components and a poor selection for optimal proliferation, monolayer cultures of established cell lines have often lost or changed their expression profiles [18-20] for specific antigens [21-25], adhesion molecules including integrins [26, 27], cadherins [28] and dystroglycans [29], cell surface proteoglycans

receptors such as syndecans, CD44 and thrombomodulin [30], cytoskeletal components [26, 31] and the phosphorylation status of focal adhesion kinases [26, 32].

Although it is generally accepted that unrestricted proliferation of monodispersed cell lines is the key to modern biopharmaceutical manufacturing, it is intuitively clear that cells may not operate and produce at a maximum outside their tissue-specific microenvironment. Furthermore, most of the metabolic energy of proliferating cell lines is devoted to reproduction rather than to heterologous protein production. Controlled proliferation technology, enabling conditional G1-phase-specific growth arrest, was the first engineering strategy, which constrained heterologous protein production to a growth-arrested tissue-mimicking phase [2, 8, 9, 15]. Proliferation-controlled cell cultures showed up to a 30-fold increase in specific productivity [8, 33, 34]. Controlled proliferation technology exemplified that engineering strategies inspired by processes orchestrating three-dimensional (3D) cellular function may enable bioengineers to increase the performance of production cell lines [1].

To date, a variety of different three-dimensional cell culture technologies have been devised to study tissue function [35-37] as well as cancer-related pathologies and therapeutic opportunities [19, 38-43]. However, the impact of a tissue-like 3D environment on specific protein productivity has never been studied from a bioengineering perspective.

In this study we have assembled a variety of transgenic cell lines and primary cells into microtissues and provide a rigorous comparative production analysis of monolayer and microtissue cultures, engineered or transduced for constitutive or regulated product gene expression. Microtissue-based production of lentiviral particles and heterologous protein secretion from vascularized microtissues [44, 45] has also been covered. Precise production management of heterologous proteins in microtissues will foster important advances in tissue engineering, gene therapy and biopharmaceutical manufacturing.

Materials and Methods

Cell culture. Baby hamster kidney cells (BHK-21, ATCC: CCL-10), human embryonic kidney cells (HEK293-T; [46]), human hepatocellular carcinoma cells (HepG2, ATCC: HB-8056), human fibrosarcoma cells (HT-1080, ATCC: CCL-121), primary human aortic fibroblasts (HAF, [44]) and normal human dermal fibroblasts (NHDF, Cat.

No. C-12300; Lot 1070402, PromoCell, Heidelberg, Germany) were expanded in Dulbecco's modified Eagle medium (DMEM, Invitrogen, Basel, Switzerland) supplemented with 10% fetal calf serum (FCS, Cat. No. 3302-P231902, Lot No. P231902, PAN biotech GmbH, Aidenbach, Germany). Human pre-adipocytes (HPA, Cat. No. SP-F-1, BioCat GmbH, Heidelberg, Germany) were cultured in specific pre-adipocyte medium (BioCat, Cat. No. PM-1). Human umbilical vein endothelial cells (HUVEC, Cat. No. C-12200, PromoCell) were expanded using endothelial cell growth medium (Cat. No. C-22010, PromoCell) containing Supplement Mix according to the provider's protocol (Cat. No. C-39215, PromoCell). Chinese hamster ovary cells (CHO-K1, ATCC: CCL-61) were expanded in FMX-8 (Cell Culture Technologies GmbH, Zurich, Switzerland) supplemented with 5% FCS.

The culture medium of transgenic CHO-K1 derivatives was supplemented with the following transgene-selecting or -inducing antibiotics: (i) CHO-WW162 (constitutive SEAP expression driven by the SV40 promoter), 60 μg/ml puromycin (Alexis Biochemicals, Lausen, Switzerland); (ii) CHO-E_1-$SEAP_1$ (erythromycin-inducible SEAP expression) [47], 400 μg/ml G418 (Calbiochem, Darmstadt, Germany), 100 μg/ml zeocin (Invitrogen) and 2μg/ml erythromycin (Fluka, Buchs, Switzerland) for SEAP induction; (iii) $_{AIR}$CHO-SEAP (transgenic for acetaldehyde-inducible SEAP expression) [48], 400 μg/ml G418, 100 μg/ml puromycin and 50 μg/ml acetaldehyde (Fluka) to induce SEAP expression, (iv) CHO-$SS101_5$ (transgenic for tetracycline-responsive SEAP and human $p27^{Kip1}$ expression) [49] 400 μg/ml G418, 6 μg/ml puromycin and 2.5 μg/ml tetracycline (Sigma Chemicals, St. Louis, MO, USA) to repress SEAP and $p27^{Kip1}$ expression. For comparative protein production analysis, CHO-K1 and their derivatives were cultivated in FMX-8 supplemented with 10% horse serum (HS, Cat. No. 16050-122, Lot No. 3036354D, Invitrogen). Additionally, ChoMaster HP-1 media (Cell Culture Technologies GmbH) was used as a high glucose media for productivity studies of CHO-WW162. All cell culture media were supplemented with 1% penicillin/streptomycin solution (Sigma Chemicals), and the cells were cultivated at 37°C in a humid 5% CO_2-containing atmosphere.

Microtissue production. Monolayer cultures of desired cell types were trypsinized (PAN biotech GmbH) and seeded at indicated cell densities (Table I) into 60-

well plates (HLA plate, Greiner Bio-One GmbH, Frickenhausen, Germany). In order to enable gravity-enforced microtissue formation in hanging drops, the 60-well plates were incubated upside down [50]. Multicellular microtissues were generated in two steps: (i) The core feeder spheroid was produced by cultivation of NHDF for two days in hanging drops and (ii) then coated by adding of monodispersed HUVECs and cultivated for six days in hanging drops containing DMEM supplemented with 10% HuS (Human serum Typ AB, Cat. No. P30-2501, PAN biotech GmbH). Coated as well as non-coated control microtissues were harvested after eight days in culture and prepared for immunofluorescence-based analysis.

The total cell number of microtissues was quantified following disassembly in cell dissociation solution (Sigma Chemicals) for 15 min at 37°C and 1200 rpm orbital shaking (Thermomixer Comfort, Eppendorf, Hamburg, Germany) using a CASY®1 counter (Schaerfe System, Reutlingen, Germany). The number of cells per layer of microtissue was calculated assuming three different packing densities (Table II).

Table I. Transduction of different monolayer and microtissue cultures using transgenic lentiviral particles

Cell type	Origin	I_C 2D [cell/cm^2]	F_C 2D [cell/cm^2]	I_C 3D [cell/well]	F_C3D [cell/well]	$I_\varnothing$ 3D (μm)	$F_\varnothing$ 3D (μm)	Viable Cells 2D/3D %
BHK-21	Hamster	2.1×10^4	$3.1\times10^5\pm 6.3\times10^4$	1.5×10^3	$1.5\times10^3\pm 4\times10^3$	220±22	256±24	65/60
CHO-K1	Hamster	2.1×10^4	$6.6\times10^5\pm 2.7\times10^5$	1.5×10^3	$1.5\times10^4\pm 4.7\times10^4$	480±24	392±57	76/91
HEK-293T	Human	2.1×10^4	$2.1\times10^5\pm 1.8\times10^5$	1×10^3	$1.3\times10^4\pm 1.4\times10^3$	310±2	455±37	85/80
HepG2	Human	2.1×10^4	$2.4\times10^5\pm 1.1\times10^5$	5×10^2	$2\times10^3\pm 1\times10^3$	275±30	355±54	55/89
HT-1080	Human	2.1×10^4	$2.7\times10^5\pm 5.5\times10^4$	1.5×10^3	$1.5\times10^3\pm 3.5\times10^2$	265±3	260±24	89/65
HAF	Human	4.2×10^4	$4.2\times10^4\pm 1.1\times10^4$	1.5×10^3	n.d	175±19	170±10	n.d
HPA	Human	4.2×10^4	$5.3\times10^4\pm 1.3\times10^4$	1.5×10^3	n.d	192±18	190±12	n.d
NHDF	Human	4.2×10^4	$5.3\times10^4\pm 6.3\times10^3$	1.5×10^3	n.d	150±11	150±6	n.d

Abbreviations: I_C, initial cell number per cm^2/well before transduction of 2D/3D cultures; F_C, final cell number per cm^2/well after 3 days post-transduction of 2D/3D cultures; $I_\varnothing$, initial microtissue diameter before transduction; $F_\varnothing$, final microtissue diameter after 3 days post- transduction; 2D, monolayer cultures; 3D, microtissue cultures; n.d, not determined due to difficult microtissue disassociation.

Table II. Estimation of transduced cells within the microtissues and determination of specific SAMY productivity using transgenic lentiviral particles.

BHK-21	Cubic lattice [a] Pd=0.5235	Ideal packed sphere[b] Pd=0.7405	Rhombododecahedron[c] Pd=1
$V_{cell}=(Pd*V_M)/N_{cell}$	$3.1\times10^3 \pm 8.7\times10^2$	$4.3\times10^3 \pm 1.2\times10^3$	$4.4\times10^3 \pm 1.9\times10^3$
$\varnothing_{cell}$	18 ± 1.7	20 ± 1.9	26 ± 3.1
$\varnothing_{TC}$	54 ± 5.1	61 ± 5.7	78 ± 9.3
$\varnothing_{NTC}$	148 ± 10.1	135 ± 11.4	100 ± 18.6
$\%_{TC}$: $[1-(V_{NTC}/V_M)]*0.7$[d]	0.57 ± 0.1	0.60 ± 0.1	0.67 ± 0.1
N_{TC}	$8.5\times10^2 \pm 1\times10^2$	$9.0\times10^2 \pm 8.7\times10^1$	$1.0\times10^2 \pm 3.6\times10^1$
Cells ml^{-1}	$2.8\times10^4 \pm 3.5\times10^3$	$3.0\times10^4 \pm 2.9\times10^3$	$3.4\times10^4 \pm 1.2\times10^3$
Productivity 3D [pg $cell^{-1}day^{-1}$]	23.6 ± 3.2	22.3 ± 2.3	19.8 ± 0.7
Productivity 2D [pg $cell^{-1}day^{-1}$]		1.1 ± 0.1	
CHO-K1	Cubic lattice [a] Pd=0.5235	Ideal packed sphere[b] Pd=0.7405	Rhombododecahedron[c] Pd=1
$V_{cell}=(Pd*V_M)/N_{cell}$	$1.1\times10^3 \pm 4.8\times10^2$	$1.6\times10^3 \pm 6.9\times10^2$	$2.1\times10^3 \pm 9.3\times10^2$
$\varnothing_{cell}$	13 ± 1.9	14 ± 2.1	20 ± 3.0
$\varnothing_{TC}$	38 ± 5.6	43 ± 6.3	61 ± 8.9
$\varnothing_{NTC}$	315 ± 11.2	306 ± 12.5	270 ± 17.7
$\%_{TC}$: $[1-(V_{NTC}/V_M)]*0.7$[d]	0.34 ± 0.2	0.37 ± 0.2	0.47 ± 0.1
N_{TC}	$5.0\times10^3 \pm 2.5\times10^3$	$5.5\times10^3 \pm 2.3\times10^3$	$7.1\times10^3 \pm 1.9\times10^3$
Cells ml^{-1}	$1.7\times10^5 \pm 8.2\times10^4$	$1.8\times10^5 \pm 7.8\times10^4$	$2.4\times10^5 \pm 6.2\times10^4$
Productivity 3D [pg $cell^{-1}day^{-1}$]	22.0 ± 5.2	20.1 ± 4.1	15.7 ± 3.4
Productivity 2D [pg $cell^{-1}day^{-1}$]		2.8 ± 0.4	
HEK-293T	Cubic lattice [a] Pd=0.5235	Ideal packed sphere[b] Pd=0.7405	Rhombododecahedron[c] Pd=1
$V_{cell}=(Pd*V_M)/N_{cell}$	$2.0\times10^3 \pm 4.9\times10^2$	$2.8\times10^3 \pm 6.9\times10^2$	$3.8\times10^3 \pm 9.3\times10^2$
$\varnothing_{cell}$	16 ± 1.3	18 ± 1.4	25 ± 2
$\varnothing_{TC}$	47 ± 3.8	53 ± 4.3	74 ± 6
$\varnothing_{NTC}$	361 ± 7.6	350 ± 8.5	306 ± 12.1
$\%_{TC}$: $[1-(V_{NTC}/V_M)]*0.7$[d]	0.35 ± 0.1	0.38 ± 0.1	0.49 ± 0.1
N_{TC}	$4.5\times10^3 \pm 1.4\times10^3$	$5.0\times10^3 \pm 1.4\times10^3$	$6.3\times10^3 \pm 1\times10^3$
Cells ml^{-1}	$1.5\times10^5 \pm 4.8\times10^4$	$1.7\times10^5 \pm 4.5\times10^4$	$2.1\times10^5 \pm 3.5\times10^4$
Productivity 3D [pg $cell^{-1}day^{-1}$]	5.2 ± 2.2	4.7 ± 1.6	3.7 ± 0.7
Productivity 2D [pg $cell^{-1}day^{-1}$]		1.5 ± 0.2	
HepG2	Cubic lattice [a] Pd=0.5235	Ideal packed sphere[b] Pd=0.7405	Rhombododecahedron[c] Pd=1
$V_{cell}=(Pd*V_M)/N_{cell}$	$6.1\times10^3 \pm 2.8\times10^3$	$8.7\times10^3 \pm 4\times10^3$	$1.2\times10^4 \pm 5.4\times10^3$
$\varnothing_{cell}$	23 ± 3.5	25 ± 3.9	36 ± 5.5
$\varnothing_{TC}$	68 ± 10.4	76 ± 11.6	108 ± 16.4
$\varnothing_{NTC}$	219 ± 20.7	202 ± 23.3	139 ± 32.9
$\%_{TC}$: $[1-(V_{NTC}/V_M)]*0.7$[d]	0.54 ± 0.1	0.57 ± 0.1	0.66 ± 0.1
N_{TC}	$1.1\times10^3 \pm 2.8\times10^2$	$1.1\times10^3 \pm 2.4\times10^2$	$1.3\times10^3 \pm 1.2\times10^2$
Cells ml^{-1}	$3.6\times10^4 \pm 9.3\times10^3$	$3.8\times10^4 \pm 8\times10^3$	$4.4\times10^4 \pm 4.1\times10^3$
Productivity 3D [pg $cell^{-1}day^{-1}$]	20.2 ± 5.1	18.9 ± 2.4	16.4 ± 1.7
Productivity 2D [pg $cell^{-1}day^{-1}$]		2.1 ± 0.1	
HT-1080	Cubic lattice [a] Pd=0.5235	Ideal packed sphere[b] Pd=0.7405	Rhombododecahedron[c] Pd=1
$V_{cell}=(Pd*V_M)/N_{cell}$	$3.2\times10^3 \pm 8.9\times10^2$	$4.5\times10^3 \pm 1.3\times10^3$	$6.1\times10^3 \pm 1.7\times10^3$
$\varnothing_{cell}$	18 ± 1.7	23 ± 1.9	29 ± 2.7
$\varnothing_{TC}$	55 ± 5.1	68 ± 5.7	87 ± 8
$\varnothing_{NTC}$	150 ± 10.1	124 ± 11.4	86 ± 16.1
$\%_{TC}$: $[1-(V_{NTC}/V_M)]*0.7$[d]	0.57 ± 0.1	0.62 ± 0.1	0.67 ± 0.1
N_{TC}	$8.5\times10^2 \pm 1\times10^2$	$9.4\times10^2 \pm 8.6\times10^1$	$1\times10^3 \pm 3.5\times10^1$
Cells ml^{-1}	$2.8\times10^4 \pm 1\times10^2$	$3.1\times10^4 \pm 1\times10^2$	$3.4\times10^4 \pm 1\times10^2$
Productivity 3D [pg $cell^{-1}day^{-1}$]	9.2 ± 1.2	8.3 ± 0.9	7.7 ± 0.3
Productivity 2D [pg $cell^{-1}day^{-1}$]		1.6 ± 0.1	

Lentivirus-based transduction technology. For production of replication-incompetent, self-inactivating lentiviral particles a mixture containing (i) 0.25 M $CaCl_2$

(Acros Organics, Geel, Belgium), (ii) 1 µg pLTR-G, encoding the pseudotyping envelope protein VSV-G of the vesicular stomatitis virus, (iii) 1 µg of the helper construct pCD/NL-BH* and (iv) 1 µg of the gene of interest (GOI)-encoding lentiviral expression vector in a final volume of 100 µl was added dropwise into 100 µl 2x HEPES-buffered saline (HBS, 280 mM NaCl; 100 mM HEPES 1.5 mM Na_2HPO_4; pH 7.1) solution and transfected after incubation for 15 min into human embryonic kidney cells (HEK-293T). Prior to transfection, 2 µl of a 25 mM chloroquine solution (Bode Chemie, Hamburg, Germany) were added to the cell culture medium. Following a medium exchange after 6 h, lentiviral particle production was continued for another 48 h prior to filtration-based harvesting of the lentiviral particles from the culture supernatant (0.45µm pore size FP 030/2 filter; Schleicher & Schuell, Dassel, Germany), to give typical titers of 2×10^7 virus TU/ml. The following lentivectors were used in this study: (i) pMF364 (5'LTR-ψ^+-ori_{SV40}-cPPT-RRE-$P_{hEF1\alpha}$-SAMY-3'$LTR_{\Delta U3}$) [51], (ii) pNL-EGFP-ΔU3 (5'LTR-ψ^+-ori_{SV40}-cPPT-RRE-P_{hCMV}-EGFP-3'$LTR_{\Delta U3}$) [52], and (iii) pBM44 (5'LTR-ψ^+-ori_{SV40}-cPPT-RRE-$P_{hEF1\alpha}$-SEAP-3'$LTR_{\Delta U3}$) [46]. (3'LTR, 3' long terminal repeat; 3'$LTR_{\Delta U3}$, enhancer-free 3'LTR; 5'LTR, 5' long terminal repeat; cPPT, central polypurine tract; EGFP, enhanced green fluorescent protein; ori_{SV40}; simian virus 40-derived origin of replication; P_{hCMV}, human cytomegalovirus immediate early promoter; $P_{hEF1\alpha}$, promoter of the human elongation factor 1α; RRE, Rev response element; SAMY, *Bacillus stearothermophilus*-derived secreted α-amylase; SEAP, human placental secreted alkaline phosphatase; ψ^+, extended lentiviral packaging signal).

For the comparative analysis of lentiviral particle production in adherent cultures and microtissues, HEK-293T monolayer cultures were trypsinized and a single-cell suspension of 1×10^5 cells/ml, in a final volume of 2 ml, was transfected with a mixture containing (i) 94 µl DMEM, ii) 6 µl FuGENE6 (Roche Diagnostics AG, Rotkreuz, Switzerland), (iii) 25 µM chloroquine, (iv)1 µg pLTR-G, (v) 1 µg helper construct pCD/NL-BH* and vi) 1 µg of pBM44 (5'LTR-ψ^+-ori_{SV40}-cPPT-RRE-$P_{hEF1\alpha}$-SEAP-3'$LTR_{\Delta U3}$) [46]. Transfected cells were seeded at indicated cell densities into the wells of 6-well (adherent cultures) or 60-well (microtissues) plates. After 72 h, viral particles were harvested from the cell culture supernatants. Lentiviral particle titer was determined by ELISA-based quantification of the *gag*-encoded lentiviral capsid protein p24 according to

the manufacturer's protocol (NEK-050, Perkin Elmer, Boston, MA, USA). 6.25×10^3 CHO-K1 cells/cm^2, cultivated in a 6-well plate with 2 ml culture medium, were infected with the lentiviral particles, which resulted from monolayer (2D, two-dimensional) and 3D cultures; SEAP production was quantified after 72 h.

Transduction of monolayers and microtissues. For comparative analysis of recombinant protein production in 2D and 3D cultures, monolayer cultures, cultivated in 24-well plates containing 0.5 ml culture medium, were transduced with 50 µl and microtissues cultivated in hanging drops with 2 µl lentiviral particle-containing supernatant. In order to maintain identical growth-arrested cell phenotypes, cell types that failed to proliferate in microtissues (BHK-21, HT-1080, HAF, HPA and NHDF) were grown to confluence as monolayers prior to transduction. CHO-K1, HEK-293T and HepG2, which remained mitotically active when grown in microtissues, were seeded at 2.1×10^4 cells/cm^2 in a 24-well plate and transduced 24 h after seeding. The same pMF364-derived lentiviral particle batch was used in all the experiments (virus titer: 1.4×10^7 TU/ml). BHK-21, HEK-293T, HepG2, HT-1080, HAF, HPA, NHDF (and CHO-K1) microtissue cultures were transduced after three days (six days) cultivation in hanging drops. Transduction efficiency, i.e. penetration of lentiviral particles into monolayer (microtissue) cultures, was analyzed using pNL-EGFP-ΔU3-derived lentiviral particles (virus titer: 1×10^7 TU/mL). To study the influence of neovascularization on the overall production capacity of HUVEC-coated NHDF microtissues, 5×10^3 NHDFs/cm^2, kept in a 10 cm (diameter) Petri dish containing 5 ml DMEM, were transduced with 9.7×10^6 TU/mL of pBM44-derived lentiviral particles before microtissue formation and coating. 24 h after transduction 5 ml DMEM supplemented with 10% FCS were added.

Immunofluorescence-based analysis. Microtissues were washed twice in phosphate-buffered saline solution (PBS; 150mM NaCl, 6.5mM Na_2HPO_4 x 2 H_2O, 2.7mM KCl, 1.5 mM KH_2PO_4, pH 7.4; Sigma Chemicals), fixed at room temperature for 1 h in PBS containing 4% paraformaldehyde (PFA, Sigma Chemicals), washed three times for 5 min in phosphate buffered Triton X-100 (PBT, PBS containing 0.002% Triton X-100; Sigma Chemicals) and permeated for 60 min in PBS containing 0.5% Triton X-100 [53]. Primary antibodies, specific for desired proteins, as well as fluorescence-labelled secondary antibodies were diluted in 1% BSA-containing Tris-buffered saline (TBS,

20 mM Tris base, 155 mM NaCl, 2 mM EGTA, 2 mM $MgCl_2$) and sequentially incubated with microtissues for 12 h at 4°C; they were washed three times during this process. Finally, the microtissues were washed in PBS and embedded on glass slides using Tris-buffered glycerol (a 3:7 mixture of 0.1 M Tris-HCl (pH 9.5) and glycerol supplemented with 50 mg/ml n-propyl-gallat). Tailored 0.5 mm silicon spacers were used to prevent crushing the microtissues between the slide and the cover slip. Immunofluorescence-based analysis of microtissues required antibodies specific for human von Willebrand Factor (F3520; Sigma Chemicals) and platelet endothelial cell adhesion molecule-1 (PECAM-1; P8590, Clone WM-59; Sigma Chemicals), all of which were visualized using Cy3-coupled anti-mouse (Jackson Immunochemicals, West Grove, PA, USA; cat. no. 115-165-146) and FITC-coupled anti-rabbit secondary antibodies (ICN Pharmaceuticals, Hyland, CA, USA).

Hematoxylin-Eosin staining. Microtissues were harvested, washed once in PBS (Sigma) and fixed for 2h at 4°C in PBS containing 4% paraformaldehyde (Sigma). Following stepwise dehydratation in ethanol, microtissues were embedded in paraffin (Fisher Scientific, Wohlen, Switzerland). Hematoxilin-Eosin staining (Fluka) of 5µm microtissue sections was performed as described before [54].

Microscopy. Confocal images were taken with an inverted fluorescence microscope (Leica Microsystems DMIRB/E; Glattbrugg, Switzerland) equipped with a 20x oil immersion objective, a confocal scanner (Leica TCS SP1) featuring argon and helium-neon lasers and a Silicon Graphics workstation (SGI, Schlieren, Switzerland) with Imaris 3D multichannel image-processing software installed (Bitplane, Zurich, Switzerland) [55]. Phase-contrast images, HE staining as well as fluorescence micrographs of monolayer cultures were obtained using an inverted microscope (DM-RB, Leica Microsystems) equipped with a digital camera (DC300FX, Leica Microsystems) and an I3 filter (Omega Optical Inc. Brattleboro, VT, USA).

Quantification of secreted α-amylase (SAMY) and secreted human placental alkaline phosphatase (SEAP). SAMY-containing cell culture supernatants (100 µl) were centrifuged at 14,000 x g for 2 min. 25 µl were transferred to an eppendorf tube, also containing 500 µl substrate solution (45 mg of blue starch corresponding to one Phadebas tablet (Pharmacia Diagnostics, Uppsala, Sweden), dissolved in 4 ml H_2O) and

incubated for 15 min. at 70°C. The reaction was stopped by adding of 125 µl 0.5M NaOH and the sample was centrifuged for 5 min at 14,000 x g before transferring 200 µl supernatant to the well of a 96-well plate to quantify absorbance at 620 nm [51]. SEAP production was analyzed by a *p*–nitrophenylphosphate-based light absorbance time course at 405 nm [51, 56] using the GeniusPro (Tecan Group Ltd., Maennedorf, Switzerland).

Glucose and lactate profiling. Glucose and lactate concentrations in the culture medium were analyzed using commercially available enzymatic assays and the protocols provided by the supplier (Beckman Coulter, Zurich, Switzerland).

Quantitative RT-PCR. Total RNA was isolated with the NucleoSpin RNA II kit (Macherey-Nagel, Oensingen, Switzerland) from 2×10^6 CHO-WW162 cells cultivated in 2D and 3D cultures according to the manufacture's protocol. Reverse transcription and relative quantification of human placental secreted alkaline phosphatase (SEAP; Acc. No: CS000429; forward primer, 5'-AGGCCCGGGACAGGAA-3'; reverse primer, 5'-GCCGTCCTTGAGCACATAGC-3' and a probe labeled with 5'FAM and 3'TAMRA dyes, 5'-CCTACACGGTCCTCCTATACGGAAACGG-3' (Sigma)) mRNA was performed in a two-step RT-PCR as describe before [57].

Results

Specific productivity of SEAP-producing CHO-K1 grown as monolayers or microtissues.

Previous experiments comparing cellular production capacities of monolayer and microtissue cultures exemplified that the specific protein productivities of cardiomyocytes, assembled in microtissues, were up to six-fold higher than those of isogenic monolayer cultures [53]. In order to determine whether a three-dimensional microenviroment also increases the heterologous protein production capacity of a biotechnologically relevant cell line, we assembled a variety of different CHO-K1-derived cell lines, engineered for constitutive or regulated reporter gene expression in microtissues, and compared their production profiles to isogenic monolayer cultures. CHO-WW162 cells, transgenic for constitutive SEAP expression (P_{SV40}-SEAP-pA), were either assembled for six days in microtissues or grown for 48 h in monolayers and then

profiled for SEAP production for two days. Although the microtissue and monolayer cultures consisted of similar cell numbers were grown without glucose limitations (Fig. 1A), microtissues showed up to 30% increase in specific SEAP productivity (Fig. 1B). Productivities of monolayer cultures at higher glucose concentration (3.5 g l^{-1}) from day 2 to day 4 were also measured (1.5 g l^{-1} of glucose; 0.31 ± 0.01 pg $Cell^{-1}$ Day^{-1} and 3.5 g l^{-1} glucose; 0.25 ± 0.01 pg $Cell^{-1}$ Day^{-1}) confirming a non-dependency of the productivity on glucose concentration. Additionally, we have quantified by quantitative RT-PCR the differences of SEAP productivity at the transcriptional level between both culture types (Ct values; 2D, 9.2 ± 0.02 and 3D, 9.0 ± 0.6) showing no significance differences and suggesting that the increase of productivity in 3D cultures may take place at the translational or secretion level.

Earlier studies have established an inverse correlation between specific productivity and cultivation temperature within a window of 30°C to 37°C [58]. Indeed, the specific SEAP productivity of CHO-WW162 monolayer cultures maintained at 30°C was 1.5-fold higher than to isogenic cultures grown at 37°C. Interestingly, microtissues did not respond to low-temperature cultivation (Fig. 1B). Furthermore, specific SEAP productivity of microtissues were insensitive to serum withdrawal; microtissues, assembled in serum-supplemented FMX-8 medium and then switched to serum-free FMX-8 medium, showed no reduction in SEAP productivity, while cell viability decreased by only 8%. In contrast, isogenic monolayer cultures exhibited viability and productivity decreases of 30% and 35%, respectively (Fig. 1C).

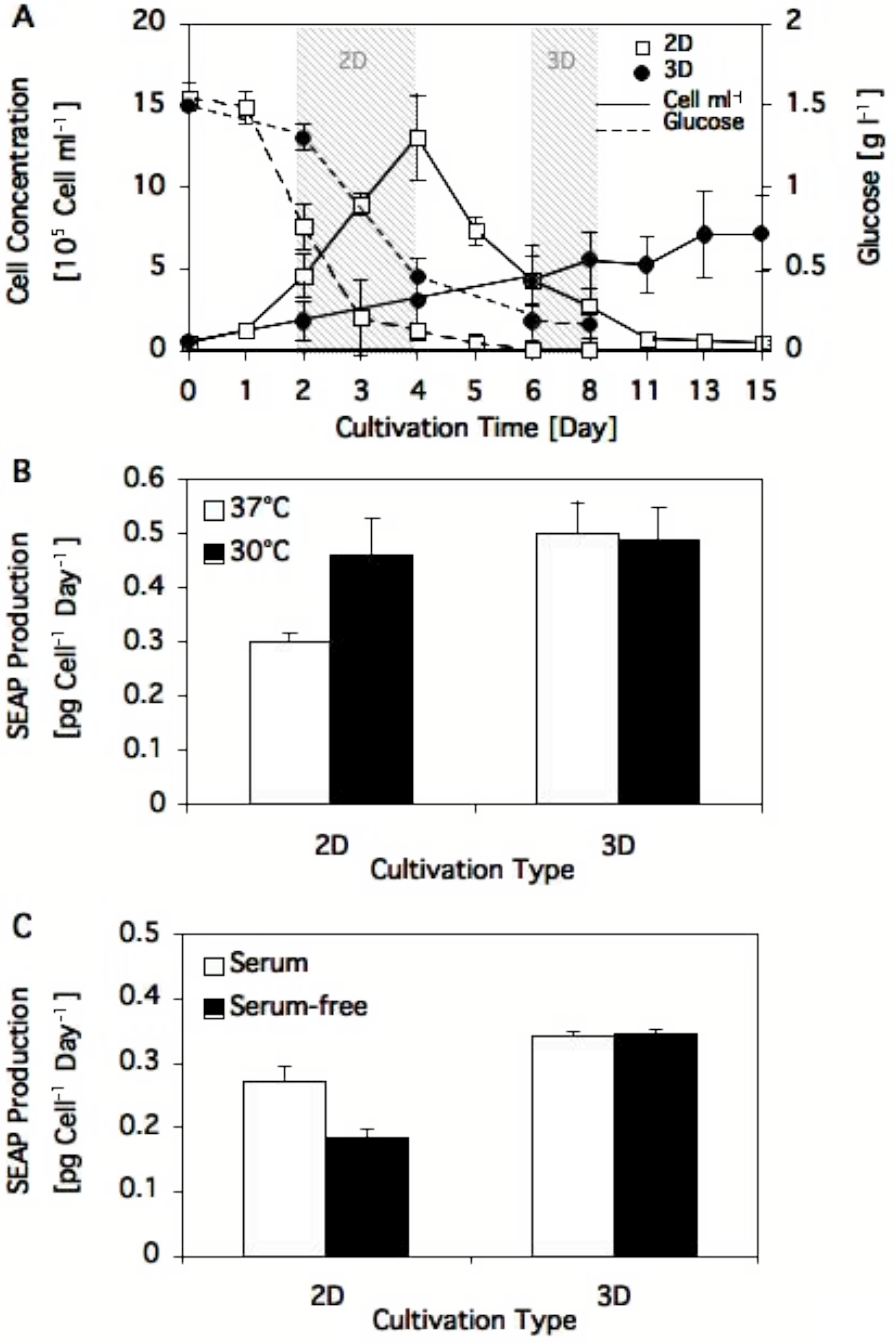

Figure 1: Growth characteristics, glucose consumption and SEAP production profiles of CHO-WW162 engineered for constitutive SEAP expression and cultivated as monolayer (2D) or microtissues (3D). (A) Growth profiles (continuous line) and glucose consumption (dotted line) of CHO-WW162, seeded at an initial cell concentration of 1×10^4 cells/cm^2 and cultivated for 15 days in 2D (□) and 3D (●). (B) Specific SEAP productivity of CHO-WW162 2D and 3D populations cultivated at different cultivation

temperatures. (C) Specific SEAP productivity of CHO-WW162 2D and 3D populations cultivated in serum-supplemented and serum-free media.

CHO-K1 cells, engineered for conditional G1-phase-specific growth arrest, showed increased specific productivities [8]. In order to assess whether the production boost observed for CHO-derived microtissues was associated with reduced proliferation of cells in a three-dimensional environment we profiled the production capacities of isogenic proliferation-controlled CHO-SS101$_5$ [49]. CHO-SS101$_5$ harbors a multicistronic tetracycline-responsive expression unit encoding the human cyclin-dependent kinase inhibitor p27^{Kip1} along with SEAP. Cultivation of this cell line in tetracycline-free medium results in ectopic p27^{Kip1} and SEAP expression and a p27^{Kip1}-mediated G1-specific growth arrest [8, 49]. Even in a proliferation-controlled cell phenotype, CHO-SS101$_5$-based microtissues outperformed isogenic monolayers in specific SEAP productivity by 40%, suggesting that production increases associated with microtissues are intimately linked to crosstalk among cells in a tissue-like microenvironment (Fig. 2A).

Since small-molecule-responsive transgene expression is of prime importance for future gene therapy and tissue engineering initiatives, we evaluated the production capacity of macrolide- [47] and gas-inducible [48] gene regulation systems in microtissue and monolayer cultures under full induction. CHO-E$_1$-SEAP$_1$ transgenic for erythromycin-inducible SEAP expression cassette [47] (Fig. 2B), and $_{AIR}$CHO-SEAP, engineered for gas-inducible SEAP expression cassette [48] (Fig. 2C), showed up to 1.5-fold higher specific SEAP productivity when cultivated in a microtissue compared to a monolayer format.

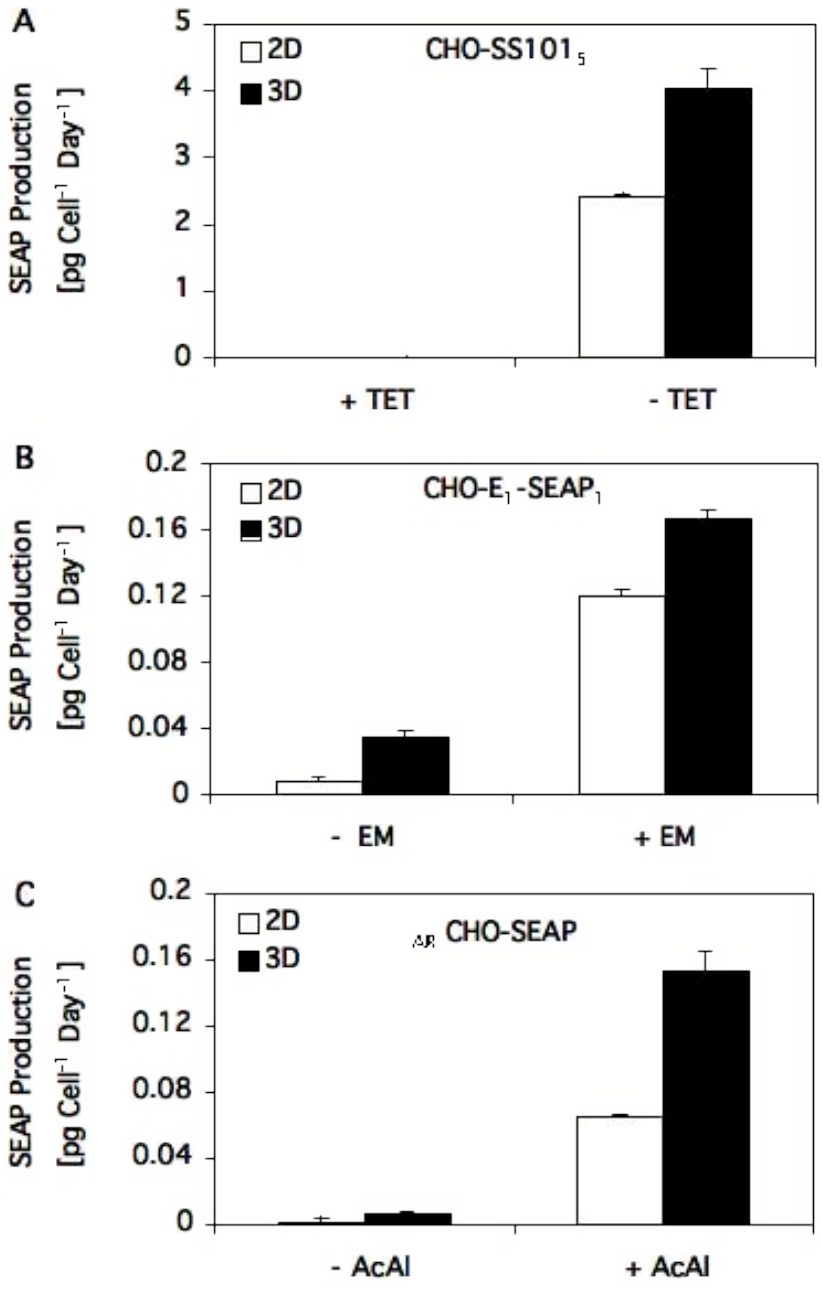

Figure 2: Specific SEAP productivities of different cell lines grown as monolayer (2D) or microtissue (3D) cultures. (A) CHO-SS101$_5$ engineered for coordinated tetracycline- (TET) responsive expression of the human cyclin-dependent kinase inhibitor p27^{Kip1} and SEAP. Both transgenes are repressed in the presence of tetracycline (+TET). In the absence of tetracycline (-TET) SEAP is produced and p27^{Kip1} expression results in a G1-phase-specific growth arrest. (B) CHO-E$_1$-SEAP$_1$ engineered for macrolide-inducible SEAP expression and cultivated in 2D/3D in the presence (+EM) and absence (-EM) of erythromycin (EM). (C) $_{AIR}$CHO-SEAP transgenic for gas-inducible SEAP expression was cultivated in 2D/3D in the presence and absence of gaseous acetaldehyde (+/- AcAl).

Microtissue-based production of lentiviral particles

Capitalizing on the greater production capacity of microtissues we evaluated the performance of 3D-cultivated HEK-293T for production of lentiviral particles. HEK-293T suspension cultures were co-transfected with lentivector pBM44 (5'LTR-ψ^+-ori$_{SV40}$-cPPT-RRE-P$_{hEF1\alpha}$-SEAP-3'LTR$_{\Delta U3}$) and appropriate helper constructs and were left to produce pBM44-derived lentiviral particles after seeding for monolayer culture or assembly in microtissues. Lentiviral particle production was assessed by quantification of *gag*-encoded lentiviral capsid protein p24. Microtissue-based production of lentiviral particles was up to three times higher (Fig. 3A) and CHO-K1 monolayer cultures transduced with those lentiviruses resulted in up to 30% higher SEAP expression compared to control scenarios using monolayer production cultures (Fig. 3B).

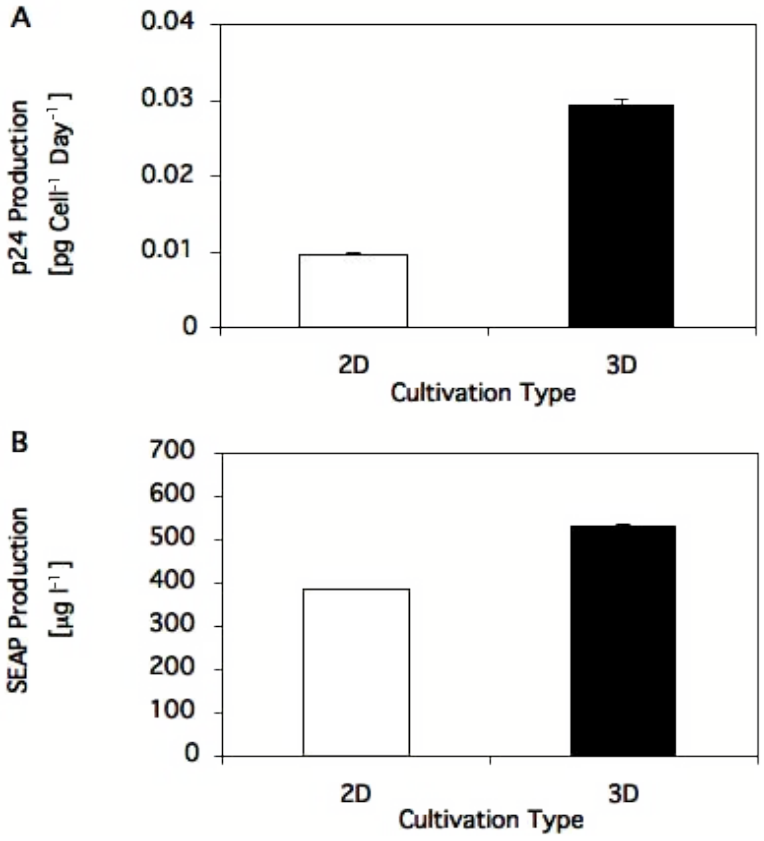

Figure 3: Lentiviral particle production of HEK-293T cultivated as monolayers (2D) or microtissues (3D). (A) ELISA-based quantification of the *gag*-encoded lentiviral capsid protein p24. 1000 pg of the gag-encoded lentiviral capsid protein p24 are equivalent to 1.2×10^{10} lentiviral particles. (B) SEAP production of CHO-K1 transduced in monolayer with pBM44-derived lentiviral particles (transgenic for constitutive SEAP production) produced in 2D and 3D cultures.

Specific productivity of transduced cell lines and primary cells cultivated as monolayers or microtissues with lentiviral particles

Microtissues and monolayer cultures were transduced with third-generation self-inactivating lentiviral particles encoding the *Bacillus stearothermophilus*-derived secreted α-amylase (SAMY; pMF364, 5'LTR-ψ^+-ori_{SV40}-cPPT-RRE-P_{hCMV}-SAMY-3'$LTR_{\Delta U3}$). Primary cells (HAF, HPA and NHDF), HT-1080 and BHK-21 monolayer cultures were grown to confluence prior to transduction in order to compare them with the proliferation-inert phenotype of these cells in microtissues and provide isogenic culture conditions for direct comparison of production performance. CHO-K1, HEK-293T and HepG2 which proliferate in monolayers and microtissues, were seeded at indicated cell densities (Table I) and transduced after 24h. In order to exclude an impact of glucose depletion, critical after any three-day culture, SAMY production of cell lines was profiled 24h post transduction. All cell types transduced in a microtissue configuration showed significantly higher specific SAMY productivities compared to isogenic monolayer cultures. For example, the specific productivity of transduced BHK-21 microtissues outperformed monolayer cultures 18-fold (Fig. 4A). Whereas BHK-21 was scored as the highest producer cell line in 3D cultures (13.4 ± 1.2 pg $Cell^{-1}$ Day^{-1}), HEK-293T was the poorest of the five cell lines analyzed (1.8 ± 0.05 pg $Cell^{-1}$ Day^{-1}). CHO-K1 and HT-1080 showed a similar four-fold relative increase in specific productivity when transduced as microtissues (Fig. 4A). Among the primary cells used in this study, human aortic fibroblasts (HAF) and normal human dermal fibroblasts (NHDF) exhibited a two-fold higher specific productivity in 3D cultures, and human pre-adipocytes (HPA) showed the highest relative 2D/3D production ratio with a three-fold increase (Fig. 4C). Glucose depletion was not observed under any of the aforementioned culture conditions (Fig. 4B and D).

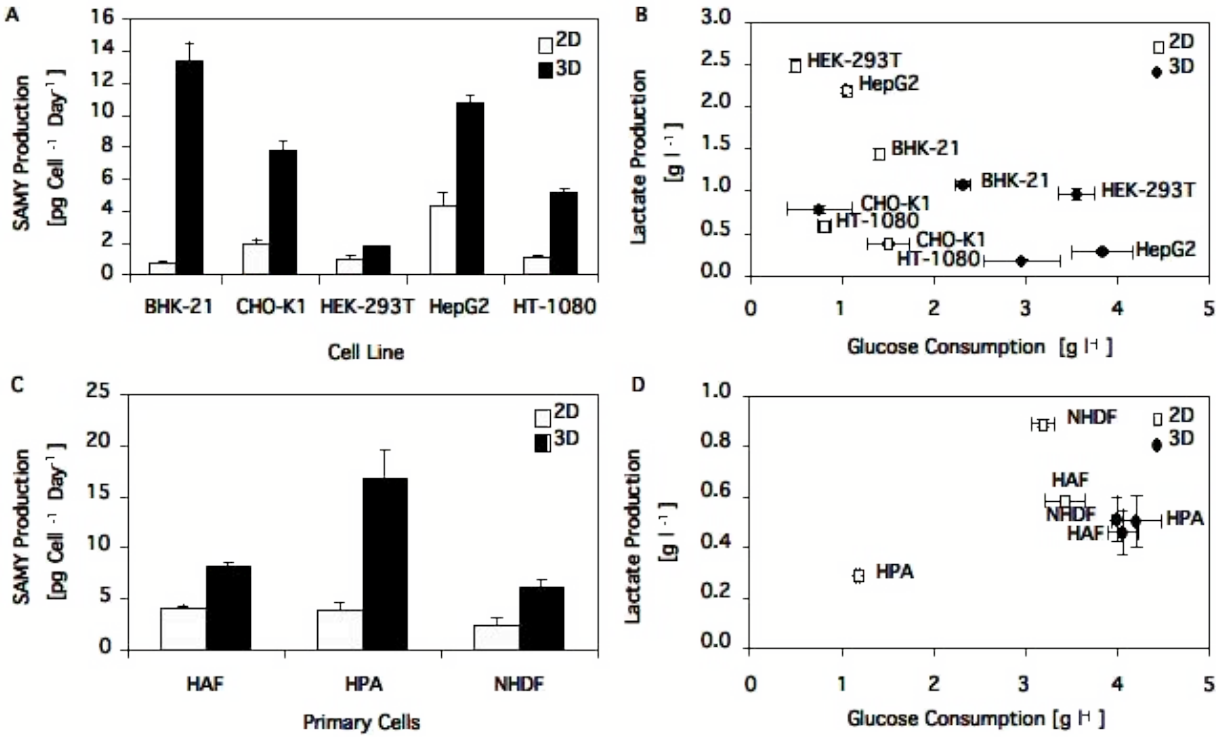

Figure 4: Quantification of specific SAMY productivity (A, C), glucose consumption and lactate production (B, D) of cell lines (A, B) and primary cells (C, D) cultivated as monolayers (2D) or microtissues (3D) and transduced by 1.4×10^7 TU/ml of pMF364-derived lentiviral particles (transgenic for constitutive SAMY production). Specific SAMY productivities of cell lines were quantified 24h after transduction in the absence of glucose limitation.

Penetration of lentiviral particles into microtissues

To evaluate the transduction efficiency and penetration of lentiviral particles into microtissue cultures, CHO-K1 monolayer/microtissues were transduced with pNL-EGFP-ΔU3- (5'LTR-ψ^+-ori$_{SV40}$-cPPT-RRE-P$_{hCMV}$-EGFP-3'LTR$_{\Delta U3}$) [52] derived lentiviral particles. Control fluorescence micrographs showed 70% transduction efficiency in monolayer cultures (Fig. 5A). As evidenced by confocal microscopy (Fig. 5B), lentiviral particles penetrated microtissues no deeper than three cell layers. Of those three layers the outermost cell layer was nearly 90% transduced. The adjoining second layer was 70% transduced and the third layer less than 50%. The number of cells per layer was calculated assuming 100% packing density of the microtissue which was supported by HE staining microtissue sections (Fig. 5C), and compared with 50% (cubic lattice) and 75% (ideal packed sphere) packed densities [59] (Table II). A rhombododecahedron was

used to model the cell geometry within the microtissue assuming 100% packing density. This approximation was consistent with the geometry acquired by the cells at maximum packing density (Fig. 5C). Using this data as a closer approximation for evaluation of the specific productivity of transduced monolayer and microtissue cultures, it is evident that the specific protein productivity of transduced cells in a microtissue is still several orders of magnitude higher compared to isogenic monolayer settings (Table II). As each cell type may generate different aggregation percentage in micortissue formation, which strongly depends on the extracellular matrix production, we used the productivity range represented by the three aggregation models (cubic lattice, ideal packing density and rhombododecahedron) of table II to accurately determine specific cell productivity in microtissues.

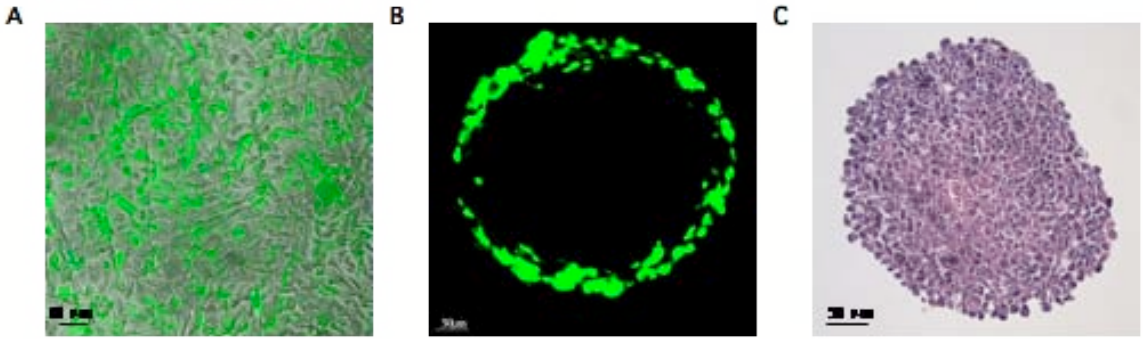

Figure 5: Fluorescence microscopy of transduced CHO-K1 cells with pNL-EGFP-ΔU3- derived lentiviral particles. Phase-contrast (A) and confocal (B) fluorescence micrographs of EGFP production in monolayer (A) and microtissue cultures (B) 72 h after transduction with 1.33×10^7 TU/ml of pNL-EGFP-ΔU3-derived lentiviral particles (engineered for constitutive EGFP production). Hematoxylin-eosin staining of CHO-K1 cells (C). EGFP expression is shown in green.

Vascularization of protein-producing microtissues

Diffusion limitations in microtissues may compromise their overall production capacity. HUVECs, coated onto NHDF spheroids managed VEGF-mediated vascularization of microtissues [44]. To determine whether vascularization positively impacts microtissue-based protein secretion, NHDF monolayer cultures were transduced with pBM44-derived lentiviral particles. 48h after transfection, the NHDFs were detached and assembled in microtissues (1×10^4 cells/microtissue), 350 ± 50 μm in

diameter, for 48h before the NHDF-derived spheroids were coated with 500 HUVECs per microtissue. Control spheroids were coated with an additional NHDF layer (500 NHDF/microtissue). Coated NHDF-HUVEC and NHDF-NHDF microtissues were cultivated for six days to allow vascularization as previously described by [44]. Confocal microscopy-based analysis revealed a highly branched capillary network in NHDF-HUVEC transduced-microtissues (Fig. 6A and B). Culture supernatants, collected on days 3 and 6 and profiled for SEAP production, showed that vascularized microtissues exhibited two-fold higher SEAP production than non-vascularized control spheroids (Fig. 6C).

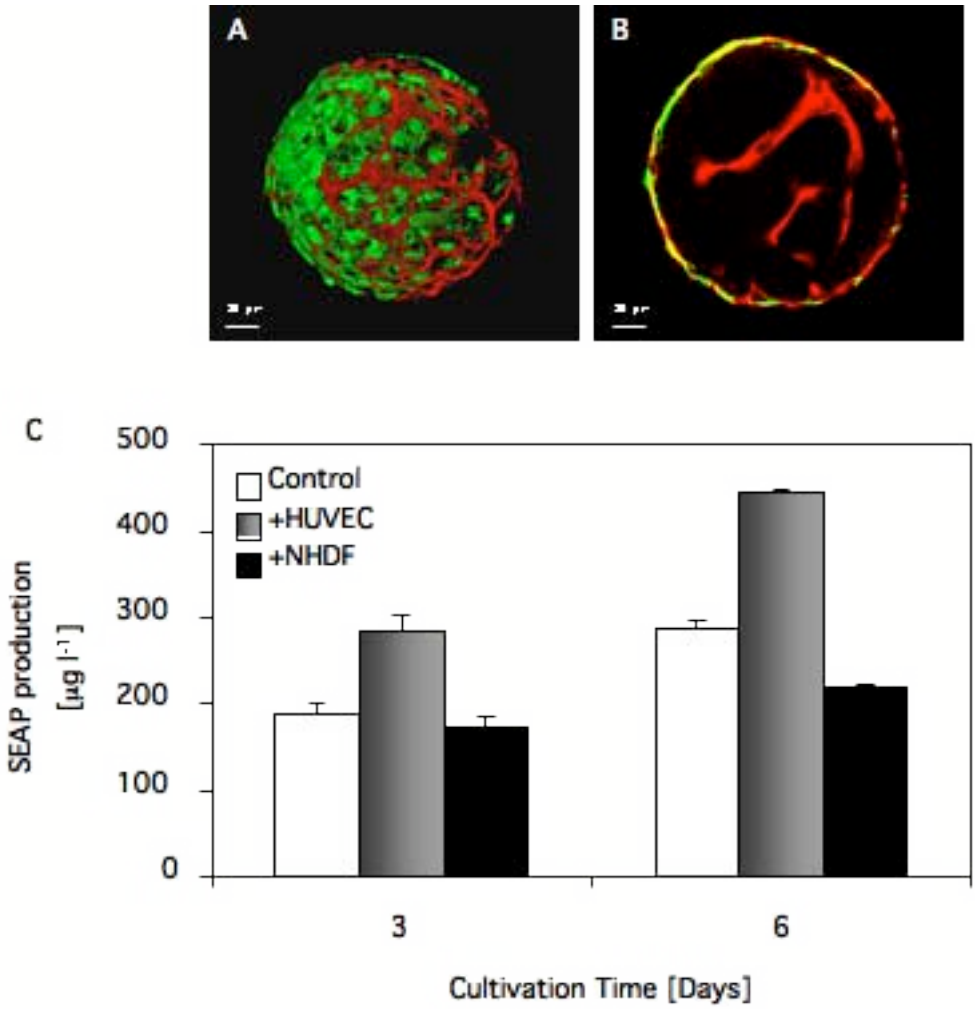

Figure 6 : SEAP production of normal human dermal fibroblasts (NHDF) transduced with 9.6×10^6 TU/ml of pBM44-derived lentiviral particles (mediating constitutive SEAP expression) and optionally

vascularized by coating with human umbilical vein endothelial cells (HUVECs). (A) Confocal fluorescence micrographs (A, 3D projection; B, central section) showing HUVEC-based vascularization six days after coating of NHDF microtissues with HUVECs. HUVECs were stained for von Willebrand factor (shown in green) and for PECAM-1 (CD31; shown in red). (C) SEAP production of NHDF microtissues transduced with pBM44-derived lentiviral particles followed by no coating (control), HUVEC coating (+HUVEC) or NHDF-based control coating (+NHDF).

Discussion

Improving specific productivity and product quality of mammalian cell-based biopharmaceutical manufacturing processes was one of the priorities of bioengineers following approval of the first tPA production process [60-63]. Strategies for increasing specific productivity of mammalian production cell lines include; (i) genetic engineering [5, 64, 65], (ii) modification of physical process parameters [10, 66] and (iii) optimization of cell culture medium [6, 67, 68]. For example, $p27^{Kip1}$-mediated G1-specific growth arrest and/or ectopic expression of the survival gene *bcl-*x_L resulted in up to 30-fold higher specific productivity [8, 13, 14, 69], low-temperature cultivation of production cell lines doubled specific productivity [58] and addition of specific media, containing rapamycin, boosted production by 2-fold [70].

With an obvious focus on improving overall production and product quality of serum-free suspension cultures the production capacity of mammalian cells assembled in tissue-like microenvironments has largely remained elusive. However, more information on production capacities of tissue-embedded cells may (i) foster advances in operating bioreactors at high tissue-like cell densities, (ii) indicate the range of a cell's utmost specific productivity and (iii) increase our understanding of *in-vivo* transgene expression dosing in gene therapy and tissue engineering initiatives. Our rigorous comparative production profiling of isogenic monolayer and microtissue cultures revealed unmatched performance levels of transgenic cell lines assembled in microtissues in every configuration. Specific productivities of CHO-WW162, transgenic for constitutive SEAP production and CHO-$SS101_5$, engineered for $p27^{Kip1}$-mediated G1-specific growth arrest, outperformed classic monolayer cultures up to 1.5-fold. Since these production values were based on SEAP quantification in the culture supernatant the actual specific productivity may be even higher due to diffusion limitations of microtissues, which may

compromise SEAP release from core cell layers [71]. The observation that vascularized microtissues exhibited two-fold higher production compared to non-vascularized control microtissues supports this notion. Furthermore, increased SEAP production of vascularized microtissues exemplifies that HUVEC-based microvessels are functional hollow structures able to connect the microtissue core to the extra-microtissue environment.

Microtissues produce not only heterologous proteins at higher levels, but also supra-molecular structures such as lentiviral particles. Intuitively, it comes as no surprise that viruses, which evolved for optimal reproduction in tissues, show higher particle production in microtissues. However, this observation should be considered on the eve of producing transgenic lentiviral particles for gene therapy trials [22, 72]. Another clinically relevant fact is the limited penetration of VSV-G-pseudotyped lentiviral particles into microtissues. Lentiviral particles transduced only three peripheral cell layers of microtissues, which will favour local rather than systemic applications in future gene therapy scenarios [22].

Mammalian cells, cultivated in a tissue-like format, show specific phenotypes associated with particular cell-cell crosstalk, production of an extracellular matrix (ECM) [41], differentiation of morphological and biochemical properties and assembly of supra-cellular secretory capabilities [73-75]. Our study confirmed that cells derived from endocrine tissues such as kidney (BHK-21 and HEK- 293T), liver (HepG2) and adipose tissues (HPA) showed higher secretory capacities when assembled in a microtissue format. Furthermore, previous studies have exemplified that HepG2-derived microtissues adopted liver-like morphologic polarization and production of liver-specific enzyme sets, the expression of which was not observed in isogenic HepG2 monolayer cultures [50, 76].

3D cultures differed from their 2D counterparts not only in specific tissue functionality, but also in their metabolic activity. In contrast to monolayer cultures, cells assembled within microtissues typically show lower proliferation and metabolic rates, diminished oxygen and glucose consumption, decreased ATP-ADP conversion and reduced glycolysis fluxes [77-82]. Proliferation-controlled monolayer cultures, by upregulation of the cyclin-dependent kinase inhibitor $p27^{Kip1}$ [8, 14, 69], mimic cell arrest within microtissues to a great extent [77, 83, 84]. However, the observation that a production

difference remains between proliferation-controlled cells cultivated as monolayers and microtissues suggests that additional parameters are at work to increase specific productivity in microtissues. Synergistic combination of (i) reduced proliferation and metabolic activities, (ii) molecular community crosstalk and (iii) specialized morphologic superstructures may result in optimal cell survival and metabolic energy conversion, which will ultimately impinge on specific productivity profiles [30, 85]. Furthermore, analyses of the human placental secreted alkaline phosphatase (SEAP) mRNA level shows no differences between 2D and 3D cultures suggesting that an increase production rate of 3D cultures may take place at the translational or secretion level. Previous comparisons at the transcriptional level between 2D and 3D cultures [83] show an upregulation in 3D cultures from Rab GTPase, which can facilitate protein transport and membrane traffic [86], and from genes related to protein processing as the translation initiation factor 2B (eIF2B) [87].

A detailed molecular understanding of production discrepancies between monolayer and microtissue cultures will help shape tomorrow's biopharmaceutical manufacturing processes, operating at the cell's production limit, facilitate the design of tissue replacements and enable therapeutic transgene expression levels required for future gene therapy initiatives.

Acknowledgements

We thank Markus Rimann and Marcia Schoenberg for critical comments on the manuscript. This work was supported by the Swiss National Science Foundation (grant no. 631-065946) and the Swiss State Secretariat for Education and Research within EC Framework 6.

References

1. Wurm, F.M. Production of recombinant protein therapeutics in cultivated mammalian cells. Nat Biotechnol **22**, 1393, 2004.
2. al-Rubeai, M. Apoptosis and cell culture technology. Adv Biochem Eng Biotechnol **59**, 225, 1998.
3. Baker, K.N., Rendall, M.H., Hills, A.E., Hoare, M., Freedman, R.B. and James, D.C. Metabolic control of recombinant protein N-glycan processing in NS0 and CHO cells. Biotechnol Bioeng **73**, 188, 2001.

4. Carvalhal, A.V., Santos, S.S., Calado, J., Haury, M. and Carrondo, M.J. Cell growth arrest by nucleotides, nucleosides and bases as a tool for improved production of recombinant proteins. Biotechnol Prog **19**, 69, 2003.
5. Chen, K., Liu, Q., Xie, L., Sharp, P.A. and Wang, D.I. Engineering of a mammalian cell line for reduction of lactate formation and high monoclonal antibody production. Biotechnol Bioeng **72**, 55, 2001.
6. deZengotita, V.M., Miller, W.M., Aunins, J.G. and Zhou, W. Phosphate feeding improves high-cell-concentration NS0 myeloma culture performance for monoclonal antibody production. Biotechnol Bioeng **69**, 566, 2000.
7. Fox, S.R., Patel, U.A., Yap, M.G. and Wang, D.I. Maximizing interferon-gamma production by Chinese hamster ovary cells through temperature shift optimization: experimental and modeling. Biotechnol Bioeng **85**, 177, 2004.
8. Fussenegger, M., Schlatter, S., Datwyler, D., Mazur, X. and Bailey, J.E. Controlled proliferation by multigene metabolic engineering enhances the productivity of Chinese hamster ovary cells. Nat Biotechnol **16**, 468, 1998.
9. Geserick, C., Bonarius, H.P., Kongerslev, L., Hauser, H. and Mueller, P.P. Enhanced productivity during controlled proliferation of BHK cells in continuously perfused bioreactors. Biotechnol Bioeng **69**, 266, 2000.
10. Kaufmann, H., Mazur, X., Marone, R., Bailey, J.E. and Fussenegger, M. Comparative analysis of two controlled proliferation strategies regarding product quality, influence on tetracycline-regulated gene expression, and productivity. Biotechnol Bioeng **72**, 592, 2001.
11. Knibbs, R.N., Dame, M., Allen, M.R., Ding, Y., Hillegas, W.J., Varani, J. and Stoolman, L.M. Sustained high-yield production of recombinant proteins in transiently transfected COS-7 cells grown on trimethylamine-coated (hillex) microcarrier beads. Biotechnol Prog **19**, 9, 2003.
12. Mastrangelo, A.J., Hardwick, J.M., Zou, S. and Betenbaugh, M.J. Part II. Overexpression of bcl-2 family members enhances survival of mammalian cells in response to various culture insults. Biotechnol Bioeng **67**, 555, 2000.
13. Meents, H., Enenkel, B., Eppenberger, H.M., Werner, R.G. and Fussenegger, M. Impact of coexpression and coamplification of sICAM and antiapoptosis determinants bcl-2/bcl-x(L) on productivity, cell survival, and mitochondria number in CHO-DG44 grown in suspension and serum-free media. Biotechnol Bioeng **80**, 706, 2002.
14. Meents, H., Enenkel, B., Werner, R.G. and Fussenegger, M. p27Kip1-mediated controlled proliferation technology increases constitutive sICAM production in CHO-DUKX adapted for growth in suspension and serum-free media. Biotechnol Bioeng **79**, 619, 2002.
15. Mueller, P.P., Schlenke, P., Nimtz, M., Conradt, H.S. and Hauser, H. Recombinant glycoprotein product quality in proliferation-controlled BHK-21 cells. Biotechnol Bioeng **65**, 529, 1999.
16. Umana, P., Jean-Mairet, J., Moudry, R., Amstutz, H. and Bailey, J.E. Engineered glycoforms of an antineuroblastoma IgG1 with optimized antibody-dependent cellular cytotoxic activity. Nat Biotechnol **17**, 176, 1999.

17. Wu, M.H., Dimopoulos, G., Mantalaris, A. and Varley, J. The effect of hyperosmotic pressure on antibody production and gene expression in the GS-NS0 cell line. Biotechnol Appl Biochem **40**, 41, 2004.
18. Abbott, A. Cell culture: biology's new dimension. Nature **424**, 870, 2003.
19. Bissell, M.J., Radisky, D.C., Rizki, A., Weaver, V.M. and Petersen, O.W. The organizing principle: microenvironmental influences in the normal and malignant breast. Differentiation **70**, 537, 2002.
20. Zhang, S. Beyond the Petri dish. Nat Biotechnol **22**, 151, 2004.
21. Girotto, D., Urbani, S., Brun, P., Renier, D., Barbucci, R. and Abatangelo, G. Tissue-specific gene expression in chondrocytes grown on three-dimensional hyaluronic acid scaffolds. Biomaterials **24**, 3265, 2003.
22. Grill, J., Lamfers, M.L., van Beusechem, V.W., Dirven, C.M., Pherai, D.S., Kater, M., Van der Valk, P., Vogels, R., Vandertop, W.P., Pinedo, H.M., Curiel, D.T. and Gerritsen, W.R. The organotypic multicellular spheroid is a relevant three-dimensional model to study adenovirus replication and penetration in human tumors in vitro. Mol Ther **6**, 609, 2002.
23. Kunz-Schughart, L.A., Wenninger, S., Neumeier, T., Seidl, P. and Knuechel, R. Three-dimensional tissue structure affects sensitivity of fibroblasts to TGF-beta 1. Am J Physiol Cell Physiol **284**, C209, 2003.
24. Roskelley, C.D., Srebrow, A. and Bissell, M.J. A hierarchy of ECM-mediated signalling regulates tissue-specific gene expression. Curr Opin Cell Biol **7**, 736, 1995.
25. Schuetz, E.G., Li, D., Omiecinski, C.J., Muller-Eberhard, U., Kleinman, H.K., Elswick, B. and Guzelian, P.S. Regulation of gene expression in adult rat hepatocytes cultured on a basement membrane matrix. J Cell Physiol **134**, 309, 1988.
26. Cukierman, E., Pankov, R., Stevens, D.R. and Yamada, K.M. Taking cell-matrix adhesions to the third dimension. Science **294**, 1708, 2001.
27. Yamada, K.M., Pankov, R. and Cukierman, E. Dimensions and dynamics in integrin function. Braz J Med Biol Res **36**, 959, 2003.
28. Duguay, D., Foty, R.A. and Steinberg, M.S. Cadherin-mediated cell adhesion and tissue segregation: qualitative and quantitative determinants. Dev Biol **253**, 309, 2003.
29. Muschler, J., Levy, D., Boudreau, R., Henry, M., Campbell, K. and Bissell, M.J. A role for dystroglycan in epithelial polarization: loss of function in breast tumor cells. Cancer Res **62**, 7102, 2002.
30. Zahir, N. and Weaver, V.M. Death in the third dimension: apoptosis regulation and tissue architecture. Curr Opin Genet Dev **14**, 71, 2004.
31. Petroll, W.M., Cavanagh, H.D. and Jester, J.V. Dynamic three-dimensional visualization of collagen matrix remodeling and cytoskeletal organization in living corneal fibroblasts. Scanning **26**, 1, 2004.
32. Wozniak, M.A., Modzelewska, K., Kwong, L. and Keely, P.J. Focal adhesion regulation of cell behavior. Biochim Biophys Acta **1692**, 103, 2004.
33. Fussenegger, M. The impact of mammalian gene regulation concepts on functional genomic research, metabolic engineering, and advanced gene therapies. Biotechnol Prog **17**, 1, 2001.

34. Fussenegger, M. and Bailey, J.E. Molecular regulation of cell-cycle progression and apoptosis in mammalian cells: implications for biotechnology. Biotechnol Prog **14**, 807, 1998.
35. Griffith, L.G. and Naughton, G. Tissue engineering--current challenges and expanding opportunities. Science **295**, 1009, 2002.
36. Lysaght, M.J. and Reyes, J. The growth of tissue engineering. Tissue Eng **7**, 485, 2001.
37. Schmeichel, K.L. and Bissell, M.J. Modeling tissue-specific signaling and organ function in three dimensions. J Cell Sci **116**, 2377, 2003.
38. Ingber, D.E. Cancer as a disease of epithelial-mesenchymal interactions and extracellular matrix regulation. Differentiation **70**, 547, 2002.
39. Jacks, T. and Weinberg, R.A. Taking the study of cancer cell survival to a new dimension. Cell **111**, 923, 2002.
40. Radisky, D., Muschler, J. and Bissell, M.J. Order and disorder: the role of extracellular matrix in epithelial cancer. Cancer Invest **20**, 139, 2002.
41. Santini, M.T., Rainaldi, G. and Indovina, P.L. Apoptosis, cell adhesion and the extracellular matrix in the three-dimensional growth of multicellular tumor spheroids. Crit Rev Oncol Hematol **36**, 75, 2000.
42. Weaver, V.M., Lelievre, S., Lakins, J.N., Chrenek, M.A., Jones, J.C., Giancotti, F., Werb, Z. and Bissell, M.J. beta4 integrin-dependent formation of polarized three-dimensional architecture confers resistance to apoptosis in normal and malignant mammary epithelium. Cancer Cell **2**, 205, 2002.
43. Weaver, V.M., Petersen, O.W., Wang, F., Larabell, C.A., Briand, P., Damsky, C. and Bissell, M.J. Reversion of the malignant phenotype of human breast cells in three-dimensional culture and in vivo by integrin blocking antibodies. J Cell Biol **137**, 231, 1997.
44. Kelm, J.M., Diaz Sanchez-Bustamante, C., Ehler, E., Hoerstrup, S.P., Djonov, V., Ittner, L. and Fussenegger, M. VEGF profiling and angiogenesis in human microtissues. J Biotechnol **118**, 213, 2005.
45. Timmins, N.E., Dietmair, S. and Nielsen, L.K. Hanging-drop multicellular spheroids as a model of tumour angiogenesis. Angiogenesis **7**, 97, 2004.
46. Mitta, B., Rimann, M., Ehrengruber, M.U., Ehrbar, M., Djonov, V., Kelm, J. and Fussenegger, M. Advanced modular self-inactivating lentiviral expression vectors for multigene interventions in mammalian cells and in vivo transduction. Nucleic Acids Res **30**, e113, 2002.
47. Weber, W., Fux, C., Daoud-el Baba, M., Keller, B., Weber, C.C., Kramer, B.P., Heinzen, C., Aubel, D., Bailey, J.E. and Fussenegger, M. Macrolide-based transgene control in mammalian cells and mice. Nat Biotechnol **20**, 901, 2002.
48. Weber, W., Rimann, M., Spielmann, M., Keller, B., Daoud-El Baba, M., Aubel, D., Weber, C.C. and Fussenegger, M. Gas-inducible transgene expression in mammalian cells and mice. Nat Biotechnol **22**, 1440, 2004.
49. Schlatter, S., Bailey, J.E. and Fussenegger, M. Novel surface tagging technology for selection of complex proliferation-controlled mammalian cell phenotypes. Biotechnol Bioeng **75**, 597, 2001.

50. Kelm, J.M., Timmins, N.E., Brown, C.J., Fussenegger, M. and Nielsen, L.K. Method for generation of homogeneous multicellular tumor spheroids applicable to a wide variety of cell types. Biotechnol Bioeng **83**, 173, 2003.
51. Schlatter, S., Rimann, M., Kelm, J. and Fussenegger, M. SAMY, a novel mammalian reporter gene derived from Bacillus stearothermophilus alpha-amylase. Gene **282**, 19, 2002.
52. Reiser, J., Harmison, G., Kluepfel-Stahl, S., Brady, R.O., Karlsson, S. and Schubert, M. Transduction of nondividing cells using pseudotyped defective high-titer HIV type 1 particles. Proc Natl Acad Sci U S A **93**, 15266, 1996.
53. Kelm, J.M., Ehler, E., Nielsen, L.K., Schlatter, S., Perriard, J.C. and Fussenegger, M. Design of artificial myocardial microtissues. Tissue Eng **10**, 201, 2004.
54. Sheehan, D. and Hrapchak Theory and Practice of Histotechnology. Ohio, 1980.
55. Messerli, J.M., van der Voort, H.T., Rungger-Brandle, E. and Perriard, J.C. Three-dimensional visualization of multi-channel volume data: the amSFP algorithm. Cytometry **14**, 725, 1993.
56. Berger, J., Hauber, J., Hauber, R., Geiger, R. and Cullen, B.R. Secreted placental alkaline phosphatase: a powerful new quantitative indicator of gene expression in eukaryotic cells. Gene **66**, 1, 1988.
57. Kramer, B.P. and Fussenegger, M. Hysteresis in a synthetic mammalian gene network. Proc Natl Acad Sci U S A **102**, 9517, 2005.
58. Kaufmann, H., Mazur, X., Fussenegger, M. and Bailey, J.E. Influence of low temperature on productivity, proteome and protein phosphorylation of CHO cells. Biotechnol Bioeng **63**, 573, 1999.
59. Martin, I., Dozin, B., Quarto, R., Cancedda, R. and Beltrame, F. Computer-based technique for cell aggregation analysis and cell aggregation in in vitro chondrogenesis. Cytometry **28**, 141, 1997.
60. Andersen, D.C. and Krummen, L. Recombinant protein expression for therapeutic applications. Curr Opin Biotechnol **13**, 117, 2002.
61. Dove, A. Uncorking the biomanufacturing bottleneck. Nat Biotechnol **20**, 777, 2002.
62. Hesse, F. and Wagner, R. Developments and improvements in the manufacturing of human therapeutics with mammalian cell cultures. Trends Biotechnol **18**, 173, 2000.
63. Kretzmer, G. Industrial processes with animal cells. Appl Microbiol Biotechnol **59**, 135, 2002.
64. Irani, N., Wirth, M., van Den Heuvel, J. and Wagner, R. Improvement of the primary metabolism of cell cultures by introducing a new cytoplasmic pyruvate carboxylase reaction. Biotechnol Bioeng **66**, 238, 1999.
65. Kim, N.S. and Lee, G.M. Overexpression of bcl-2 inhibits sodium butyrate-induced apoptosis in Chinese hamster ovary cells resulting in enhanced humanized antibody production. Biotechnol Bioeng **71**, 184, 2000.
66. Kim, M.S., Kim, N.S., Sung, Y.H. and Lee, G.M. Biphasic culture strategy based on hyperosmotic pressure for improved humanized antibody production in Chinese hamster ovary cell culture. In Vitro Cell Dev Biol Anim **38**, 314, 2002.

67. Cruz, H.J., Moreira, J.L. and Carrondo, M.J. Metabolic shifts by nutrient manipulation in continuous cultures of BHK cells. Biotechnol Bioeng **66**, 104, 1999.
68. Siegwart, P., Cote, J., Male, K., Luong, J.H., Perrier, M. and Kamen, A. Adaptive control at low glucose concentration of HEK-293 cell serum-free cultures. Biotechnol Prog **15**, 608, 1999.
69. Mazur, X., Fussenegger, M., Renner, W.A. and Bailey, J.E. Higher productivity of growth-arrested Chinese hamster ovary cells expressing the cyclin-dependent kinase inhibitor p27. Biotechnol Prog **14**, 705, 1998.
70. Balcarcel, R.R. and Stephanopoulos, G. Rapamycin reduces hybridoma cell death and enhances monoclonal antibody production. Biotechnol Bioeng **76**, 1, 2001.
71. Muschler, G.F., Nakamoto, C. and Griffith, L.G. Engineering principles of clinical cell-based tissue engineering. J Bone Joint Surg Am **86-A**, 1541, 2004.
72. Smith, P.G., Burchill, S.A., Brooke, D., Coletta, P.L. and Whitehouse, A. Efficient infection and persistence of a herpesvirus saimiri-based gene delivery vector into human tumor xenografts and multicellular spheroid cultures. Cancer Gene Ther **12**, 248, 2005.
73. Juliano, R.L. Signal transduction by cell adhesion receptors and the cytoskeleton: functions of integrins, cadherins, selectins, and immunoglobulin-superfamily members. Annu Rev Pharmacol Toxicol **42**, 283, 2002.
74. Khalil, M., Shariat-Panahi, A., Tootle, R., Ryder, T., McCloskey, P., Roberts, E., Hodgson, H. and Selden, C. Human hepatocyte cell lines proliferating as cohesive spheroid colonies in alginate markedly upregulate both synthetic and detoxificatory liver function. J Hepatol **34**, 68, 2001.
75. Vournakis, J.N. and Runstadler, P.W., Jr. Optimization of the microenvironment for mammalian cell culture in flexible collagen microspheres in a fluidized-bed bioreactor. Biotechnology **17**, 305, 1991.
76. Kelm, J.M. and Fussenegger, M. Microscale tissue engineering using gravity-enforced cell assembly. Trends Biotechnol **22**, 195, 2004.
77. Desoize, B. and Jardillier, J. Multicellular resistance: a paradigm for clinical resistance? Crit Rev Oncol Hematol **36**, 193, 2000.
78. Freyer, J.P. Decreased mitochondrial function in quiescent cells isolated from multicellular tumor spheroids. J Cell Physiol **176**, 138, 1998.
79. Kunz-Schughart, L.A., Doetsch, J., Mueller-Klieser, W. and Groebe, K. Proliferative activity and tumorigenic conversion: impact on cellular metabolism in 3-D culture. Am J Physiol Cell Physiol **278**, C765, 2000.
80. Kunz-Schughart, L.A., Habbersett, R.C. and Freyer, J.P. Mitochondrial function in oncogene-transfected rat fibroblasts isolated from multicellular spheroids. Am J Physiol **273**, C1487, 1997.
81. Kunz-Schughart, L.A., Habbersett, R.C. and Freyer, J.P. Impact of proliferative activity and tumorigenic conversion on mitochondrial function of fibroblasts in 2D and 3D culture. Cell Biol Int **25**, 919, 2001.
82. Mueller-Klieser, W. Three-dimensional cell cultures: from molecular mechanisms to clinical applications. Am J Physiol **273**, C1109, 1997.

83. Li, S., Lao, J., Chen, B.P., Li, Y.S., Zhao, Y., Chu, J., Chen, K.D., Tsou, T.C., Peck, K. and Chien, S. Genomic analysis of smooth muscle cells in 3-dimensional collagen matrix. Faseb J **17**, 97, 2003.
84. St Croix, B., Florenes, V.A., Rak, J.W., Flanagan, M., Bhattacharya, N., Slingerland, J.M. and Kerbel, R.S. Impact of the cyclin-dependent kinase inhibitor p27Kip1 on resistance of tumor cells to anticancer agents. Nat Med **2**, 1204, 1996.
85. Dang, C.V. and Semenza, G.L. Oncogenic alterations of metabolism. Trends Biochem Sci **24**, 68, 1999.
86. Zerial, M. and McBride, H. Rab proteins as membrane organizers. Nat Rev Mol Cell Biol **2**, 107, 2001.
87. Proud, C.G. eIF2 and the control of cell physiology. Semin Cell Dev Biol **16**, 3, 2005.

Conclusions and Outlook

Three-dimensional (3D) cultures have been shown to reproduce chemical and molecular gradients, which are relevant in differentiation, cell fate, organ development, signal transduction and other biological processes. The metabolism and gene expression patterns of cells expanded in two-dimensional (2D) cultures are frequently altered, and such standard cultures can significantly reduce production of the ECM and create morphological changes which affect cell sensitivity (non-optimal orientation of the receptors), cell communication and thus cell functionality [1]. Therefore is not surprising the need to move *in vitro* cell experimentation into 3D cultures, which more authentically represent a cell's environment, in order to create more predictive studies prior to *in vivo* assays. Attempts in cultivating cells in 3D structures have expanded the science of material design. However cells attached to microfibers are still strictly considered as 2D environments. More accurate 3D environments require scaffold fibers and pores smaller than the cells. But, although they do have the right scale, cells expanded in such biomaterials make it difficult for controlled studies.

Artificial microtissues produced by the hanging drop technique have been demonstrated as an advantageous alternative to scaffold 3D cell culture systems for gene-function assays prior to *in vivo* assays. Thus, suggesting the impeding adaptation of scaffold-free in the research, development and production areas of biopharmaceutical industries. This work sought to provide examples of novel applications of artificial microtissues in physiological assays, transdifferentiation studies and productivity yields.

The ability to engineer and regulate tissue electrophysiology will facilitate great advances in the understanding of cardiac cell behavior and in the development of novel therapies to treat cardiac contractility disorders. Myocardial microtissues cultivated onto CMOS-based high-density microelectrode arrays provide a system to determine in real time cardiac functionality for; (i) pre-clinical and experimental electrophysiology tests, (ii) novel gene-function studies with potential therapeutic effect and (iii) as a pre-implantation quality control. In particular, BMP-2 gene expression was demonstrated to restore cardiac contractility of myocardial microtissues and contraction rhythm. Therefore BMP-2 might represent a therapeutic molecule for the recovery of cardiomyocyte function when cardiac contractility is the cause of reduced heart function.

Myocardial microtissues genetically engineered for regulable BMP-2 expression present an opportunity for *in vivo* transplantation of a biological pacemaker-like device, which responds to external signals in order to control cardiac electrical activity.

The ability to engineer cell fate using 3D cell culture models will foster important advances in the understanding of developmental processes and age-related diseases, and in regenerative therapies. Adipose-like microtissues were here demonstrated to be an excellent model to study differentiation and transdifferentiation processes at the molecular and cellular levels. ECM characterization in 3D cultures was required for in-depth study of functional and morphogenetic tissue-specific properties. Transduction with ΔFosB induced partially de-differentiation of mature adipocytes enabling the conversion of the ECM into a bone-like matrix, thus presenting ΔFosB as a potential molecule to treat osteoporosis and a novel pathway for transdifferentiation processes. Importantly, three-dimensional cultures provided a superior *ex vivo* system for the improved characterization of phenotypical and functional alterations resulting from interventions directed toward differentiation processes.

Improving specific productivity and product quality of mammalian cell-based manufacturing processes is one of the priorities of the biopharmaceutical industry. Mammalian cells cultivated in tissue-like format showed higher secretory capacities than cells cultivated on standard tissue culture plates. This suggests a synergistic combination of reduced proliferation and metabolic activities, molecular community crosstalk and specialized morphologic superstructures, which resulted in optimal cell survival and metabolic energy conversion, thus affecting specific productivity profiles. Microtissues also produce at higher levels supra-molecular structures such as lentiviral particles. Production capacities of tissue-embedded cells will (i) enable advances in operating bioreactors at high tissue-like cell densities, (ii) indicate the range of cell's utmost specific productivity and (iii) increase the understanding of in-vivo transgene expression in gene therapy and tissue engineering initiatives.

Overall, we demonstrated that artificial scaffold-free microtissues provide a tool for *in vitro* cell-based studies, which could be introduced as a standard cell culture technology in molecular and cellular laboratories for the investigation, screening and production of potent therapeutic molecules.

Potential additional applications of artificial microtissues in cell-based studies would be the study of cell type to cell type interaction/influence in cell physiology and cell fate. For instance, the electrophysiological influence of endothelial cells for future cardiac regeneration therapies. Endothelial cells are known to influence cardiac development but also cardiomyocyte function and survival, and in the normal myocardium they surround cardiomyocytes [2]. In addition, cell fate influence of chondrocytes in adipose transdifferentiation to bone. Chondrocytes are known to enhanced osteogenic differentiation by production of morphogenetic signals [3, 4]. As mentioned in the thesis, adipose-like microtissues could represent a closer *in vivo* model for the study and the screening of drugs to treat obesity-related diseases. For example, increasing the sensitivity of adipose tissue to insulin in order to treat type II diabetes [5] or prevention of adipocyte differentiation/growth as a target for obesity [6, 7]. Another topic of interest would be to model bone tissue by co-culturing osteoblasts with endothelial cells and fibroblasts as a drug-screening model for bone-related diseases or to further tissue transplant for wound healing. Finally, microtissues formed by high producers cell lines (BHK-21 showed a higher productivity growing as aggregates) cultured in high-density bioreactors, such as flow perfusion bioreactor, could optimize productivity and reduce cell death [8]. Therefore in order to up-scaled microtissue cultures and to perform high-throughput screening techniques an automatic system for microtissue production would be essential.

References

1. Zhang, S. Beyond the Petri dish. Nature biotechnology **22**, 151, 2004.
2. Hsieh, P.C., Davis, M.E., Lisowski, L.K. and Lee, R.T. Endothelial-cardiomyocyte interactions in cardiac development and repair. Annual review of physiology **68**, 51, 2006.
3. Gerstenfeld, L.C., Barnes, G.L., Shea, C.M. and Einhorn, T.A. Osteogenic differentiation is selectively promoted by morphogenetic signals from chondrocytes and synergized by a nutrient rich growth environment. Connective tissue research **44 Suppl 1**, 85, 2003.
4. Gerstenfeld, L.C., Cruceta, J., Shea, C.M., Sampath, K., Barnes, G.L. and Einhorn, T.A. Chondrocytes provide morphogenic signals that selectively induce osteogenic differentiation of mesenchymal stem cells. J Bone Miner Res **17**, 221, 2002.

5. Kadowaki, T., Hara, K., Yamauchi, T., Terauchi, Y., Tobe, K. and Nagai, R. Molecular mechanism of insulin resistance and obesity. Experimental biology and medicine (Maywood, N.J **228**, 1111, 2003.
6. Friedman, J.M. and Halaas, J.L. Leptin and the regulation of body weight in mammals. Nature **395**, 763, 1998.
7. Powell, K. Obesity: the two faces of fat. Nature **447**, 525, 2007.
8. Geserick, C., Bonarius, H.P., Kongerslev, L., Hauser, H. and Mueller, P.P. Enhanced productivity during controlled proliferation of BHK cells in continuously perfused bioreactors. Biotechnol Bioeng **69**, 266, 2000.

Acknowledgements

I thank to Martin Fussenegger for giving me the opportunity to perform my PhD studies at the ETH in Zurich. To Josep Vendrell for accepting being the tutor of my thesis at the Universtiy Autònoma of Barcelona.

To Jens Kelm for introducing me in to the world of tissue engineering and for becoming an important motivation during my PhD studies. To Barbara Guarino and Nadja Giuliani for welcoming and helping me during the first years and for still keeping a deep friendship. To David Fluri for being an extremely nice lab mate and for his advises. To Valeria Gonzalez-Nicolini for her advises, support and the nice chats. To Laetitia Malphettes and Shizuka Hartenbach for their friendship and help in the lab and outside the lab. To David Greber not only for his english corrections but also for creating a great atmosphere in the lab, for his productive discussions and for his nice friendship. And to all the people of the Fussengger's group for their help during my PhD studies, for the coffee breaks, the BBQs at Hönggerberg and the Friday beers.

To all the lunch mates for making the lunch breaks an enjoyable time, which I will really miss.

To all the people I meet in Zurich (Alex, Cristina F., Nacho, Bea, Daniele, Betta, Yanela, Francesca B., Francesca F., Serena, Helen, Vanessa, Sebastian, Justine, Cristina C., Ana, Olga, Stefania, Elena y Rosario) for making my time in Zurich unforgettable and with whom I hope and I know I will keep the friendship.

To my friends Amaya and Mar because they have been always there. To Carol for giving me always motivation during PhD.

To my grandparents, uncles and cousins for their love and support. To my parents who have been always next to me and continuously supporting me.

To Jacob for his unconditional love during the last eight years, my traveling partner and my eternal fellow.

Agradecimientos

Le agradezco a Martin Fussenegger por darme la oportunidad de hacer el doctorado en su grupo en el ETH de Zurich. A Josep Vendrell por aceptar ser el tutor de mi tesis en la Universidad Autònoma de Barcelona.

A Jens Kelm por introducirme en el mundo de la ingeniería de tejidos y por convertirse en una importante motivación durante mis estudios de doctorado. A Barbara Guarino y Nadja Giuliani por su recibimiento y ayuda durante los primeros años del doctorado y por mantener aún una profunda amistad. A David Fluri por ser un excelente compañero de laboratorio y por sus consejos. A Valeria Gonzalez-Nicolini por su consejos, su ayuda y por las divertidas charlas. A Laetitia Malphettes and Shizuka Hartenbach por su amistad y ayuda tanto en el laboratorio como fuera. A David Greber no sólo por sus correcciones de ingles sino también por crear un magnifico ambiente en el laboratorio, por sus productivas discusiones y por su bonita amistad. Y a toda la gente del grupo de M. Fussenegger por su ayuda durante el doctorado, por los ratos del café, por las barbacoas y por las cervezas los viernes por la tarde.

A todos los compañeros de la comida por hacer del rato de la comida una divertida hora, las echaré mucho de menos.

A toda la gente que he conocido en Zurich (Alex, Cristina F., Nacho, Bea, Daniele, Betta, Yanela, Francesca B., Francesca F., Serena, Helen, Vanessa, Sebastian, Justine, Cristina C., Ana, Olga, Stéphanie and Rosario) por hacer de mi tiempo en Zurich una experiencia inolvidable y con los que espero y se mantendré la amistad.

A mis amigas Mar y Amaya por siempre estar ahí. A Carol por darme siempre ánimos.

A mis abuelos, tíos y primos por su amor y por la fuerza que me transmiten. A mis padres quienes han estado siempre ha mi lado continuamente ayudándome y apoyándome.

A Jacob por su amor incondicional durante los últimos ocho años, por ser mi compañero de viaje y mi eterno aliado.

Curriculum Vitae

Carlota Díaz Sánchez-Bustamante

Spanish nationality

Hügelstrasse 13, CH-8002, Zurich

Education

- 2003-Present: **Doctoral:** PhD studies on "Biotechnological Applications of Artificial Microtissues" under the supervision of Prof. Dr. Martin Fussenegger at the Institute of Chemical and Bio-engineering (ETH, Zurich).
- 2002-2003: **Research training:** "*In Vitro* Induction of Angiogenesis in a 3-dimensional Microtissue Co-Culutre Model" in Prof. Dr. Martin Fussenegger's group at the Institute of Biotechnology (ETH, Zurich).
- 1998-2003: **Tertiary:** Bachelor in Biotechnology/*Licenciatura en Biotechnología***.** Universitat Autònoma de Barcelona (UAB), Barcelona.
- 1992-1998: **Secondary**: Colegio Jesús-María. Barcelona.

List of scientific publications

Sanchez-Bustamante CD, Frey U, Kelm JM, Greve F, Hierlemann A, Fussenegger M. 2007a. Control of Cardiomyocyte Electrical Properties by Regulated BMP-2 Expression. Tissue Engineering. *Submitted.*

Sanchez-Bustamante CD, Kelm JM, Egermann M, Djonov V, Fussenegger M. 2007b. Ectopic Expression of deltaFosB mediates transdifferentiation of Adipose-Like Spheroids Into Osteo-Like Microtissues. Tissue Engineering. *In Press*.

Frey U, Sanchez-Bustamante CD, Ugniwenko T, Heer F, Sedivy J, Hafizovic S, Roscic B, Fussenegger M, Blau A, Egert U and others. 2007. Cell Recordings with a CMOS High-density Microelectrode Array. IEEE Engineering in Medicine and Biology Society. *In press.*

Gonzalez-Nicolini V, Sanchez-Bustamante CD, Hartenbach S, Fussenegger M. 2006. Adenoviral vector platform for transduction of constitutive and regulated tricistronic or

triple-transcript transgene expression in mammalian cells and microtissues. J Gene Med 8(10):1208-22

Kelm JM, Djonov V, Hoerstrup SP, Guenter CI, Ittner LM, Greve F, Hierlemann A, Sanchez-Bustamante CD, Perriard JC, Ehler E and others. 2006. Tissue-transplant fusion and vascularization of myocardial microtissues and macrotissues implanted into chicken embryos and rats. Tissue Eng 12(9):2541-53.

Sanchez-Bustamante CD, Kelm JM, Mitta B, Fussenegger M. 2006. Heterologous protein production capacity of mammalian cells cultivated as monolayers and microtissues. Biotechnol Bioeng 93(1):169-80.

Kelm JM, Diaz Sanchez-Bustamante C, Ehler E, Hoerstrup SP, Djonov V, Ittner L, Fussenegger M. 2005. VEGF profiling and angiogenesis in human microtissues. J Biotechnol 118(2):213-29.

Oral and poster presentations

The Swiss Cardiovascular Research and Training Network. February 2007. University of Bern. "Control of cardiac myocyte electrophysiology by regulation of BMP-2 expression" Carlota Diaz Sanchez-Bustamante, Urs Frey, Frauke Greve, Jens M. Kelm, Andreas Hierlermann and Martin Fussenegger.

IDEA Leage Summer School. September 2006. Centro Stefano Franscini, Monte Verita, Ascona. "Generation of biological pacemaker-like activity with NRC cells and microtissues compatible with a 3D culture screening system" Carlota Diaz Sanchez-Bustamante, Frauke Greve, Jens M. Kelm, Valeria Gonzalez-Nicolini, Jean-Claude Perriard, Andreas Hierlermann and Martin Fussenegger.

D-BIOL Symposium. May 2006. Congress-Center Davos. "Generation of biological pacemaker-like activity with NRC cells and microtissues compatible with a 3D culture screening system". Carlota Diaz Sanchez-Bustamante, Frauke Greve, Jens M. Kelm, Valeria Gonzalez-Nicolini, Jean-Claude Perriard, Andreas Hierlermann and Martin Fussenegger.

D-BIOL Symposium. May 2004. Congress-Center Davos. "Heterlogous Protein Production Capacity of Mammalian Cells in 2D and 3D Cultures". Carlota Diaz Sanchez-Bustamante, Jens M. Kelm, Barbara Mitta and Martin Fussenegger.